

**SYNTHESIS OF BORON AND CERIUM CODOPED  
TITANIUM DIOXIDE PHOTOCATALYSTS FOR  
ANTIBIOTIC DEGRADATION AND MICROBIAL  
DISINFECTION UNDER SOLAR LIGHT**

**Thesis**

Submitted in partial fulfillment of the requirements for the degree of

**DOCTOR OF PHILOSOPHY**

by

**MANASA M**

Registration no. 177043CH002



**DEPARTMENT OF CHEMICAL ENGINEERING  
NATIONAL INSTITUTE OF TECHNOLOGY KARNATAKA,  
SURATHKAL, MANGALURU-575025**

**JULY, 2022**

## DECLARATION

I hereby declare that the research thesis entitled “**SYNTHESIS OF BORON AND CERIUM CODOPED TITANIUM DIOXIDE PHOTOCATALYSTS FOR ANTIBIOTIC DEGRADATION AND MICROBIAL DISINFECTION UNDER SOLAR LIGHT**” which is being submitted to the **National Institute of Technology Karnataka, Surathkal** in partial fulfillment of the requirements for the award of the degree of **Doctor of Philosophy** in Chemical Engineering is a *bonafide report of the research work carried out by me*. The material contained in this research thesis has not been submitted to any University or Institution for the award of any degree.

Manasa.M

MANASA M

177043CH002

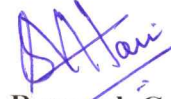
Department of Chemical Engineering

Place: Surathkal

Date: 01/08/2022

## CERTIFICATE

This is to certify that the research thesis entitled “**SYNTHESIS OF BORON AND CERIUM CODOPED TITANIUM DIOXIDE PHOTOCATALYSTS FOR ANTIBIOTIC DEGRADATION AND MICROBIAL DISINFECTION UNDER SOLAR LIGHT**” submitted by **MANASA M (177043CH002)** as the record of the research work carried out by her, *is accepted as the research thesis submission* in partial fulfillment of the requirements for the award of degree of **Doctor of Philosophy**.



**Research Guide**

Dr. Hari Mahalingam

Associate Professor

Department of Chemical Engineering

NITK, Surathkal



Head of the Department  
विभागाध्यक्ष

**Chairman - DRPC**  
Department of Chemical Engineering  
रासायनिक अभियांत्रिकी विभाग

National Institute of Technology Karnataka - Surathkal  
राष्ट्रीय प्रौद्योगिकी संस्थान कर्नाटक, सुरात्कल  
PO Srinivasnagar, Mangalore - 575025 Karnataka  
पी.ओ. श्रीनिवासनगर, मंगलूर - ५७५०२५, कर्नाटक

## ACKNOWLEDGEMENTS

I take this opportunity to acknowledge each and every individual who has contributed in different ways for my research work carried out in the Department of Chemical Engineering at NITK, Surathkal.

I wish to express special gratitude to my research guide, Dr. Hari Mahalingam, Associate Professor, Department of Chemical Engineering, NITK, Surathkal for his valuable guidance, unflinching support, constant encouragement, and patience.

I sincerely thank and express my gratitude to the RPAC committee members, Dr. Basavaraju Manu, Department of Civil Engineering and Dr. Hari Prasad Dasari, Department of Chemical Engineering. Their suggestions and guidance have helped me to improve my research work in innumerable ways.

I express my sincere gratitude to the Director, NITK. I wish to extend my gratitude to all the HODs (Prof. Raj Mohan, B., Dr. Hari Mahalingam, Dr. Prasanna Belur, D., and Dr. P. E. Jagadeeshbabu) for providing support throughout the research work. I also wish to thank all teachers and research scholars in the Department of Chemical Engineering for their support and encouragement. I thank MoE, GOI for providing stipend throughout my research work.

I would like to extend my thanks to Mr. Sadashiva, Mrs. Trithila, Mrs. Vijetha, Mrs. Bhavya Shree, Mrs. Shashikala, Mr. Jnaneshwar, and all other non-teaching staffs of Department of Chemical Engineering for their timely help and support in the laboratory for the research work. I also thank Central Research Facility (CRF), Department of Physics, Chemistry, & Metallurgy, NITK, MNIT (Jaipur), STIC (Kochi), CNMS, Jain University, (Bengaluru) and CAF, Manipal University (Jaipur) for providing their instrumentation facilities.

Finally, I would like to thank my parents, brother, friends for their support and care throughout the research work.

MANASA M





## ABSTRACT

In recent years, antimicrobial resistance has been a global emerging problem due to the emergence of superbugs which poses a major threat to human health and the environment. The presence of antibiotic residues is the primary source of this emerging problem. Photocatalysis, for decades, has been a promising treatment technology in removing recalcitrant organic compounds from the environment. In this study, a systematic series of B and Ce monodoped (0.1 and 1 at.% Ce-TiO<sub>2</sub>, 1 and 2 at.% B-TiO<sub>2</sub>) and codoped (B<sub>x</sub>Ce<sub>1-x</sub>TiO<sub>2</sub>, x = 0.9, 0.8 and 0.7 at.%) catalysts were synthesized using a facile green EDTA-citrate method. The synthesized catalysts were evaluated for the degradation of ciprofloxacin (CIP, antibiotic) and disinfection of *E.coli* under sunlight in both suspended and immobilized forms. For immobilization, waste expanded polystyrene (EPS) beads were used as a substrate along with the best performing codoped catalyst. The catalysts were characterized for particle size, BET surface area, surface morphology (SEM and TEM analysis), crystal structure (XRD analysis), surface chemistry (XPS and RAMAN analysis), bandgap (DRS analysis), and recombination (PL analysis). XRD analysis showed anatase rutile and Ce peaks, and no B peaks were detected which is due to the difference in ionic radius of the dopants. From XPS analysis, the elemental compositions of the doped catalysts (suspended form) and the actual amount of photocatalyst added during the film preparation (immobilized form) were in accordance with the selected compositions. Lesser recombination with lower PL intensity was observed for the doped catalysts. The reaction parameters such as catalyst loading, initial concentrations of antibiotic, mineralization (COD/TOC reduction), and reusability were studied, and the degradation pathways were elucidated (LC-MS analysis). The degraded sample was evaluated for the residual antibacterial activity to confirm the degradation of antibiotic. Real water matrices (tap water and river water) were considered in the study. Among the monodoped series, highest degradation of 93.22% was shown by 1 at.% Ce-TiO<sub>2</sub> and 93.16% by 1 at.% B-TiO<sub>2</sub> after 180 min. Whereas, among the codoped series of catalysts, B<sub>0.8</sub>Ce<sub>0.2</sub>TiO<sub>2</sub> showed the highest degradation of 97.43% (suspended form) and 81.36% (immobilized form) after 180 min. Immobilized form

showed 89.17% degradation of CIP at the end of 240 min. In terms of disinfection, the codoped catalyst was found to be 10 times more effective (corresponding to 1 log higher reduction) than the monodoped catalysts. Low molecular weight and less harmful degraded products were observed from LC-MS analysis. Reusability studies up to five consecutive runs proved the stability of these catalysts both in suspended and immobilized forms. The active role of electrons, holes, and OH<sup>·</sup> species in the degradation was observed from the scavenging studies. The degradation and disinfection efficiencies in the real water samples were slightly lesser than the deionized water, which might be due to the presence of anions and natural organic matter. The performance of the codoped catalysts (in terms of both degradation and disinfection) was better than monodoped catalysts and superior when compared to TiO<sub>2</sub>. Overall, these boron and cerium (monodoped and codoped) doped catalysts can serve as an efficient solar light active catalysts for both antibiotic degradation and bacterial disinfection.

**Keywords:** Doping, EDTA-citrate method, Sunlight, Ciprofloxacin, *E.coli*, Waste EPS beads

# CONTENTS

CHAPTER	TITLE	PAGE NO.
	<b>ABSTRACT</b>	i
	<b>CONTENTS</b>	iii
	<b>LIST OF FIGURES</b>	vii
	<b>LIST OF TABLES</b>	xii
	<b>NOMENCLATURE</b>	xiv
<b>1</b>	<b>INTRODUCTION</b>	
1.1	BACKGROUND	1
1.2	WATER POLLUTION: PHARMACEUTICALS AND ANTIMICROBIAL RESISTANCE (AMR)	1
1.3	MECHANISMS OF AMR AND CLASSIFICATION OF ANTIBIOTICS	2
1.4	ANTIBIOTIC POLLUTION	5
1.4.1	Sources	5
1.4.2	Global Status	5
1.4.3	Indian Scenario	6
1.4.4	Initiatives to minimize or control antibiotic pollution	8
1.4.5	Effects on human health and the environment	9
1.5	ARTICLES/CASE STUDIES REPORTED ON THE PRESENCE OF ANTIBIOTIC RESIDUES AND SUPERBUGS IN THE ENVIRONMENT	9
1.6	TREATMENT TECHNOLOGIES AVAILABLE FOR PHARMACEUTICAL WASTEWATER TREATMENT	10
1.7	DISADVANTAGES OF CONVENTIONAL PHARMACEUTICAL WASTEWATER TREATMENT METHODS	10
1.8	ADVANCED OXIDATION PROCESSES (AOPS)	11
1.9	PHOTOCATALYSIS	11
1.9.1	Different forms of the photocatalyst	12
1.9.1.1	Suspended form	12
1.9.1.2	Immobilized/floating form	12

CHAPTER	TITLE	PAGE NO.
1.10	GENERAL MECHANISM OF PHOTOCATALYSIS	13
<b>2</b>	<b>LITERATURE REVIEW</b>	
2.1	HISTORICAL DEVELOPMENT OF PHOTOCATALYSTS	16
2.2	TITANIUM DIOXIDE (TiO <sub>2</sub> )	17
2.3	FACTORS AFFECTING THE PHOTOCATALYTIC PROCESS	17
2.3.1	Effect of catalyst loading	17
2.3.2	Effect of initial concentration of pollutant	18
2.3.3	Effect of pH	18
2.3.4	Effect of size and surface area of photocatalyst	18
2.3.5	Effect of irradiation time and light intensity	18
2.3.6	Effect of temperature	19
2.3.7	Effect of inorganic ions and water matrix	19
2.3.8	Effect of dopants	20
2.3.9	Effect of bandgap	20
2.3.10	Effect of immobilization on/into suitable support	20
2.3.11	Effect of crystallinity	21
2.4	VISIBLE-LIGHT ACTIVE CATALYSTS	21
2.4.1	Doping	21
2.5	PHOTOCATALYTIC DEGRADATION OF ANTIBIOTICS USING TiO <sub>2</sub>	22
2.6	PHOTOCATALYSIS USING B AND Ce AS DOPANTS (DEGRADATION AND DISINFECTION)	24
2.7	RECENT PHOTOCATALYSTS: DEGRADATION OF CIP, OTHER ORGANIC POLLUTANTS AND DISINFECTION	32
2.8	SIMULTANEOUS PHOTOCATALYTIC DEGRADATION AND DISINFECTION (DISINFECTION IN THE PRESENCE OF ANTIBIOTICS)	40
2.9	IMMOBILIZATION OF PHOTOCATALYSTS TO OVERCOME THE DISADVANTAGES OF SUSPENDED FORM	49

CHAPTER	TITLE	PAGE NO.
2.10	EFFECT OF REAL WATER MATRICES	57
2.11	SYNTHESIS METHODS	57
2.12	RESEARCH GAPS	58
2.13	SELECTION OF DOPANTS: BORON AND CERIUM	59
2.14	SCOPE AND OBJECTIVES	60
<b>3</b>	<b>MATERIALS AND METHODS</b>	
3.1	MATERIALS	63
3.2	METHODS	63
3.2.1	Synthesis of boron and cerium doped (monodoped/codoped) TiO <sub>2</sub> photocatalysts (B-TiO <sub>2</sub> /Ce-TiO <sub>2</sub> and B <sub>x</sub> Ce <sub>1-x</sub> TiO <sub>2</sub> )	63
3.2.2	Preparation of photocatalytic EPS film	65
3.2.3	Model pollutant and organism: Ciprofloxacin (CIP) and <i>Escherichia coli</i> ( <i>E.coli</i> )	66
3.2.4	Characterization	67
3.2.5	Measurement of photocatalytic degradation of CIP	69
3.2.6	Identification of the degraded products	71
3.2.7	Role of reactive species in the degradation of CIP (scavenging studies)	71
3.2.8	Residual antibacterial activity of the degraded CIP solution	72
3.2.9	Preparation of bacterial cells and enumeration	72
3.2.10	Photocatalytic disinfection in the absence and presence of antibiotic	73
3.2.10.1	Regrowth studies and determination of K <sup>+</sup> ions	74
3.2.11	Recyclability/reusability studies	74
3.2.12	Real water matrices	74
<b>4</b>	<b>PHOTOCATALYTIC DEGRADATION: SUSPENDED FORM</b>	
4.1	CHARACTERIZATION OF THE SYNTHESIZED PHOTOCATALYSTS	77
4.1.1	Particle size and BET surface area measurements	77
4.1.2	SEM Analysis	78
4.1.3	TEM Analysis	80
4.1.4	XRD analysis	82
4.1.5	XPS analysis	84

CHAPTER	TITLE	PAGE NO.
4.1.6	RAMAN spectroscopy	87
4.1.7	DRS and PL analysis	87
4.2	PHOTOCATALYTIC TREATMENT OF CIP	90
4.2.1	Effect of catalyst loading	90
4.2.2	Effect of initial concentration and kinetics	92
4.2.3	Mineralization of CIP	94
4.2.4	Factors contributing to the synergy of the dopants (B and Ce)	96
4.2.5	Effect of pH	98
4.2.6	Recyclability studies	99
4.2.7	Scavenging studies and possible mechanism of CIP degradation	100
4.3	ANALYSIS OF DEGRADED CIP SAMPLE	102
4.3.1	Residual antibacterial activity of the degraded CIP sample	102
4.3.2	LC-MS analysis	103
<b>5</b>	<b>PHOTOCATALYTIC DEGRADATION: IMMOBILIZED FORM</b>	
5.1	CHARACTERIZATION OF THE IMMOBILIZED FILM	109
5.1.1	FESEM analysis	109
5.1.2	XRD spectra analysis	111
5.1.3	FTIR spectra analysis	112
5.1.4	XPS spectra analysis	113
5.15	Contact angle measurement and leaching studies	114
5.2	PHOTOCATALYTIC TREATMENT OF CIP	115
5.2.1	Effect of solvent volumes and amount of EPS beads	115
5.2.2	Effect of catalyst loading	116
5.2.3	Effect of CIP initial concentrations and kinetic studies	117
5.2.4	Effect of pH	118
5.2.5	Reusability studies	119
5.3	ANALYSIS OF DEGRADED CIP SAMPLE	120
5.3.1	TOC analysis and antibacterial activity of the degraded CIP sample	120

CHAPTER	TITLE	PAGE NO.
5.3.2	LC-MS analysis	121
5.4	COMPARISON OF PERFORMANCE OF THE B <sub>0.8</sub> CE <sub>0.2</sub> TIO <sub>2</sub> PHOTOCATALYST: SUSPENDED AND IMMOBILIZED FORMS, OTHER ANTIBIOTICS, SUNLIGHT AND UV-A IRRADIATION	124
5.5	BATCH SCALE-UP STUDY AND EFFECT OF H <sub>2</sub> O <sub>2</sub> CONCENTRATIONS	125
<b>6</b>	<b>PHOTOCATALYTIC DISINFECTION IN THE ABSENCE &amp; PRESENCE OF ANTIBIOTIC AND EFFECT OF REAL WATER MATRICES</b>	
6.1	PHOTOCATALYTIC DISINFECTION USING <i>E.coli</i>	129
6.1.1	Disinfection in the absence of antibiotic (suspended and immobilized form)	129
6.1.2	Disinfection in the presence of antibiotic (suspended and immobilized form)	131
6.1.3	Regrowth studies	131
6.1.4	Disinfection kinetics	132
6.1.5	Determination of K <sup>+</sup> ions using ICP-OES in the disinfected sample (suspended and immobilized forms)	134
6.2	EFFECT OF REAL WATER MATRICES	135
<b>7</b>	<b>CONCLUSIONS AND SCOPE FOR FUTURE WORK</b>	
7.1	SUMMARY	137
7.2	CONCLUSIONS	139
7.3	SCOPE FOR FUTURE WORK	146
	<b>REFERENCES</b>	147
	<b>APPENDIX I</b>	187
	<b>APPENDIX II</b>	191
	<b>BIO-DATA</b>	201



## LIST OF FIGURES

FIGURES	CAPTION	PAGE NO.
1.1	Mechanisms of bacterial resistance to antibiotics	3
1.2	Antibiotic residues: Sources and effects	5
1.3	Suspended form of the photocatalyst	12
1.4	Immobilized/floating form of the photocatalyst and common supports used for immobilization	13
1.5	Mechanism of photocatalytic degradation of organic pollutants	14
1.6	Mechanism of photocatalytic disinfection	15
2.1	Historical development of photocatalysts to remove organic pollutants from the environment	16
2.2	Enhancement of visible light utilization through doping	22
2.3	Lattice positions of B: interstitial and substitutional	60
3.1	Synthesis of boron and cerium doped photocatalysts by EDTA-citrate method	64
3.2	Summary of photocatalysts synthesized in this study	65
3.3	Preparation of EPS film	65
3.4	Chemical structure of CIP	66
3.5	Characterizations of TiO <sub>2</sub> , synthesized photocatalysts and immobilized film	68
3.6	Experimental set-up view of batch photocatalytic studies carried out under sunlight	70
3.7	Standard calibration curve of the model pollutant: CIP	70
3.8	(a) MTCC culture grown in LB broth and (b) Enumeration of cells through serial dilution and plate count method	73
3.9	Antibiotic resistance assay	74
4.1	SEM images of TiO <sub>2</sub> and the synthesized photocatalysts (Left image is at X500 and the right image is at X1000 magnifications)	79

FIGURES	CAPTION	PAGE NO.
4.2	Elemental mapping (a) 1 at.% Ce-TiO <sub>2</sub> , (b) 1 at.% B-TiO <sub>2</sub> and (c) B <sub>0.9</sub> Ce <sub>0.1</sub> TiO <sub>2</sub>	80
4.3	TEM images and SAED patterns of [a-c]TiO <sub>2</sub> , [d-f] 1Ce-TiO <sub>2</sub> , [g-i] 1B-TiO <sub>2</sub> and [j-l] B <sub>0.9</sub> Ce <sub>0.1</sub> TiO <sub>2</sub>	81
4.4	XRD spectra of TiO <sub>2</sub> and the synthesized photocatalysts	83
4.5	XPS spectra TiO <sub>2</sub> and the synthesized photocatalysts	86
4.6	RAMAN spectra of TiO <sub>2</sub> and the synthesized photocatalysts	87
4.7	(a) Wavelength vs. absorbance plot, (b-i) Tauc plot showing the bandgap of TiO <sub>2</sub> and the synthesized photocatalysts	88
4.8	PL spectra of TiO <sub>2</sub> and the synthesized photocatalysts	90
4.9	Effect of catalyst loading on the degradation of CIP using (a) TiO <sub>2</sub> , (b) Ce-TiO <sub>2</sub> & B-TiO <sub>2</sub> series and (c) B <sub>x</sub> Ce <sub>1-x</sub> TiO <sub>2</sub> series	91
4.10	Effect of initial concentrations of CIP on the degradation using (a) 1Ce-TiO <sub>2</sub> , (b) 1B-TiO <sub>2</sub> , (c) B <sub>0.8</sub> Ce <sub>0.2</sub> TiO <sub>2</sub> , (d-f) Kinetics plot, and (g) Summary of kinetics data	93
4.11	Mineralization of CIP under sunlight	95
4.12	Comparison of CIP degradation efficiency of codoped catalyst with the literature	96
4.13	(a) Point of zero charge (pzc) of B <sub>0.8</sub> Ce <sub>0.2</sub> TiO <sub>2</sub> and (b) Effect of pH on CIP degradation	99
4.14	Degradation (%) in consecutive photocatalytic cycles of recyclability	100
4.15	Scavenging experiments for identification of reactive oxygen species in the photocatalytic degradation	101
4.16	Possible degradation mechanism of CIP using (a) Ce-TiO <sub>2</sub> , (b) B-TiO <sub>2</sub> , and (c) B <sub>x</sub> Ce <sub>1-x</sub> TiO <sub>2</sub>	102
4.17	Residual antibacterial activity of the degraded CIP sample using the best performing photocatalysts and their corresponding degradation	103
4.18	Possible degradation pathways of CIP (a) Ce-TiO <sub>2</sub> & B-TiO <sub>2</sub> series and (b) B <sub>x</sub> Ce <sub>1-x</sub> TiO <sub>2</sub> series	107

FIGURES	CAPTION	PAGE NO.
5.1	FESEM images of plain EPS film and film with the immobilized catalyst (before and after five times of reuse)	110
5.2	Thickness of the $B_{0.8}Ce_{0.2}TiO_2$ immobilized EPS film	111
5.3	XRD spectra of [a] EPS film, [b] $B_{0.8}Ce_{0.2}TiO_2$ immobilized EPS film after using five times, [c] $B_{0.8}Ce_{0.2}TiO_2$ immobilized EPS film	112
5.4	FTIR spectra of plain EPS film, unused EPS film, and EPS film after five times of reuse	113
5.5	XPS analysis of the immobilized $B_{0.8}Ce_{0.2}TiO_2$ photocatalyst film	114
5.6	Effect of solvents on the photocatalytic degradation of CIP using $B_{0.8}Ce_{0.2}TiO_2$ immobilized EPS film [A1: 3 g EPS + 10 mL Acetone (5 wt.%), A2: 3 g EPS + 10 mL Acetone (10 wt.%), B1: 4 g EPS + 10 mL Acetone (5 wt.%), C1: 3 g EPS + 8 mL Acetone + 2 mL Ethanol (5 wt.%), C2: 3 g EPS + 8 mL Acetone + 2 mL Ethanol (10 wt.%)]	115
5.7	EPS films prepared by varying the quantity of EPS and solvents: [a] 3 g EPS + 10 mL Acetone, [b] 4 g EPS + 10 mL Acetone, and [c] 3 g EPS + 8 mL Acetone + 2 mL ethanol	116
5.8	(a) Effect of catalyst loading on the photocatalytic CIP degradation [CIP = 10 ppm], (b) Photocatalytic degradation of CIP for 20 wt.% EPS film at a longer time scale	117
5.9	(a) Variation of initial concentrations of CIP with the optimum catalyst loading of 20 wt.%, (b) Kinetics plot and (c) Summary of kinetics data	118
5.10	Effect of pH on CIP degradation	119
5.11	Reusability of EPS film performed for five consecutive cycles	120
5.12	Antimicrobial activity of the degraded CIP sample	121
5.13	Possible degradation pathways of CIP from LC-MS analysis	123
5.14	(a) Comparison of CIP degradation efficiency in suspended and immobilized forms, (b) Comparison of CIP degradation efficiency under sunlight and UV-A irradiation and (c) Degradation of other antibiotics using the $B_{0.8}Ce_{0.2}TiO_2$ both in suspended and immobilized form	125

FIGURES	CAPTION	PAGE NO.
5.15	(a) Batch scale-up studies using 550 ml of CIP solution under sunlight and (b) Effect of H <sub>2</sub> O <sub>2</sub> as an oxidizing agent on degradation of CIP	126
6.1	Disinfection using TiO <sub>2</sub> and best-performing catalysts under sunlight (Initial cell concentration -10 <sup>8</sup> CFU/mL, duration -180 min)	130
6.2	Photocatalytic disinfection in the absence and presence of antibiotic	131
6.3	Kinetics plot of disinfection in the absence and presence of 1 ppm CIP using B <sub>0.8</sub> Ce <sub>0.2</sub> TiO <sub>2</sub> (a-b) Suspended form and (c-d) Immobilized form	133
6.4	Release of K <sup>+</sup> ions during disinfection with an increase in the treatment time (a) Suspended form and (b) Immobilized form	134
6.5	Photocatalytic degradation of CIP under different water matrices (a) suspended form and (b) immobilized form; Photocatalytic disinfection of <i>E.coli</i> (c) suspended form and (d) immobilized form <b>Experimental conditions:</b> Suspended form: B <sub>0.8</sub> Ce <sub>0.2</sub> TiO <sub>2</sub> - 0.5 g/L, CIP - 10 ppm/ <i>E.coli</i> - 10 <sup>8</sup> CFU/mL, under sunlight - 180 min, Immobilized form: 20 wt.% B <sub>0.8</sub> Ce <sub>0.2</sub> TiO <sub>2</sub> EPS immobilized film, CIP - 10 ppm/ <i>E.coli</i> - 10 <sup>8</sup> CFU/mL, under sunlight - 180 min	136

## LIST OF TABLES

TABLES	CAPTION	PAGE NO.
1.1	Classification of antibiotics based on chemical structure	4
1.2	Studies reported on the occurrence of antibiotic in the environment across the globe	6
1.3	Most commonly reported antibiotics concentration in rivers and wastewater treatment plants (WTPs)/sewage treatment plants (STPs) in India	7
2.1	Degradation of antibiotics using TiO <sub>2</sub>	23
2.2	Degradation of organic pollutants using monodoped and codoped catalysts with boron/cerium as dopants	26
2.3	Disinfection studies using monodoped and codoped catalysts with boron/cerium as dopants	29
2.4	Degradation of CIP using TiO <sub>2</sub> and latest generation photocatalysts	34
2.5	Summary of photocatalytic degradation of other organic pollutants and disinfection	38
2.6	Simultaneous photocatalytic degradation and disinfection studies	44
2.7	Summary of loss of antimicrobial activity of photocatalytically treated antibiotics and photocatalytic disinfection of multidrug resistant (MDR) micro-organisms	47
2.8	Photocatalytic studies of organic pollutants and disinfection in immobilized forms	52
3.1	Physico-chemical data of CIP	66
3.2	Characteristics of real water samples	75
4.1	Particle size of TiO <sub>2</sub> and the synthesized photocatalysts	78
4.2	XRD parameters of TiO <sub>2</sub> and the synthesized photocatalysts	84
4.3	Elemental composition of TiO <sub>2</sub> and the synthesized photocatalysts from XPS analysis	86
4.4	Bandgap energy values of the photocatalysts from the Tauc plot	89
4.5	Kinetics of CIP degradation	94

<b>TABLES</b>	<b>CAPTION</b>	<b>PAGE NO.</b>
<b>4.6</b>	CIP degraded products identified by LC-MS analysis	105
<b>5.1</b>	Kinetics data of CIP degradation	118
<b>5.2</b>	Degradation products of CIP	122
<b>6.1</b>	Kinetics of <i>E.coli</i> disinfection in the absence and presence of CIP using $B_{0.8}Ce_{0.2}TiO_2$ catalyst	133
<b>7.1</b>	Performance of photocatalysts under the study based on crystallite size, bandgap energy, adsorption, degradation, COD/TOC reduction, and disinfection (suspended and immobilized forms)	138
<b>7.2</b>	Kinetics data of best-performing catalysts	140
<b>7.3</b>	Degradation efficiencies of various antibiotics using $B_{0.8}Ce_{0.2}TiO_2$ catalyst	142
<b>7.4</b>	Comparison of CIP degradation efficiency of this work with some latest generation photocatalysts	144

## NOMENCLATURE

AMR – Antimicrobial resistance

AOPs – Advanced oxidation processes

B – Boron

BET – Brunauer–Emmett–Teller

CB – Conduction band

Ce – Cerium

CFU – Colony forming units

CIP – Ciprofloxacin

COD – Chemical oxygen demand

DRS – Diffuse reflectance spectroscopy

e<sup>-</sup> – Electrons

eV – Electron volt

ECs – Emerging contaminants

EDCs – Endocrine-disrupting compounds

EPS – Expanded polystyrene

FDA – Food and Drug Administration

FESEM – Field emission scanning electron microscopy

FTIR – Fourier Transform Infrared Spectroscopy

h<sup>+</sup> – Holes

ICP-OES – Inductively coupled plasma-optical emission spectrometry

MTCC – Microbial Type Culture Collection and Gene Bank

LCMS – Liquid chromatography-mass spectrometry

LEV – Levofloxacin

µg/L – Microgram per liter

MOX – Moxifloxacin

ng/L – Nanogram per liter

NOR – Norfloxacin

O<sub>2</sub><sup>•-</sup> – Superoxide radicals

OH<sup>•</sup> – Hydroxyl radicals

ppm – Parts per million

PL – Photoluminescence

PNEC – Predicted no-effect concentration

ROS – Reactive oxygen species

SEM – Scanning electron microscopy

TEM – Scanning electron microscopy

TiO<sub>2</sub> – Titanium dioxide

TOC – Total organic carbon

UV – Ultraviolet

VB – Valence band

XRD – X-ray diffraction

XPS –X-ray photoelectron spectroscopy





## **CHAPTER 1**

### **INTRODUCTION**

#### **1.1. BACKGROUND**

Water pollution from the last three decades is a major environmental problem that needs an immediate solution (Boretti and Rosa 2019). Out of the total water available (on, in, and above the earth, 1385 km in diameter), freshwater accounts for 20% (272.8 km in diameter) and only 4% of surface water (56.2 km in diameter) is available for serving the growing population (Shiklomanov 1993). The common water pollutants are heavy metals, pathogens, pharmaceuticals, and dyes (Owa 2014). In recent years, emerging contaminants (ECs) have been one of the major threats throughout the globe. Pesticides, herbicides, heavy metals/industrial chemicals, personal care products, pharmaceuticals, and endocrine-disrupting compounds (EDCs) are some of the key examples of ECs (Herman 2014). Since many years, pharmaceuticals have improved the quality of life and lengthened the life spans by curing millions of people from deadly diseases. However, in the past three decades, pharmaceutical residues have been detected in almost all environmental sources, and this has led to the evolution of resistant microbes or superbugs. Pharmaceutical discharge is unregulated (Larsson 2014; Tijani et al. 2016), and these residues are considered to be emerging compounds due to their adverse impacts on human health and the environment (Kümmerer 2009). The pharmaceutical market in India is among the top 10 globally (Friend et al. 2010) and is a major contributor to water pollution, facilitating the rise of drug-resistant infections, considered to be a significant health threat by 2050 (Thomas 2020). The global antibiotic consumption increased by 65% in 2015, and is expected to increase 15% by 2030 (Klein et al. 2018).

#### **1.2. WATER POLLUTION: PHARMACEUTICALS AND ANTIMICROBIAL RESISTANCE (AMR)**

Rapid urbanization, industrialization, and unethical human activities like untreated/partially treated wastewater being released into the environment etc. are the major factors contributing to water pollution. The common contaminants of water

pollution are organic, inorganic, biological pollutants, metals, debris, dyes, oil and grease, sewage, trash, micro-organisms, etc. Wastewater treatment plants with domestic effluents and industrial effluents from various industries such as chemicals, petrochemicals and refining, pharmaceuticals, pulp and paper, distillery, textile, and food processing are the major sources of water pollution (Owa 2014).

Emerging pollutants include a wide range of chemicals and microbial pollutants that enter the water bodies from major sources such as industrial effluents, wastewater treatment plants, and agricultural runoff. They are also referred to as emerging contaminants (ECs) or contaminants of emerging concern. ECs are mainly grouped into pesticides, pharmaceuticals, personal care products, and industrial & household chemicals (Sagasta et al. 2018). These ECs interfere with the metabolism and hormone biosynthesis in humans and animals and are hence regarded as endocrine-disrupting compounds (EDCs) (Diamanti-Kandarakis et al. 2009).

In particular, pharmaceuticals detected in the water bodies are of emerging concern as they affect human health and the environment (Sagasta et al. 2018). Pharmaceuticals include analgesics, antipyretics, antibiotics, and antihistamines. The presence of antibiotic residues in the water bodies with their concentrations exceeding the predicted no-effect concentration (PNEC) (in the range of  $\mu\text{g/L}$ – $\text{ng/L}$ ) postulated for prevention of resistance development leads to the potential development of antimicrobial resistance (AMR), and thus the emergence of superbugs (antibiotic-resistant bacteria). Hence, antibiotics are considered as emerging contaminants (Herman 2014).

### **1.3. MECHANISMS OF AMR AND CLASSIFICATION OF ANTIBIOTICS**

The main mechanisms of bacterial resistance to antimicrobial agents (antibiotics) (Cesur and Demiröz 2013; Dever and Dermondy 1991; Munita and Arias 1982) are given below and depicted in **Figure 1.1**.

➤ Genetic basis of AMR

- Mutational resistance - decreased affinity for the antibiotic, decreased uptake of antibiotic, activation of efflux pump (to release the harmful molecule), and changes in the metabolic pathways

- Horizontal gene transfer - conjugation: transfer of resistance genes occurs between microbes when they come in contact with each other, transformation: microbe picks up the resistance genes released from the live or dead organism, and transduction: transfer of resistance genes occurs from one microbe to another via phages
- Mechanistic basis of AMR
- Modifications of antibiotics
    - ❖ Chemical alterations - biochemical reactions: acetylation, phosphorylation, adenylation
    - ❖ Destruction of antibiotics
  - Decreased penetration of antibiotics and efflux
    - ❖ Decreased uptake of antibiotics
    - ❖ Efflux pumps
  - Modifications in target sites
    - ❖ Protection of target (avoiding the antibiotic in reaching the target site, decreased affinity for the antibiotic)
    - ❖ Mutations (changes in DNA and RNA) and enzymatic alteration (production of alternative enzymes)
    - ❖ Replacement of target site or bypass– biochemical functions of susceptible bacteria are altered by the resistant bacteria. Bypass of metabolic pathway by overproducing the antibiotic target

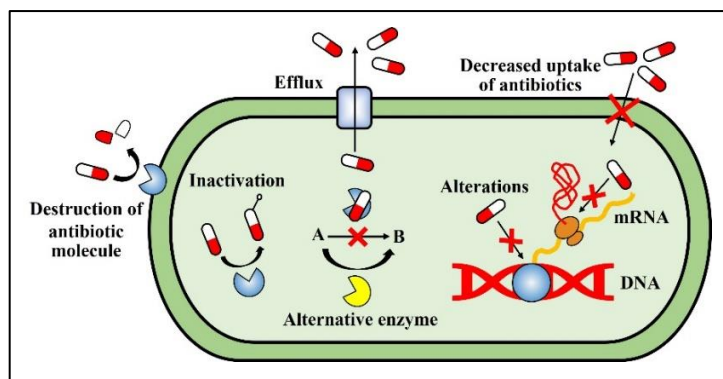


**Figure 1.1.** Mechanisms of bacterial resistance to antibiotics (Adapted from Wistrand-Yuen et al. 2018)

**Table 1.1** summarizes the classification of antibiotics according to their structure and corresponding mechanisms of AMR (Bayan et al. 2021; Cesur and Demiröz 2013; Dever and Dermondy 1991). The antibiotics structure is complex, reactive, and stable in the environment. The structural groups of antibiotic molecules determine the kinetics of degradation activity on the catalyst surface. Hence, the mechanism of AMR in each class of antibiotics varies depending on their chemical structure.

**Table 1.1.** Classification of antibiotics based on chemical structure

CHEMICAL STRUCTURE	CLASS OF ANTIBIOTICS	EXAMPLES	MECHANISM OF RESISTANCE
Containing $\beta$ -lactam ring	Penicillin	Penicillin, ampicillin, benzylpenicillin, oxacillin, amoxicillin	Enzymatic inactivation and modification, alteration of protein penicillin-binding proteins
	Cephalosporins	Cefazolin, cephalixin, cefotaxime, ceftriaxone	
	Carbapenems	Meropenem, imipenem	Enzymatic inactivation
	Monobactams	Aztreonam	
Containing amino sugars	Aminoglycosides	Streptomycin, gentamicin, kanamycin, neomycin	Enzymatic modification, ribosomal alteration, and decreased uptake of antibiotic
Containing four condensed six-membered cycles	Tetracyclines	Tetracycline, oxytetracycline, metacycline	Active efflux
Containing phenylpropanoid structure	Amphenicols	Chloramphenicol, thiamphenicol	Enzymatic inactivation
Containing a macrocyclic lactone ring	Macrolides	Erythromycin, Azithromycin, clarithromycin	Enzymatic modification
Consist of glycosylated cyclic or polycyclic non-ribosomal peptides	Glycopeptides	Vancomycin	Enzymatic modification
Derives 4-aminobenzenesulfonic acid	Sulfonamides	Sulfadimethoxine, sulfadiazine	Using an alternative metabolic pathway
Nitrogen-containing heterocycles	Quinolones	Ciprofloxacin, moxifloxacin, ofloxacin	Decreased drug permeability, alteration of subunit A of DNA gyrase

## 1.4. ANTIBIOTIC POLLUTION

### 1.4.1. Sources

Even though AMR is a naturally occurring phenomenon, the excessive/increasing use of antibiotics has led to the evolution of superbugs. The anthropogenic sources of these antibiotic residues are partially or untreated effluent from hospitals, pharmaceutical manufacturing industries, wastewater treatment plants, and domestic sewage (excretion from the human body). In livestock, the excess antibiotics usage (through excretion) reaches the water bodies (**Figure 1.2**) (Gani and Kazmi 2017; Hirsch et al. 1998).

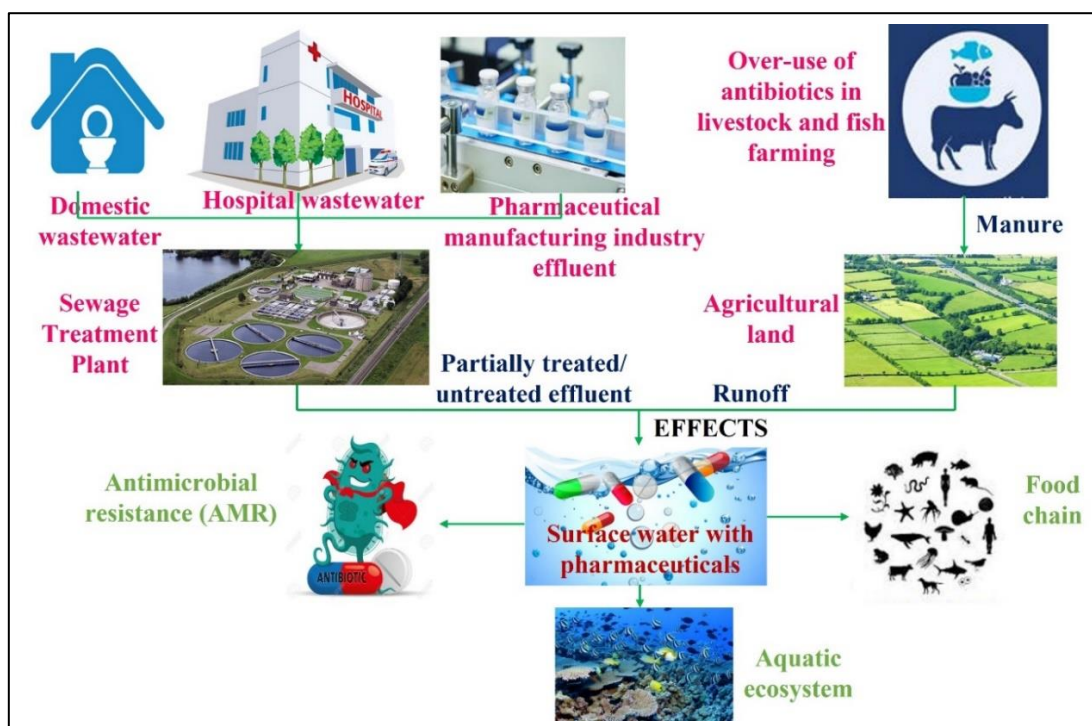


**Figure 1.2.** Antibiotic residues: Sources and effects

### 1.4.2. Global Status

Pharmaceuticals have been widely reported in rivers (drinking water source), groundwater, industrial effluents and wastewater treatment plants, raising concerns on human health and the environment. It has been reported in India, Ghana, China, Korea, Israel and USA in the order of mg/L (at very high concentrations) (Gaonkar 2022; Larsson 2014; Segura et al. 2015). In China, antibiotic residues were detected in

major rivers, residential tap waters, in the concentration range of 0.1 to 1000 ng/L (Anh et al. 2021). In the African rivers, trimethoprim, ciprofloxacin, sulfamethoxazole and erythromycin have been reported (Singh et al. 2019). The rivers in Italy and France were detected with 22 pharmaceutical compounds at concentrations greater than 100 ng/L (Al Aukidy et al. 2012). In US, 27 antibiotics have been reported to be present in the surface waters (Deo 2014). Studies on presence of antibiotics reported globally are tabulated in **Table 1.2**.

**Table 1.2.** Studies reported on the occurrence of antibiotic in the environment across the globe

COUNTRY	RIVERS/ EFFLUENT	DETECTED CONCENTRATION LEVELS OF ANTIBIOTICS	REFERENCE
China	Effluent, Surface water	Oxytetracycline – 19.5 mg/L, 712 µg/L Penicillin G and its metabolites – 44 mg/L, 11.6 mg/L Sulfamethoxazole – 1.34 mg/L Ibuprofen – 1.5 mg/L	(Li et al. 2008a; b; Lin and Tsai 2009)
India	Effluent, Surface water, Ground water	Ciprofloxacin: Effluent: 14-31 mg/L Groundwater: 770 ng/L Surface water: 6.5 mg/L River sediment: 914 mg/kg organic material Soil: 7.2 µg/g organic matter  Cetirizine: Groundwater: 28 µg/L	(Archana et al. 2016; Fick et al. 2009; Kristiansson et al. 2011; Mutiyar and Mittal 2014; Rutgersson et al. 2014)
Ghana	Rivers	12 antibiotics, and among them Sulfamethoxazole (2861 ng/L) was found to be present in highest concentration	(Azanu et al. 2018)
Italy	River Po	Ciprofloxacin, ofloxacin, lincomycin and vancomycin: 5-10 ng/L	(Zuccato et al. 2010)
USA	Hudson river, estuarine waters of Puget Sound	Sulfamethoxazole and trimethoprim, 16 antibiotics in three local estuaries	(Cantwell et al. 2018; Meador et al. 2016)
Korea	Yeongsan river	Sulfamethoxazole (113.2 ng/L) and Clarithromycin (42.7 ng/L)	(Na et al. 2019)
Israel	Effluent	Venlafaxine (11.7 mg/L)	(Larsson 2014; Lester et al. 2013)

### 1.4.3. Indian Scenario

The commonly reported classes of antibiotics in Indian rivers are fluoroquinolones, cephalosporins, and carbapenems (Balakrishna et al. 2017). The wells around the

Patencheru Effluent Treatment Plant (PETL) near Hyderabad, which received effluents from 90 drug manufacturing units of Hyderabad, were detected with ciprofloxacin, enoxacin, ofloxacin, trimethoprim, norfloxacin (Larsson et al. 2007) and their concentration range are given below in **Table 1.3**. Beta-lactam antibiotics produce degradable residues that are less detectable but contribute to resistance (Lundborg and Tamhankar 2017). Among various class of antibiotics, fluoroquinolones especially ciprofloxacin were reported at higher concentrations in rivers and wastewater treatment plants of India (Fick et al. 2009; Mutiyar and Mittal 2014; Sharma et al. 2019). The most common resistance mechanism reported for quinolone class of antibiotics are alteration of target enzyme/membrane permeability (Aoyama et al. 1987; Hirai et al. 1987; Inoue et al. 1978; Legakis et al. 1989; Sato et al. 1986), decreased penetration of drugs due to minimal expression of OmpF (an integral membrane protein in the outer membrane of *Escherichia coli* (*E.coli*)) (Hooper et al. 1986, 1989; Yamamoto et al. 1986).

**Table 1.3.** Most commonly reported antibiotics concentration in rivers and wastewater treatment plants (WTPs)/sewage treatment plants (STPs) in India

ANTIBIOTIC	RIVERS/ WTPs/ETPs	DETECTED CONCENTRATION LEVELS	PNEC (resistance selection) (Bengtsson-Palme and Larsson 2016)	REFERENCE
Ciprofloxacin	PETL, Hyderabad	28000 – 31000 µg/L	0.064 µg/L	(Larsson et al. 2007)
Norfloxacin	PETL, Isakavagu and Nakkavagu Rivers, Hyderabad	390–420 µg/L	0.5 µg/L	(Fick et al. 2009; Larsson et al. 2007)
Ofloxacin	PETL, Isakavagu and Nakkavagu Rivers, Hyderabad	150 –160 µg/L	0.5 µg/L	
Ampicillin	WTP, India	21 µg/L	0.25 µg/L	(Mutiyar and Mittal 2014)
Clarithromycin	Rivers and WTPs, South Africa	0.30 µg/L	0.25 µg/L	(Faleye et al. 2018)
Tetracyclines and oxytetracycline	Aquaculture water, Thailand	180 ng/L	1 µg/L and 0.5 µg/L	(Shimizu et al. 2013)



ANTIBIOTIC	RIVERS/ WTPs/ETPs	DETECTED CONCENTRATION LEVELS	PNEC (resistance selection) (Bengtsson-Palme and Larsson 2016)	REFERENCE
Enrofloxacin	PETL, Hyderabad	780–900 µg/L	0.064 µg/L	(Larsson et al. 2007)
Sulfamethoxazole	WTPs, India	3–2260 ng/L	16 µg/L	(Balakrishna et al. 2017)
Erythromycin	WTPs, India	12 ng/L	1 µg/L	
Levofloxacin	WTPs, India	86700–107900 ng/L	0.25 µg/L	
Clindamycin	WTPs, India	5.16 –210 ng/L	1 µg/L	
Lincomycin	WTPs, India	15.2–730 ng/L	2 µg/L	
Cefuroxime	WTPs, India	0–212 ng/L	0.5 µg/L	
Trimethoprim	WTPs, India	3–4010 ng/L	0.5 µg/L	

#### 1.4.4. Initiatives to minimize or control antibiotic pollution

In 2005, WHO has developed a global action plan on prevention and management of AMR. However, there is no defined criteria for treated effluents from antibiotic manufacturing industries in the fight against AMR. In 2016, National Plan against Micropollutants (2016-2021) was launched, which focussed on pharmaceutical residues in water - hazards and exposure, identification of metabolites, and assessment of analytical capacities with regard to the development of an early monitoring system. In 2018, nearly 100 companies/industries signed a declaration on AMR, which focused on reducing the development of AMR and the environmental impact of manufacturing. Further, in 2018 (revised in 2021), these companies published the first list of discharge targets based on Predicted No-Effect Concentrations (PNEC) for the most common antibiotics used globally to guide environmental risk assessments for the manufacture of antibiotics. Recently, Sweden has approved greater environmental considerations in international and EU pharmaceutical legislation (2020) – various specific measures were considered to reduce the pharmaceutical impact on the environment (Gaonkar 2022).

#### **1.4.5. Adverse impacts on human health and the environment**

The potential effects owing to the presence of antibiotic residues in trace quantities (**Figure 1.2**) (Balakrishna et al. 2017; Giannakis et al. 2017; Gothwal and Shashidhar 2015; Kalyva 2017; Kümmerer 2009; Sagasta et al. 2018) are as follows:

- Crops irrigated with contaminated water and manure of livestock – lead to bioaccumulation in the food chain, as there is excessive use of antibiotics in the livestock, and finally, it reaches the humans in the food chain.
- The transfer of pathogenic (antibiotic-resistant) genes into healthy microbes promotes an increase in superbugs – transfer of genes occurs through horizontal gene transfer mechanisms of conjugation, transformation, and transduction.
- The aquatic ecosystem is imbalanced due to hindrance of the light penetration – imbalance is due to a disturbance in the photosynthetic activity and the metabolism of aquatic plants and animals respectively.
- Antibiotic residues, through adsorption onto the soil or sediments (through water contaminated with effluents or animal manure reaching the soil used for growing crops), undergo biological or photochemical transformations.

#### **1.5. ARTICLES/CASE STUDIES REPORTED ON THE PRESENCE OF ANTIBIOTIC RESIDUES AND SUPERBUGS IN THE ENVIRONMENT**

Various water bodies (especially in rivers throughout the world) have been detected with the residual antibiotics and their concentrations exceeding the acceptable threshold limit and, consequently, the development of antimicrobial resistance (AMR) (Bardsley 2019). The resistance development by *Helicobacter pylori* (commonly found in the digestive tract of humans) to levofloxacin, metronidazole, and clarithromycin antibiotics is a cause for serious concern (Mendonsa 2019). Another article has highlighted the assessment of the river Ganga with the presence of bacterial isolates of *Escherichia*, *Enterobacter*, *Salmonella*, *Shigella*, and *Vibrio*; and bacteriophages in higher proportion (Koshy 2019a). Antibiotic resistance rates in India are significantly higher when compared to other countries. (Koshy 2019b) River Netravathi and Swarna have been detected with the

presence of personal care products and pharmaceuticals (Sanjeev 2020). A recent study conducted by IIT Madras, has reported the presence of pharmaceutical contaminants such as ibuprofen and diclofenac (anti-inflammatories), atenolol and isoprenaline (anti-hypertensives), perindopril (enzyme inhibitor), caffeine (stimulants), carbamazepine (antidepressant), and ciprofloxacin (antibiotic) in the river Cauvery (Renganathan et al. 2021).

By 2050, antibiotic resistance could be the global most significant cause of death due to their injudicious usage, with an estimated 10 million deaths annually. Asia alone may witness around 5 million deaths (Thomas 2020). Because of these reasons, it is necessary to treat the antibiotic residues and minimize the antimicrobial resistance problem even though it is not quantified yet.

#### **1.6. TREATMENT TECHNOLOGIES AVAILABLE FOR PHARMACEUTICAL WASTEWATER TREATMENT**

Physio-chemical and biological methods are available for the pharmaceutical treatment of wastewater. The conventional physical methods are filtration, flocculation, reverse osmosis, sedimentation, and adsorption. Precipitation, ion exchange, reduction, neutralization, and calcination are chemical methods. Thermal methods include pyrolysis and incineration. Anaerobic digestion, activated sludge, trickling filters, and aerated lagoons are the biological methods (Ahmed et al. 2015; Homem and Santos 2011; Onesios et al. 2009; Patel et al. 2019). In the physical methods, pharmaceuticals merely shift from aqueous to solid phase. Whereas in the chemical and biological methods, new metabolites or degradation products are formed from the chemical reaction of pharmaceuticals (Joss et al. 2005; Sirés and Brillas 2012).

#### **1.7. DISADVANTAGES OF CONVENTIONAL PHARMACEUTICAL WASTEWATER TREATMENT METHODS**

The conventional treatment methods have the disadvantages of clogging of membranes, carbon regeneration, limitation of size exclusion range, disposal problems (physio-chemical treatment); biomass accumulation, slow process and

requirement of long startup periods (biological treatment) (Deegan et al. 2011; Guo et al. 2017b; Li and Yang 2018; Patel et al. 2019). These primary and secondary wastewater treatment methods are inefficient in the removal of low biodegradable pharmaceuticals/antibiotic residues, thus leading to contamination of receiving water bodies with these emerging contaminants. Hence, an efficient alternative treatment method is necessary. In this regard, advanced oxidation processes (AOPs) can remove antibiotic residues effectively from water and wastewater. Photocatalysis, a promising AOP, can degrade emerging pollutants and inactivate micro-organisms, thus reducing the above problem of AMR through an efficient visible-light active photocatalyst (Nagar and Pradeep 2020; Patel et al. 2019).

## **1.8. ADVANCED OXIDATION PROCESSES (AOPs)**

The different types of AOPs available for wastewater treatment are non-photochemical processes (Fenton, ozonation, sonolysis, electrochemical); photochemical processes (photo-Fenton, UV oxidation, photocatalysis); hybrid processes (photoelectrocatalysis, sono-photolysis, photocatalytic ozonation, sono-biphotocatalysis) (Kanakaraju et al. 2018).

## **1.9. PHOTOCATALYSIS**

Photocatalysis is the “change in the rate of a chemical reaction or its initiation under the action of ultraviolet, visible radiation in the presence of a substance—the photocatalyst—that absorbs light and is involved in the chemical transformation of the reaction partners”. A photocatalyst is a “catalyst able to produce, upon absorption of light, chemical transformations of the reaction partners. The excited state of the photocatalyst repeatedly interacts with the reaction partners forming reaction intermediates and regenerates itself after each cycle of such interactions” (McNaught and Wilkinson 1997).

Photocatalysis, a promising advanced oxidation process (AOPs), has the capability of degrading the recalcitrant compounds to less harmful products through the generation of powerful hydroxyl radicals due to its strong oxidizing ability ( $E^\circ = +2.80 \text{ V}$ ), which is placed next to fluorine ( $E^\circ = +3.03 \text{ V}$ ) (Kanakaraju et al. 2014,

2018). Heterogeneous and homogeneous are the two categories of photocatalytic processes based on differences in phases of reactant and catalyst. In heterogeneous photocatalysis, reactant and pollutant exist in two different phases (solid-liquid, solid-gas), whereas in homogeneous photocatalysis, both the reactant and pollutant exist in the same phase (usually liquid phase) (Byrne et al. 2015).

### 1.9.1. Different forms of the photocatalyst

#### 1.9.1.1. Suspended form

It is the most widely used form (**Figure 1.3**). It provides a high photocatalyst surface area to volume ratio. The main disadvantages are low irradiation utilization due to the opacity of slurry, loss of catalyst, and recovery/reuse of the photocatalyst post-treatment is expensive (solid/liquid phase separation) (Srikanth et al. 2017; Xing et al. 2018b).

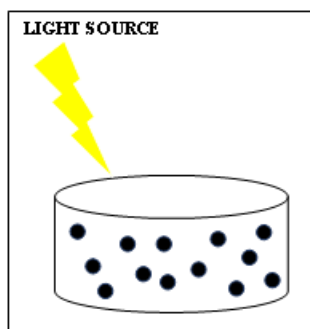


**Figure 1.3.** Suspended form of the photocatalyst

#### 1.9.1.2. Immobilized/floating form

This helps in achieving the feasibility of the catalysts for large-scale purposes through the reuse of photocatalysts, thus reducing the operational costs and preventing the loss of photocatalysts. It also provides for constant operation of the reactor. The disadvantage is the lesser accessibility of catalysts to photons.

The most commonly used supports are glass beads, cork, perlite, polymers, zeolites, vermiculate, clay, and ceramics (**Figure 1.4**). The widely used methods for immobilization are sol-gel and sputtering. Apart from these, there are other methods

such as dip coating, chemical vapour deposition, thermal treatment, electrophoretic deposition, and sol-spray (Srikanth et al. 2017; Xing et al. 2018b).

In view of the above-mentioned water pollution problems, application of the immobilized/floating forms of photocatalyst due to less catalyst loss and lower operational cost plays a significant role in the photocatalytic degradation of organic contaminants in real water samples.

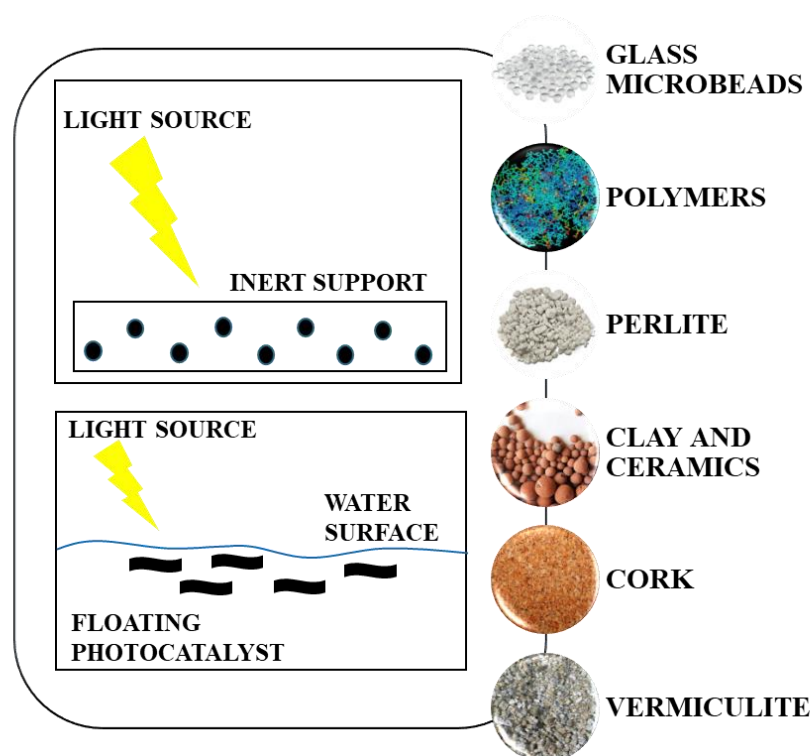


**Figure 1.4.** Immobilized/floating form of the photocatalyst and common supports used for immobilization

## 1.10. GENERAL MECHANISM OF PHOTOCATALYSIS

When a light energy (equivalent to or higher than the band gap of semiconductor) is irradiated upon a semiconductor, electrons ( $e^-$ ) get excited from the valence band (VB) to the conduction band (CB), leaving behind free holes ( $h^+$ ) in the VB (Eq. 1.1). Reduction reaction occurs between these excited electrons and electron acceptors adsorbed by the surface thus producing superoxide radicals ( $O_2^{\cdot-}$ ) (Eq. 1.2). The holes are directly oxidized or react with surface hydroxyl groups to produce hydroxyl radicals ( $OH^{\cdot}$ ), a powerful oxidizing agent (Eq. 1.3). These generated reactive oxygen

species (ROS:  $e^-$ ,  $h^+$ ,  $O_2^{\cdot-}$ ,  $OH^{\cdot}$ ) degrade pollutants to less harmful products such as carbon dioxide and water (Eq. 1.4). If these oxygen reduction and pollutant oxidation reactions do not occur simultaneously, there is accumulation of  $e^-$  in the CB, thereby causing an increase in the rate of recombination of electron-hole pairs. Thus, the prevention of electron accumulation is necessary for effective photocatalysis. These redox reactions constitute the fundamental mechanism of photocatalysis (**Figure 1.5**).

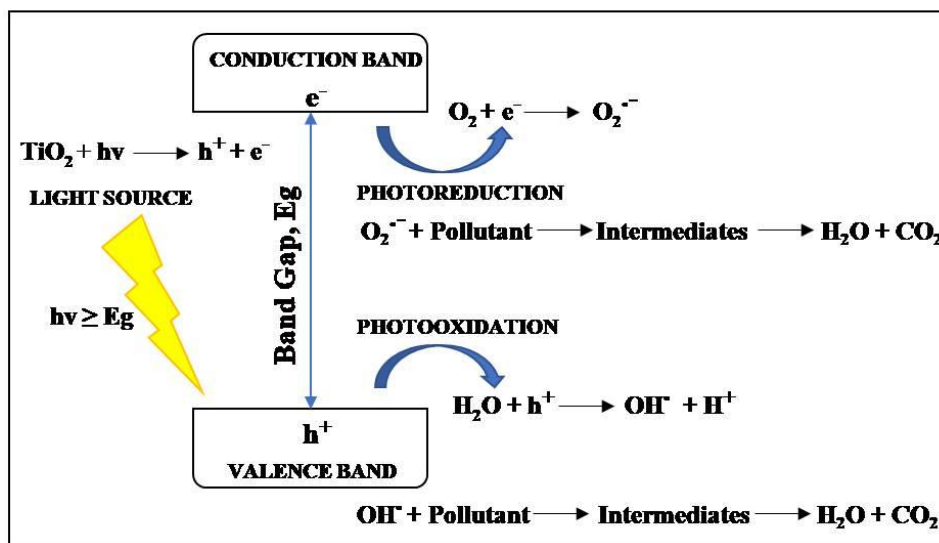
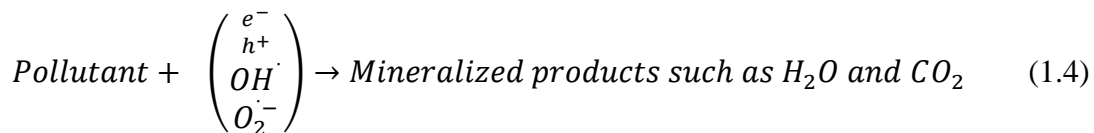


**Figure 1.5.** Mechanism of photocatalytic degradation of organic pollutants (Adapted from Pawar et al. 2018)

Regarding disinfection, most of the researchers have reported that the reactive oxygen species produced due to oxidative stress or oxidation & reduction reactions, damage the cell membrane permeability and other cell components like nucleic acids (DNA/RNA), lipids and proteins (which constitute to about 96% of cell's dry weight).

The membrane damage leads to leakage of potassium ions from the cell and finally leads to cell death (**Figure 1.6**).

Other possible mechanisms include the electromagnetic attraction between the organism and the photocatalyst surface (as the micro-organism possess a negative charge and metal oxide photocatalyst possess a positive charge). Also, the uneven and rough texture of the photocatalysts causes mechanical damage to the cell membrane (Arumugam et al. 2015; Arun et al. 2019; Ferro et al. 2015; Yan et al. 2020).

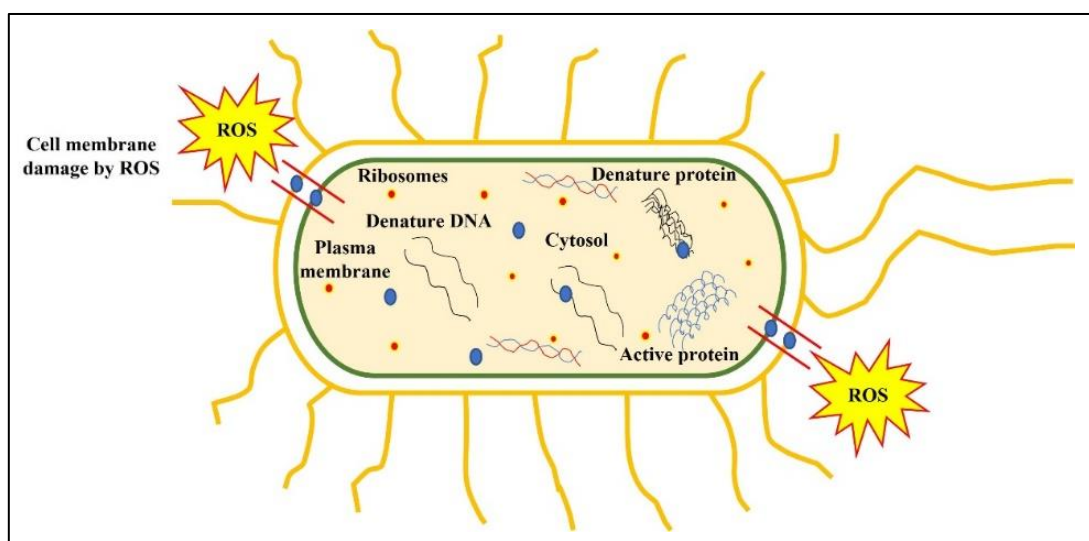


**Figure 1.6.** Mechanism of photocatalytic disinfection (Adapted from Arumugam et al. 2015)

This study uses a facile green EDTA-citrate method to synthesize a systematic series of monodoped and codoped photocatalysts (using B and Ce as dopants). The synthesized catalysts were investigated for antibiotic degradation and bacterial disinfection under sunlight both in suspended and immobilized forms. Reaction parameters such as catalyst loading, initial concentration of antibiotic, and pH were varied. The degraded antibiotic sample was evaluated for residual antibacterial activity and mineralization (COD/TOC reduction). The possible degradation pathways were elucidated using the m/z values of degraded products identified from LCMS analysis. The stability of catalysts and the immobilized film after reuse was evaluated. The real water matrices (tap water and river water) were employed to evaluate the effectiveness of these catalysts for real-world application on a large-scale basis.



## CHAPTER 2

### LITERATURE REVIEW

#### 2.1. HISTORICAL DEVELOPMENT OF PHOTOCATALYSTS

Since 1960, photocatalysis has been an environmentally friendly technology for water pollution purification due to the self-cleaning and self-sterilizing properties of the photocatalyst. It began with a photoelectrochemical process – discovery of hydrogen evolution from water by Fujishima and Honda using a  $\text{TiO}_2$  electrode; environmental photocatalysis – a series of sulfides, metal oxides, and composite metal oxide were developed to treat various organic pollutants such as dyes, heavy metals, pesticides, and industrial wastewater; and a commercialized  $\text{TiO}_2$ -based photocatalytic process using Degussa P25  $\text{TiO}_2$ . New materials based on titania have been developed in recent years, and visible/solar light sensitivity has improved (**Figure 2.1**).  $\text{TiO}_2$  photocatalysis has been one of the promising treatment methods in the elimination of recalcitrant organic pollutants from the environment. The strong oxidation potential of the reactive radicals generated during the photocatalytic process makes them suitable for removing/eliminating organic pollutants (Fujishima et al. 2008; Fujishima and Honda 1972; Fujishima and Zhang 2006; Long et al. 2020).

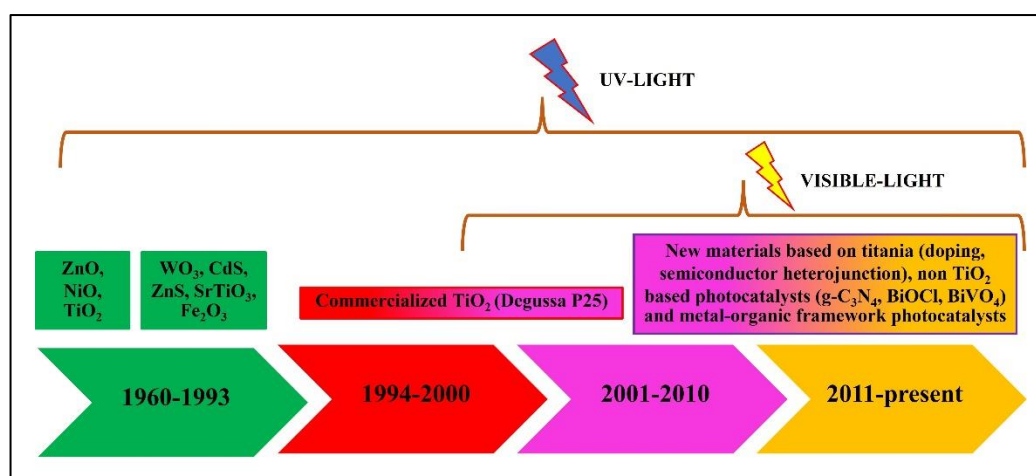


**Figure 2.1.** Historical development of photocatalysts to remove organic pollutants from the environment (Adapted from Long et al. 2020)

## **2.2. TITANIUM DIOXIDE (TiO<sub>2</sub>)**

TiO<sub>2</sub> is the most extensively used photocatalyst as it is a good semiconductor, easily available, non-toxic, chemically, and mechanically stable. Various applications include as self-cleaning glass and self-cleaning ceramics due to antifogging properties, antibacterial material by sterilizing areas of micro-organisms, air purification by neutralizing toxic gases, sewage treatment, and wastewater purification by degrading pollutants into CO<sub>2</sub> and water (Fujishima and Zhang 2006). TiO<sub>2</sub> with a bandgap of 3.0-3.2 eV can work effectively only under UV light (100-400 nm) which accounts for only about 5% of the electromagnetic spectrum (Riaz et al. 2015). Hence, there is a need for visible light active catalysts.

TiO<sub>2</sub> exists in three phases – anatase, rutile, and brookite. Among these phases, brookite is rarely used for photocatalysis. Anatase is preferred/active than rutile phase as the anatase phase prolongs the lifetime of charge carriers and reduces the recombination reactions. The higher photocatalytic activity is also attributed to the position of conduction band (-4.05 eV, more negative than rutile) which results in higher reduction of adsorbed pollutants (Fujisawa et al. 2017).

## **2.3. FACTORS AFFECTING THE PHOTOCATALYTIC PROCESS**

Several reaction parameters are responsible for an efficient photocatalytic system to degrade the organic pollutants into less harmful products. The significance of reaction parameters is discussed below.

### **2.3.1. Effect of catalyst loading**

An optimum catalyst loading is essential for achieving effective degradation to avoid excess catalyst use and to ensure effective absorption of photons. With an increase in the catalyst loading beyond the optimal value, the degradation efficiency decreases as less number of photons penetrate (shielding effect) the solution due to an increase in the turbidity of the solution (Das et al. 2018; Kumar et al. 2016).

### **2.3.2. Effect of initial concentration of pollutant**

An increase in the pollutant concentration causes a decrease in the degradation efficiency as excessive number of pollutant molecules compete for the catalyst's active site, resulting in the requirement of more number radicals and prolonged reaction time for complete degradation of pollutant. Also, the radicals generated remain constant for a particular irradiation time, the intensity of light, and catalyst amount (Das et al. 2018; Seddigi et al. 2017; Wen et al. 2018).

### **2.3.3. Effect of pH**

At alkaline pH conditions, the TiO<sub>2</sub> surface is negatively charged and positively charged at acidic pH conditions. As noted from the literature (Das et al. 2018; Van Doorslaer et al. 2011; Guo et al. 2017a; Shah et al. 2018b), the optimum pH for the degradation of antibiotics is in the range of 7.0-9.0. In view of real water sample applications, the pH of Indian rivers and lakes lies in the range of 6.5-8.5 (BIS – IS: 10500 – 2012 Standards for drinking water). Also, the effluent with antibiotic residues from the sources mentioned earlier (section 1.4.1) has a pH in the range of 6.7-7.7 (effluent discharge standards for industries and hospitals) (Das et al. 2018; Gupta et al. 2017).

### **2.3.4. Effect of size and surface area of photocatalyst**

A catalyst with a higher surface area and a smaller particle size provides a better contact between pollutant and catalyst, which promotes efficient photocatalytic activity (Kumar and Pandey 2017). Also, the shorter migration distance (from the point of generation to the surface of charge carriers) in particles with smaller sizes promotes higher photocatalytic activity (Seddigi et al. 2017).

### **2.3.5. Effect of irradiation time and light intensity**

Different light sources emit different intensities or energy of light. At lower light intensity, lesser generation of electron-hole pairs, and the rate of degradation of pollutants is directly proportional to the light intensity. However, at a higher light intensity, the degradation rate is independent of the light intensity as electron-hole

pairs recombination is predominant (separation of electron-hole pairs competes with the recombination process) (Kumar and Pandey 2017).

The degradation efficiency (photodegradation) of organic pollutants increases with an increase in time of irradiation. The reaction rate decreases with time of irradiation as it follows pseudo-first-order kinetics typically as competition between pollutant and intermediate products exist during the photocatalytic process. In addition, the reaction rate decreases due to the deposition of intermediate products on active sites of the catalysts leading to their inactivation or reducing the lifetime of the catalyst (Kumar and Pandey 2017). Other reasons for the slow rate of reaction are: short-chain aliphatics of a pollutant have difficulty in reacting with  $\cdot\text{OH}$  radicals and N-, S-atoms of the pollutant do not participate directly in the oxidation of compounds (Konstantinou and Albanis 2004).

### **2.3.6. Effect of temperature**

In general, the higher reaction temperature promotes photocatalytic activity due to the generation of free radicals quickly. However, it is the electron-hole pair generation (interfacial charge transfer) and better adsorption of pollutant molecules that enhances the photocatalytic activity. Hence, at higher temperatures ( $> 80^\circ\text{C}$ ), degradation efficiency decreases due to recombination of electron-hole pairs and there is an increase in stability of pollutants (disfavoring the adsorption of pollutant molecules) on exposure to heat stress (Das et al. 2018; Kumar and Pandey 2017). There is an increase in the activation energy for temperatures near to  $0^\circ\text{C}$ . Thus, the temperature range between  $20\text{-}80^\circ\text{C}$  is more desirable for effective photocatalytic activity.

### **2.3.7. Effect of inorganic ions and water matrix**

In natural water and wastewater, the degradation efficiency of a pollutant decreases due to the presence of anions such as sulphate, phosphate, chloride, bicarbonate, and dissolved organic matter (humic acids and nitrates), which act as scavengers of  $\cdot\text{OH}$  radicals. The presence of such inorganic ions and organic matter might hinder the adsorption of pollutants onto the catalyst surface by competing for available catalyst

active sites (García-Fernández et al. 2015; Giraldo-Aguirre et al. 2015; Jojoa-Sierra et al. 2017; Kumar and Pandey 2017; Yoon et al. 2017).

#### **2.3.8. Effect of dopants**

Doping enhances photocatalytic activity through narrowing of bandgap, formation of new energy levels, and oxygen vacancies. Nowadays, codoping with metals and non-metals has attracted much attention due to the change in the optical, crystal and morphological characteristics of TiO<sub>2</sub> which promotes the photocatalytic activity in the visible-light range. (Gnanaprakasam et al. 2015; Huang et al. 2016a; Khairy and Zakaria 2014; Kumar and Pandey 2017; Marschall and Wang 2014; Tan et al. 2011; Vieira et al. 2018; Wang et al. 2016c; Zaleska 2008).

#### **2.3.9. Effect of bandgap**

In an insulator or semiconductor, bandgap energy is the minimum energy required for electrons to move from the valence band to the conduction band. In TiO<sub>2</sub>, the mixture of anatase and rutile phase (better crystallinity) has narrowed the bandgap by reducing the defects which acts as electron-hole traps. Codoping with metals and non-metals, on the other hand, causes a shift in the absorption edge towards the visible light range, thus narrowing the bandgap and promotes separation of photogenerated electron-hole pairs through the formation of new energy levels/impurity bands (Samsudin and Hamid 2017; Xu et al. 2015).

#### **2.3.10. Effect of immobilization on/into suitable support**

Slurry/suspended form of photocatalyst has a large surface area (larger the surface area - higher is the photocatalytic activity) when compared to the immobilized form of the same photocatalyst. The immobilized form helps in reuse of the catalyst and reduces the operational cost in large-scale applications (Gnanaprakasam et al. 2015; Srikanth et al. 2017; Xing et al. 2018a; b).

### **2.3.11. Effect of crystallinity**

Higher crystallinity reduces the formation of electron traps which results in fewer recombination centers of photogenerated charge carriers (lack of defects that promotes the recombination) and thus improves the photocatalytic activity (Fischer et al. 2017; Tian et al. 2009; Xu et al. 2015).

## **2.4. VISIBLE-LIGHT ACTIVE CATALYSTS**

Nowadays, the focus on visible light-active catalysts has been increasing due to their effective degradation ability of pollutants and enhancement in the utilization of broad spectrum of sunlight (a renewable form of energy) (Huang et al. 2016). Various strategies employed for bandgap engineering of the TiO<sub>2</sub> (visible light utilization) are metal and non-metal doping, compositing with metal oxides, formation of surface heterojunctions, and plasmonic metallic particle decoration (Li et al. 2018; Marschall and Wang 2014; Samsudin and Hamid 2017).

### **2.4.1. Doping**

Metal, non-metal, and codoping (metal/non-metal) are the various doping methods (Huang et al. 2016). In particular, doping with metals/non-metals has received much attention as they induce physiochemical modifications in the catalyst (Akpan and Hameed 2010; Basavarajappa et al. 2020; Jaiswal et al. 2012, 2016; Marschall and Wang 2014; Shi et al. 2019). Physical modifications result in smaller crystallite size, higher anatase phase content/crystallinity, and larger surface area (Maarisetty and Baral 2019; Tan et al. 2011). The effect of chemical modifications includes the promotion of adsorption ability (dopants can act as active sites for adsorption of pollutants) and the creation of new energy levels (impurity bands) for effective photogenerated charge separation with reduced recombination (Jaiswal et al. 2016; Tan et al. 2011; Vieira et al. 2018; Wang et al. 2016b). In general, metal dopants facilitate better adsorption of pollutants through surface modifications and effective separation of photogenerated charges. Contrarily, non-metal dopants cause a shift in the absorption edge towards visible light and thus bandgap narrowing of TiO<sub>2</sub> (**Figure 2.2**) (Tan et al. 2011).

Metal dopants include transition metals, rare earth metals, and other metals. The most commonly used transition metals are iron, tungsten, copper, cobalt, molybdenum, zinc, manganese, nickel, vanadium, and chromium, which have unfilled inner d electron shells and exhibit two or more oxidation states. Rare earth metals are cerium, lanthanide, gadolinium, europium, and yttrium. Other metal doping elements are lithium, silicon, germanium, tin, lead, and bismuth. Non-metals such as boron, phosphorous, sulfur, nitrogen, and carbon are used. Chlorine, bromine, and iodine are also used as dopants with bismuth oxyhalides (Huang et al. 2016a). Thus, codoping with metals (Ce, Y, Zn, Fe, V, Ni) and non-metals (B, N, C, S) provides a synergistic effect of the above-mentioned properties and thus enhances the photocatalytic activity.

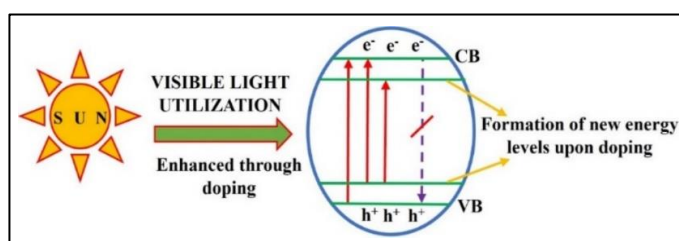


**Figure 2.2.** Enhancement of visible light utilization through doping (Adapted from Huang et al. 2016a)

## 2.5. PHOTOCATALYTIC DEGRADATION OF ANTIBIOTICS USING $\text{TiO}_2$

$\text{TiO}_2$  as a conventional photocatalyst with a bandgap of 3.0-3.2 eV has been reported for the degradation of a variety of pharmaceuticals such as sulfamethoxazole, amoxicillin, tetracycline, diclofenac, ibuprofen, naproxen, ciprofloxacin (Fagan et al. 2016). Using commercial anatase  $\text{TiO}_2$ , degradation of ciprofloxacin (CIP) (GadAllah et al. 2011), and degradation of ciprofloxacin, enrofloxacin, ofloxacin, & norfloxacin (Li et al. 2012) was examined under simulated sunlight. MOX (moxifloxacin) and CIP were studied under UV-A and UV-C (Van Doorslaer et al. 2011). Other antibiotics, such as azithromycin and esomeprazole, were examined for degradation using  $\text{TiO}_2$  under UV light (Pratap et al. 2015). All these studies were performed under UV light which showed lesser degradation efficiency (in the range of 60-82%) when compared to simulated sunlight which showed better degradation efficiency (in the range of 96-100%) and have been summarized in **Table 2.1**. Hence, there is a need for visible light-active photocatalysts through doping.

**Table 2.1.** Degradation of antibiotics using TiO<sub>2</sub>

PHOTOCATALYST	SLURRY FORM/ IMMOBILIZED FORM	LIGHT SOURCE	MODEL POLLUTANT	REFERENCE
TiO <sub>2</sub>	Slurry form	Simulated sunlight	Ciprofloxacin C <sub>0</sub> – 50 mg/L Degradation – 99% (1 g/L) T – 120min Analysis – HPLC	(Gad-Allah et al. 2011)
TiO <sub>2</sub>	Slurry form	UV-A and UV-C	Ciprofloxacin (CIP) C <sub>0</sub> – 45.3 mg/L Morfloxacin (MIP) C <sub>0</sub> – 37.4mg/L Degradation – 78% and 82% (0.5 g/L) T – 15min Analysis – HPLC	(Van Doorslaer et al. 2011)
TiO <sub>2</sub>	Slurry form	Simulated sunlight	Ofloxacin, norfloxacin, ciprofloxacin and enrofloxacin C <sub>0</sub> – 0.028, 0.031, 0.027 and 0.028 mmol L <sup>-1</sup> respectively Degradation – 100%, 99%, 96%, and 100% respectively (0.5 g/L, 82.5 mg/L H <sub>2</sub> O <sub>2</sub> ) T – 150 min Analysis – HPLC, TOC reduction Residual toxicity <i>Bacillus subtilis</i> Inhibition halo method	(Li et al. 2012)
TiO <sub>2</sub>	Slurry form, Sol-gel	UV	Azithromycin and Esomeprazole C <sub>0</sub> – 150 mg/L and 40 mg/L Degradation – 67% and 60% (1 g/L) T – 150 min Analysis – COD reduction	(Pratap et al. 2015)

C<sub>0</sub> – Initial pollutant concentration/bacterial cell concentration, T – Duration



## 2.6. PHOTOCATALYSIS USING B AND Ce AS DOPANTS (DEGRADATION AND DISINFECTION)

Various studies have been reported for degradation and disinfection using B and Ce as dopants. Boron doped TiO<sub>2</sub> (B-TiO<sub>2</sub>) has been studied for degradation of phenol, metoprolol, 4-nitrophenol, p-nitrophenol, methylene blue, rhodamine B, and reduction of NADH (Bettinelli et al. 2007; Bilgin Simsek 2017; Cavalcante et al. 2015; Chen et al. 2006; Grabowska et al. 2009; Jaiswal et al. 2016; Lu et al. 2010; May-Lozano et al. 2014; Patel et al. 2015; Xu et al. 2009; Yadav et al. 2020). Cerium doped TiO<sub>2</sub> (Ce-TiO<sub>2</sub>) for degradation of phenol, chlorophenol, methylene blue, rhodamine B, polyvinylpyrrolidone, and reduction of CO<sub>2</sub> (Amoresi et al. 2019; Ellappan and Miranda 2014; Fan et al. 2006; Fonseca de Lima et al. 2015; Maarisetty and Baral 2019; Maddila et al. 2017; Martin et al. 2015; Matějová et al. 2014, 2017; Mikaeili et al. 2018; Muñoz-Batista et al. 2014; Priyanka et al. 2014; Silva et al. 2009; Tsega and Dejene 2016; Vieira et al. 2018; Yan et al. 2012). B–Ce–TiO<sub>2</sub> has been studied for degradation of Acid Red B dye (Chao-hai et al. 2007), and B–Fe–Ce–TiO<sub>2</sub> for degradation of 2,4-dichlorophenol (DCP) (Ling et al. 2008). B and Ce as one of the codopants have been reported for degradation of various dyes (Alim et al. 2019; Feng et al. 2011, 2013; Han et al. 2018; In et al. 2007; Zhang et al. 2014; Zhang and Liu 2008; Zhao et al. 2015a). A recent study (Stoyanova et al. 2021) using cerium-boron codoped TiO<sub>2</sub> nanoparticles has been reported for degradation of malachite green dye under UV-A light.

As noted from the literature, boron is a well-known disinfectant. B-TiO<sub>2</sub> has been reported for disinfection of *E.coli*, *Staphylococcus aureus* and *Candida albicans* (Wang et al. 2014; Xue et al. 2013) and Ce- TiO<sub>2</sub> for *E.coli* (Ali et al. 2016). B and Ce codoped catalysts have been employed for disinfection of *S. aureus* (Wang et al. 2016b), *E.coli* and *S. aureus* (Wang et al. 2018). Other combinations with boron include boron/yttrium codoped TiO<sub>2</sub> for *S.aureus* and *E. coli* (Wang et al. 2016c), (Ce, Y, or B)-doped Zn-TiO<sub>2</sub> for *E.coli* (Wang et al. 2017b). The above-reported studies have been summarized in **Tables 2.2** and **2.3**.

The enhancement in the photocatalytic activity in the above-reported studies is attributed to higher crystallinity (anatase phase), narrowed bandgap (absorption of visible light), reduced electron-hole recombination, higher adsorption capacity of Ce, and presence of B in the interstitial lattice position through the effective separation of photogenerated charges. The dopant concentration levels in the above-reported studies are quite arbitrary. Also, there is no insight into the basis of the selection of dopant concentrations, which play a major role in achieving higher photocatalytic activity. As noted from the literature (Huang et al. 2008; Sakthivel et al. 2004), above a certain/optimum level of dopant concentration, the photocatalytic activity decreases, which is attributed to the recombination of photogenerated electron-hole pairs, the excess dopants block active sites of TiO<sub>2</sub> and a reduction in the adsorption capacity of pollutant. B and Ce dopants have not been investigated/explored for both degradation of antibiotics and disinfection under sunlight.

**Table 2.2.** Degradation of organic pollutants using monodoped and codoped catalysts with boron/cerium as dopants

<b>PHOTOCATALYST</b>	<b>SLURRY FORM/ IMMOBILIZED FORM, PREPARATION METHOD</b>	<b>LIGHT SOURCE</b>	<b>MODEL POLLUTANT</b>	<b>REFERENCE</b>
B-TiO <sub>2</sub>	Slurry form, Sol-gel	Visible light (250 W high pressure mercury lamp)	Photoregeneration of reduced nicotinamide adenine dinucleotide (NADH)	(Chen et al. 2006)
Ce-TiO <sub>2</sub>	Slurry form, Sol-gel	UV-A	Phenol	(Fan et al. 2006)
B-TiO <sub>2</sub>	Slurry form, Grinding anatase	UV and visible (1000 W Xenon lamp)	Phenol	(Grabowska et al. 2009)
Ce-TiO <sub>2</sub>	Slurry form, Solvothermolysis	Visible light (medium pressure mercury lamp)	Chlorophenol	(Silva et al. 2009)
B-TiO <sub>2</sub>	Slurry form, Hydrothermal	Artificial sunlight (250 W halogen lamp)	Reactive red-2 and 4-chlorophenol	(Xu et al. 2009)
B-TiO <sub>2</sub>	Immobilized form, Hydrothermal dip coating onto a glass slide	UV and visible	Rhodamine B	(Lu et al. 2010)
Ce-TiO <sub>2</sub>	Slurry form, Sol-gel	30 W fluorescent lamp	Methylene blue	(Yan et al. 2012)
CeO <sub>2</sub> nanocrystals	Microwave-assisted solution	-	-	(Kumar et al. 2013)
Ce-TiO <sub>2</sub>	Slurry form, Sol-gel	Visible light	Nitrobenzene	(Ellappan and Miranda 2014)

Ce-TiO <sub>2</sub>	Slurry form, Sol-gel	UV-C	Reduction of CO <sub>2</sub>	(Matějová et al. 2014)
B-TiO <sub>2</sub>	Slurry form, Sol-gel	UV-A	Orange-II	(May-Lozano et al. 2014)
CeO <sub>2</sub> -TiO <sub>2</sub>	Slurry form, Microemulsion	Four fluorescent UV lamps	Toulene	(Muñoz-Batista et al. 2014)
Ce-TiO <sub>2</sub>	Slurry form, Sol-gel	Sunlight	Methylene blue	(Priyanka et al. 2014)
Cerium in doped anatase TiO <sub>2</sub>	Slurry form, Solvothormal	Visible light (300 W Xenon lamp)	Water reduction	(Fonseca de Lima et al. 2015)
B-TiO <sub>2</sub>	Slurry form, Sol-gel	Simulated sunlight	Metoprolol	(Cavalcante et al. 2015)
Ce-TiO <sub>2</sub>	Slurry form, Sol-gel	UV and visible	Phenol	(Martin et al. 2015)
B-TiO <sub>2</sub>	Slurry form, Sol-gel	Visible light (150 W Xenon lamp)	p-nitrophenol and methylene blue	(Patel et al. 2015)
Ce-TiO <sub>2</sub>	Slurry form, Sol-gel	-	-	(Tsega and Dejene 2016)
Ce-TiO <sub>2</sub>	Slurry form, Sol-gel	Visible light (500 W Xenon lamp)	Chlorophenol	(Maddila et al. 2017)
Ce-TiO <sub>2</sub>	Slurry form, Sol-gel	UV-C (8W mercury lamp)	Decomposition of N <sub>2</sub> O and reduction of CO <sub>2</sub>	(Matějová et al. 2017)
B-TiO <sub>2</sub>	Slurry form,	UV-A	2,4-dichlorophenol, bisphenol-A,	(Bilgin

	Solvo-thermal	(Phillips 8W×18)	ibuprofen, and flurbiprofen	Simsek 2017)
Ce-TiO <sub>2</sub>	Slurry form, Flame spray pyrolysis	Visible light (150 W Xenon lamp)	Methylene blue	(Mikaeili et al. 2018)
CeO <sub>2</sub> /TiO <sub>2</sub> nanostructures	Slurry form, Hydrothermal	Visible light (medium mercury vapour lamp)	Methylene blue and polyvinylpyrrolidone	(Vieira et al. 2018)
CeO <sub>2</sub> nanoparticles	Slurry form, Microwave assisted hydrothermal	UV-C	Rhodamine B	(Amoresi et al. 2019)
Ce-TiO <sub>2</sub>	Slurry form, Sol-gel	Sunlight	Rhodamine B	(Maarisetty and Baral 2019)
B- TiO <sub>2</sub>	Slurry form, Sol-gel	UV-A (123 W mercury lamp)	4-nitrophenol	(Yadav et al. 2020)
B/Ce-TiO <sub>2</sub>	Slurry form, Sol-gel	UV (253.7 nm)	Acid Red B (ARB)	(Chao-hai et al. 2007)
B/V-TiO <sub>2</sub>	Slurry form, Sol-gel	Visible light (450 W medium mercury vapour lamp)	Methylene blue	(Bettinelli et al. 2007)
B/N-TiO <sub>2</sub>	Slurry form, Sol-gel	Visible light	Methyl tertiary butyl ether (MTBE)	(In et al. 2007)
B-Fe-Ce-TiO <sub>2</sub>	Slurry form, Sol-gel	Visible light	2,4-Dichlorophenol-(DCP)	(Ling et al. 2008)
B/Ni/Ce-TiO <sub>2</sub>	Sol-gel	-	-	(Zhang and Liu 2008)
B/N-TiO <sub>2</sub>	Slurry form, Sol-gel	Visible light	Rhodamine B	(Feng et al. 2011)
B/Ag-TiO <sub>2</sub>	Slurry form, Solvo-thermal	Sunlight	Methylene blue	(Feng et al. 2013)
La/B-TiO <sub>2</sub>	Slurry form, Sol-gel	Visible light (500 W commercial)	Azo-dye acid orange 7 (AO7)	(Lan et al. 2014)

			tungsten halogen lamp)	
La/B-TiO <sub>2</sub>	Slurry form, Sol-gel	Visible light (500 W Xenon lamp)	Methyl orange	(Zhang et al. 2014)
B/N-TiO <sub>2</sub>	Slurry form, Hydrothermal	-	-	(Zhao et al. 2015a)
Co/B-TiO <sub>2</sub>	Slurry form, Sol-gel	Visible light (150 W Xenon lamp)	p-nitrophenol and rhodamine B	(Jaiswal et al. 2016)
S/B-TiO <sub>2</sub>	Slurry form, Melamine as precursors	Visible light (300 W Xenon lamp)	Rhodamine B	(Han et al. 2018)
Cu/B-TiO <sub>2</sub>	Slurry form, Sol-gel	Visible light (400 w metal halide lamp)	Lissamine Green B	(Alim et al. 2019)
Cerium doped and cerium-boron codoped TiO <sub>2</sub>	Slurry form, Sol-gel	UV-A	Malachite green	(Stoyanova et al. 2021)

**Table 2.3.** Disinfection studies using monodoped and codoped catalysts with boron/cerium as dopants

PHOTOCATALYST	SLURRY FORM/ IMMOBILIZED FORM, PREPARATION METHOD	LIGHT SOURCE	EXPERIMENTAL CONDITIONS/ MAJOR RESULTS	REFERENCE
B-TiO <sub>2</sub>	Slurry form, Sol-gel	Visible light	<i>E.coli</i> (Inhibition ring method) Disinfection – 8.3 mm - 500°C 8.5 mm – 600°C 8.0 mm – 700°C 5.5 mm – 800°C 4.5 mm – 900°C (4g/L)	(Xue et al. 2013)
B-TiO <sub>2</sub>	Slurry form, Sol-gel	Visible light (15 × 18 W fluorescent	<i>Candida albicans</i> , <i>Escherichia coli</i> , and <i>Staphylococcus aureus</i> (Inhibition ring method)	(Wang et al. 2014)

		tubes)	$C_0 - 10^4 - 10^5$ CFU/mL Disinfection – 16 mm, 10 mm and 7 mm respectively (4g/L)	
Ce-TiO <sub>2</sub>	Slurry form, Sol-gel	Visible light	<i>E. coli</i> Kirby Bauer test Disinfection- 15-18 mm (1 mg/mL)	(Ali et al. 2016)
B-TiO <sub>2</sub> , Ce-TiO <sub>2</sub> , B/Ce-TiO <sub>2</sub>	Slurry form, Sol-gel	Visible light	<i>Staphylococcus aureus</i> (Shake flask method) $C_0 - 10^5 - 10^6$ CFU/mL Disinfection – B/Ce-TiO <sub>2</sub> – 97.62% B-TiO <sub>2</sub> – 87.41% Ce-TiO <sub>2</sub> – 25% (4g/L) T – 120 min	(Wang et al. 2016b)
TiO <sub>2</sub> , B-TiO <sub>2</sub> , Y-TiO <sub>2</sub> , B/Y-TiO <sub>2</sub>	Slurry form, Sol-gel	Visible light	<i>E. coli</i> (Shake flask method) $C_0 - 10^5 - 10^6$ CFU/mL Disinfection – TiO <sub>2</sub> - 0% and 0% B-TiO <sub>2</sub> – 41% and 42% Y-TiO <sub>2</sub> – 64.5% and 60% B/Y--TiO <sub>2</sub> – 99.43% (4g/L) T – 120 min	(Wang et al. 2016c)
Zn-TiO <sub>2</sub> , Zn/Ce-TiO <sub>2</sub> , Zn/Y-TiO <sub>2</sub> , Zn/B-TiO <sub>2</sub>	Slurry form, Sol-gel	Visible light	<i>E. coli</i> (Inhibition zone and shake flask method) $C_0 - 10^5 - 10^6$ CFU/mL Disinfection – 94.98% for Zn-TiO <sub>2</sub> – 500°C, 99.9% for Zn/Ce-TiO <sub>2</sub> – 600°C, 99.99% for Zn/Y-TiO <sub>2</sub> – 700°C, 99.68% for Zn/B-TiO <sub>2</sub> – 500°C (4g/L) T – 120 min	(Wang et al. 2017b)

Boron and cerium codoped TiO <sub>2</sub>	Slurry form, Sol-gel	Visible light	<p><i>E. coli</i> and <i>S. aureus</i> (Inhibition zone and Shake-flask method) C<sub>0</sub> – 10<sup>5</sup>-10<sup>6</sup> CFU/mL Disinfection – KR [Killing rate = log (N<sub>sc</sub>/N<sub>s</sub>)] 500°C – 0 and 0 600°C – 1.8 and 4.2 700°C – 1.7 and 1.3 800°C – 1.2 and 1.0 (4g/L) T – 120 min</p>	(Wang et al. 2018)
--	-------------------------	---------------	---	-----------------------

C<sub>0</sub> – Initial pollutant concentration/bacterial cell concentration, T – Duration



## 2.7. RECENT PHOTOCATALYSTS: DEGRADATION OF CIP, OTHER ORGANIC POLLUTANTS AND DISINFECTION

Studies which have investigated the photocatalytic degradation of ciprofloxacin include TiO<sub>2</sub> and ZnO (Silva et al. 2016), Ag<sub>2</sub>O/Ag<sub>2</sub>CO<sub>3</sub>/MWNTs composite (Wang et al. 2016a), N-doped TiO<sub>2</sub> (Shetty et al. 2017), Fe<sub>3</sub>O<sub>4</sub>/SiO<sub>2</sub>/TiO<sub>2</sub> (Teixeira et al. 2017), Ag/AgCl/Ag<sub>2</sub>O heterostructures (Yang et al. 2017), Fe doped ZnO (Das et al. 2018), Ag/Ag<sub>2</sub>MoO<sub>4</sub> composites (Li et al. 2018), CeO<sub>2</sub>-Ag/AgBr (Wen et al. 2018), AgI/BiOBr (Yu et al. 2018), graphitized mesoporous carbon (GMC)-TiO<sub>2</sub> nanocomposite (Zheng et al. 2018), AgBr/Ag<sub>3</sub>PO<sub>4</sub>@natural hematite heterojunction (Chen et al. 2019), exfoliated g-C<sub>3</sub>N<sub>4</sub> and bulk g-C<sub>3</sub>N<sub>4</sub> catalysts (Pattnaik et al. 2019), Zn doped Cu<sub>2</sub>O catalyst (Yu et al. 2019), FeWO<sub>4</sub>/NC (nitrogen-doped carbon) nanocomposite (Ahamad et al. 2021), AgNPs@BP (black phosphorus nanosheets) (Chen et al. 2020), S-C<sub>3</sub>N<sub>4</sub>/ZnO hybrid heterojunction (Gupta et al. 2020), TiO<sub>2</sub>/g-C<sub>3</sub>N<sub>4</sub> heterojunction (Hu et al. 2020), black Ti<sup>3+</sup>/N-TiO<sub>2</sub> (b-N-TiO<sub>2</sub>) (Sarafraz et al. 2020), Bi<sub>2</sub>WO<sub>6</sub>/C<sub>3</sub>N<sub>4</sub>/Ti<sub>3</sub>C<sub>2</sub> composite (Wu et al. 2020), Zn doped BiOCl nanosheets (Xu et al. 2020), Sm-doped g-C<sub>3</sub>N<sub>4</sub>/Ti<sub>3</sub>C<sub>2</sub> MXene heterojunction (Yu et al. 2020), and TiO<sub>2</sub>-pillared multilayer graphene nanocomposites (Zeng et al. 2020). Heterojunction and nanocomposites are advanced/latest generation photocatalysts as they exhibit broad light range response and are effective in the spatial separation of electron-hole pairs (Dey and Gogate 2021; Low et al. 2017). These studies are summarized in **Table 2.4**.

Other organic pollutants such as dyes, phenol, and pesticides have been studied along with disinfection, summarized in **Table 2.5**. Amaranth (azo pigment) & *S.aureus* using g-C<sub>3</sub>N<sub>4</sub> loaded Ag nanoparticles (Xu et al. 2019), RhB & *E.coli* using Ce-TiO<sub>2</sub> (Kasinathan et al. 2016), methyl orange & *E.coli* using Rh doped SrTiO<sub>3</sub> (Kiss et al. 2017), methylene blue & *E.coli* using TiO<sub>2</sub> (Wang et al. 2013b), B/F-TiO<sub>2</sub> (Wang et al. 2013a), phenol & *E.coli* using Ag@AgSCN (Zhao et al. 2018), lindane & *E.coli* using TiO<sub>2</sub> (Omar et al. 2017). All these visible light active photocatalysts (except (Wang et al. 2013a)) showed their effective role both in degradation and disinfection through narrowed bandgap with

the introduction of impurity band (shift in absorption edge towards visible light), reduction of recombination, and effective charge separation. Lesser crystallite size and a larger surface area of the catalysts have also contributed to an efficient degradation/disinfection. Overall, these advanced/latest generation photocatalysts were effective for most of the organic pollutants under UV-A, visible light, and sunlight. However, B and Ce doped photocatalysts have not been studied for their effectiveness of degradation of antibiotics and disinfection.

**Table 2.4.** Degradation of CIP using TiO<sub>2</sub> and latest generation photocatalysts

<b>PHOTOCATALYST</b>	<b>SLURRY FORM/ IMMOBILIZED FORM, PREPARATION METHOD</b>	<b>LIGHT SOURCE</b>	<b>EXPERIMENTAL CONDITIONS/ MAJOR RESULTS</b>	<b>REFERENCE</b>
TiO <sub>2</sub> and ZnO	Slurry form	UV-A	CIP C <sub>0</sub> – 0.3 mg/L Degradation – 85%-TiO <sub>2</sub> , 63%-ZnO (1 g/L) T – 45 min Analysis – HPLC-MS, toxicity test	(Silva et al. 2016)
Ag <sub>2</sub> O/ Ag <sub>2</sub> CO <sub>3</sub> /MWNTs composite	Slurry form, Calcination of precipitate	Visible light (300 W Xenon lamp)	CIP C <sub>0</sub> – 10 mg/L Degradation – 58.3% (0.5 g/L) T – 60 min Analysis – UV-Vis spectrophotometer	(Wang et al. 2016a)
Fe <sub>3</sub> O <sub>4</sub> /SiO <sub>2</sub> /TiO <sub>2</sub>	Slurry form, Co-precipitation	UV-A (Phillips 8W lamps)	CIP, norfloxacin, ibuprofen, methylene blue C <sub>0</sub> – 5 mg/L, 5 mg/L, 15 mg/L and 2 mg/L respectively Degradation – 95%, 95%, 60%, and 95% respectively (1 g/L) T – 90 min Analysis – UV-Vis spectrophotometer	(Teixeira et al. 2017)
N-TiO <sub>2</sub> , Aeroxide-P25-TiO <sub>2</sub>	Slurry form, Sol-gel	Visible tungsten lamp with power output of 400 W-artificial radiation, solar radiation	CIP C <sub>0</sub> – 100 mg/L Degradation – Visible – 99%, 90% (1 g/L) Solar – 100%, 100% (1 g/L) T – 60 min Analysis – UV-Vis spectrophotometer, liquid chromatography-tandem mass chromatography (LC-MS/MS)	(Shetty et al. 2017)

Ag/AgCl/Ag <sub>2</sub> O heterostructures	Slurry form, Precipitation	Visible light (250 W Xenon lamp)	CIP C <sub>0</sub> - 10 mg/L Degradation - 91.2% (0.1 g/L) T - 100 min Analysis - UV-Vis spectrophotometer, TOC reduction	(Yang et al. 2017)
Ag/Ag <sub>2</sub> MoO <sub>4</sub> composites	Slurry form, In-situ reduction reaction	Visible light (500 W Xenon lamp)	CIP C <sub>0</sub> - 10 mg/L (0.4 g/L) Degradation - 99.5 % T - 60 min Analysis - UV-Vis spectrophotometer	(Li et al. 2018)
Fe-doped ZnO	Slurry form, Precipitation	Sunlight	CIP C <sub>0</sub> - 10 mg/L Degradation - 69% (0.15 g/L) T - 210 min Analysis - UV-Vis spectrophotometer, Residual Antimicrobial activity of Antibiotics	(Das et al. 2018)
CeO <sub>2</sub> -Ag/AgBr	Slurry form, In-situ co-precipitation	Visible light (300 W Xenon lamp)	CIP C <sub>0</sub> - 10 mg/L Degradation - 90% (1 g/L) T - 120 min Analysis - UV-Vis spectrophotometer, LCMS	(Wen et al. 2018)
AgI/BiOBr	Slurry form, Chemical deposition	Visible light (300 W Xenon lamp)	CIP C <sub>0</sub> - 10 mg/L (0.5 g/L) Degradation - 90.9% T - 60 min Analysis - UV-Vis spectrophotometer, LCMS	(Yu et al. 2018)

Graphitized mesoporous carbon (GMC)-TiO <sub>2</sub> nanocomposite	Slurry form, Resorcinol-formaldehyde	UV-C	CIP C <sub>0</sub> – 15 mg/L Degradation – 100% (0.35 g/L) T – 120 min Analysis – HPLC-MS, TOC, toxicity test	(Zheng et al. 2018)
AgBr/Ag <sub>3</sub> PO <sub>4</sub> @natural hematite heterojunction	Slurry form, In-situ deposition	Simulated sunlight (300 W Xenon lamp with 808 nm long-pass filter)	Norfloxacin, CIP, ofloxacin, enoxacin, and penicillin C <sub>0</sub> – 15 mg/L Degradation – 83%, 53%, 40%, 70%, and 20% respectively (0.17 g/L) T – 90 min Analysis – HPLC, TOC reduction	(Chen et al. 2019)
g-C <sub>3</sub> N <sub>4</sub> and Exfoliated g-C <sub>3</sub> N <sub>4</sub>	Slurry form, Urea and bi-thermal aqueous	Sunlight	CIP C <sub>0</sub> – 10 mg/L Degradation – 78% (1 g/L) T – 60 min Analysis – UV-Vis spectrophotometer	(Pattnaik et al. 2019)
Zn doped-Cu <sub>2</sub> O	Slurry form, Solvothermal	Visible light (500 W metal halide lamp)	CIP C <sub>0</sub> – 20 mg/L Degradation – 78% (0.6 g/L) T – 60 min Analysis – UV-Vis spectrophotometer, HPLC-MS/MS	(Yu et al. 2019)
AgNPs@BP (black phosphorus nanosheets)	Slurry form, In-situ deposition	Simulated sunlight (300 W Xenon lamp with an AM 1.5 G filter)	CIP, NOR, sulfadiazine (SDZ), and tetracycline (TTC) C <sub>0</sub> – 1 mg/L Degradation – 95%, 95%, 93% and 79% respectively (5 mmol/L) T – 30 min Analysis – TOC reduction, UV-Vis spectrophotometer, HPLC	(Chen et al. 2020)

S-C <sub>3</sub> N <sub>4</sub> /ZnO hybrid heterojunction	Slurry form	UV (Two 15 W Philips tube), Visible light (CFL, 25 W, Philips)	CIP C <sub>0</sub> – 20 mg/L Degradation – 98.8%, 75.8% (1 g/L)  T – 210 min Analysis – UV-Vis spectrophotometer, LC-MS	(Gupta et al. 2020)
TiO <sub>2</sub> /g-C <sub>3</sub> N <sub>4</sub> heterojunction	Slurry form, Hydrothermal	Simulated sunlight (500 W Xenon lamp)	CIP C <sub>0</sub> – 20 μmol/L Degradation – 93.4% (0.2 g/L) T – 60 min Analysis – HPLC	(Hu et al. 2020)
Black Ti <sup>3+</sup> /N-TiO <sub>2</sub> (b-N-TiO <sub>2</sub> )	Slurry form, Impregnation method with urea	Visible light (5 W LED lamp)	CIP C <sub>0</sub> – 0.5 mg/L Degradation – 100% (0.4 g/L) T – 70 min Analysis- HPLC, TOC, Toxicity	(Sarafraz et al. 2020)
Bi <sub>2</sub> WO <sub>6</sub> /C <sub>3</sub> N <sub>4</sub> /Ti <sub>3</sub> C <sub>2</sub> composite	Slurry form, Hydrothermal	Visible light (300 W Xenon lamp)	CIP C <sub>0</sub> – 10 mg/L Degradation – 87.4% (1.5 g/L) T – 70 min Analysis – UV-Vis spectrophotometer	(Wu et al. 2020)
Zn doped BiOCl nanosheets	Slurry form, Hydrothermal	Visible light (300 W Xenon lamp)	CIP C <sub>0</sub> – 10 mg/L Degradation – 98% (1 g/L) T – 80 min Analysis – UV-Vis spectrophotometer	(Xu et al. 2020)
Sm-doped g-C <sub>3</sub> N <sub>4</sub> /Ti <sub>3</sub> C <sub>2</sub> MXene heterojunction	Slurry form, Prepolymerization and solid mixture-calcination	Visible light (300 W Xenon lamp)	CIP C <sub>0</sub> – 20 mg/L Degradation – 99% (0.2 g/L) T – 60 min Analysis – UPLC	(Yu et al. 2020)

TiO <sub>2</sub> -pillared multilayer graphene nanocomposites	Slurry form, Hydrothermal	Visible light (5 W LED lamp)	CIP C <sub>0</sub> – 15 mg/L Degradation – 78% (0.5 g/L) T – 150 min Analysis – UV-Vis spectrophotometer	(Zeng et al. 2020)
FeWO <sub>4</sub> /NC (nitrogen doped carbon) nanocomposite	Slurry form, Hydrothermal	Visible light (1000 W Xenon lamp)	CIP C <sub>0</sub> – 20 mg/L Degradation – 92.23% (10 mg/L) T – 100 min Analysis – UV-Vis spectrophotometer, TOC, LC-MS	(Ahamad et al. 2021)
Ni-doped Ag <sub>2</sub> O nanoparticles	Slurry form, Hydrothermal	Visible light (14 W Phillips cool LED bulb)	CIP C <sub>0</sub> – 4.5 mg/L Degradation – 59% (33 mg/L) T – 20 min Analysis – UV-Vis spectrophotometer	(De and Sinha 2022)

**Table 2.5.** Summary of photocatalytic degradation of other organic pollutants and disinfection

PHOTOCATALYST	LIGHT SOURCE	DEGRADATION	DISINFECTION	REFERENCE
B/F-TiO <sub>2</sub>	Visible light (300 W Xenon lamp)	Methylene blue C <sub>0</sub> – 20 mg/L Degradation – 99% (0.625 g/L) T – 300 min Analysis – UV-visible spectrophotometer	<i>E.coli</i> Standard plate count method Disinfection – 99.55% (0.2 mg/mL) T – 30 min	(Wang et al. 2013a)
TiO <sub>2</sub>	UV-A	Methylene blue Initial – 8 mg/L Degradation – 50% (0.5 g/L) T – 25 min Analysis – UV-visible spectrophotometer	<i>E.coli</i> Initial – 10 <sup>8</sup> CFU/mL Standard serial dilution and plate counting method Disinfection – 99.9% (0.5 g/L) T – 150 min	(Wang et al. 2013b)

Ce-TiO <sub>2</sub>	Visible light (Phillips 15W and 18W)	RhB C <sub>0</sub> – 1mM Degradation – 99.89% (0.5 g/L) T – 8 h Analysis – UV-visible spectrophotometer	<i>E.coli</i> , <i>S. aureus</i> , <i>P. vulgaris</i> and <i>S. pneum</i> C <sub>0</sub> – 5×10 <sup>4</sup> CFU/mL Well diffusion method Disinfection – 5mm, 5.4mm, 12 mm, 15 mm (50 µg/L)	(Kasinathan et al. 2016)
Rh doped SrTiO <sub>3</sub>	Visible light (300 W Xenon lamp)	Methyl orange C <sub>0</sub> – 0.02 g/L Degradation – 86% (1 g/L) T – 30 min Analysis – UV-visible spectrophotometer	<i>E.coli</i> C <sub>0</sub> – 10 <sup>5</sup> CFU/mL Standard serial dilution and plate counting method Disinfection – 100% (0.1 W/V%) T – 360 min	(Kiss et al. 2017)
TiO <sub>2</sub>	Sunlight	Lindane C <sub>0</sub> – 100 µg/L Degradation – 80% (0.2 g/L) T – 60 min Analysis – GC-MS	<i>E.coli</i> C <sub>0</sub> – 1986 MPN/100mL IDEXX Colilert Method Disinfection – 90% (2g/L) T – 60 min	(Omar et al. 2017)
Ag@AgSCN	Visible light (400 W tungsten halogen lamp)	Phenol C <sub>0</sub> – 20 ppm Degradation – 100% (2 g/L) T – 15 min Analysis – UV-visible spectrophotometer	<i>E.coli</i> C <sub>0</sub> – 10 <sup>7</sup> CFU/mL Standard serial dilution and plate counting method Disinfection – 100% 0.6 g/L) T – 2.5 h	(Zhao et al. 2018)
g-C <sub>3</sub> N <sub>4</sub> loaded Ag nanoparticles	Visible light (500 W Xenon lamp)	Amaranth (azo pigment) C <sub>0</sub> – 1.5×10 <sup>-5</sup> M Degradation – 70% (0.2 g/L) T – 240 min Analysis – UV-visible spectrophotometer	<i>S.aureus</i> C <sub>0</sub> – 10 <sup>7</sup> CFU/mL Standard plate counting method Disinfection – 99.99% (0.2 g/L) T – 240 min	(Xu et al. 2019)

C<sub>0</sub> – Initial pollutant concentration/bacterial cell concentration, T – Duration



## 2.8. SIMULTANEOUS PHOTOCATALYTIC DEGRADATION AND DISINFECTION (DISINFECTION IN THE PRESENCE OF ANTIBIOTICS)

In view of the problem of antimicrobial resistance, both antibiotics and microorganisms which develops resistance for the antibiotics must be removed/eliminated from the environment.  $\text{TiO}_2$  has been studied for both the degradation of antibiotics and disinfection (Biancullio et al. 2019; Bosio et al. 2018; Pablos et al. 2012). However, these studies are limited to the UV light range.  $\text{Ag}_2\text{O}/\text{TiO}_2$ -modified chitosan was studied for degradation of ampicillin, methyl orange, and disinfection of *E.coli* under visible-light (Zhao et al. 2017). Some of the visible-light active photocatalysts have been employed for simultaneous degradation, and disinfection as these catalysts could be of great importance in the pharmaceutical community. Vanadium and nitrogen codoped  $\text{TiO}_2$  (Eswar et al. 2016) under visible-light have shown a synergistic effect towards the simultaneous photocatalytic degradation of chloramphenicol and inactivation of *E.coli*. Cerium doped  $\text{TiO}_2$ /diatomite granular (GCTD) composite (Chen et al. 2018) was examined for the degradation of oxytetracycline and disinfection of *E.coli*, *S.aureus*, and *K.pneumoniae* under visible light. Sulfur-doped carbon quantum dots loaded hollow tubular g- $\text{C}_3\text{N}_4$  (HTCN-C) (Wang et al. 2019b) were evaluated for degradation of tetracycline and disinfection of *E.coli*. Magnetic Ag/Fe, N- $\text{TiO}_2/\text{Fe}_3\text{O}_4@\text{SiO}_2$  photocatalyst (He et al. 2019) was examined for both degradation of bisphenol A (BPA) and disinfection of *E.coli* under visible light. La-doped  $\text{TiO}_2$ /calcium ferrite/diatomite (La-TCD) ternary composite (Wu and Zhang 2020) was evaluated for the photocatalytic degradation of oxytetracycline and *E.coli* disinfection under visible light. Silver also has been reported as a good disinfectant. BiOCl-Ag heterojunction nanocomposites (Zhu et al. 2016) were studied for degradation of sulfanilamide (SAM) and disinfection of *E.coli* and *B.subtilis* under simulated sunlight. Ag/ $\text{Fe}_2\text{O}_3/\text{ZnO}$  heterostructures (Kaur et al. 2019) were investigated for degradation of ciprofloxacin and disinfection of *E.coli* under sunlight.  $\text{Bi}_4\text{O}_5\text{I}_2/\text{AgI}$  hybrid (Yang et al. 2019) under visible-light was investigated for the degradation of tetracycline and disinfection of *E.coli*.

Post-irradiation bacterial regrowth/repairing the light damage is an important evaluation indicator as bacteria can utilize nutrients from various sources (Giannakis et al. 2014, 2015; Villegas- Guzman et al. 2017). The regrowth can be attributed to survival and capability of microbial species to use carbon sources generated from oxidation of recalcitrant organic compounds (Biancullo et al. 2019).

The residual antimicrobial activity/toxicity of the photo catalytically treated antibiotic solution is an important aspect that needs to be considered after treatment of antibiotics as the degraded products/intermediates might be toxic when compared to the parent compound. TiO<sub>2</sub> treated CIP solution was assessed for its toxicity using *Bacillus subtilis* (Li et al. 2012), TiO<sub>2</sub> treated solution of oxacillin (Giraldo-Aguirre et al. 2015), and Fe doped ZnO treated CIP (Das et al. 2018) were examined for the residual antibiotic activity using *S.aureus* and *E.coli* respectively by disc diffusion method/inhibition halo method. The toxicity of graphitized mesoporous carbon (GMC)-TiO<sub>2</sub> nanocomposite treated CIP solution was studied using *Vibrio fischeri* by measuring the bioluminescence inhibition (luminiscence inhibition percentage) (Zheng et al. 2018). The absence or decrease in the inhibition zone/lesser inhibition rate of the treated antibiotic samples with an increase in the photocatalytic treatment time indicated the loss of antimicrobial activity or the degradation of antibiotics to less harmful form.

Some of the studies have been reported on disinfection of multidrug resistant (MDR) organisms. Disinfection of *E.coli* resistant to 10 antibiotics belonging to antibiotic groups of penicillin, cephalosporins, fluoroquinolones and tetracyclines (multi-drug resistant) was investigated using Fe doped ZnO (Das et al. 2017), N doped TiO<sub>2</sub> (Rizzo et al. 2014) was evaluated for disinfection of *E.coli* resistant to ciprofloxacin (CIP), tetracycline (TET), cefuroxime (CEF), and vancomycin (VAN). Other AOPs (TiO<sub>2</sub>/sunlight, H<sub>2</sub>O<sub>2</sub>/sunlight, H<sub>2</sub>O<sub>2</sub>/TiO<sub>2</sub>/sunlight, and photo-Fenton) (Ferro et al. 2015) have been reported for the disinfection of *E.coli* resistant to ampicillin (AMP), ciprofloxacin (CIPR), cefuroxime (CXM), and nitrofurantoin (NI).

The cell membrane integrity or cell membrane damage was reported in the literature for disinfection of *E.coli* using Ag/AgBr/g-C<sub>3</sub>N<sub>4</sub> hybrid photocatalyst under visible light (Yan et al. 2020), using Fe-doped ZnO nanoparticles under solar light (Das et al. 2017) and using Rh doped SrTiO<sub>3</sub> under visible light (Kiss et al. 2017). The changes in the metabolism of bacterial cells were detected through cell membrane permeability, lipid peroxidation (MDA, malondialdehyde), iron leakage, ATP levels in cells, and antioxidant enzyme activity. The integrity of membrane or cell membrane damages was identified through LIVE/DEAD cell staining (fluorescence staining assay) and FESEM analysis (changes in membrane structure). The destruction of cells from the reactive species was indicated through the fluorescence colour where the viable cells with green colour intensity decreased (green-fluorescent nucleic acid stain, SYTO<sup>®</sup>9) and the dead cells with red colour intensity increased (red-fluorescent nucleic acid stain, propidium iodide) with an increase in the photocatalytic treatment time. Due to the damage of the cell the K<sup>+</sup> ions leak from the cytoplasm (measured using an optical emission spectrophotometer) and oxidation of lipids (increase in the concentration of MDA measured using lipid peroxidation assay kit) through peroxidation reaction takes place by the reactive species. The protein contents were determined using the bicinchoninic acid (BCA) method. The bacteria produce enzymes like SOD (superoxide dismutase-catalyzes dismutation of O<sub>2</sub><sup>•-</sup> to H<sub>2</sub>O<sub>2</sub> and O<sub>2</sub>) and CAT (catalase-converts H<sub>2</sub>O<sub>2</sub> to O<sub>2</sub> and H<sub>2</sub>O), which acts as an antioxidant for the oxidative stress induced by the reactive species. The decrease in the ATP concentration (measured using ATP fluorescence detector) indicates the inhibition of ATP synthesis, thereby reducing the energy of the cell and finally leading to cell death. These changes in the bacterial activity indicate the role of reactive species in bacterial disinfection through the damage of cell membrane, the release of ions, fragmentation of proteins, and finally, inactivation. The disinfection of the MDR organisms was quantitatively analyzed using K<sup>+</sup> ions release and MDA assays.

Thus, these solar photocatalytic treatments serve as a promising tool in achieving the disinfection of MDR organisms and, in turn, minimize the problem of antimicrobial resistance. However, the reuse of the suspended form of catalysts is a time and cost-

consuming process which should be considered for large-scale application of treatment of water and wastewater. Simultaneous photocatalytic degradation and disinfection studies have been summarized in **Table 2.6** and studies involving multidrug-resistant organisms in **Table 2.7**.

**Table 2.6.** Simultaneous photocatalytic degradation and disinfection studies

Photocatalyst	Light source	Degradation	Disinfection	Reference
TiO <sub>2</sub> (slurry and immobilized)	UV-A (6 W black light lamp)	Diclofenac sodium salt, Hydrochlorothiazide, Sulfamethoxazole, and 4- acetamidoantipyrine C <sub>0</sub> – 10 mg/L each Degradation – Slurry: 70%, 62%, 60%, 60% respectively (0.1 g/L) Immobilized: 86%, 76%, 84%, and 88% respectively (6 × 6 mm glass Raschig rings) T – 360 min Analysis – HPLC, LC-MS	<i>E. coli</i> C <sub>0</sub> – 10 <sup>6</sup> CFU/mL Standard serial dilution and plate count method Disinfection – Slurry: 98% (0.1 g/L) Immobilized: 99.99% (6 × 6 mm glass Raschig rings) T – 360 min	(Pablos et al. 2012)
		Simultaneous degradation and disinfection in deionised water (DI) and a SWTP effluent with TiO <sub>2</sub> in suspended form (C <sub>0</sub> -20 µg/L, 10 <sup>3</sup> CFU/mL) Degradation – 100%, 70%, 100%, 100% (DI) 100%, 80%, 100%, 60% (SWTP) (0.1g/L) Disinfection – 99.99% (DI), 99% (SWTP) T – 50 min (DI), 150 min (SWTP) (0.1g/L)		
V–N codoped TiO <sub>2</sub>	Visible light (400 W metal halide lamp)	Chloramphenicol C <sub>0</sub> – 25 ppm Degradation – 88% (1 g/L) T – 120 min Analysis – UV-visible spectrophotometer	<i>E. coli</i> C <sub>0</sub> – 2×10 <sup>9</sup> CFU/mL Spread plate method Disinfection – 99.99% (1 g/L) T – 120 min	(Eswar et al. 2016)
		Simultaneous Degradation – 90% (1 g/L) Disinfection – 99.9% (1 g/L) T – 120 min		

BiOCl nanodiscs deposited with Ag	Simulated sunlight (200 W Xe arc lamp)	Sulphonamide C <sub>0</sub> – 10 ppm Degradation – 92% (1 g/L) T – 300 min Analysis – HPLC	<i>E. coli</i> and <i>Bacillus subtilis</i> C <sub>0</sub> – 3×10 <sup>7</sup> CFU/mL Spread plate method Disinfection – 100% (1 g/L) T – 120 min	(Zhu et al. 2016)
Ag <sub>2</sub> O/TiO <sub>2</sub> -modified chitosan	UV-visible light (150 W tungsten-halogen lamp)	Methyl orange (MO), Ampicillin (AMP) C <sub>0</sub> – MO – 10 mg/L, AMP – 20 mg/L Degradation – 96%, 100% (1.5 g/L) Duration – 15 min, 3 h Analysis – UV-visible spectrophotometer, HPLC, TOC analysis	<i>E. coli</i> C <sub>0</sub> – 10 <sup>4</sup> CFU/mL Disc diffusion method Disinfection – 99.99% (1.5 g/L) Duration – 30 min	(Zhao et al. 2017)
TiO <sub>2</sub> (immobilized on glass beads)	UV-A (125 W mercury vapour lamp), sunlight	Alprazolam (ALP), clonazepam (CZP), diazepam (DZP), lorazepam (LZP), and carbamazepine (CBZ) C <sub>0</sub> – 100 µg/L Degradation – Slurry: 80-85% (ultrapure water) Immobilized: 85-90% (ultrapure water), wastewater: 15-30% (0.1 g/L) T – 120 min Analysis – HPLC	<i>E. coli</i> , and total coliform bacteria (TCB) Colilert method	(Bosio et al. 2018)
Ce- TiO <sub>2</sub> /diatomite granular composite	Visible light (Xenon lamp)	Oxytetracycline C <sub>0</sub> – 20 mg/L Degradation – 93% (5 g/L) T – 240 min Analysis – UV-visible spectrophotometer, TOC analysis	<i>E. coli</i> , <i>S. aureus</i> , and <i>K. pneumoniae</i> Standard plate count method C <sub>0</sub> – 10 <sup>5</sup> CFU/mL Disinfection – 86.4%, 87.9%, and 84.7% respectively (5 g/L) T – 120 min	(Chen et al. 2018)

TiO <sub>2</sub>	UV-A (9 W LED)	Azithromycin, trimethoprim, ofloxacin, and sulfamethoxazole/ clindamycin C <sub>0</sub> – 100 µg/L Degradation – 99%, 99%, 100%, and 100% respectively (1 g/L) T – 80 min Analysis – UHPLC-MS/MS	<i>Heterotrophs, enterococci, and E.coli</i> Membrane filtration method C <sub>0</sub> – 7.7 log (CFU/100 mL), 5.7 log (CFU/100 mL), and 5.9 log (CFU/100 mL) Disinfection – 65%, 61%, and 64% respectively (1 g/L) T – 60 min	(Biancullo et al. 2019)
		Secondary urban wastewater Degradation – 100%, 100%, 100%, 100% (1 g/L) Disinfection – 10%, 70%, 76% (1 g/L) T – 60 min		
Ag/Fe, N- TiO <sub>2</sub> /Fe <sub>3</sub> O <sub>4</sub> @SiO <sub>2</sub>	Visible light (8 W compact fluorescent lamps)	Bisphenol A C <sub>0</sub> – 2 mg/L Degradation – 100% (1 g/L) T – 120 min Analysis – HPLC, LC-MS	<i>E.coli</i> C <sub>0</sub> – 10 <sup>6</sup> CFU/mL Spread plate method Disinfection – 99.99% (1 g/L) T – 120 min	(He et al. 2019)
		Simultaneous Degradation – 90% (1 g/L) Disinfection – 99.99% (1 g/L) T – 120 min Sewage Degradation – 100%, 360 min (1 g/L) Disinfection – 99.99%, 210 min (1 g/L)		
Ag/Fe <sub>2</sub> O <sub>3</sub> /ZnO heterostructure	Sunlight	Ciprofloxacin C <sub>0</sub> – 10 mg/L Degradation – 76.4% (0.3 g/L) T – 210 min Analysis – UV-visible spectrophotometer	<i>E.coli</i> Standard plate count method C <sub>0</sub> – 3×10 <sup>7</sup> CFU/mL Disinfection – 100% (200 µg/mL) T – 120 min	(Kaur et al. 2019)
Bismuth oxyiodide/Silver iodide hybrid (Bi <sub>4</sub> O <sub>5</sub> I <sub>2</sub> /AgI)	Visible light (300 W Xe lamp)	Tetracycline C <sub>0</sub> – 20 mg/L Degradation – 82% (0.5 g/L) T – 30 min	<i>E.coli</i> Standard plate count method C <sub>0</sub> – 3×10 <sup>7</sup> CFU/mL Disinfection-100% (0.4 g/L)	(Yang et al. 2019)

		Analysis – UV-visible spectrophotometer	T – 30 min	
Sulfur doped carbon quantum dots (S-CQDs) loaded hollow tubular g-C <sub>3</sub> N <sub>4</sub> (HTCN-C)	Visible light (300 W Xenon lamp)	Tetracycline C <sub>0</sub> – 20 mg/L Degradation – 82.67% (1 g/L) T – 60 min Analysis – UV-visible spectrophotometer, TOC analysis	<i>E.coli</i> Serial dilution and plating method C <sub>0</sub> – 3×10 <sup>7</sup> CFU/mL Disinfection – 99.99% (1 g/L) T – 40 min	(Wang et al. 2019b)
La doped TiO <sub>2</sub> /calcium ferrite/diatomite (La-TCD) ternary composite	Visible light (150 W Xe lamp)	Oxytetracycline (OTC) C <sub>0</sub> – 10 mg/L Degradation – 93% (2 g/L) T – 150 min Analysis – UV-visible spectrophotometer	<i>E.coli</i> Standard plate count method C <sub>0</sub> – 10 <sup>5</sup> CFU/mL Disinfection – 94% (2 g/L) T – 120 min	(Wu and Zhang 2020)
Ag-TiO <sub>2</sub>	Slurry form, Photochemical reduction	Visible light (artificial lamp)	CIP, NOR C <sub>0</sub> – 3 mg/L each Degradation – 92%, 94% (0.3 g/L) T – 240 min Analysis – UV-Vis spectrophotometer  <i>Escherichia coli</i> C <sub>0</sub> – 10 <sup>8</sup> cells/mL (Modified streaking method) Disinfection – No growth (0.3 g/L) T – 180 min	(Wang et al. 2021)

**Table 2.7.** Summary of loss of antimicrobial activity of photocatalytically treated antibiotics and photocatalytic disinfection of multidrug resistant (MDR) micro-organisms

Photocatalyst	Light source	Degradation	Multi-drug resistant (MDR) micro-organism disinfection/ Residual antimicrobial activity or Toxicity	Reference
N-TiO <sub>2</sub>	Simulated sunlight	-	MDR disinfection <i>E.coli</i> (Resistant to CIP, CEF, TET, VAN) C <sub>0</sub> – 10 <sup>7</sup> CFU/mL	(Rizzo et al. 2014)



			Disinfection – 80%, 10 min (0.2 g/L)	
H <sub>2</sub> O <sub>2</sub> /sunlight, TiO <sub>2</sub> /sunlight, H <sub>2</sub> O <sub>2</sub> /TiO <sub>2</sub> /sunlight, natural photo-Fenton	Sunlight	-	MDR disinfection <i>E.coli</i> (Resistant to AMP, CIPR, CXM, NI) C <sub>0</sub> – 10 <sup>9</sup> CFU/mL Disinfection – H <sub>2</sub> O <sub>2</sub> /sunlight – 100%, 180 min TiO <sub>2</sub> /sunlight – 100%, 180 min H <sub>2</sub> O <sub>2</sub> /TiO <sub>2</sub> /sunlight – 100%, 180 min Photo-Fenton – 100%, 240 min (TiO <sub>2</sub> – 100 mg/L, H <sub>2</sub> O <sub>2</sub> – 0.588 mM, Fe <sup>2+</sup> - 0.09 mM)	(Ferro et al. 2015)
Fe doped ZnO	Sunlight	-	MDR disinfection <i>E.coli</i> (Resistant to 10 antibiotics belonging to groups- penicillin, cephalosporins, fluoroquinolones and tetracyclines) C <sub>0</sub> – 1.2×10 <sup>7</sup> CFU/mL Disinfection – 100%, 90 min (0.5 g/L)	(Das et al. 2017)
TiO <sub>2</sub>	UV (Phillips, 150 W)	Oxacillin C <sub>0</sub> – 1.5×10 <sup>-5</sup> M Degradation – 70% (2 g/L) T – 240 min Analysis – HPLC	Residual antimicrobial activity <i>S.aureus</i> C <sub>0</sub> – 10 <sup>5</sup> CFU/mL Inhibition halo method	(Giraldo-Aguirre et al. 2015)
Graphitized mesoporous carbon (GMC)-TiO <sub>2</sub> nanocomposite	UV-C	CIP C <sub>0</sub> – 15 mg/L Degradation – 100% (15 mg/L) T – 120 min Analysis – HPLC-MS, TOC, toxicity test	Toxicity <i>Vibrio fischeri</i> C <sub>0</sub> – 10 <sup>8</sup> CFU/mL Bioluminescence inhibition	(Zheng et al. 2018)
Fe doped ZnO	Sunlight	CIP C <sub>0</sub> – 10 ppm Degradation – 66% (0.15 g/L) T – 210 min Analysis – UV-visible spectrophotometer	Residual antimicrobial activity <i>E.coli</i> C <sub>0</sub> – 10 <sup>8</sup> CFU/mL Inhibition halo method	(Das et al. 2018)

C<sub>0</sub> – Initial pollutant concentration/bacterial cell concentration, T – Duration

## **2.9. IMMOBILIZATION OF PHOTOCATALYSTS TO OVERCOME THE DISADVANTAGES OF SUSPENDED FORM**

Photocatalysts are commonly used in slurry or suspended forms; however, the photocatalyst is difficult to recover post-treatment and to reuse, thus limiting its large-scale applications. This limitation can be overcome by immobilization of the photocatalyst onto a suitable inert support. Immobilized/floating forms of photocatalysts help in achieving the feasibility of catalysts in large-scale applications through its reuse, and thus reducing the operational costs (Shan et al. 2010; Srikanth et al. 2017; Xing et al. 2018b). Various supports such as cork (Sboui et al. 2017), perlite (Długosz et al. 2015; Hosseini et al. 2007), polymers (Ata et al. 2017; Colmenares and Kuna 2017; Duca et al. 2013; Koysuren and Koysuren 2017; Nawawi et al. 2016; Rtimi et al. 2014; Rtimi and Kiwi 2017; Singh et al. 2013b; Sökmen et al. 2011; Zhang et al. 2013), glass beads/glass spheres (Cunha et al. 2018; Daneshvar et al. 2010; Miranda-García et al. 2010; Shen et al. 2017; Xing et al. 2018a), zeolites (Gou et al. 2017; Li et al. 2020), clay (Oliveira et al. 2020; Paul et al. 2012), chitosan (Zhao et al. 2017) (Fakhri et al. 2018), and calcium alginate beads (Dalponte et al. 2019; Sarkar et al. 2015) are available for immobilization of the photocatalysts. Borosilicate glass tubes are used as supports in compound parabolic collector (CPC) reactors (Alrousan et al. 2012; Palacios-villarreal et al. 2020). Other supports include acrylic films (Bonfond et al. 2015), quartz filter/porous titanium substrate (Arlos et al. 2016), stainless steel mesh (Murgolo et al. 2017), glass fibres (Suárez et al. 2017). The supporting material must provide a large surface area, strongly adhere the catalyst, must have excellent degradation stability against strong oxidative radicals, and must be able to adsorb pollutants onto its surface for an efficient photocatalytic activity.

The widely employed methods for immobilization of photocatalysts for the degradation of organic pollutants are dip-coating, solvent casting, electrophoretic deposition, photo-etching, chemical vapour deposition, polymer assisted hydrothermal decomposition, cold plasma discharge, radio frequency (RF) magnetron sputtering

(Malakootian et al. 2019; Shankaraiah et al. 2016; Sökmen et al. 2011; Srikanth et al. 2017; Xing et al. 2018b).

Among various supports, polymers are the most suitable ones as they are cost-effective and readily available. Polymers include polyethylene, polystyrene, polyamide, polymethyl methacrylate, polyethylene terephthalate, polyvinyl alcohol, polycaprolactone, polyacrylonitrile, polyvinylidene fluoride (Cámara et al. 2018; Colmenares and Kuna 2017; Sökmen et al. 2011). Polystyrene/expanded polystyrene (EPS) beads are widely used as packaging materials (in food, electronic goods, and other fragile products), thus creating an enormous amount of waste polymers that need to be reused in a circular economy. These waste polymers can be upcycled for the development of floating photocatalysts and thus solving a major environmental problem – ‘white pollution’ (Mangalara and Varughese 2016). These low-density polymers float on the liquid surface, thus ensuring effective utilization of light energy for optimum photocatalytic activity (Singh et al. 2013b).

In recent years, polystyrene/EPS beads in the form of thin films (Ata et al. 2017; Das and Mahalingam 2019a; Magalhães and Lago 2009; Singh and Gupta 2014; Singh et al. 2013a, 2015) as a support for immobilization has attracted much attention due to its, low cost, non-toxicity, and chemical inertness (Vaiano et al. 2018). However, these studies are limited to dyes and disinfection (Fabiyyi and Skelton 2000; Lee et al. 2021; Magalhães and Lago 2009; Varnagiris et al. 2020). These studies have been performed under UV light, and other immobilization studies carried out for degradation of dyes, antibiotics & disinfection are summarized in **Table 2.8**.

Some of the studies reported on degradation of ciprofloxacin, other antibiotics and disinfection using the immobilized forms of photocatalyst are as follows: TiO<sub>2</sub> reduced graphene oxide (TiO<sub>2</sub>-rGO) immobilized on side-glowing optical fibers (SOFs) was studied for degradation of ibuprofen, carbamazepine, and sulfamethoxazole (Lin et al. 2017). TiO<sub>2</sub> nanoparticles immobilized onto a glass plate was examined for degradation of ciprofloxacin under UV-C (Malakootian et al. 2019). Photocatalytic activity of

ciprofloxacin using N-TiO<sub>2</sub> immobilized on glass spheres under visible light was explored (Xing et al. 2018a). g-C<sub>3</sub>N<sub>4</sub>@Co-TiO<sub>2</sub> (CNCT) fibrous membrane was prepared and evaluated for the degradation of tetracycline hydrochloride (TC-H), oxytetracycline hydrochloride (OTC-H), doxycycline hydrochloride (DC-H), & ciprofloxacin (CIP), and disinfection of *E.coli* under visible light (Song et al. 2020). Trimethoprim (TMP) & sulfamethoxazole (SMX) degradation and inactivation of *E.coli* was investigated using Ce-ZnO nanoparticles (Zammit et al. 2019) coated onto a silica interlayer disc. Using a real wastewater sample, the disinfection of *E.coli*, other coliforms and *P.aeruginosa* was performed in the presence of antibiotics ofloxacin and ciprofloxacin after checking for the resistance of antibiotics.

**Table 2.8.** Photocatalytic studies of organic pollutants and disinfection in immobilized forms

PHOTOCATALYST	IMMOBILIZED FORM, PREPARATION METHOD	LIGHT SOURCE	EXPERIMENTAL CONDITIONS/ MAJOR RESULTS	REFERENCE
TiO <sub>2</sub> -coated polystyrene beads	Sprinkle and heat-fixing	UV-A	Methylene blue	(Fabiya and Skelton 2000)
TiO <sub>2</sub> P25 grafted on expanded polystyrene (EPS) beads	Grafting	UV-A	Methylene blue, indigo carmine and drimaren red	(Magalhães and Lago 2009)
TiO <sub>2</sub> immobilized onto glass spheres	Dip-coating	Sunlight [Pilot compound parabolic collector (CPC) plant]	Acetaminophen, Caffeine, Ofloxacin, Antipyrine, Sulfamethoxazole, Carbamazepine, Flumequine, Keterolac, Atrazine, Isoproturon, Hydroxybiphenyl, Diclofenac, Ibuprofen, Progesterone, Triclosan	(Miranda-García et al. 2010)
TiO <sub>2</sub> films immobilized on inner surface of borosilicate glass tube of CPC reactor	Dip coating	UV-A	<i>E.coli</i> C <sub>0</sub> – 10 <sup>6</sup> CFU/mL Disinfection – 99.999% (0.5 g/L) T – 5 h	(Alroushan et al. 2012)
TiO <sub>2</sub> / polystyrene	Solvent-casting	UV-A	Methyl orange and methylene blue	(Singh et al. 2013a)
Polyethylene (PE)-TiO <sub>2</sub> films	Direct current magnetron sputtering	UV-C	<i>E.coli</i> K12 C <sub>0</sub> – 10 <sup>6</sup> CFU/mL Disinfection – 100% (0.096 wt.% TiO <sub>2</sub> /wt. PE) T – 180 min	(Rtimi et al. 2014)
Ag doped TiO <sub>2</sub> polystyrene	Liquid impregnation, Solvent-casting	UV-C, Sunlight	Methylene blue	(Singh et al. 2014)
TiO <sub>2</sub> supported on autoclaved cellular concrete	Oven dried	UV-A	Indigo carmine	(Andrade et al. 2015)

Hybrid acrylic TiO <sub>2</sub> films	Casting TiO <sub>2</sub> pickering stabilized acrylic latexes	Simulated sunlight	<i>E.coli</i> C <sub>0</sub> – 10 <sup>6</sup> CFU/mL Disinfection – 100% (10 wbm% of TiO <sub>2</sub> ) T – 200 min	(Bonnefond et al. 2015)
TiO <sub>2</sub> -Calcium alginate beads	Entrapping	UV-A	Chlorhexidine digluconate	(Sarkar et al. 2015)
TiO <sub>2</sub> / polystyrene	Solvent-casting	UV-A	Methylene blue	(Singh et al. 2015)
TiO <sub>2</sub> / quartz filter / porous titanium substrate	Sol-gel	UV-LED	Carbamazepine and atorvastatin	(Arlos et al. 2016)
Polyethylene (PE)-TiO <sub>2</sub> films	Immersing PE film in TiO <sub>2</sub> suspension	UV-A	Methylene blue	(Suárez et al. 2016)
Graphitic carbon nitride on polyethylene terephthalate nanofibres	Thermal decomposition of urea, Electrospinning	Sunlight	Sulfaquinoxaline	(Qin et al. 2016)
N-TiO <sub>2</sub> immobilized on polystyrene plates	Solvent-casting	Visible light (8W)	Methylene blue, phenol C <sub>0</sub> – 10 mg/L and 50 mg/L respectively Degradation – 98% and 72% respectively T – 300 min and 180 min respectively (0.2 wt.% N-TiO <sub>2</sub> /wt.% PS) Analysis – UV-visible spectrophotometer, TOC reduction <i>E.coli</i> C <sub>0</sub> – 10 <sup>5</sup> CFU/mL Standard plate counting method Disinfection – 97% (0.2 wt.% N-TiO <sub>2</sub> /wt.% PS) T – 60 min	(Ata et al. 2017)
TiO <sub>2</sub> -reduced graphene oxide coated side-glowing optical fibers	Polymer assisted hydrothermal deposition	UV-A and visible light	Ibuprofen, Carbamazepine, and Sulfamethoxazole	(Lin et al. 2017)

TiO <sub>2</sub> films on stainless steel meshes	Metal-organic chemical vapour deposition	UV-A	Warfarin, Trimethoprim, Carbamazepine, Metoprolol, and Gemfibrozil	(Murgolo et al. 2017)
CuO <sub>x</sub> -TiO <sub>2</sub> -PET	Direct current magnetron sputtering	Simulated sunlight	<i>E.coli</i> C <sub>0</sub> – 4 × 10 <sup>6</sup> CFU/mL Disinfection – 100% (0.08 wt.% Cu/wt. PE, 0.11 wt.% TiO <sub>2</sub> /wt. PE) T – 150 min	(Rtimi et al. 2017)
TiO <sub>2</sub> -PANI/Cork	Using binder and cork	Sunlight	Methyl orange	(Sboui et al. 2017)
Ce-TiO <sub>2</sub> immobilized on porous glass	Dip coating	Visible light (300 W Xenon lamp)	Methyl orange and Rhodamine B	(Shen et al. 2017)
Glass fiber (GF) TiO <sub>2</sub> -Cu mats	Dipping GF mats in TiO <sub>2</sub> suspension	UV-C	Methylene blue <i>E.coli</i> K12 C <sub>0</sub> – 10 <sup>6</sup> CFU/mL Disinfection – 100% (15.4% by weight TiO <sub>2</sub> , 0.45% by weight by Cu) T – 180 min	(Suárez et al. 2017)
WS <sub>2</sub> decorated and immobilized on chitosan and polycaprolactone	Electrospinning	UV-A	Neomycin	(Fakhri et al. 2018)
ZnO supported on polystyrene pellets	Solvent-casting	UV-LED	Caffeine and paracetamol	(Vaiano et al. 2018)
N- TiO <sub>2</sub> immobilized on glass spheres	Using sodium silicate as binder	Visible light (500 W Xenon lamp)	CIP C <sub>0</sub> – 20 mg/L Degradation – 97.5% (3 g/L) T – 180 min Analysis – UPLC-Q-TOF MS	(Xing et al. 2018a)
TiO <sub>2</sub> /Calcium alginate beads	Dripping (Ionotropic gelation)	UV-A	Tartrazine	(Dalponte et al. 2019)

TiO <sub>2</sub> / polystyrene	Solvent-casting	UV-C	Remazol Turquoise Blue	(Das and Mahalingam 2019a)
TiO <sub>2</sub>	Dip-coating	UV-C (6 W Phillips lamp)	CIP C <sub>0</sub> – 3 mg/L Degradation – 92.81% (1 g/L) T – 105 min Analysis – HPLC, COD reduction	(Malakootian et al. 2019)
Ce-ZnO (Immobilized onto a silica interlayer disc)	Dip-coating	UV-A (18 W lamps)	Trimethoprim (TMP) & sulfamethoxazole (SMX) C <sub>0</sub> – 7.258 µg/L & 6.332 µg/L Degradation – 6.71×10 <sup>-3</sup> min <sup>-1</sup> & 1.09×10 <sup>-2</sup> min <sup>-1</sup> T – 320 min Analysis – UHPLC/MS-MS <i>E.coli</i> Membrane filtration method C <sub>0</sub> – 10 <sup>5</sup> and 10 <sup>6</sup> CFU/mL Disinfection –100%, 180 min –10 <sup>5</sup> CFU/mL 99%, 210 min –10 <sup>6</sup> CFU/mL (15 wt.%) Wastewater <i>E.coli</i> , coliforms and <i>P.aeruginosa</i> – as expected did not show significant activity	(Zammit et al. 2019)
Ni-doped ZnO	RF sputtering	UV-A (6W)	CIP C <sub>0</sub> – 5 mg/L Degradation – 100% (0.75 g/L) T – 90 min Analysis – HPLC, TOC	(Hosseini et al. 2020)
TiO <sub>2</sub> thin films (immobilized glass substrate)	Spray pyrolysis	Simulated sunlight	CIP C <sub>0</sub> – 5 mg/L Degradation – 93% (5 wt.%) T – 90 min Analysis – UV-visible spectrophotometer	(Kerli and Eskalen 2020)
TiO <sub>2</sub> /PMMA (poly methyl methacrylate) film	Inverted phase	UV-A	Methylene blue	(Ounas et al. 2020)



TiO <sub>2</sub> immobilized on cylindrical borosilicate glass tubes	Dip coating	Simulated sunlight	Acetaminophen, Diclofenac, Carbamazepine, Atenolol, Propranolol, Albuterol, Ofloxacin, Ciprofloxacin, Azithromycin, Erythromycin, Hydrochlorothiazide, Furosemide	(Palacios-villarreal et al. 2020)
g-C <sub>3</sub> N <sub>4</sub> @Co-TiO <sub>2</sub> (CNCT) fibrous membranes with core-shell nanostructures	Electrospinning	Visible light (300 W Xe lamp)	Tetracycline hydrochloride (TC-H), doxycycline hydrochloride (DC-H), oxytetracycline hydrochloride (OTC-H), and ciprofloxacin (CIP) C <sub>0</sub> – 20 mg/L each Degradation – TC-H – 90.8%, DC-H – 82.2%, OTC-H – 75.3%, CIP – 60.2% T – 60 min Analysis – UV-visible spectrophotometer <i>E.coli</i> C <sub>0</sub> – 10 <sup>6</sup> CFU/mL Spread plate method Disinfection – 6 log reduction, 99.99% (5 mg of membrane, 2 × 2 cm <sup>2</sup> ) T – 90 min	(Song et al. 2020)
Polystyrene beads with TiO <sub>2</sub> film	Physical vapour deposition	UV-B	Methylene blue <i>E.coli</i> C <sub>0</sub> – 6 × 10 <sup>9</sup> cells/mL Disinfection – 100% (1 g/10 mL, 5 mmol/L EDTA) T – 45 min	(Varnagiris et al. 2020)
Waste EPS–TiO <sub>2</sub> composite (W-TiEPS)	Dissolving using acetone and water	UV-A	Methylene blue and Cr (VI) reduction	(Lee et al. 2021)
P/Ag/Ag <sub>2</sub> O/Ag <sub>3</sub> PO <sub>4</sub> / TiO <sub>2</sub> (PAgT)	Sol-gel/hydrpthermal two-step method	Visible light	<i>E.coli</i> , <i>Salmonella</i> , <i>S.aureus</i> , and <i>Enterococcus</i> C <sub>0</sub> – 10 <sup>7</sup> CFU/mL Disinfection – 100% (0.5 g/L) T – 20 min, 30 min, 180 min, and 360 min	(Liu et al. 2021)

C<sub>0</sub> – Initial pollutant concentration/bacterial cell concentration, T – Duration

## 2.10. EFFECT OF REAL WATER MATRICES

The photocatalytic activity is affected by the water composition as real/natural water contains many inorganic ions such as  $\text{CO}_3^{2-}$ ,  $\text{PO}_4^{3-}$ ,  $\text{NO}_3^-$ ,  $\text{SO}_4^{2-}$ ,  $\text{Cl}^-$ ,  $\text{Na}^+$ ,  $\text{K}^+$ ,  $\text{Ca}^{2+}$ ,  $\text{Mg}^{2+}$  and natural organic matter (NOM) such as humic acid. These ions either act as scavengers or react with the reactive oxygen species (Sahoo et al. 2020; Sarafraz et al. 2020; Wang et al. 2017a; Yang et al. 2020). Hence, for real-world applications on large-scale basis, the immobilization of photocatalysts and their application in real water matrices are the essential factors that need to be considered.

## 2.11. SYNTHESIS METHODS

Sol-gel, co-precipitation, hydrolysis, hydrothermal, and solvothermal are widely used for the synthesis of photocatalysts. However, these methods require controlled experimental conditions, use of surfactant and also result in less yield of the photocatalyst/nanoparticles (Sharma et al. 2015). Biological methods include synthesis using bacteria, fungi, yeast, algae (micro-organisms) and plant extracts. These methods have disadvantages such as safety risk, production of variable size nanoparticles, temperature-controlled conditions must be provided which increases the operation cost (Jamkhande et al. 2019).

The EDTA-citrate method helps in molecular level mixing of ions through homogeneous dispersion of metal-EDTA complex within the citric matrix. This method provides a higher catalyst yield, with improved catalyst properties such as higher crystallinity (Prasad et al. 2012). A study on the synthesis of cerium molybdate nanoparticles using the EDTA-citrate method has been reported (Sena et al. 2017).

The solvent employed during the synthesis is water, which has a high dielectric constant, and this helps in the formation of particles with smaller crystallite or particle size (Becker et al. 2011). Also, water is regarded as a green solvent (non-toxic to the environment and human health) compared to the organic and volatile solvents usually employed in other synthesis methods (Castro-Puyana et al. 2017).

As noted from the literature, B has a unique role towards disinfection activity and Ce has a role towards enhancing the photocatalytic activity through higher adsorption

ability. Also, both B and Ce dopants are highly active under visible light. The unique properties of B and Ce dopants are discussed in detail in section 2.13. Thus, utilizing/combining the unique properties of each of these dopants through doping with TiO<sub>2</sub> enhances the visible light utilization and aids in the removal of antibiotic & micro-organism from the environment which is a major contributor for the development of antimicrobial resistance, posing a serious threat in recent decades. In the earlier studies reported using B and Ce as dopants (monodoped or codoped), the dopants concentration levels are quite arbitrary, and there is no insight into the basis of the selection of dopant concentrations, which play a major role in achieving higher photocatalytic activity. The selection of concentration of dopants (for codoping) by studying the individual dopants photocatalytic activity (monodoping) helps in identifying the appropriate concentration of a dopant for solving a particular problem and minimizes the chemicals required for bulk synthesis.

## **2.12. RESEARCH GAPS**

This study aims to identify a suitable visible light active photocatalyst which is capable of both degradation and disinfection thus addressing the emerging problem of AMR. Keeping in mind, the advantages (physiochemical modifications) of metal and non-metal doping as mentioned in section 2.4.1 which results in shifting of absorption edge towards visible light. As noted from literature, the excellent disinfection ability of boron and higher adsorption ability of Ce results in effective degradation of antibiotics and disinfection under visible light through their synergistic effect. Also, there are no particular insights (in the studies reported for boron and cerium doped catalysts the dopants concentration are chosen arbitrarily) that would be useful in the rational design of boron and cerium doped (monodoping and codoping) photocatalysts.

The major research gaps observed from the literature review are as follows:

- EDTA-citrate synthesis method has not been employed for development of boron and cerium codoped catalysts to the best of our knowledge.

- Boron and cerium doped catalysts (monodoping/codoping) have been employed for degradation of organic pollutants such phenols, dyes, etc. but not evaluated for degradation of antibiotics.
- Immobilization of the boron and cerium doped catalysts and evaluation of their photocatalytic activity.
- No studies have been reported on disinfection activity in the presence of antibiotics using boron and cerium doped catalysts.
- Effect of photocatalytic efficiency in real water matrices.

### **2.13. SELECTION OF DOPANTS: BORON AND CERIUM**

Among the metal dopants, rare-earth metal Ce narrows the bandgap with the appearance of new energy levels below the conduction band, enhances photogenerated charge separation, and promotes the adsorption capacity (providing better contact between catalysts and pollutants for efficient photocatalytic activity) (Reszczyńska et al. 2015; Vieira et al. 2018). The narrowing of the bandgap is due to the hybridization of O 2p (conduction band) and Ce 4f orbitals (valence band) (Chao-hai et al. 2007). Thus, Ce ions can interact directly with the pollutant molecules through f orbital, and the formation of Ce-O-Ti bonds favor adsorption of water molecules to form OH<sup>•</sup> radicals, which eventually react with the pollutants (Maarisetty and Baral 2019; Silva et al. 2009).

Non-metal dopants like B ions occupy substitutional (dopant concentration  $\geq 2$  at.%) and interstitial (dopant concentration  $\sim 1$  at.%) lattice positions of TiO<sub>2</sub> (Feng et al. 2011; Patel et al. 2015; Shi et al. 2019); the former position helps in narrowing of the bandgap through the formation of B-O-Ti bond, creation of new energy levels above the valence band and shifting of the absorption edge towards visible light while the latter position promotes effective electron-hole separation and reduces the recombination (Jaiswal et al. 2016). The decrease in the bandgap can be attributed to the mixing of B p orbital with O 2p orbital as reported in the literature (Wang et al. 2016b; Zhao et al. 2004). Also, B is found to be an effective disinfectant (Arumugam et al. 2015; Jaiswal et al. 2016).

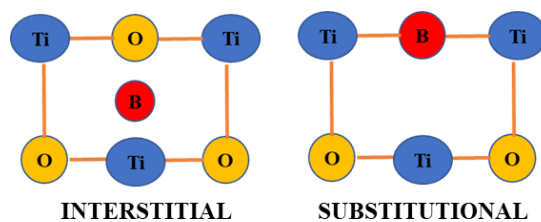


**Figure 2.3.** Lattice positions of B: interstitial and substitutional

In this way, the synergistic effect of dopants enhances the photocatalytic activity under visible/solar light, and there is effective degradation of the organic pollutant as well as disinfection.

## 2.14. SCOPE AND OBJECTIVES

In view of the problem of antimicrobial resistance, there is a need to identify a bi-functional/dual role photocatalyst that is suitable for both degradation of antibiotics and disinfection. As noted from the literature, boron is a good disinfectant and cerium has good adsorption ability, thus using B and Ce as dopants in the development of bi-functional photocatalyst serves the above purpose. Thus, the following objectives were put forward.

- To synthesize a variety of B-TiO<sub>2</sub>, Ce-TiO<sub>2</sub> and B/Ce-TiO<sub>2</sub> photocatalysts in suspended form using EDTA–Citrate method
  - 0.1 and 1 at.% Ce-TiO<sub>2</sub>
  - 1 and 2 at.% B-TiO<sub>2</sub>
  - B<sub>x</sub>Ce<sub>1-x</sub>TiO<sub>2</sub> (x = 0.9, 0.8, 0.7 at.%)
- To immobilize the above-synthesized photocatalysts onto suitable support (EPS beads)
- Characterization of the synthesized photocatalysts
  - Particle size and BET surface area
  - SEM & TEM (SAED) – morphology, diffraction rings
  - XRD – crystalline phase and structural properties
  - XPS – elemental composition and electronic state
  - RAMAN – crystal phase transformation
  - DRS and PL – bandgap and recombination of electron-hole pairs

- To study the photocatalytic degradation activity of the model pollutant (ciprofloxacin) both in suspended and immobilized forms under sunlight.
- To investigate the photocatalytic disinfection of bacterial species (*E.coli*, both in the absence and presence of antibiotic) both in suspended and immobilized forms under sunlight.
- To study the degradation and disinfection activities using real water matrices.

**This page is left blank**

## CHAPTER 3

### MATERIALS AND METHODS

This chapter describes the chemicals used for the experimental work and methods followed for the synthesis and characterization of photocatalysts followed by analysis of the samples after photocatalytic treatment.

#### 3.1. MATERIALS

Degussa P25 TiO<sub>2</sub> (99.9% pure) was obtained from Evonik, Japan; EDTA (99% extra pure), citric acid (99% extra pure), boric acid (99.5% extra pure), ammonia (99% extra pure), citric acid (99.5% extra pure), hydrochloric acid (35%) and sodium chloride was procured from Loba Chemie Pvt Ltd., India; cerium nitrate hexahydrate (99% trace metal basis), ciprofloxacin ( $\geq 98\%$  HPLC grade, CAS: 85721-33-1), acetone, triethanolamine, and isopropyl alcohol procured from Sigma Aldrich Co., USA. Ethanol from Biological Scientific solutions (India), benzoquinone from TCI Chemicals (India) Pvt. Ltd. Sodium hydroxide from Spectrum Reagents and Chemicals Pvt. Ltd (India). Luria Bertani broth and agar from HiMedia Laboratories Pvt. Ltd., Mumbai. The chemicals were used without further purification. Waste expanded polystyrene beads were obtained from the filling of discarded beanbags. Deionized water was used for preparation of all the solutions.

#### 3.2. METHODS

##### 3.2.1. Synthesis of boron and cerium doped (monodoped/codoped) TiO<sub>2</sub> photocatalysts (B-TiO<sub>2</sub>/Ce-TiO<sub>2</sub> and B<sub>x</sub>Ce<sub>1-x</sub>TiO<sub>2</sub>)

The facile EDTA-citrate method was employed for the synthesis photocatalysts in this study (**Figure 3.1**). To synthesize 'x' g of catalyst, a known amount of EDTA was dissolved in water using ammonia solution. The cerium and boron precursor solutions (known amounts) were then added to the EDTA solution. Then citric acid was added followed by the adjustment of pH to 9.0 using ammonia solution. The mole



ratio of metal/boric acid: EDTA: citric acid was kept as 1:1:1.5. The above mixture was kept under constant heating and stirring until the formation of an organometallic gel, followed by drying for 24 h at 150°C in a hot air oven. The dried samples were calcined in the first stage at 350°C for 12 h and in the second stage at 600°C for 5 h. Finally, the powder nanoparticles were stored for further use.

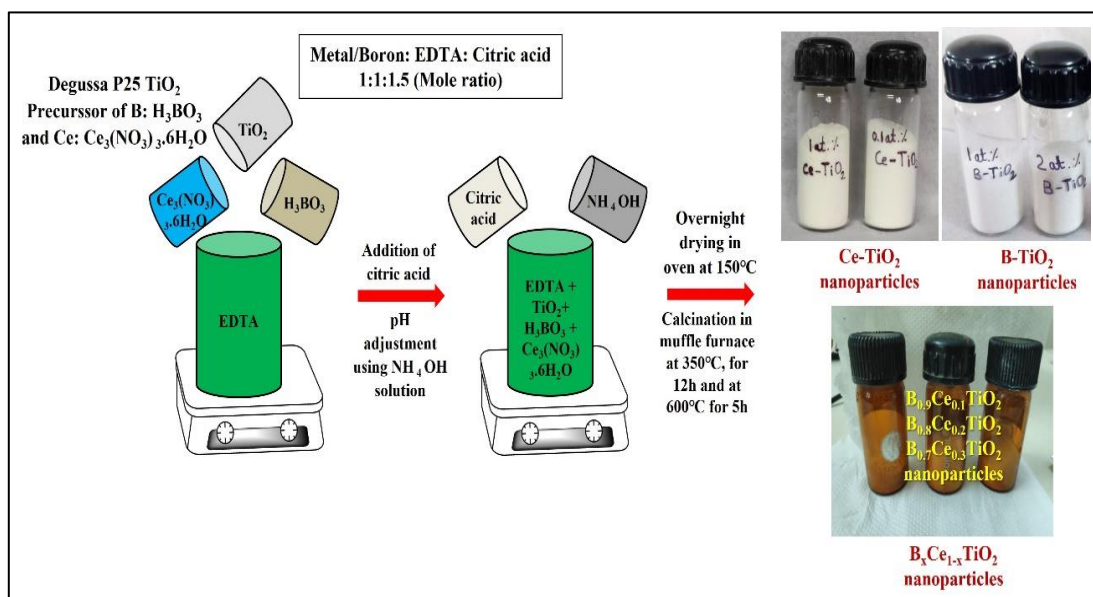


**Figure 3.1.** Synthesis of boron and cerium doped photocatalysts by EDTA-citrate method

In this study, four monodoped catalysts, namely 0.1 at.% & 1 at.% Ce-TiO<sub>2</sub> and 1 at.% & 2 at.% B-TiO<sub>2</sub> were synthesized. These compositions have been reported as the best-performing catalysts in the literature (Jaiswal et al. 2016; Martin et al. 2015). Accordingly, the catalyst samples were denoted as 0.1Ce-TiO<sub>2</sub>, 1Ce-TiO<sub>2</sub>, 1B-TiO<sub>2</sub>, and 2B-TiO<sub>2</sub>. Three codoped catalysts (B<sub>x</sub>Ce<sub>1-x</sub>TiO<sub>2</sub>) were synthesized with values of  $x$  chosen to be 0.7, 0.8 and 0.9 at.% (the reasons for choosing these  $x$  values are discussed in chapter 4) and denoted as B<sub>0.7</sub>Ce<sub>0.3</sub>TiO<sub>2</sub>, B<sub>0.8</sub>Ce<sub>0.2</sub>TiO<sub>2</sub>, and B<sub>0.9</sub>Ce<sub>0.1</sub>TiO<sub>2</sub> (**Figure 3.2**). Water, regarded as green solvent (Castro-Puyana et al. 2017) compared to volatile organic solvents generally used in other synthesis methods, is employed here and hence this procedure can be considered as a green synthesis method.

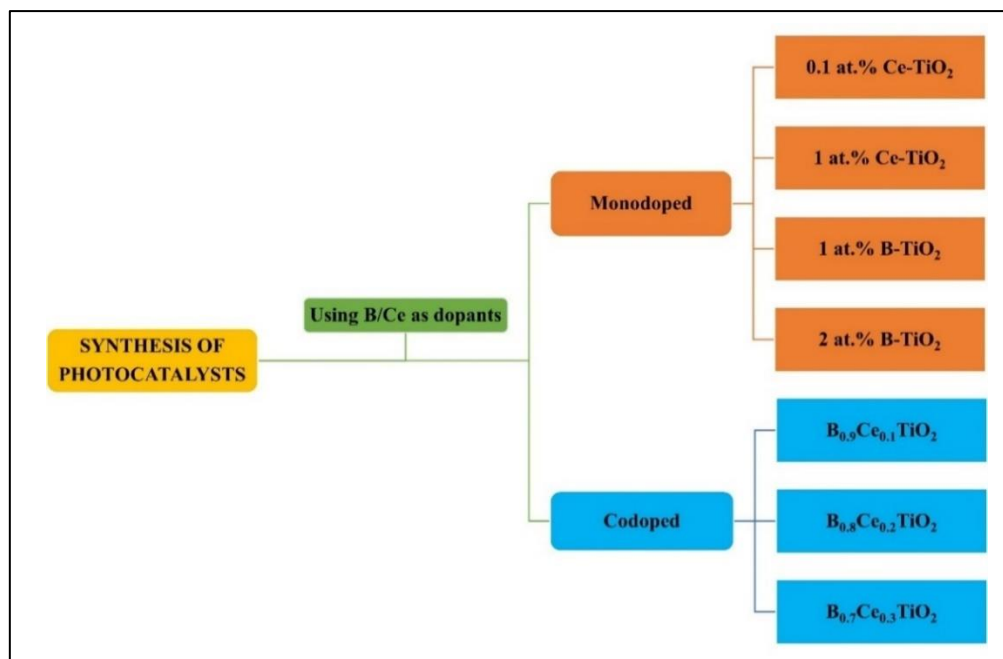


**Figure 3.2.** Summary of photocatalysts synthesized in this study

### 3.2.2. Preparation of photocatalytic EPS film

The photocatalytic EPS film was prepared by a simple solvent casting method. The photocatalyst solution (catalyst: a certain wt. % with respect to the mass of EPS beads used + 8 mL acetone + 2 mL ethanol) was homogenized through sonication for 15 min in an ultrasonic water bath. Then this solution was poured into a petri plate, followed by the addition of 3 g of EPS (expanded polystyrene) beads. The resulting film was left overnight at room temperature for solvent evaporation (**Figure 3.3**).

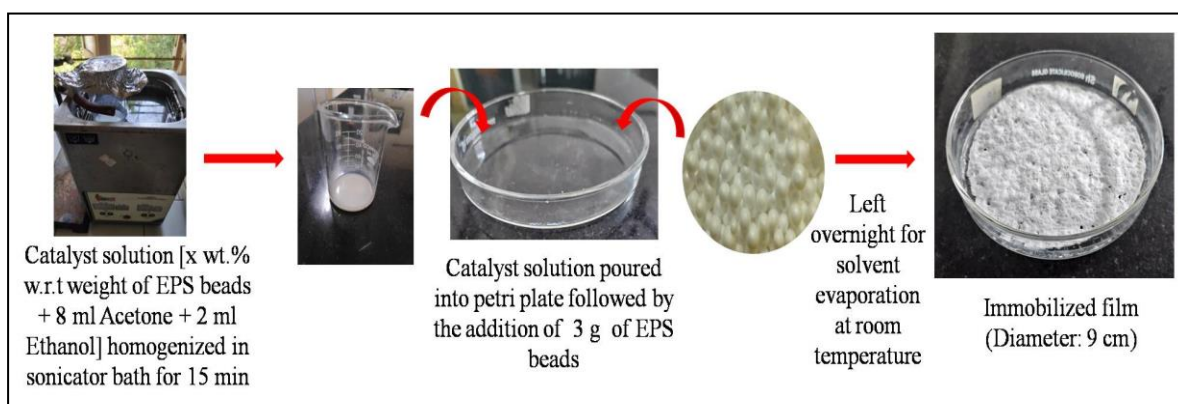


**Figure 3.3.** Preparation of EPS film

The prepared film was then gently washed with deionized water to remove any loosely bound catalyst particles. The specific amounts of solvents used in the preparation are the optimized amounts based on a preliminary evaluation of the degradation performance for the resulting film (discussed in chapter 5).

### 3.2.3. Model pollutant and organism: Ciprofloxacin (CIP) and *Escherichia coli* (*E.coli*)

The structure of the model pollutant: Ciprofloxacin (CIP), is illustrated in **Figure 3.4**, and its physico-chemical data is given in **Table 3.1**. CIP is a broad-spectrum fluoroquinolone antibiotic. It consists of N-aryl piperazine and quinolone moiety. It is insoluble in alcohol and water but soluble in dilute aqueous acid (0.1 N HCl). It is highly active against gram-negative bacteria. It is amphoteric in nature with two dissociation constant values of  $pK_{a1} = 6.09$  (carboxylic acid group) and  $pK_{a2} = 8.74$  (nitrogen on piperazinyl ring).

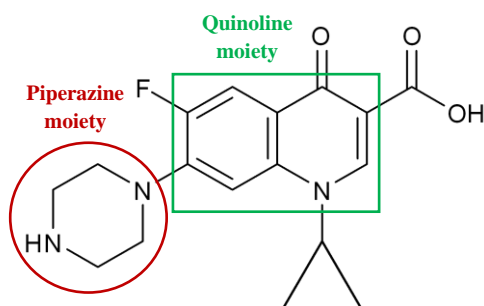


**Figure 3.4.** Chemical structure of CIP

(Source: <https://pubchem.ncbi.nlm.nih.gov/compound/ciprofloxacin>)

**Table 3.1.** Physico-chemical data of CIP

PROPERTIES	CIP
Molecular formula	$C_{17}H_{18}FN_3O_3$
Molecular weight	331.34 g/mol
Drug class	Second generation fluoroquinolone antibiotic
Mode of action	Inhibition of bacterial DNA gyrase
Medication	Used to treat bacterial infections (respiratory and urinary tract infections, skin infections)

(Source: <https://pubchem.ncbi.nlm.nih.gov/compound/ciprofloxacin>)

*Escherichia coli* (*E.coli*, a gram-negative bacterium), MTCC 9541 strain, was used as the model organism for disinfection studies. It was isolated from the river Ganga in view of the antimicrobial resistance present in this river.

#### 3.2.4. Characterization

The characterizations carried out for the catalysts, and the immobilized film are shown in **Figure 3.5**. The particle size of the synthesized photocatalysts was analyzed using a nanoparticle size analyzer (Horiba SZ-100, Kyoto, Japan) and surface area using BET (Brunauer-Emmett-Teller) surface area analyzer (MicrotracBEL-BELSORP Max, Osaka, Japan). The morphology was analyzed by scanning electron microscopy (SEM; JEOL JSM-6380LA, Peabody, Massachusetts, USA) and transmission electron microscopy (TEM; JEOL/ JEM 2100, Peabody, Massachusetts, USA). The structural phase and crystallinity were identified by X-ray diffraction (XRD, Rigaku Ultima-IV diffractometer, Rigaku, Tokyo, Japan) using Cu K $\alpha$  ( $\lambda = 0.15418$  nm) in the range of  $2\theta = 20-65^\circ$  with an increment of  $0.02^\circ$  and by Raman spectroscopy (BRUKER - RFS27, Billerica, Massachusetts, USA). X-ray photoelectron spectroscopy (XPS; Omicron ESCA+, Chanhassen, Minnesota, USA) with Al K $\alpha$  monochromator as X-ray source is used to identify the Ti (2p), O (1s), B (1s), and Ce (3d) peaks. The bandgap energy values were determined from diffuse reflectance spectroscopy (DRS; Agilent Cary 5000, Santa Clara, California, USA). Photoluminescence analysis was carried out to analyze the recombination of electron-hole pairs (PL; Horiba FluoroMax-4 spectrometer, Piscataway, New Jersey, USA) at an excitation wavelength of 325 nm. The absorbance values of the solution were analyzed by UV-Visible spectrophotometer (GBC CINTRA 103, Hampshire, USA) at  $\lambda_{\max} = 280$  nm was used to determine the concentration of degraded samples. COD (chemical oxygen demand) reduction was measured using a COD reactor (DRB 200, HACH, Loveland, Colorado, USA) by the closed reflux method/ TOC analyzer (TOC-V-CSN, Shimadzu, Osaka, Japan). The degraded products of photocatalytic treatment were identified by Liquid Chromatography-Mass Spectrometry (LCMS-2020, Shimadzu, Kyoto, Japan).

The morphology of the photocatalyst immobilized film was analyzed using FE-SEM (ZEISS GeminiSEM 300, Oberkochen, Germany) with different magnifications of X100, X500, and X3000. Surface roughness was measured using a profilometer (Taylor Hobson Taly Surf 50, Illinois, USA). The XRD analysis (Panalytical Empyrean series 3, Malvern, UK) was carried out for a  $2\theta$  range of  $5^\circ$ – $80^\circ$  with an increment of  $0.05^\circ$ . FTIR (FT-IR Bruker Alpha spectrometer, Bangalore, India) analysis was carried out to determine the functional groups and chemical bonds. ATR mode was used and analyzed over the range of  $4000$ – $500\text{ cm}^{-1}$ . A contact angle analyzer (KRÜSS, Drop shape analyzer-DSA 100E, Hamburg, Germany) was used to determine the polarity of the film. The elements leached from the immobilized film were determined using ICP-OES (Agilent Technologies, 5100, California, USA).

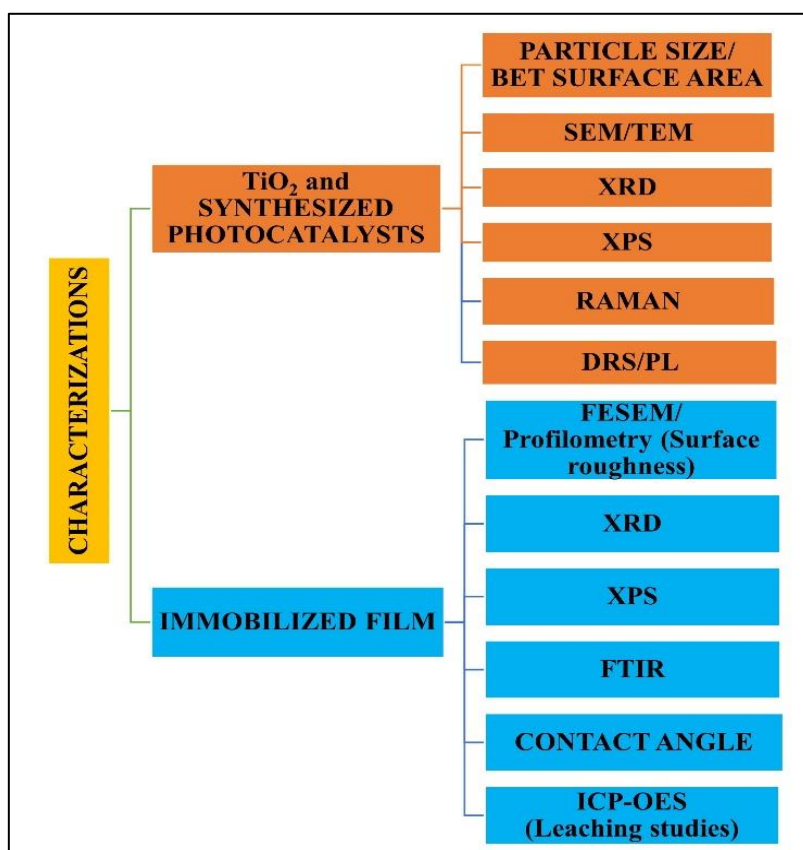


**Figure 3.5.** Characterizations of TiO<sub>2</sub>, synthesized photocatalysts and immobilized film

From XRD analysis, the crystallite size of the photocatalysts is calculated using the Debye-Scherrer equation (Eq. 3.1) for both anatase and rutile peaks. The percentage rutile content ( $X_r$ ) is calculated using Spurr and Myers equation (Eq. 3.2).

$$D_p = \frac{0.9\lambda}{\beta \cos\theta} \quad (3.1)$$

where,  $D_p$  is the average crystallite size (nm),  $\lambda$  is the x-ray wavelength (1.5418 Å),  $\beta$  is the peak width at full width half maximum (FWHM), and  $\theta$  is the diffraction angle

$$X_r(\%) = 1 - \left[1 + 1.265 \frac{I_r}{I_a}\right]^{-1} \times 100 \quad (3.2)$$

where,  $X_r$  = weight fraction of rutile,  $I_r$  = intensity of rutile (110) peak,  $I_a$  = intensity of anatase (101) peak.

From XPS analysis, the elemental composition is evaluated by the elemental sensitive factor method (Greczynski and Hultman 2020; Meng et al. 2010; Shi et al. 2019) using the relative sensitive factor (RSF) of Ti 2p<sub>1/2</sub> – 2.001, Ti 2p<sub>3/2</sub> – 1.334, O 1s – 2.93, B 1s – 5, Ce 3d<sub>3/2</sub> – 8.808 and Ce 3d<sub>5/2</sub> – 5.282.

From DRS analysis, the bandgap energy values are determined from the Tauc plot using the following equation (Eq. 3.3):

$$\alpha h\nu = A(h\nu - E_g)^{n/2} \quad (3.3)$$

where,  $E_g$  – bandgap (eV),  $\alpha$  – absorption co-efficient,  $h$  – Planck's constant,  $\nu$  – frequency of light,  $A$  – constant,  $n = 4$  (for indirect transition). The plot of  $(\alpha h\nu)^{1/2}$  versus  $(h\nu)$  determines the bandgap. The bandgap energy value is obtained by extrapolating the linear portion of the curve to the x-axis.

### 3.2.5. Measurement of photocatalytic degradation of CIP

TiO<sub>2</sub> and the synthesized photocatalysts were evaluated for the photocatalytic degradation of CIP under sunlight (at NITK Surathkal whose GPS coordinates are 13°0'40" N 74°47'44" E, from 12 to 3 p.m.) for 3 h irradiation time with an average irradiation intensity of 80,000 ± 6,000 lx and an average temperature of 33°C. The batch experiments were carried out with 200 mL of 10 mg/L of pollutant solution in a crystallizing dish (100 × 50 mm) (**Figure 3.6**). The catalyst loading was varied as 0.1, 0.5, 1.0 and 1.5 g/L. The experiments were carried out at neutral pH. Before

irradiation, the solution was kept in the dark for 30 min to achieve the adsorption-desorption equilibrium. The required samples were collected, filtered, and centrifuged for absorbance measurement. The stock solution was prepared by dissolving CIP using small amounts of 0.1 N HCl and then the volume was made up with deionized water. The calibration graph was constructed using the absorbance values of standard working concentrations of CIP (in the range of 0 - 40 ppm) at  $\lambda_{\max}$  of 280 nm. The coefficient of determination,  $R^2 = 0.999$  for CIP, was observed (**Figure 3.7**). The error bars represent the standard deviation of duplicate measurements.



**Figure 3.6.** Experimental set-up view of batch photocatalytic studies carried out under sunlight

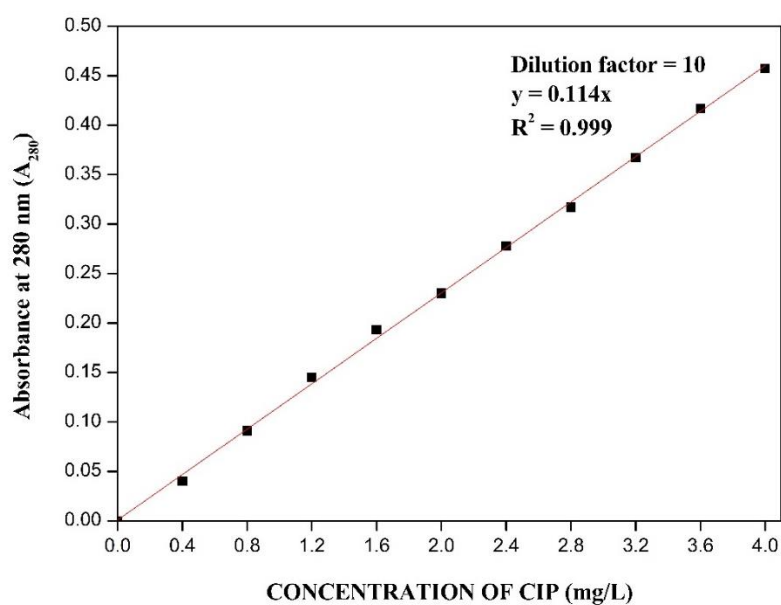


**Figure 3.7.** Standard calibration curve of the model pollutant: CIP

The percentage of CIP degradation (Eq. 3.4), COD reduction (Eq. 3.5), and kinetics (Eq. 3.6) are calculated according to the following equations:

$$\text{Degradation (\%)} = \frac{C_0 - C}{C_0} \times 100 \quad (3.4)$$

$$\text{COD reduction (\%)} = \frac{COD_0 - COD}{COD_0} \times 100 \quad (3.5)$$

$$-\ln \left[ \frac{C}{C_0} \right] = kt \quad (3.6)$$

where,  $C_0$  - initial concentration (mg/L),  $C$  - final concentration (mg/L),  $COD_0$  - initial COD (mg/L),  $COD$  - final COD (mg/L),  $k$  - rate constant of the reaction ( $\text{min}^{-1}$ ),  $t$  - reaction time (min).

The slope of the plot  $-\ln \left[ \frac{C}{C_0} \right]$  versus time, gives the rate of the reaction ( $k$ ). As reported in the literature (Li et al. 2012; Shetty et al. 2017), the degradation of antibiotics is found to usually follow a pseudo-first order reaction.

### 3.2.6. Identification of the degraded products

LC-MS with a UV detector and a column (5  $\mu\text{m}$  C-18 column, 4.6  $\times$  250 mm) was used to determine the degraded products of CIP after photocatalytic treatment. 0.1% formic acid in acetonitrile and 0.1% formic acid in water (16:84) was used as mobile phase. Injected volume was 10  $\mu\text{L}$  with a flow rate of 0.5 mL/min and a column temperature of 30°C. The analysis was carried out for 20 min at a maximum absorbance wavelength of 280 nm.

### 3.2.7. Role of reactive species in the degradation of CIP (scavenging studies)

The dominant reactive oxygen species such as electrons ( $e^-$ ), holes ( $h^+$ ), hydroxyl ( $\cdot\text{OH}$ ), and superoxide ( $\cdot\text{O}_2^-$ ) radicals responsible for the photocatalytic degradation were determined by performing the scavenging experiments. 1 mM triethanolamine (TEOA), 1 mM isopropyl alcohol (IPA), 1mM benzoquinone (BQ), and 50 mL ethanol were used as scavenging agents for  $h^+$ ,  $\cdot\text{OH}$ ,  $\cdot\text{O}_2^-$ , and  $e^-$  respectively (Wang et al. 2016a).



### 3.2.8. Residual antibacterial activity of the degraded CIP solution

After photocatalytic treatment, the degraded CIP solution was tested to assess its residual antibacterial activity against *E.coli* (MTCC 9541) by the agar well diffusion method. 100  $\mu$ L of *E.coli* was spread onto agar plates using L-shaped rod. Wells were punched on the solidified agar in the petri plates. 100  $\mu$ L of treated CIP solution collected at regular intervals (every 1 h sample) was added to each well. The plates were incubated at 37°C for 24 h to determine the zone of inhibition.

### 3.2.9. Preparation of bacterial cells and enumeration

All the glass and plastic wares were sterilized prior to use at 15 psi for 20 min in an autoclave. The *E.coli* strain (MTCC-9541) was grown in a Luria Bertani (LB) broth. A flask with 20 mL broth was inoculated with 100  $\mu$ L of bacterial culture and kept at 37°C under shaking conditions at 60 rpm for 24 h. The cells were harvested through centrifugation at 8000 rpm for 10 min at 8°C. The cells were then resuspended in a 0.9% saline solution (NaCl) and stored for further use. The viable cells were enumerated/quantified by the standard plate count method through a serial dilution (10-fold). 0.1mL of each diluted sample was plated onto Luria Bertani agar plates. Colonies were counted (using Eq. 3.7) after incubation at 37°C for 24h. A bacterial count of  $75 \times 10^8$  CFU (colony forming unit)/mL was obtained with a limit of detection (LOD) equal to 15 colonies (**Figure 3.8**). Further, the initial cell concentration was adjusted to  $10^8$  CFU/mL for the photocatalytic experiments. The range of number of colonies counted for analysis is 25-250 CFU/plate (as per the FDA Bacterial Analytical Manual).

$$\frac{CFU}{mL} = \frac{CFU \times Dilution\ factor}{Volume\ of\ Sample} = \frac{75 \times 10^7}{0.1} = 75 \times 10^8 \quad (3.7)$$

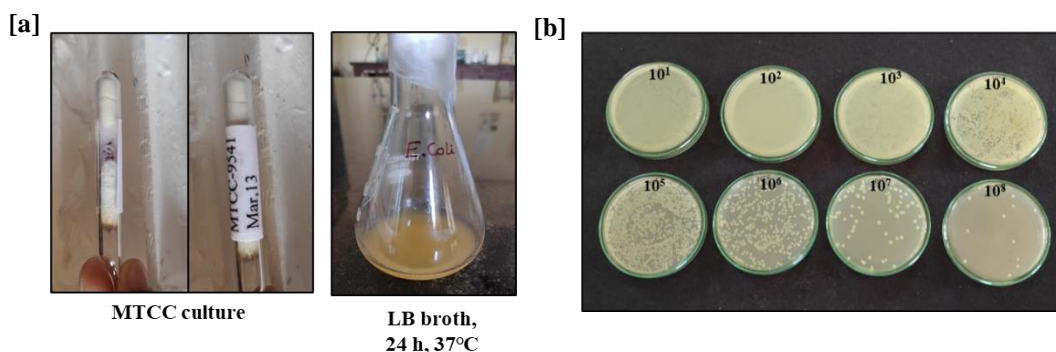


**Figure 3.8.** (a) MTCC culture grown in LB broth and (b) Enumeration of cells through serial dilution and plate count method

### 3.2.10. Photocatalytic disinfection in the absence and presence of antibiotic

Batch disinfection experiments (200 mL of reaction volume) were carried out with 10<sup>8</sup> CFU/mL as an initial *E.coli* cell concentration under sunlight for 180 min in the absence of antibiotic. Photolysis was performed using bacterial suspension alone.

Initially, *E.coli* was tested for resistance against various concentrations of ciprofloxacin, namely 1, 5, 10, and 100 ppm (Antibiotic resistance assay). Sterile deionized water was used as a control. Inhibition zones were observed for all these concentrations except 1 ppm (**Figure 3.9**). Hence, disinfection experiments in the presence of antibiotic were also carried out 10<sup>8</sup> CFU/mL (as an initial *E.coli* cell concentration) and 1 ppm of CIP under sunlight for 180 min. Photolysis was carried out by suspending bacteria in CIP solution without catalyst under sunlight for 180 min. At regular intervals of 15 min, the samples were collected, serially diluted, and plated onto agar plates. These plates were then incubated for 24 h at 37°C. Duplicate measurements were performed, and the average number of colonies with error bars was plotted. The log reduction was calculated using the following equation (Eq. 3.8).

$$\text{Log reduction} = \log_{10}(N_0 - N) \quad (3.8)$$

where,  $N_0$  - initial CFU/mL,  $N$  - final CFU/mL.

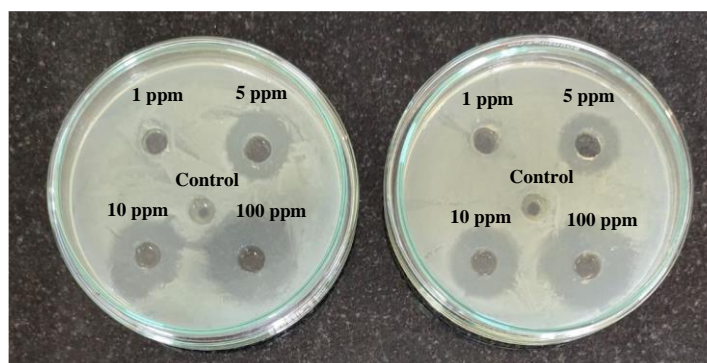


**Figure 3.9.** Antibiotic resistance assay

### **3.2.10.1. Regrowth studies and determination of $K^+$ ions**

The presence of organic matter (recalcitrant compounds – especially antibiotics) might help to utilize available carbon sources and contribute towards the survival of bacteria (Thayanukul et al. 2013; Zhao et al. 2014). The potential regrowth of bacteria in the photocatalytically treated sample was evaluated by storing the bacterial plates with zero number of colonies (observed after incubation) for 3 days in the dark at room temperature (Biancullò et al. 2019).

The release of  $K^+$  ions was determined using ICP-OES, as these are the major intracellular cations in the bacteria (Zacchia et al. 2016). This provides indirect evidence of cell membrane damage/loss of cell membrane integrity (Das et al. 2017; Foster et al. 2011).

### **3.2.11. Recyclability/reusability studies**

To determine the stability, the catalyst (suspended form)/ immobilized film was reused for five consecutive runs. After each run, the catalyst was recovered (suspended form) through centrifugation (8000 rpm, 15 min, 25°C), washing, and drying. The immobilized film was gently washed with deionized water after each run and dried overnight at room temperature. For each run (cycle), a fresh CIP solution was used.

### **3.2.12. Real water matrices**

The degradation and disinfection efficiencies of the best performing catalyst were determined using real water samples (tap water and river water). For experiments, 200

mL of real water samples were spiked with CIP (10 ppm) and *E.coli* ( $10^8$  CFU/mL). The river water was collected from the Kumaradhara River (Subramanya, Karnataka, India, 33°C) by grab sampling. The sample was stored on the same day in the refrigerator for further use. Tap water as available in laboratory was used. The characteristics of river water and tap water are given in **Table 3.2**.

**Table 3.2.** Characteristics of real water samples

<b>WATER SAMPLES</b>	<b>pH</b>	<b>Conductivity (mS/cm)</b>
Tap water	7.0	0.193
River water	7.0	0.068

**This page is left blank**

## CHAPTER 4

### PHOTOCATALYTIC DEGRADATION: SUSPENDED FORM

A series of B & Ce monodoped and codoped catalysts were synthesized using the green EDTA-citrate method as described in section 3.2.1. Four monodoped catalysts, namely, 0.1 at.% & 1 at.% Ce-TiO<sub>2</sub> and 1 at.% & 2 at.% B-TiO<sub>2</sub> were subjected to various characterizations (section 3.2.4) to evaluate their functional aspects. Accordingly, the catalyst samples are denoted as 0.1Ce-TiO<sub>2</sub>, 1Ce-TiO<sub>2</sub>, 1B-TiO<sub>2</sub>, and 2B-TiO<sub>2</sub>. The interplay between the B and Ce dopants in the codoped series (B<sub>x</sub>Ce<sub>1-x</sub>TiO<sub>2</sub>) is examined by keeping the overall dopant concentration at 1 at.% (on the basis of the best performing monodoped catalysts) in order to identify the synergistic effects resulting in improved photocatalytic performance. The B dopant level was represented as 'x' with a relatively higher concentration (nearer to 1 at.%). Thus, the values of 'x' are 0.9, 0.8, and 0.7 at.%, which means that the dopant levels of Ce are 0.1, 0.2, and 0.3 at.%, respectively.

The photocatalytic activity was determined using ciprofloxacin as the model pollutant and *E.coli* as the model organism (section 3.2.3) under sunlight. The degraded sample was analyzed for COD reduction and residual antibacterial activity (section 3.2.8). The degraded products were analyzed using LC-MS (section 3.2.6).

#### 4.1. CHARACTERIZATION OF THE SYNTHESIZED PHOTOCATALYSTS

##### 4.1.1. Particle size and BET surface area measurements

The particle size of the photocatalysts is in the range of 28-90 nm, while the surface area is in the range of 30-43 m<sup>2</sup>/g, and the results are tabulated in **Table 4.1**. It is well known that the particles of lesser size aid in higher photocatalytic activity due to the shorter migration distance from the point of generation to the surface of charge carriers (Jaiswal et al. 2016; Kumar et al. 2016; Seddigi et al. 2017). As observed from the Table 4.1, among the synthesized catalysts B<sub>0.8</sub>Ce<sub>0.2</sub>TiO<sub>2</sub> showed least particle size of 15.2 nm and B<sub>0.7</sub>Ce<sub>0.3</sub>TiO<sub>2</sub> showed highest surface area of 43.198 m<sup>2</sup>/g. These values are lesser in terms of particle size and higher in terms of surface

area when compared to TiO<sub>2</sub>. The variation in the particle size among the doped catalysts is discussed in the next section.

**Table 4.1.** Particle size of TiO<sub>2</sub> and the synthesized photocatalysts

PHOTOCATALYSTS	PARTICLE SIZE (nm)	BET surface area (m <sup>2</sup> /g)
TiO <sub>2</sub>	28	35
0.1 at.% Ce-TiO <sub>2</sub>	70.6	30.84
1 at.% Ce-TiO <sub>2</sub>	89.5	41.486
1 at.% B-TiO <sub>2</sub>	61.8	30.124
2 at.% B-TiO <sub>2</sub>	42.4	29.955
B <sub>0.9</sub> Ce <sub>0.1</sub> TiO <sub>2</sub>	38.7	31.323
B <sub>0.8</sub> Ce <sub>0.2</sub> TiO <sub>2</sub>	<b>15.2</b>	32.115
B <sub>0.7</sub> Ce <sub>0.3</sub> TiO <sub>2</sub>	58.5	<b>43.198</b>

#### 4.1.2. SEM Analysis

The surface morphologies of TiO<sub>2</sub>, Ce-TiO<sub>2</sub>, B-TiO<sub>2</sub>, and B<sub>x</sub>Ce<sub>1-x</sub>TiO<sub>2</sub> photocatalysts were characterized by SEM, and the images are shown in **Figure 4.1**. No specific treatment was provided to the TiO<sub>2</sub> sample prior to SEM analysis as it was commercially available. However, in the case of doped catalysts prior to SEM analysis, they were sonicated for 10 min and then dried.

The doped photocatalyst particles appeared as loosely packed irregular/elongated aggregates with a coarse surface, whereas TiO<sub>2</sub> particles appeared as closely packed small aggregates with a smooth surface. Similar results were observed in the literature (Karkare 2014; Wojcieszak et al. 2017). As seen in **Figure 4.1**, the 1Ce-TiO<sub>2</sub> SEM image exhibited a higher agglomeration than that of 0.1Ce-TiO<sub>2</sub>, although the latter has a smaller particle size. This higher agglomeration with an increase in the Ce dopant concentration can be attributed to the larger ionic radius of Ce than that of Ti, implying that it cannot enter the lattice of TiO<sub>2</sub>, and therefore, Ce peaks were observed in the XRD spectra (**Figure 4.4**). However, an opposite trend of a decrease in agglomeration (as well as particle size) with an increase in boron dopant concentration was observed. The decrease in agglomeration and particle size can be attributed to the smaller ionic radius of B than that of Ti, due to which it enters the TiO<sub>2</sub> lattice. Hence, no prominent B peaks were observed in the XRD spectra.

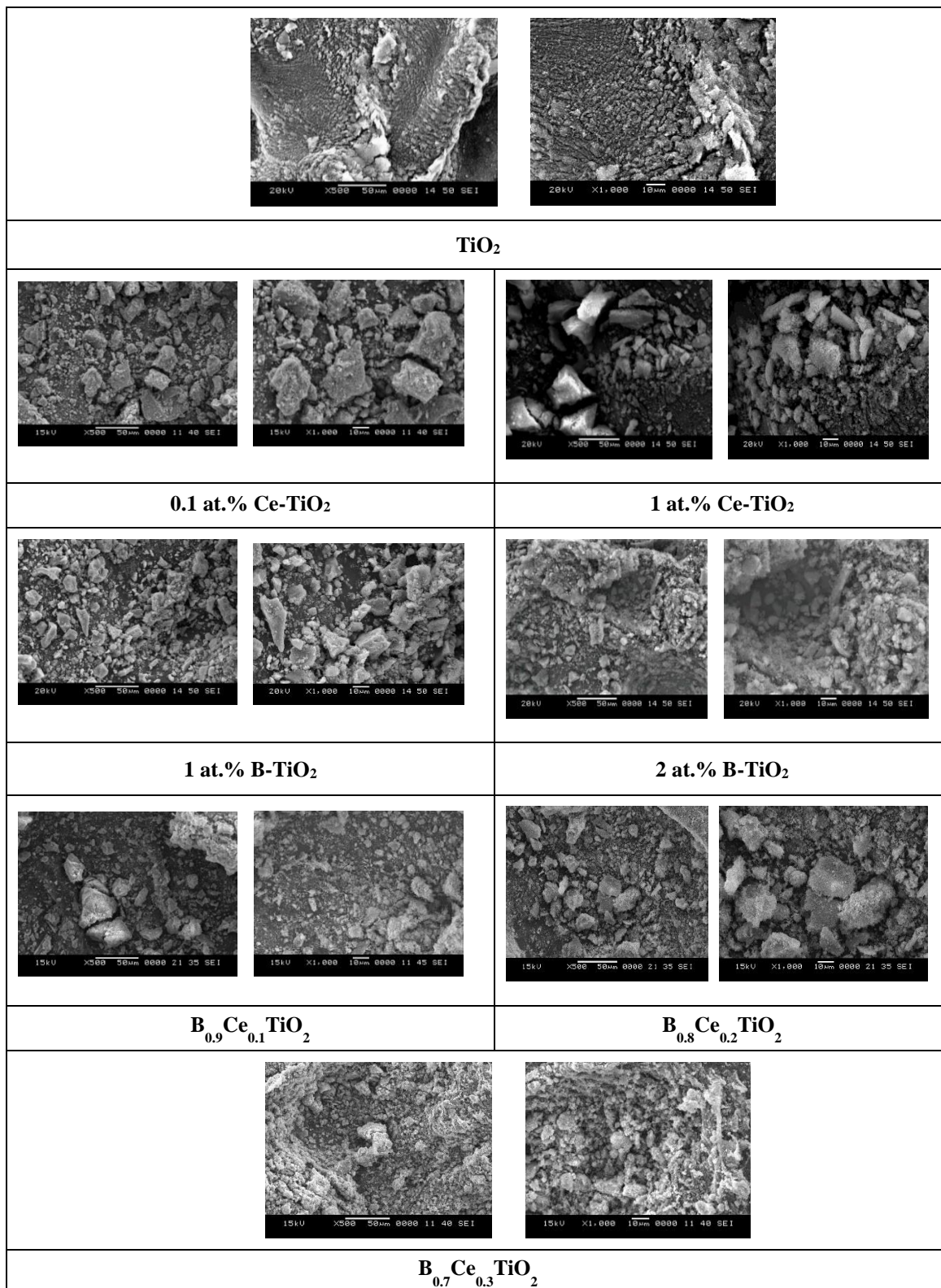


**Figure 4.1.** SEM images of TiO<sub>2</sub> and the synthesized photocatalysts (Left image is at X500 and the right image is at X1000 magnifications)



In the case of codoped catalysts, the agglomeration increased with an increase in Ce dopant concentrations (corresponding to a decrease in B dopant concentrations). Similar results about the ionic radius affecting the agglomeration and particle size have been mentioned in the literature (Pal et al. 2015). The elemental mapping (Figure 4.2 (a-c)) shows the distribution of cerium and boron dopants in the respective doped samples.

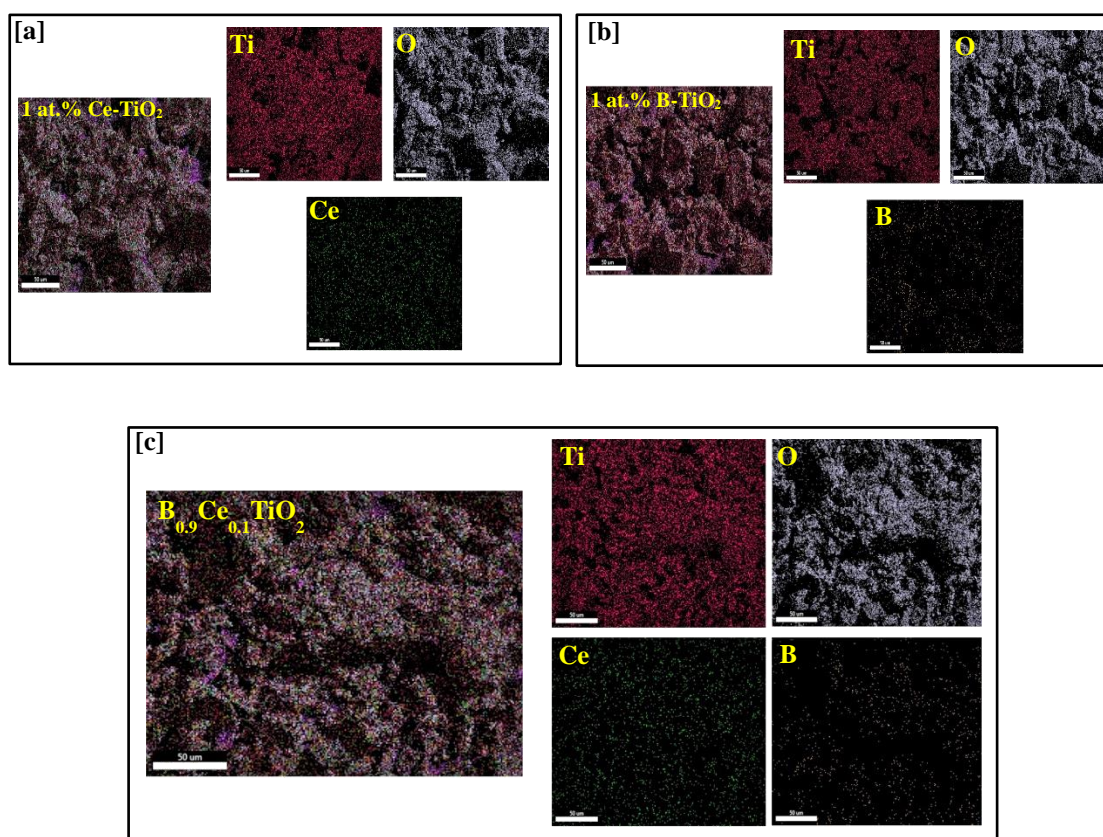
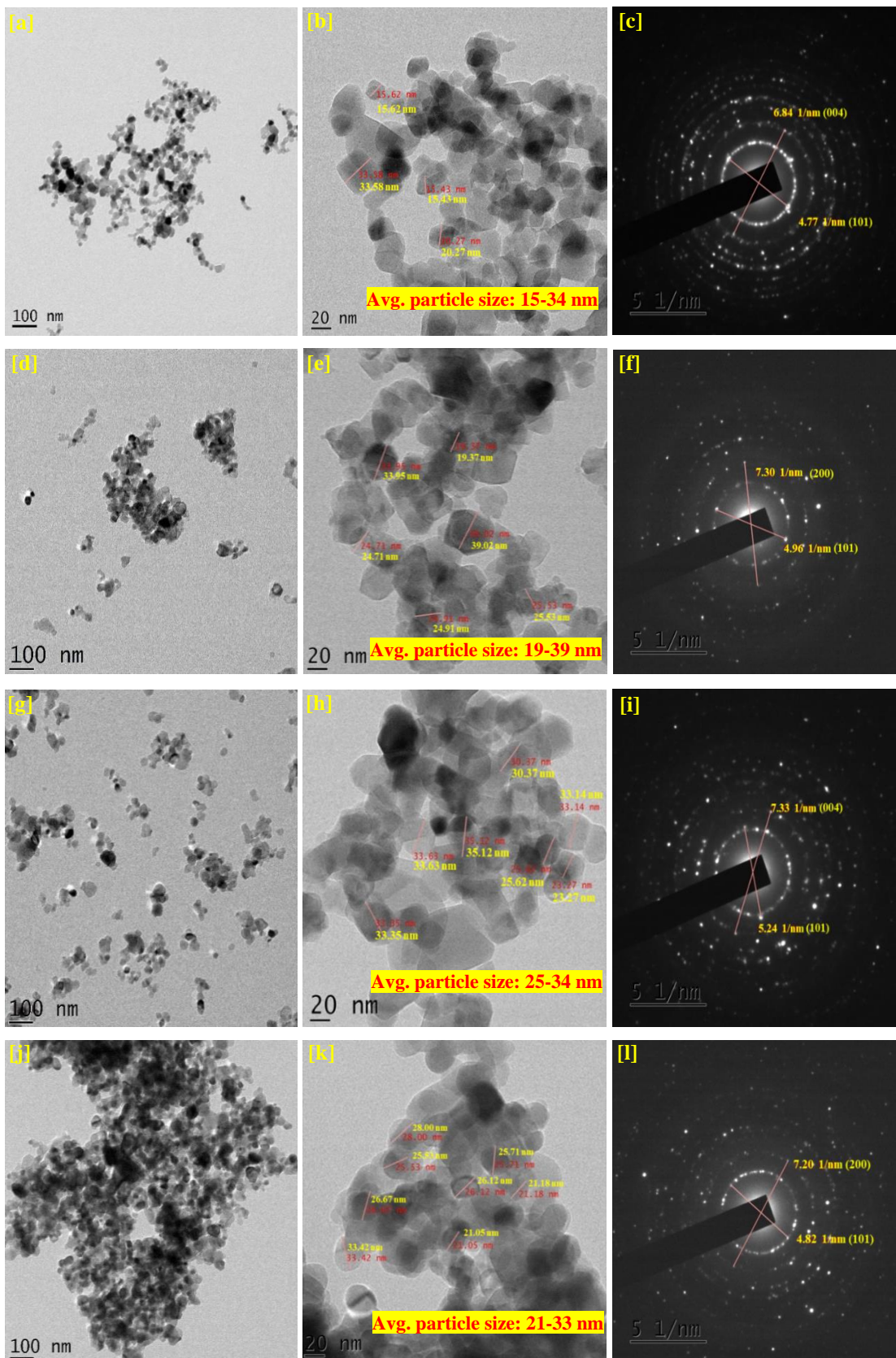


Figure 4.2. Elemental mapping (a) 1 at.% Ce-TiO<sub>2</sub>, (b) 1 at.% B-TiO<sub>2</sub> and (c) B<sub>0.9</sub>Ce<sub>0.1</sub>TiO<sub>2</sub>

#### 4.1.3. TEM Analysis

The detailed morphology of TiO<sub>2</sub> and three of the synthesized photocatalysts was evaluated by TEM as shown in Figure 4.3 (a-l). The synthesized photocatalysts appeared to be roughly spherical, with an average particle size in the range of 19–39 nm for 1Ce-TiO<sub>2</sub>, 25–34 nm range for 1B-TiO<sub>2</sub>, and 21–33 nm for B<sub>0.9</sub>Ce<sub>0.1</sub>TiO<sub>2</sub>. As observed in Figure 4.3 (c, f, i, l), the bright spots in the SAED (selected area electron diffraction) pattern affirm the crystalline nature of the photocatalyst.



**Figure 4.3.** TEM images and SAED patterns of [a-c]TiO<sub>2</sub>, [d-f] 1Ce-TiO<sub>2</sub>, [g-i] 1B-TiO<sub>2</sub> and [j-l] B<sub>0.9</sub>Ce<sub>0.1</sub>TiO<sub>2</sub>

The rings assigned with hkl values (101) and (004) correspond to the anatase phase, while those with (200) correspond to the CeO<sub>2</sub> phase. The hkl values were obtained from the literature for TiO<sub>2</sub> (Wang et al. 2016c) and for CeO<sub>2</sub> (Wen et al. 2017).

#### 4.1.4. XRD analysis

The effect of B and Ce dopants on the structure of TiO<sub>2</sub> was examined from the XRD spectra as shown in **Figure 4.4**. The anatase planes at around 25.26° (101), 36.9° (103), 37.9° (004), 38.7° (112), 48.07° (200), 53.99° (105), 55.07° (211), and 62.70° (204) (Vieira et al. 2018; Zhao et al. 2015b) and the rutile planes at around 27.37° (110), 36.11° (101), 41.35° (111), and 56.65° (220) (Li et al. 2014) were observed (TiO<sub>2</sub> JCPDS 21-1276 for anatase and JCPDS 21-1272 for rutile). The absence of B peak indicates the homogeneous commingling (uniform distribution) of boron in the synthesized photocatalysts. The Ce element exists in the form of CeO<sub>2</sub> and was observed at around 28.8° (111) and 56.90° (311) (JCPDS 43-1002) (Wen et al. 2017, 2018). Ce<sup>3+</sup> and Ce<sup>4+</sup> ions have a larger ionic radius (0.103 nm and 0.093 nm, respectively) than the Ti<sup>4+</sup> ions (0.068 nm). Hence either they exist on the TiO<sub>2</sub> surface as CeO<sub>2</sub> (Wang et al. 2016c), or Ti<sup>4+</sup> ions enter the Ce lattice with the formation of Ti-O-Ce bonds (El-Bahy et al. 2009; Vieira et al. 2018). The B ions with an ionic radius of 0.023 nm enter into the TiO<sub>2</sub> lattice, causing a rearrangement of atoms in the lattice (Wang et al. 2016c) with the formation of B-O-Ti bonds (Jaiswal et al. 2016). An intense crystalline peak (~ 25.30°) was observed in all the samples. Similar peaks were noted in the literature (Li et al. 2014; Thamaphat et al. 2008; Vieira et al. 2018; Wen et al. 2017; Zhao et al. 2015b). After doping, a slight shift in anatase and rutile peaks was observed, which suggests the creation of defects with oxygen vacancies (Mikaeili et al. 2018), thus enhancing the charge separation and, in turn, improving the photocatalytic activity.

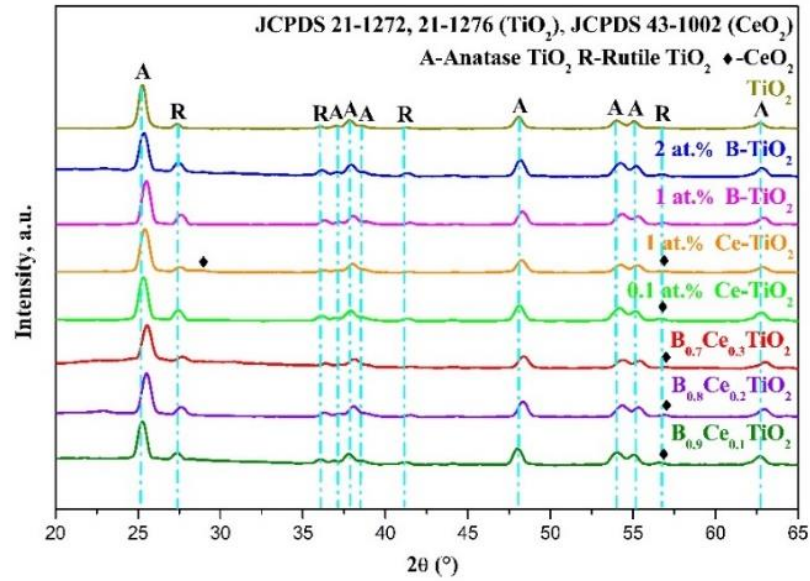


**Figure 4.4.** XRD spectra of  $\text{TiO}_2$  and the synthesized photocatalysts

Scherrer's equation was used to calculate each photocatalyst's crystallite size for both the anatase & rutile peaks, and this along with the lattice constants (variations in lattice parameters due to peak shift) are listed in **Table 4.2**. It is observed that, the lattice constants decreased with increasing Ce dopant concentrations (corresponding to an increase of lattice constants with an increase in B dopant concentrations). Also, the increase in the c-axis lattice constants with increasing B dopant concentrations suggests the incorporation of B into the  $\text{TiO}_2$  lattice (interstitial lattice position), leading to the occupation of O sites and thus is correlated with increasing oxygen vacancies (Wang et al. 2016c). Similarly, for the monodoped catalysts, a decrease ( $\text{Ce-TiO}_2$ ) and an increase ( $\text{B-TiO}_2$ ) in the lattice parameters were observed. These consistent variations suggest the synergistic effect of dopants in the codoped catalysts.

To estimate the proportion of anatase to rutile crystalline phases in the synthesized catalysts, the percentage of rutile  $X_r(\%)$ , was calculated using the Spurr and Myers equation as mentioned in section 3.2.4 (Eq 3.2). The computed  $X_r$  values are listed in **Table 4.2** and gives the following order in terms of increasing rutile phase content:  $1\text{Ce-TiO}_2 < 1\text{B-TiO}_2 / \text{B}_{0.8}\text{Ce}_{0.2}\text{TiO}_2 < \text{B}_{0.9}\text{Ce}_{0.1}\text{TiO}_2 < \text{B}_{0.7}\text{Ce}_{0.3}\text{TiO}_2 < 0.1\text{Ce-TiO}_2 < 2\text{B-TiO}_2$ .

**Table 4.2.** XRD parameters of TiO<sub>2</sub> and the synthesized photocatalysts

Photocatalysts	Crystallite size (nm)		Unit cell parameters				X <sub>r</sub> (%)
			Anatase		Rutile		
	Anatase	Rutile	a(b), Å	c, Å	a(b), Å	c, Å	
TiO <sub>2</sub>	15.99	30.05	3.784	9.715	6.51	2.690	12.18
0.1 at.% Ce-TiO <sub>2</sub>	14.06	25.20	3.782	9.563	6.502	2.690	23.57
1 at.% Ce-TiO <sub>2</sub>	16.95	23.21	3.772	9.445	6.458	2.680	14.13
1 at.% B-TiO <sub>2</sub>	19.82	26.24	3.768	9.314	6.476	2.677	22.61
2 at.% B-TiO <sub>2</sub>	17.96	26.45	3.776	9.540	6.494	2.687	28.50
B <sub>0.9</sub> Ce <sub>0.1</sub> TiO <sub>2</sub>	20.52	28.94	3.788	9.628	6.516	2.697	25.78
B <sub>0.8</sub> Ce <sub>0.2</sub> TiO <sub>2</sub>	17.33	21.10	3.766	9.306	6.458	2.677	22.61
B <sub>0.7</sub> Ce <sub>0.3</sub> TiO <sub>2</sub>	16.83	18.89	3.762	9.234	6.442	2.674	26.25

#### 4.1.5. XPS analysis

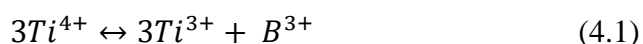
The Ti 2p, O 1s, B 1s, and Ce 3d spectra obtained from XPS measurements are shown in **Figure 4.5**. The standard value of 458.7 eV is assigned to the Ti 2p<sub>3/2</sub> and 464.4 eV to the Ti 2p<sub>1/2</sub> orbits, indicating the presence of Ti<sup>4+</sup>. From **Figure 4.5a**, the Ti 2p peak appears to be slightly shifted from the standard values of binding energy for the doped catalysts, indicating the presence of Ti<sup>3+</sup>. This peak shift indicates the incorporation of B dopant into the TiO<sub>2</sub> lattice (Shi et al. 2019) without the formation of prominent B peaks as indicated in the XRD analysis, partial substitution of O atoms in the TiO<sub>2</sub> lattice by the B atoms (Xu et al. 2009), and also to the efficient transfer of electrons (Maarisetty and Baral 2019).

The O 1s peaks appeared at around 529-530 eV (**Figure 4.5b**), corresponding to principally the surface OH<sup>-</sup> group (529.8 eV)(Jaiswal et al. 2016)/lattice oxygen (529.5 eV; 529.8 eV)(Maarisetty and Baral 2019; Zhao et al. 2015b). The lattice oxygen leads to the Ti-O-Ce bond formation (as observed from XRD analysis), favoring adsorption. The higher binding energy in the case of codoped catalysts (when compared to 529.34 eV observed for TiO<sub>2</sub>) suggests the existence of a Ti-O-B bond as observed from XRD analysis (Shi et al. 2019). As reported in the literature



(Gharagozlou and Bayati 2014), OH<sup>-</sup> groups combine with oxygen vacancies; hence these OH<sup>-</sup> groups indicate the presence of oxygen vacancies in the photocatalysts.

As reported in the literature (Jaiswal et al. 2016; Patel et al. 2015), interstitial boron is attributed to the binding energy between 191 eV and 192 eV. The B 1s standard binding energy in H<sub>3</sub>BO<sub>3</sub> or B<sub>2</sub>O<sub>3</sub> corresponds to 193 eV (B-O bond) and in TiB<sub>2</sub> corresponds to 187.5 eV (B-Ti bond) (Chen et al. 2006; Wang et al. 2014). In **Figure 4.5c**, a broad peak corresponding to interstitial B appeared at 190.95 eV and 192.33 eV for 1B-TiO<sub>2</sub> and 2B-TiO<sub>2</sub>, respectively. In 2B-TiO<sub>2</sub>, a small additional peak at 188.10 eV has appeared, corresponding to substitutional B. This indicates that as the concentration of B increases, it occupies both interstitial and substitutional lattice positions. In the case of codoped catalysts, 191.94 eV (B<sub>0.9</sub>Ce<sub>0.1</sub>TiO<sub>2</sub>) and 191.81 eV (B<sub>0.8</sub>Ce<sub>0.2</sub>TiO<sub>2</sub>, B<sub>0.7</sub>Ce<sub>0.3</sub>TiO<sub>2</sub>) can be attributed to the formation of B-O-Ti bonds with B occupying the interstitial lattice position. Also, the increase in the c-axis lattice constant with an increase in B dopants concentration indicates that the B ions occupy the interstitial lattice position, as confirmed from the XRD results. The presence of interstitial boron results in the reduction of Ti<sup>4+</sup> to Ti<sup>3+</sup> (facilitating photogenerated charge separation effectively, thereby enhancing the photocatalytic activity) as per the following equation:(Wang et al. 2016c)



In the case of Ce, the Ce 3d peaks (**Figure 4.5d**) appeared at 903.03 eV, 916.08 eV, which corresponds to 3d<sub>3/2</sub> orbit whereas 883.12 eV and 899.32 eV corresponds to 3d<sub>5/2</sub> orbit. 903.1 eV and 884.3 eV peaks correspond to Ce<sup>4+</sup>, according to the literature (Wang et al. 2018). In the doped catalysts, the Ce 3d peaks corresponding to 3d<sub>3/2</sub> orbit appeared at around 901-903 eV, and 3d<sub>5/2</sub> orbit appeared at around 883-884 eV. This is attributed to the presence of Ce<sup>4+</sup> and results from the transfer of electrons from O 2p to an empty Ce 4f orbital (Liu et al. 2005; Wang et al. 2016c).

The elemental compositions of the doped catalysts are in accordance with the selected compositions and are given in **Table 4.3**.

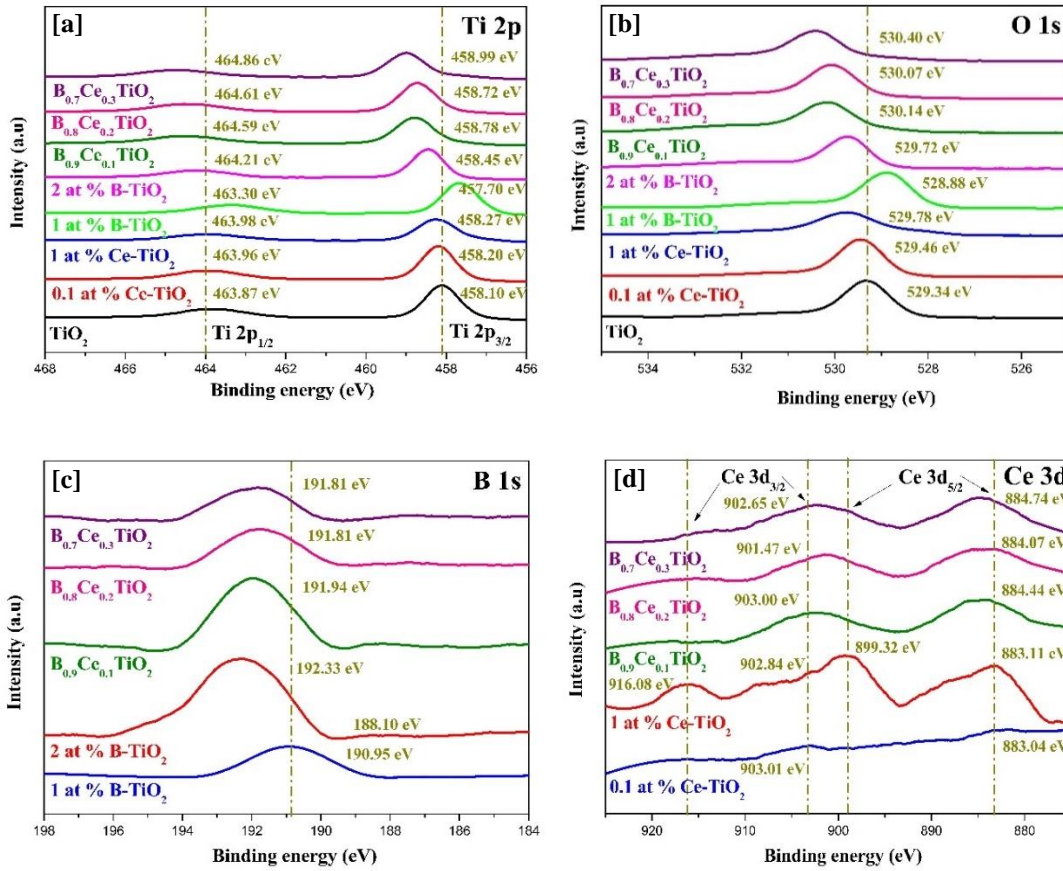


Figure 4.5. XPS spectra  $\text{TiO}_2$  and the synthesized photocatalysts

Table 4.3. Elemental composition of  $\text{TiO}_2$  and the synthesized photocatalysts from XPS analysis

Photocatalysts	XPS (atomic %)			
	Ti	O	B	Ce
$\text{TiO}_2$	65.38	34.62	-	-
0.1 at.% Ce- $\text{TiO}_2$	66.01	33.86	-	0.13
1 at.% Ce- $\text{TiO}_2$	52.06	46.85	-	1.09
1 at.% B- $\text{TiO}_2$	72.55	26.38	1.07	-
2 at.% B- $\text{TiO}_2$	54.84	43.07	2.09	-
$\text{B}_{0.9}\text{Ce}_{0.1}\text{TiO}_2$	58.66	40.12	1.12	0.10
$\text{B}_{0.8}\text{Ce}_{0.2}\text{TiO}_2$	53.66	45.39	0.77	0.18
$\text{B}_{0.7}\text{Ce}_{0.3}\text{TiO}_2$	59.19	39.79	0.71	0.31

An increase in peak area corresponding to  $\text{Ti}^{3+}$  indicates the removal of oxygen from the lattice or the formation of oxygen vacancies (Bharti et al. 2016). The  $\text{Ti}^{3+}/\text{Ti}^{4+}$  ratio was calculated using the XPS peak area values and the results are as follows:  $\text{B}_{0.9}\text{Ce}_{0.1}\text{TiO}_2 - 0.097 > 1\text{Ce-TiO}_2 - 0.095 > 1\text{B-TiO}_2 - 0.087 >$

$B_{0.8}Ce_{0.2}TiO_2 - 0.086 > 0.1CeTiO_2 - 0.079 > B_{0.7}Ce_{0.3}TiO_2 - 0.056 > 2B-TiO_2 - 0.053$ . These results are in agreement with the results of the PL analysis (see section 4.1.7), indicating lower recombination as  $Ti^{3+}$  defects promote the separation of photoelectrons and holes effectively (creating trap centers), thus reducing the recombination of photoexcited charges (Huang et al. 2016b; Xu et al. 2017).

#### 4.1.6. RAMAN spectroscopy

The vibrational modes of Raman spectroscopy illustrate the crystal phase structure. As depicted in **Figure 4.6**, anatase Raman modes of  $E_{g(1)}$ ,  $E_{g(2)}$ ,  $E_{g(3)}$ ,  $B_{1g}$ , and  $A_{1g} + B_{1g}$  correspond to the wavenumbers: ( $144\text{ cm}^{-1}$ ), ( $196\text{ cm}^{-1}$ ), ( $638\text{ cm}^{-1}$ ), ( $396\text{ cm}^{-1}$ ), and ( $517\text{ cm}^{-1}$ ) respectively were observed for all the photocatalysts. Similar results have been reported in the literature (Apopei et al. 2014; Bettinelli et al. 2007; Ho et al. 2015; Jaiswal et al. 2016; Lan et al. 2014; Li et al. 2014; Martin et al. 2015; Zhang et al. 2000). The intensity of  $E_{g(1)}$  peak was higher in all the photocatalysts as reported in the literature (Martin et al. 2015). Even though it is a sensitive technique, no rutile and Ce peaks were detected. Here also, the absence of boron signal was noticeable, as observed earlier in the XRD analysis.

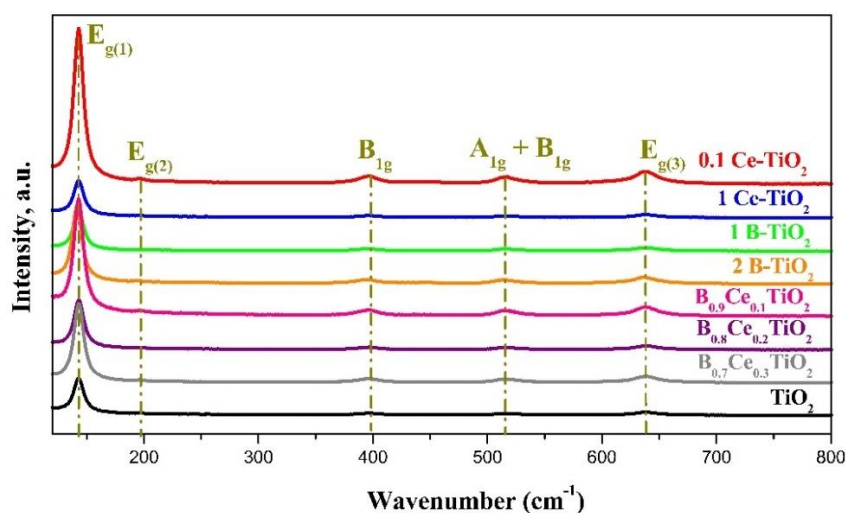


**Figure 4.6.** RAMAN spectra of  $TiO_2$  and the synthesized photocatalysts

#### 4.1.7. DRS and PL analysis

The diffuse reflectance spectra (DRS) of  $TiO_2$  and the synthesized photocatalysts are illustrated in **Figure 4.7a**.  $TiO_2$  is assumed to be an indirect semiconductor (Wang



et al. 2016c), and the bandgap energy ( $E_g$ ) values are calculated using equation 3.3 (section 3.2.4).

From the plot of  $(ah\nu)^{1/2}$  versus  $(h\nu)$ , the bandgap energy values were determined (Table 4.4). The Tauc plots of the synthesized photocatalysts are represented in Figure 4.7 (b-i).

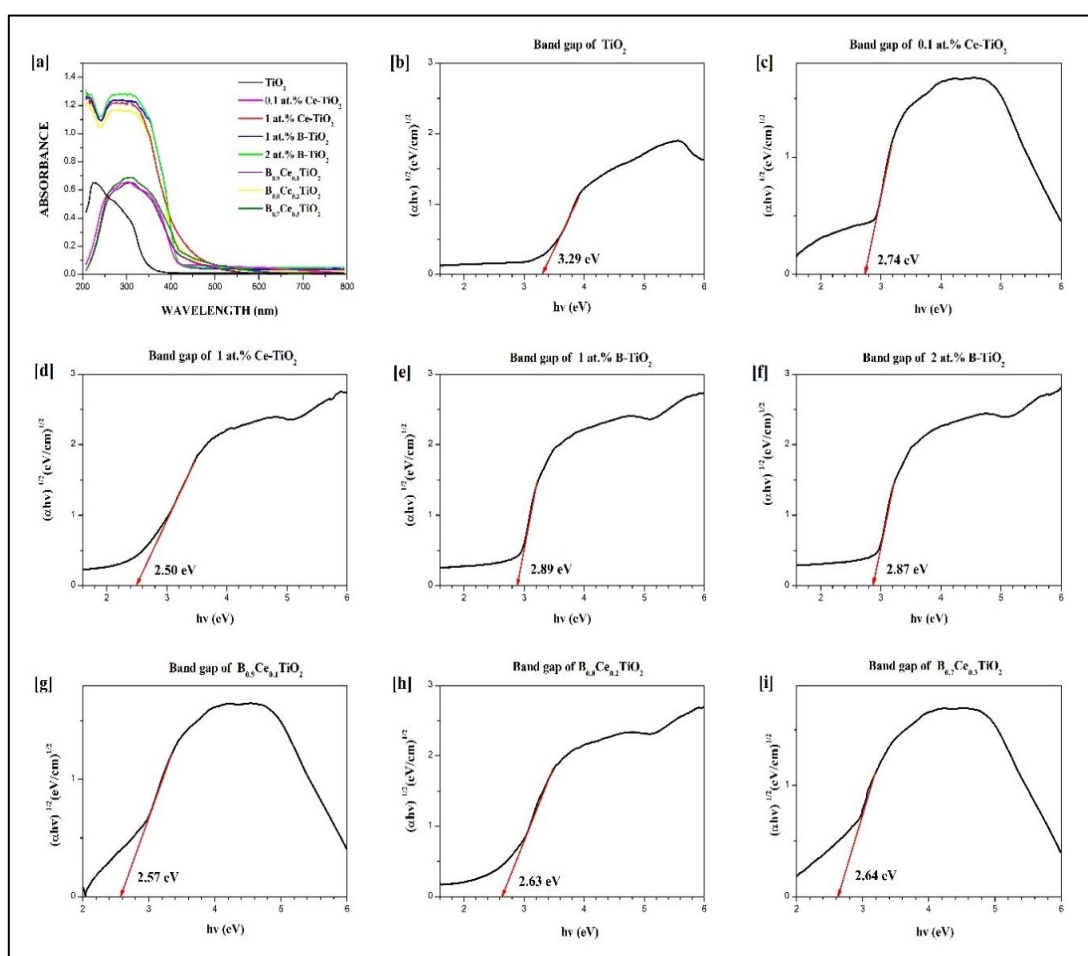


**Figure 4.7.** (a) Wavelength vs. absorbance plot, (b-i) Tauc plot showing the bandgap of  $\text{TiO}_2$  and the synthesized photocatalysts

In all the doped catalysts, the absorption edges were located at a wavelength longer than 420 nm. This shift of absorption spectra indicates the addition of new energy levels, which effectively separate the photogenerated charges required for the photocatalytic activity. The hybridization between Ti, B, and O states leads to the formation of B-O-Ti bond, as confirmed from XRD analysis, which is responsible for narrowing the bandgap through the formation of new bands (Jaiswal et al. 2016). In

the case of Ce, hybridization of O 2p with Ce 4f (as observed from the XPS result) produces an impurity band that narrows the bandgap, traps, and transfers the photogenerated charges effectively for an efficient photocatalytic activity (Maarisetty and Baral 2019). Co-doping has narrowed the bandgap energy values observed as:  $B_{0.9}Ce_{0.1}TiO_2$  (2.57 eV),  $B_{0.8}Ce_{0.2}TiO_2$  (2.63 eV),  $B_{0.7}Ce_{0.3}TiO_2$  (2.64 eV). These values are in between the range of bandgap energy values observed for the monodoped catalysts (2.5 – 2.9 eV), suggesting a synergistic effect of the dopants. A similar range of bandgap values has been reported in the literature (Wang et al. 2016c).

**Table 4.4.** Bandgap energy values of the photocatalysts from the Tauc plot

PHOTOCATALYSTS	Bandgap (eV)	Bandgap (eV) in literature (Wang et al. 2016c)
$TiO_2$	3.29	3.2
<b>0.1 at.% Ce-<math>TiO_2</math></b>	2.74	2.48
<b>1 at.% Ce-<math>TiO_2</math></b>	2.50	
<b>1 at.% B-<math>TiO_2</math></b>	2.89	2.95
<b>2 at.% B-<math>TiO_2</math></b>	2.87	
<b><math>B_{0.9}Ce_{0.1}TiO_2</math></b>	2.57	2.69
<b><math>B_{0.8}Ce_{0.2}TiO_2</math></b>	2.63	
<b><math>B_{0.7}Ce_{0.3}TiO_2</math></b>	2.64	

Photoluminescence (PL) emission spectra of  $TiO_2$  and the doped catalysts are depicted in **Figure 4.8**. Three distinct peaks were recorded. Two peaks around 470 nm and 570 nm in the visible light range are attributed to oxygen vacancies arising from surface defects. These observations are consistent with (470 nm)(Wang et al. 2016c) and (572 nm)(Jaiswal et al. 2016). Another peak around 380 nm corresponds to bandgap recombination (Wang et al. 2016c). From **Figure 4.8**, the decrease in PL intensity is of the following order:  $TiO_2 > 2B-TiO_2 > B_{0.7}Ce_{0.3}TiO_2 > 0.1Ce-TiO_2 > 1B-TiO_2 > B_{0.8}Ce_{0.2}TiO_2 > B_{0.9}Ce_{0.1}TiO_2 > 1Ce-TiO_2$ . The lower the PL intensity, the higher the separation of electron-hole pairs trapped in dopant sites. Thus, these monodoped and codoped catalysts showed lower recombination, suggesting effective separation of photogenerated charges for promising/higher photocatalytic activity.

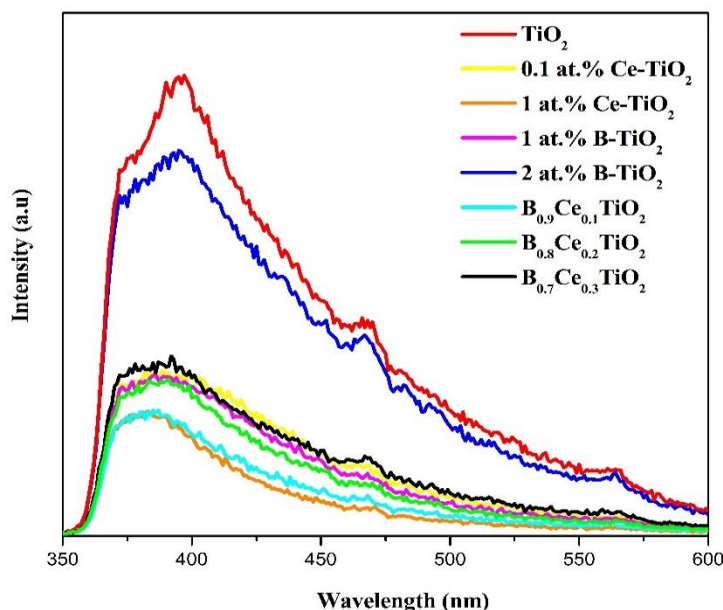


Figure 4.8. PL spectra of TiO<sub>2</sub> and the synthesized photocatalysts

## 4.2. PHOTOCATALYTIC TREATMENT OF CIP

### 4.2.1. Effect of catalyst loading

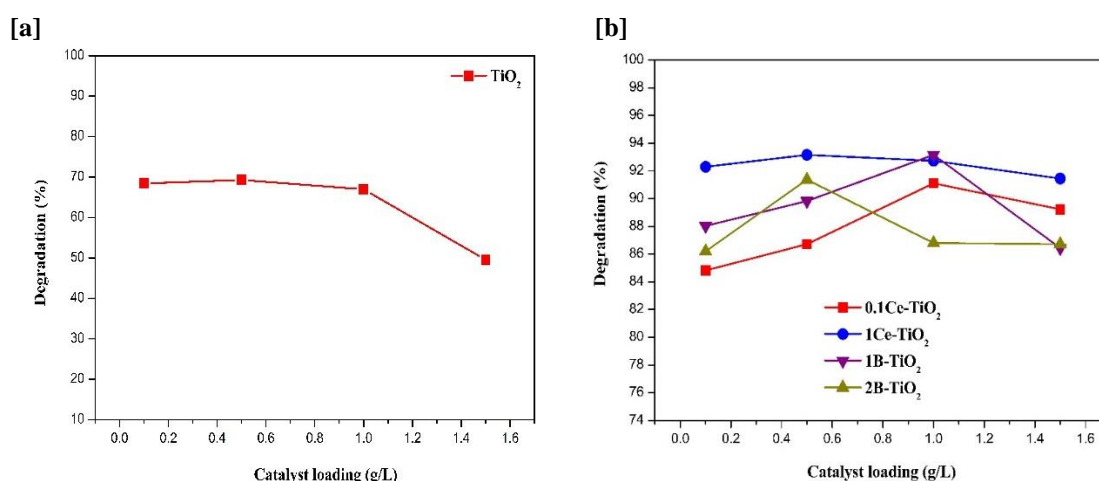
The effect of varying catalyst loading (0.1, 0.5, 1.0 and 1.5 g/L) on the degradation of CIP (10 ppm solution) was ascertained using TiO<sub>2</sub> for comparison, Ce-TiO<sub>2</sub>, B-TiO<sub>2</sub>, and B<sub>x</sub>Ce<sub>1-x</sub>TiO<sub>2</sub> series of catalyst and the results are illustrated in **Figure 4.9 (a-c)**. TiO<sub>2</sub> showed 69.29% degradation (**Figure 4.9a**) at an optimum catalyst loading of 0.5 g/L.

1B-TiO<sub>2</sub> and 2B-TiO<sub>2</sub> showed 93.16% and 91.37% degradation (**Figure 4.9b**) at an optimum catalyst loading of 1.0 g/L and 0.5 g/L, respectively. B-TiO<sub>2</sub> catalysts showed adsorption percentages in the range of 13-16% only (**Figure 4.11**). Similar results are reported for rhodamine B dye degradation (Jaiswal et al. 2016). The optimum catalyst loading obtained in the case of 0.1Ce-TiO<sub>2</sub> is 1.0 g/L and 0.5 g/L for 1Ce-TiO<sub>2</sub> (**Figure 4.9b**). 0.1Ce-TiO<sub>2</sub> and 1Ce-TiO<sub>2</sub> showed 91.11% and 93.22% degradation respectively. A higher rate of adsorption of 24.77% and 48.71% (**Figure 4.11**) was observed for 0.1Ce-TiO<sub>2</sub> and 1Ce-TiO<sub>2</sub>, respectively. The difference in the optimum catalyst loading value between boron and cerium dopants was due to the lower bandgap energy and higher adsorption which promoted an effective charge

separation and reduced recombination. Also, from the scavenging studies (see section 4.2.7), it is evident that electrons are the dominant reactive species responsible for photocatalytic activity, especially in the case of Ce-TiO<sub>2</sub>, thus implying the effective photogenerated charge separation.

An optimum catalyst dosage of 0.5 g/L was observed for all the codoped catalysts. As seen in **Figure 4.9c**, the co-doped catalysts showed CIP degradation efficiency in the order of: B<sub>0.8</sub>Ce<sub>0.2</sub>TiO<sub>2</sub> (97.43%) > B<sub>0.9</sub>Ce<sub>0.1</sub>TiO<sub>2</sub> (92.55%) > B<sub>0.7</sub>Ce<sub>0.3</sub>TiO<sub>2</sub> (91.57%). Interestingly, B<sub>0.7</sub>Ce<sub>0.3</sub>TiO<sub>2</sub>, with the higher surface area among the synthesized catalysts, did not show the highest degradation activity, possibly due to the lower degree of crystallinity (**Table 4.2**). Catalysts with a higher degree of crystallinity and a lower surface area have shown higher photocatalytic activity (Mazinani et al. 2014).

As reported in the literature (Das et al. 2018; Kumar et al. 2016), with an increase in the catalyst loading, the photocatalytic efficiency decreases due to the shielding effect, thus reducing the penetration of light in the solution. Also, the turbidity of the solution (catalyst shielding) increases with a corresponding reduction in opacity. Additionally, blockage of the catalyst's active sites can occur due to agglomeration, causing a decrease in the surface area. Hence, the efficiency has increased up to an optimum catalyst loading value, and then it has either decreased or remained constant.



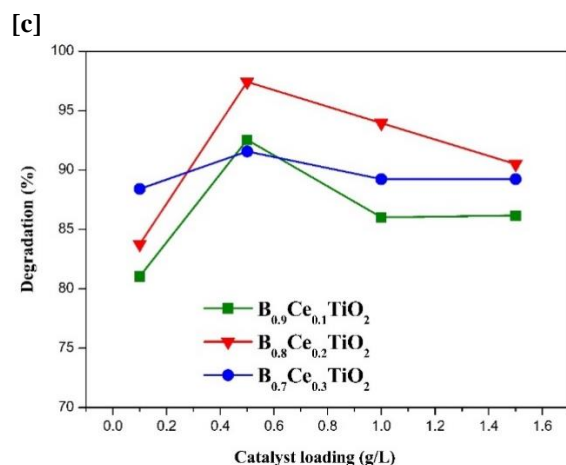
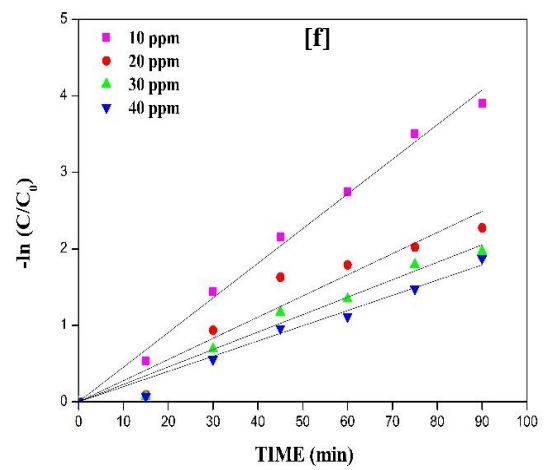
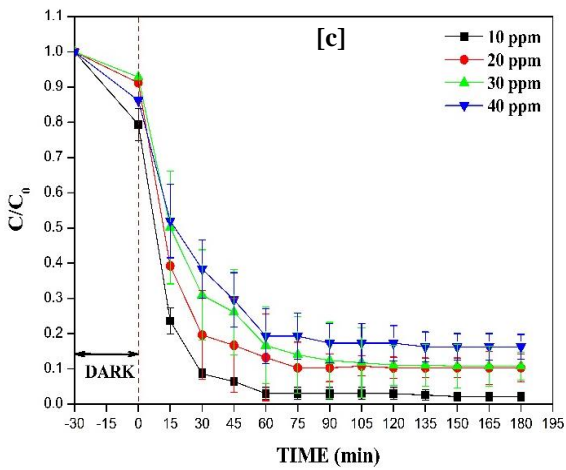
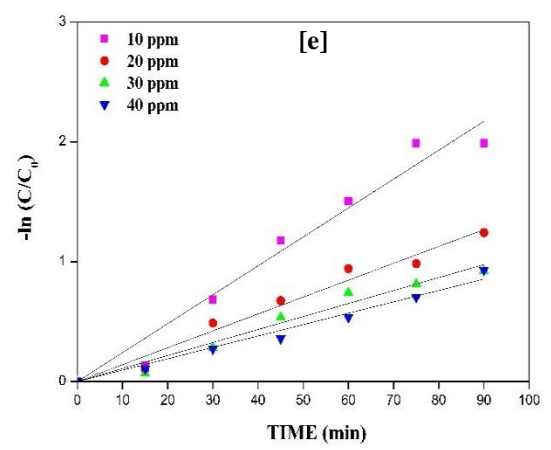
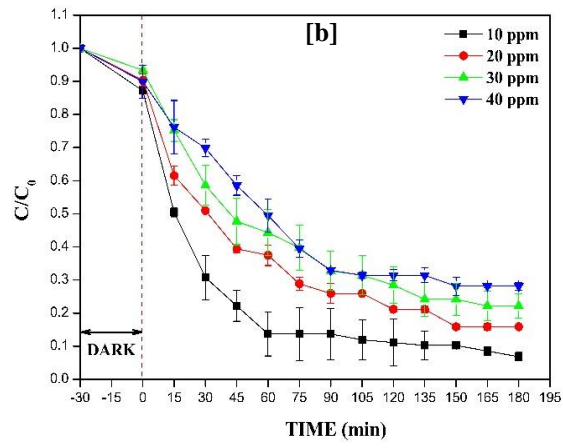
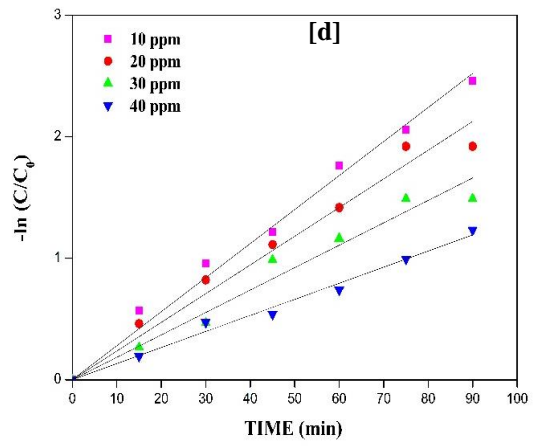
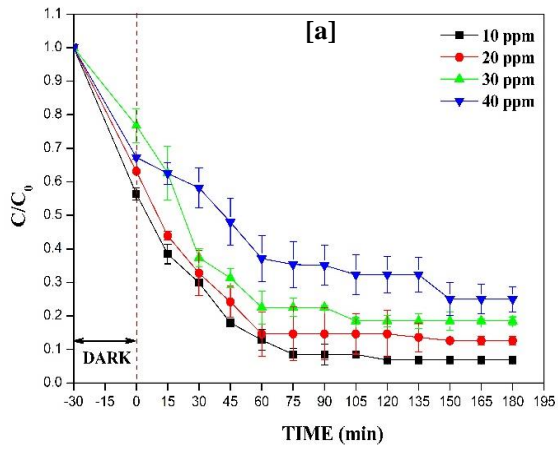


**Figure 4.9.** Effect of catalyst loading on the degradation of CIP using (a)  $TiO_2$ , (b) Ce- $TiO_2$  & B- $TiO_2$  series and (c)  $B_xCe_{1-x}TiO_2$  series

#### 4.2.2. Effect of initial concentration and kinetics

For the best performing catalysts (1Ce- $TiO_2$ , 1B- $TiO_2$ , and  $B_{0.8}Ce_{0.2}TiO_2$ ) at their optimum catalyst dosage, the initial concentrations of CIP were varied from 10–40 mg/L. The kinetics plot of the same is given in **inset Figure 4.10 (a-c)**. The reaction kinetics follows a pseudo-first-order reaction. The  $k$  and  $R^2$  values are tabulated in **Table 4.5** and summarized in **Figure 4.5d**. The rate constant ( $k$ ) decreased with an increase in the initial concentrations of the pollutant.

With increasing initial concentrations, the degradation efficiency decreased, which can be ascribed to the competition from the excess pollutant molecules for the catalyst active sites and a decrease in the availability of photons. Also, the ratio of radicals generated/pollutant molecules decreases as the catalyst loading and light energy remains constant. A similar trend of decrease in the degradation efficiency ( $k$  value) with an increase in the initial pollutant concentrations has been reported in the literature (Das et al. 2018).



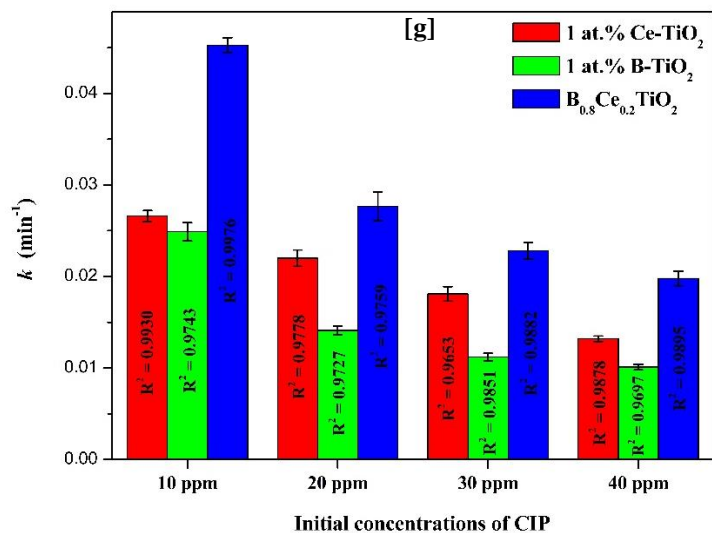


**Figure 4.10.** Effect of initial concentrations of CIP on the degradation using (a) 1Ce-TiO<sub>2</sub>, (b) 1B-TiO<sub>2</sub>, (c) B<sub>0.8</sub>Ce<sub>0.2</sub>TiO<sub>2</sub>, (d-f) Kinetics plot, and (g) Summary of kinetics data

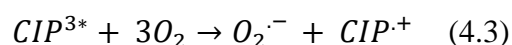
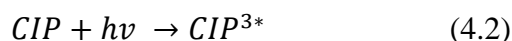
**Table 4.5.** Kinetics of CIP degradation

PHOTOCATALYSTS	$k$ (min <sup>-1</sup> )				$R^2$			
	10 ppm	20 ppm	30 ppm	40 ppm	10 ppm	20 ppm	30 ppm	40 ppm
1 at.% Ce-TiO <sub>2</sub>	0.0266 ± 0.0006	0.0220 ± 0.0009	0.0181 ± 0.0008	0.0132 ± 0.0003	0.9930	0.9778	0.9653	0.9878
1 at.% B-TiO <sub>2</sub>	0.0249 ± 0.0010	0.0141 ± 0.0005	0.0112 ± 0.0004	0.0101 ± 0.0003	0.9743	0.9727	0.9851	0.9697
B <sub>0.8</sub> Ce <sub>0.2</sub> TiO <sub>2</sub>	0.0452 ± 0.0008	0.0276 ± 0.0016	0.0228 ± 0.0009	0.0198 ± 0.0008	0.9976	0.9759	0.9882	0.9895

### 4.2.3. Mineralization of CIP

The photolysis, photocatalytic degradation, and COD reduction efficiencies are illustrated in **Figure 4.11**. In the absence of the catalyst, CIP showed 32% degradation, which indicates the stability of the pollutant even after photolysis, and hence further treatment with the synthesized photocatalysts is essential. The photolytic degradation of CIP, as observed, might have occurred through photooxygenation reactions, as reported by Salma et al. (2016). These reactions depend on the electronically excited CIP (Eq. 4.2), which might form radicals through single bond homolysis. Peroxyl radicals (CIP-O-O<sup>•</sup>) formed can decompose and

generate oxidation products. Other mechanism includes the formation of a superoxide radical anion and a substrate radical cation through  $e^-$  transfer to molecular oxygen, and these radical cations hydrolyze or recombine to produce the final products (Eq. 4.3).



0.1 and 1Ce-TiO<sub>2</sub> photocatalysts showed 68% and 92% of COD reduction, respectively, whereas 1B-TiO<sub>2</sub> and 2B-TiO<sub>2</sub> showed 93% and 64% of COD reduction, respectively. In the case of codoped catalysts, 82% (B<sub>0.9</sub>Ce<sub>0.1</sub>TiO<sub>2</sub>), 96% (B<sub>0.8</sub>Ce<sub>0.2</sub>TiO<sub>2</sub>), and 80% (B<sub>0.7</sub>Ce<sub>0.3</sub>TiO<sub>2</sub>) reduction was observed. The COD reduction was marginally lesser than the observed degradation, which may be ascribed to the formation of stable intermediate products of degradation (Paul et al. 2007). Also, it was noted that the complete mineralization of the organic compounds is generally a time-dependent process (Chen et al. 2019). Thus, it is noted that the B<sub>0.8</sub>Ce<sub>0.2</sub>TiO<sub>2</sub> photocatalyst showed the highest COD reduction.

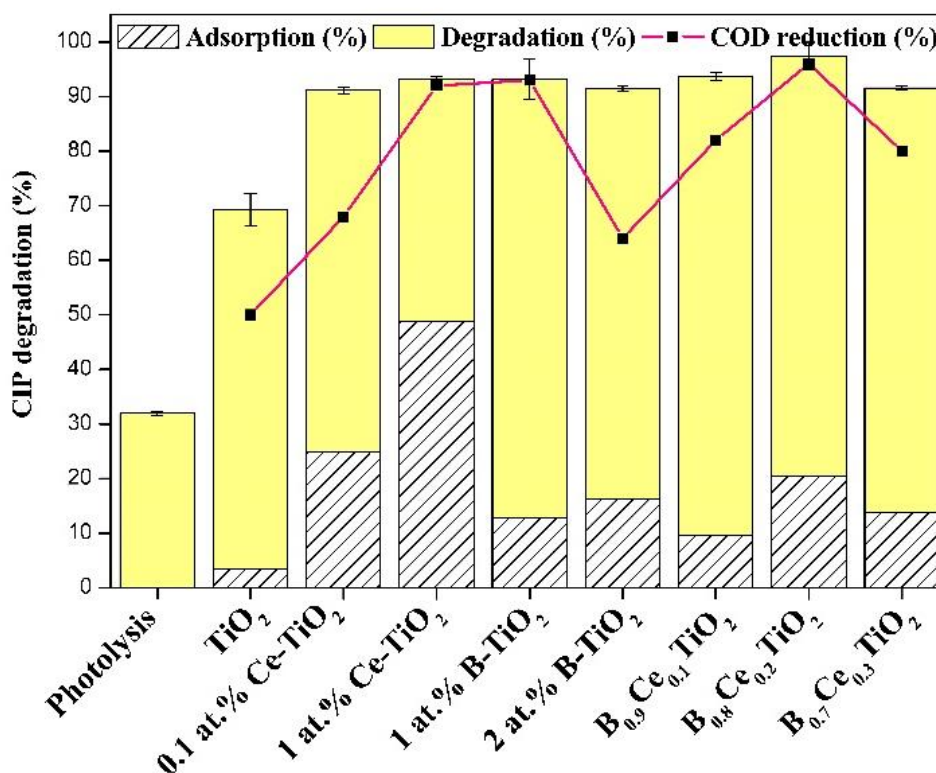
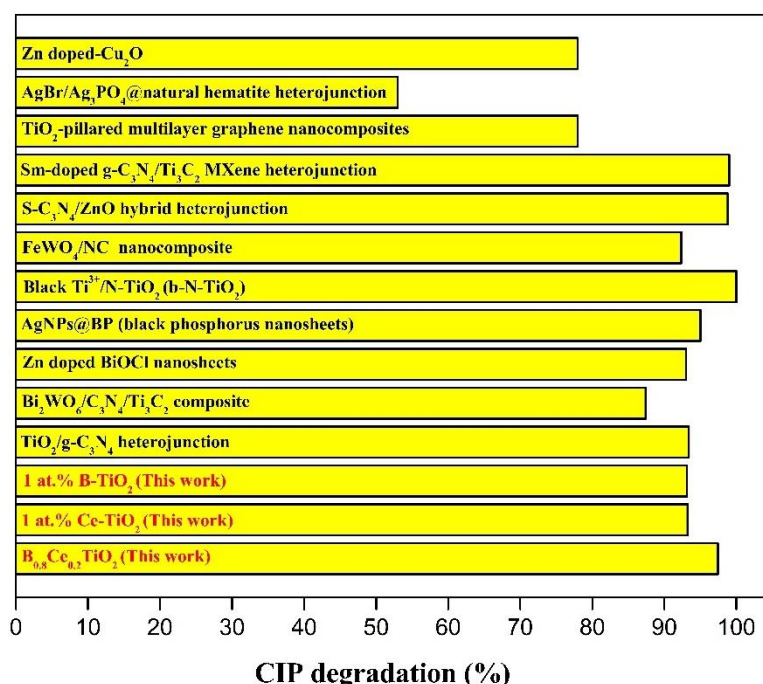


Figure 4.11. Mineralization of CIP under sunlight



#### 4.2.4. Factors contributing to the synergy of the dopants (B and Ce)

In summary, the best performance was shown by the  $B_{0.8}Ce_{0.2}TiO_2$  photocatalyst. The performance of the codoped catalysts was better than that of the mono-doped catalysts (1 at.% Ce- $TiO_2$ : 93.22%, and 1 at.% B- $TiO_2$ : 93.16%). However, superior performance was observed when compared to that of bare  $TiO_2$ . In comparison with recent literature involving the CIP antibiotic and advanced/latest generation photocatalysts (**Table 2.4** and **Figure 4.12**), it is evident that these codoped catalysts are as efficient or perhaps better than some of the catalysts listed therein. Also, with regard to the mineralization of the pollutants, the performance of  $B_{0.8}Ce_{0.2}TiO_2$  was the best among the catalysts and also better than those listed in the literature.



**Figure 4.12.** Comparison of CIP degradation efficiency of codoped catalyst with the literature

A higher/improved adsorption capacity indicates the interaction between pollutant and catalyst for efficient photocatalytic activity. The higher adsorption capacity for  $CeO_2/TiO_2$  catalysts (Vieira et al. 2018) has been reported in the literature. And the water adsorbed surface acts as photoexcited hole traps and helps in the generation of hydroxyl radicals through the adsorption of  $OH^-$  ions onto the surface of  $CeO_2$  (Wang

et al. 2016c). Similarly, in this study, cerium doped TiO<sub>2</sub> has shown higher adsorption, thus, contributing to higher activities. However, in the case of B-TiO<sub>2</sub>, adsorption does not appear to be the major factor. In the case of 1B-TiO<sub>2</sub>, boron occupying the interstitial lattice position of TiO<sub>2</sub> (the presence of B-O-Ti bond traps photogenerated charges due to the existence of Ti<sup>3+</sup>, as observed from XPS) and visible light absorption has contributed to its higher photocatalytic activity. In the case of 2B-TiO<sub>2</sub>, boron occupies both the interstitial and substitutional lattice positions, due to which it cannot trap the photogenerated charges as effectively, thereby leading to a lesser activity in terms of both degradation and COD. The codoped catalysts showed the following order of adsorption capacity: B<sub>0.8</sub>Ce<sub>0.2</sub>TiO<sub>2</sub> (20.51%) > B<sub>0.7</sub>Ce<sub>0.3</sub>TiO<sub>2</sub> (13.82%) > B<sub>0.9</sub>Ce<sub>0.1</sub>TiO<sub>2</sub> (9.57%).

Researchers consider the degree of crystallinity (Mazinani et al. 2014) and anatase content (Bellardita et al. 2018) as important criteria in correlation to photocatalytic activity. It is seen (**Table 4.2**) that 1Ce-TiO<sub>2</sub>, 1B-TiO<sub>2</sub>, and B<sub>0.8</sub>Ce<sub>0.2</sub>TiO<sub>2</sub> catalyst has the lowest rutile content ( $X_r$ ) or, conversely, more of the anatase crystalline phase, indicating that the anatase phase possibly significantly influences the mineralization of the pollutant molecules. Also, a higher degree of crystallinity has promoted higher photocatalytic activity (Mazinani et al. 2014), even with lower surface areas. A higher crystallinity reduces the formation of electron traps which results in fewer recombination centers (as observed from PL spectra of the codoped catalysts) and thus improves the photocatalytic activity through effective separation of photogenerated charges.

With an increase in dopant concentration of Ce (corresponding to a decrease in the dopant concentration of B), the photocatalytic activity was found to be decreasing, which can be attributed to the broadening of the impurity band and narrowing of the charge separation gap, thus leading to slight recombination of electrons and holes (as observed from PL spectra). Similar effects for varying B and Ce dopants concentrations have been mentioned in the literature (Chao-hai et al. 2007). Thus, these results suggest the synergistic role of dopants in improving photocatalytic activity through their higher adsorption capacity, improved optical properties (narrowed bandgap and lower recombination), and higher anatase phase content.

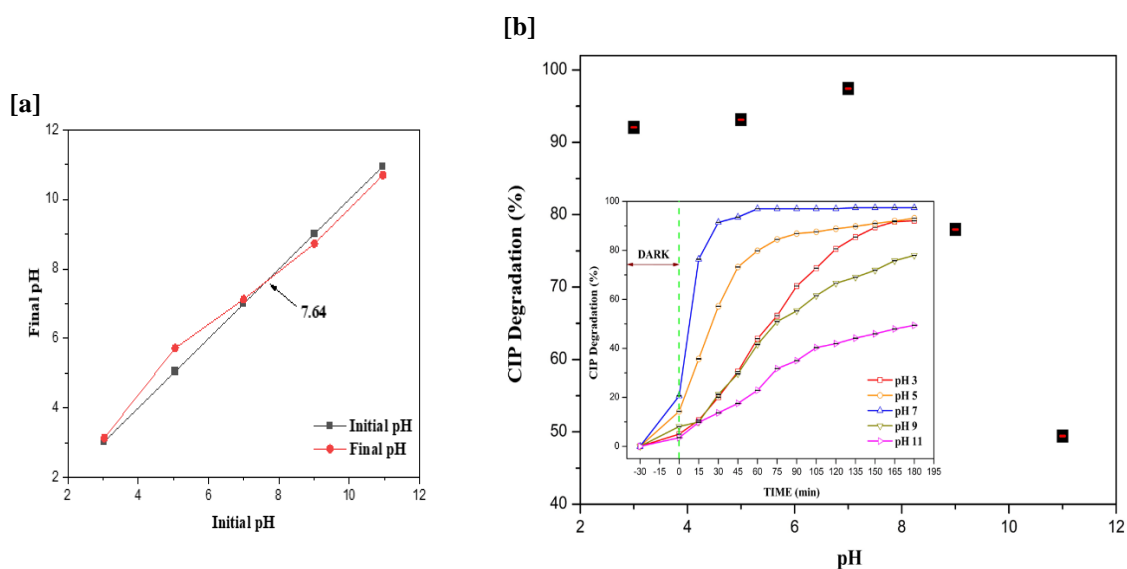
Overall, the following factors have contributed to effective photocatalytic activity:

- Narrowed bandgap (2.50-2.89 eV) with lower PL intensity: promotes effective charge separation and minimizes the recombination.
- Higher crystallinity/anatase phase content: anatase phase prolongs the lifetime of charge carriers, reduces the formation of electron traps resulting in fewer recombination centers (as observed from PL spectra), and thus improves the photocatalytic activity through effective separation of photogenerated charges.
- Higher adsorption capacity of Ce: provides better contact between pollutant and photocatalyst.
- Interstitial lattice position of B: helps in trapping of photogenerated charges effectively.

#### 4.2.5. Effect of pH

The pH of a solution is an important aspect as it determines the properties of surface charge of the photocatalyst and the adsorption behavior of pollutant molecules (Das et al. 2018; Shetty et al. 2017). It can affect changes in the ionic state of pollutants, surface charge of the photocatalyst, and concentrations of reactive oxygen species. Thus, pH greatly influences photocatalytic degradation of the CIP (Hassani et al. 2017; Sayed et al. 2018; Shah et al. 2018b). The effect of pH on CIP degradation was studied by varying the pH as 3, 5, 7, 9, 11 using the best performing codoped catalyst ( $B_{0.8}Ce_{0.2}TiO_2$ ) under optimum conditions. pH was adjusted using 1M HCl and 1M NaOH. The CIP has two dissociation constant values of  $pK_{a1} = 6.09$  (carboxylic acid group) and  $pK_{a2} = 8.74$  (nitrogen on piperazinyl ring). From **Figure 4.13a**, the point of zero charge of  $B_{0.8}Ce_{0.2}TiO_2$  was found to be 7.64 (below which catalyst is positively charged and above which it is negatively charged). From **Figure 4.13b (inset)**, the adsorption was found to be highest at pH 7 and much lower at pH 11 (pH 7 > pH 5 > pH 9 > pH 3 > pH 11). The CIP degradation efficiency at pH 3 and pH 5 was good but slightly lesser than that of pH 7 (**Figure 4.13b**). This might be due to the higher oxidation potential of hydroxyl radicals (standard  $\cdot OH/H_2O - 2.59$  eV) for the degradation of organic pollutants at low pH (Hassani et al. 2017) even though both CIP and catalyst are positively charged. Under alkaline conditions, at pH 9 and pH 11, degradation efficiency decreased to 77.96% and 49.42%. This might be due to

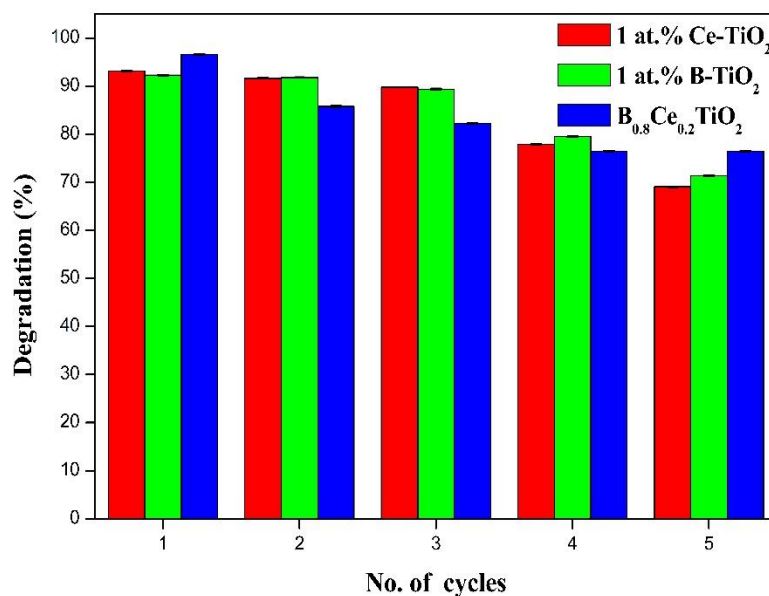
the repulsion effect from both negatively charged CIP and the catalyst. Similar results have been reported in the literature (Shetty et al. 2017). Overall, at pH 7, both adsorption and degradation were found to be highest. Thus, all studies were performed at pH 7.



**Figure 4.13.** (a) Point of zero charge (pzc) of B<sub>0.8</sub>Ce<sub>0.2</sub>TiO<sub>2</sub> and (b) Effect of pH on CIP degradation

#### 4.2.6. Recyclability studies

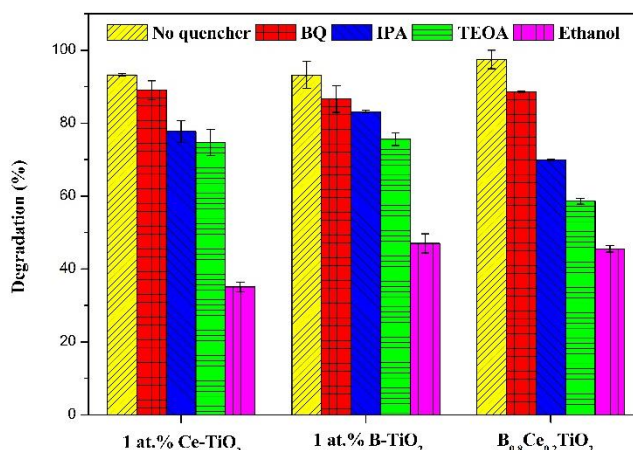
The recyclability studies were carried out to determine the stability of the best performing photocatalysts – 1Ce-TiO<sub>2</sub>, 1B-TiO<sub>2</sub>, and B<sub>0.8</sub>Ce<sub>0.2</sub>TiO<sub>2</sub> under optimized conditions. Five consecutive runs were performed under sunlight at optimized conditions. As observed in **Figure 4.14**, the CIP degradation efficiency decreased from 93% to 69% in the case of monodoped catalysts and from 97% to 76% in the case of codoped catalysts at the end of five consecutive runs. These results with a marginal decrease in the degradation efficiency (~ 20%) confirm the stability of the photocatalysts.



**Figure 4.14.** Degradation (%) in consecutive photocatalytic cycles of recyclability

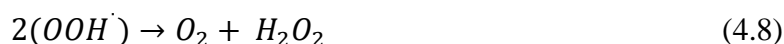
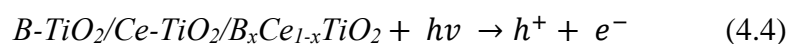
#### 4.2.7. Scavenging studies and possible mechanism of CIP degradation

The dominant reactive oxygen species such as electrons ( $e^-$ ), holes ( $h^+$ ), hydroxyl ( $\cdot\text{OH}$ ) and superoxide ( $\cdot\text{O}_2^-$ ) radicals responsible for the degradation of CIP were determined from scavenging experiments. 1 mM triethanolamine (TEOA), 1 mM isopropyl alcohol (IPA), 1mM benzoquinone (BQ), and 50 mL ethanol were used as scavenging agents for  $h^+$ ,  $\cdot\text{OH}$ ,  $\cdot\text{O}_2^-$ , and  $e^-$  respectively (Wang et al. 2016a). From **Figure 4.15**, it is seen that ethanol ( $e^-$ ) exhibited the highest quenching effect (35-47%). The results indicate that TEOA ( $h^+$ ) and IPA ( $\cdot\text{OH}$ ) also played a role in the quenching process/influenced degradation. BQ ( $\cdot\text{O}_2^-$ ) showed a lesser decrease in degradation (%), and hence it has no major effect. Overall, the results suggest that the degradation of CIP has occurred mainly through the effect of  $e^-$ ,  $h^+$ , and  $\cdot\text{OH}$  species.



**Figure 4.15.** Scavenging experiments for identification of reactive oxygen species in the photocatalytic degradation

**Figure 4.16 (a-c)** shows the postulated mechanism of the doped catalysts. Upon irradiation of visible/solar light energy, the electrons get excited from O 2p level/B p level to Ti 3d level/Ce 4f level. Ce 4f level and Bp level formation were confirmed from the XPS results. More electron-hole pairs were generated, and these electrons could be captured by the surface CeO<sub>2</sub> (as observed from the XRD results). The generated holes reach the surface of the catalyst and react with the OH<sup>-</sup> to produce OH<sup>·</sup>. The electrons react with the surface absorbed O<sub>2</sub> to produce O<sub>2</sub><sup>-·</sup>. From the scavenging studies, the electrons were found to be the dominant species, followed by holes and hydroxyl radicals. Therefore, higher photocatalytic activity can be attributed to the synergistic effect of Ce doping which has narrowed the bandgap, and B doping which has promoted the efficient separation of electron-hole pairs. The possible chemical reactions occurring during the degradation of CIP are given in the following equations (Eq. 4.4-4.11):



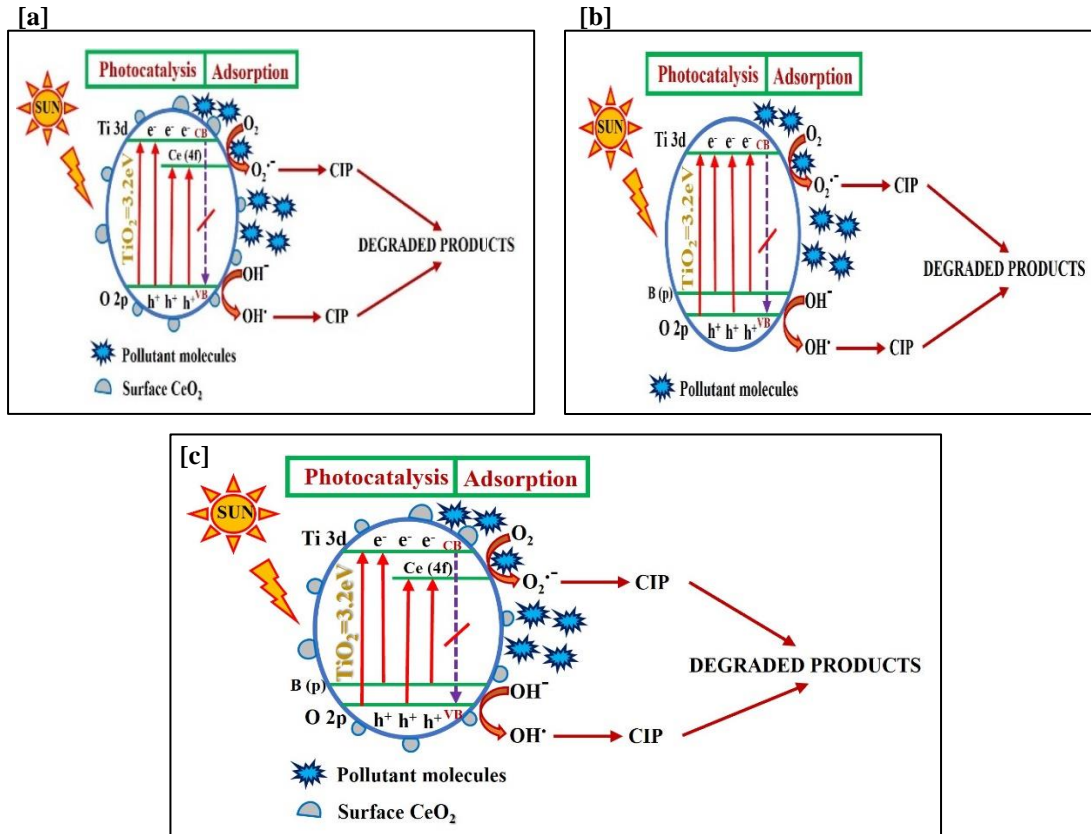
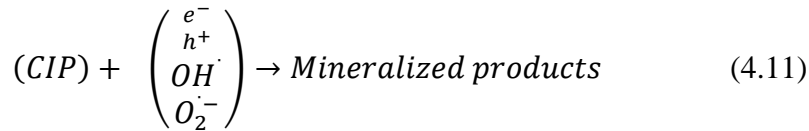
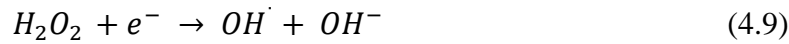


**Figure 4.16.** Possible degradation mechanism of CIP using (a) Ce-TiO<sub>2</sub>, (b) B-TiO<sub>2</sub>, and

(c) B<sub>x</sub>Ce<sub>1-x</sub>TiO<sub>2</sub>

### 4.3. ANALYSIS OF DEGRADED CIP SAMPLE

#### 4.3.1. Residual antibacterial activity of the degraded CIP sample

The degraded CIP sample was analyzed for residual antibacterial activity using *E.coli* as the test organism by the agar well diffusion method (as mentioned in section 3.2.7). As seen in **Figure 4.17**, no inhibition zones were observed after 60 min, this is in accordance with the degradation trend observed which remains constant after 60

min. The decrease in the zone of inhibition (absence of zones) suggests the loss of antibiotic activity of the degraded sample.

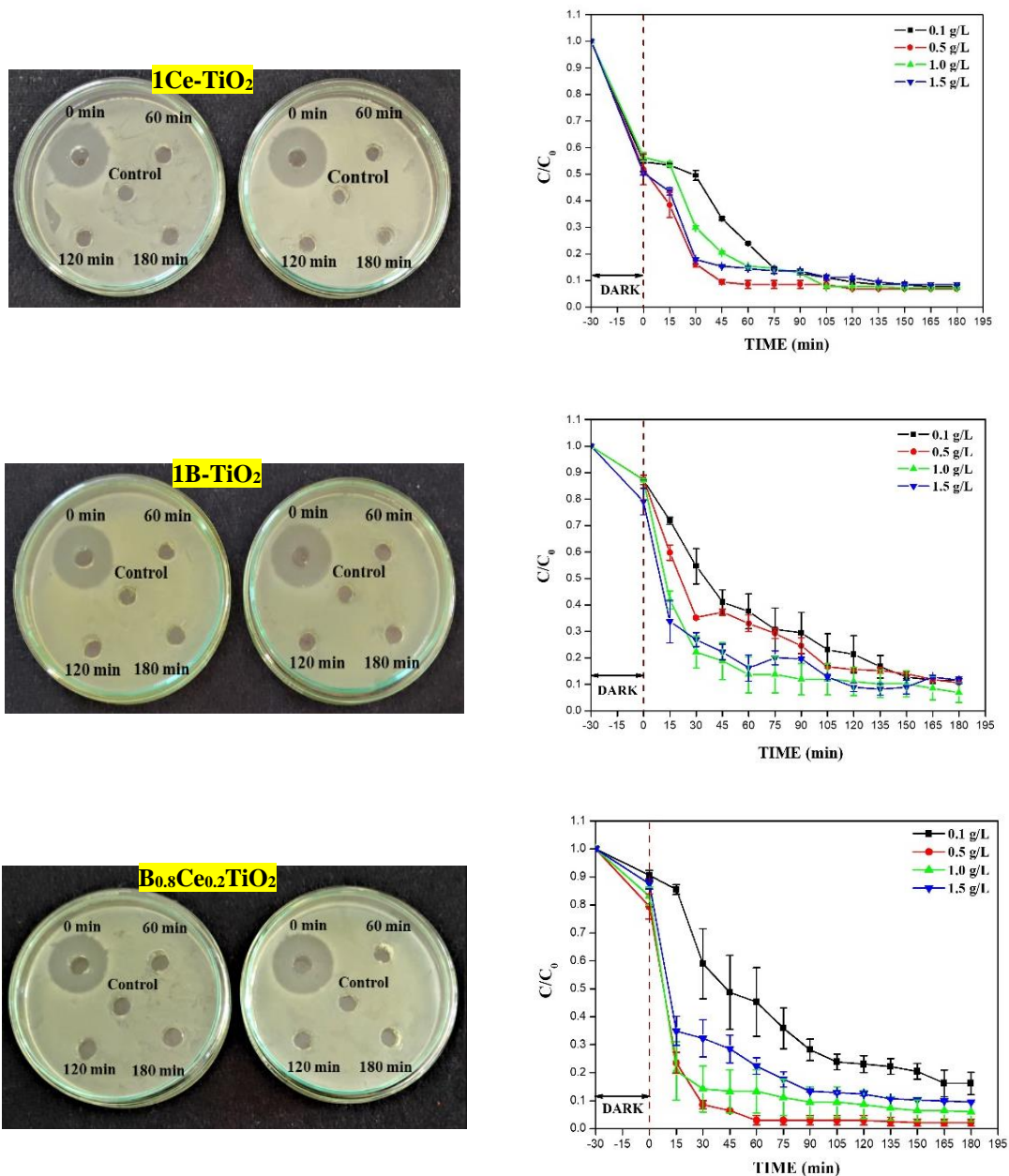


**Figure 4.17.** Residual antibacterial activity of the degraded CIP sample using the best performing photocatalysts and their corresponding degradation

#### 4.3.2. LC-MS analysis

The degraded products (DP) of CIP identified by LC-MS are tabulated in **Table 4.6**. The  $m/z$  data of DP were compared to those reported in the literature as there are



no specific standards/libraries available to identify the degraded by-products. At a retention time of 7.2 min, CIP showed a peak in HPLC with the corresponding  $m/z$  of 331 containing piperazine and quinolone moieties. The black line in HPLC spectra (**Figure A1 (a-d)** monodoped series, **(e-g)** codoped series, Appendix I) represents the initial sample, and the coloured lines in each spectrum represent the corresponding degraded sample.

As seen in **Figure 4.18a** for the monodoped series of catalysts, pathway I occurred through piperazine ring transformation with the products of  $m/z$ : 263 (piperazine ring-opening)  $\rightarrow$  229 (elimination of piperazine ring). Pathway II occurred through defluorination with the products of  $m/z$ : 315  $\rightarrow$  287 (loss of F atom and opening of piperazine ring)  $\rightarrow$  229 (loss of F atom and elimination of piperazine moiety). Pathway III occurred through decarboxylation with the products of  $m/z$ : 287 (removal of carboxyl group). In pathway IV, keto derivatives were formed with the products of  $m/z$ : 362  $\rightarrow$  334/332 (keto derivatives with a carbonyl group on N atom)  $\rightarrow$  291 (formation of hydroxyl keto group by the loss of N atom). Finally, the product of  $m/z$ : 200, was formed with partial loss of piperazine ring, loss of F atom, and decarboxylation. Further, low molecular weight and less harmful products like acrylate and carbon trioxide with  $m/z$  of 71 and 68 respectively were formed.

As seen in **Figure 4.18b** for the codoped series of catalysts, pathway I occurred through piperazine ring transformation with the products of  $m/z$ : 361 (piperazine ring-opening)  $\rightarrow$  263 (elimination of piperazine ring). In pathway II, keto derivatives were formed with the products of  $m/z$ : 361  $\rightarrow$  332/334 (keto derivatives with a carbonyl group on N atom)  $\rightarrow$  291 (loss of N atom with the formation of keto group)  $\rightarrow$  263 (by loss of CO). Pathway III occurred through defluorination with the products of  $m/z$ : 315 (loss of F atom and opening of piperazine ring)  $\rightarrow$  229 (loss of F atom and elimination of piperazine moiety). Finally, the product of  $m/z$ : 200, was formed with partial loss of piperazine ring, loss of F atom, and decarboxylation. Further, low molecular weight and less harmful products like acrylate and carbon trioxide with  $m/z$  of 71 and 68 respectively were formed.

**Table 4.6.** CIP degraded products identified by LC-MS analysis

Degradation Products	Experimental m/z	Literature m/z	Molecular formula	Proposed Structure	References
<b>CIP</b>	331	331	$C_{17}H_{18}FN_3O_3$		(Gupta and Garg 2018; Hubicka et al. 2013; Maia et al. 2014; Shetty et al. 2017; Wang et al. 2019a; Yu et al. 2018, 2019; Zhang et al. 2015)
<b>D1</b>	333	332 334	$C_{17}H_{19}FN_3O_3$ + $C_{16}H_{17}FN_3O_4$ +		(Huo et al. 2019; Moongraksathum and Chen 2018; Sahoo et al. 2020; Yu et al. 2019)
<b>D2</b>	363 365	362 361	$C_{17}H_{17}FN_3O_5$ + $C_{17}H_{16}FN_3O_5$		(Ahamad et al. 2021; Gupta and Garg 2018; Hubicka et al. 2013; Maia et al. 2014; Shetty et al. 2017; Wang et al. 2019a; Xiao et al. 2018; Yu et al. 2019; Zhang et al. 2015)
<b>D3</b>	314 315	315	$C_{16}H_{17}N_3O_4$		(Maia et al. 2014)
<b>D4</b>	293	291	$C_{14}H_{12}FN_2O_4$ +		(Gupta and Garg 2018; Maia et al. 2014; Sahoo et al. 2020; Wang et al. 2019a; Yu et al. 2018, 2019; Zhang et al. 2015)

Degradation Products	Experimental m/z	Literature m/z	Molecular formula	Proposed Structure	References
<b>D5</b>	287	287	$C_{16}H_{18}FN_3O$ $C_{15}H_{17}N_3O_3$		(Gupta and Garg 2018; Maia et al. 2014)
<b>D6</b>	261 265	263	$C_{13}H_{12}FN_2O_3$ +		(Gupta and Garg 2018; Maia et al. 2014; Sahoo et al. 2020; Wang et al. 2019a; Yu et al. 2018, 2019; Zhang et al. 2015)
<b>D7</b>	227	229	$C_{13}H_{11}NO_3$		Haddad and Kümmerer (2014)
<b>D8</b>	201	200	$C_{12}H_{12}N_2O$		Haddad and Kümmerer (2014)

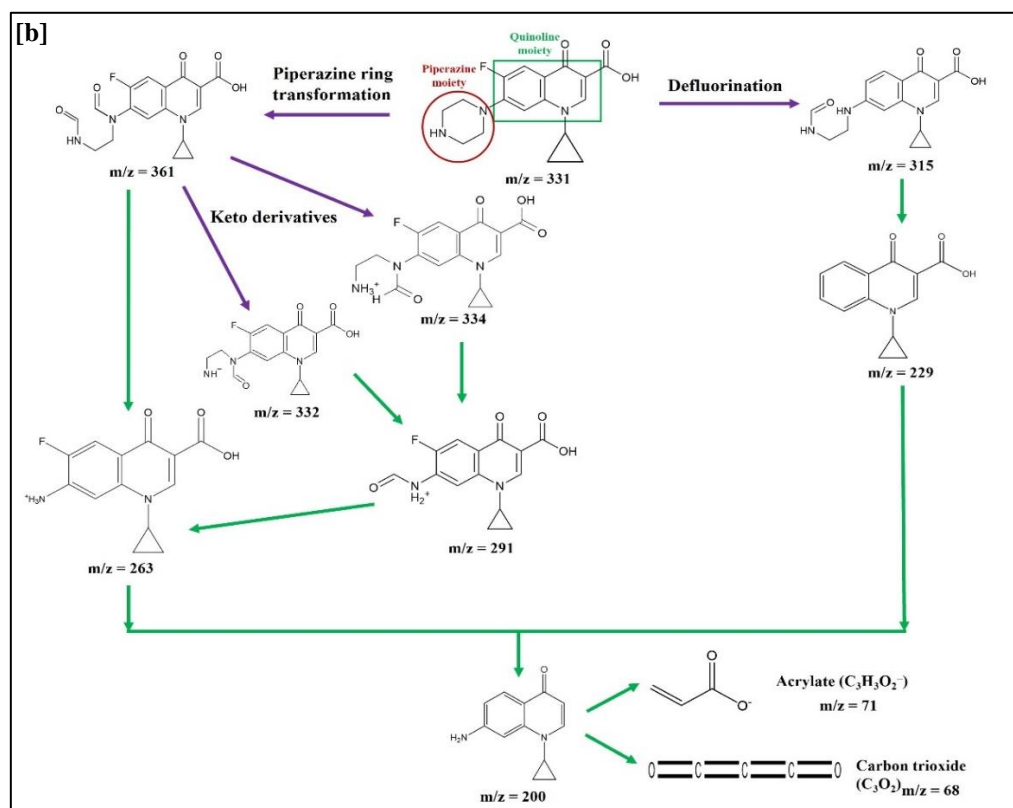
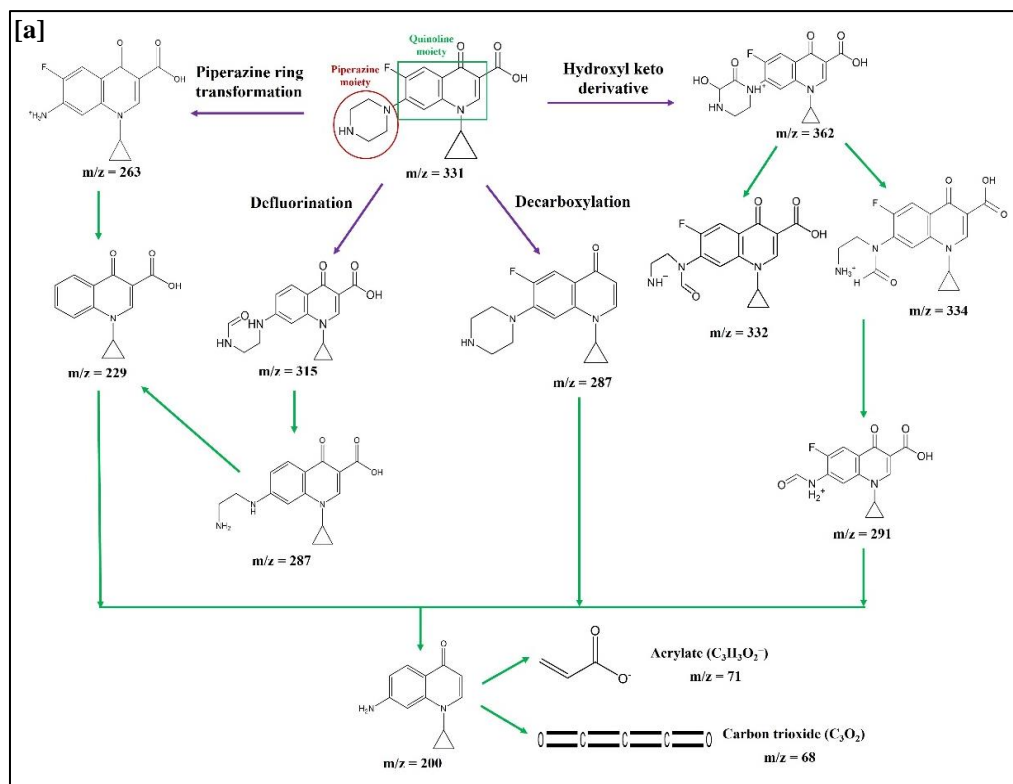


**Figure 4.18.** Possible degradation pathways of CIP (a) Ce-TiO<sub>2</sub> & B-TiO<sub>2</sub> series and (b) B<sub>x</sub>Ce<sub>1-x</sub>TiO<sub>2</sub> series

Overall, from the suspended form studies, the codoped catalyst -  $B_{0.8}Ce_{0.2}TiO_2$  was the best performing catalyst through the synergy of boron and cerium dopants. Hence,  $B_{0.8}Ce_{0.2}TiO_2$  catalyst was immobilized using waste expanded polystyrene beads and studied for degradation of CIP under sunlight.

## CHAPTER 5

### PHOTOCATALYTIC DEGRADATION: IMMOBILIZED FORM

As discussed in section 2.9, the disadvantages of using the catalyst in suspended form can be overcome through immobilization of the photocatalyst onto a suitable support. In this regard, waste expanded polystyrene (EPS) beads were employed to immobilize the best performing codoped ( $B_{0.8}Ce_{0.2}TiO_2$ ) photocatalyst.  $B_{0.8}Ce_{0.2}TiO_2$  immobilized EPS film was prepared by solvent casting method as described in section 3.2.2. The film was then subjected to various characterizations, as discussed in section 3.2.4. Photocatalytic activity was determined using ciprofloxacin as the model pollutant (section 3.2.3) under sunlight. The degraded sample was analyzed for TOC reduction and residual antibacterial activity (section 3.2.8). The degraded products were analyzed using LC-MS analysis (section 3.2.6). Reusability of the film was studied to determine its stability, and leachability studies were carried out using ICP-OES.

#### 5.1. CHARACTERIZATION OF THE IMMOBILIZED FILM

##### 5.1.1. FESEM analysis

**Figure 5.1** (FESEM images) shows the morphology of plain EPS film, unused EPS film with  $B_{0.8}Ce_{0.2}TiO_2$  catalyst particles distributed on the film surface. Pores created on the surface of the EPS film are clearly visible, and these pores act as active sites for photocatalytic activity. After reusing the EPS film five times, no significant morphological changes were observed. From FESEM, an average thickness of 1087  $\mu m$  (**Figure 5.2**) and from profilometer measurements, an average roughness of 15.4323  $\mu m$  was observed.





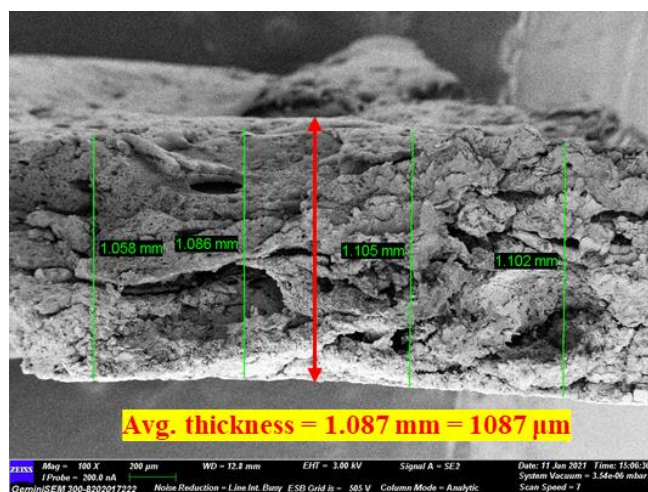


**Figure 5.2.** Thickness of the  $B_{0.8}Ce_{0.2}TiO_2$  immobilized EPS film

### 5.1.2. XRD spectra analysis

The XRD spectra of plain EPS film, immobilized EPS photocatalytic film before and after five times of reuse are given in **Figure 5.3**. In the plain film, two peaks were observed at  $9.975^\circ$  - amorphous polymer and  $19.625^\circ$  - crystalline polymer (Wankasi and Dikio 2014). After the catalyst immobilization, crystalline peaks of  $TiO_2$  (anatase and rutile) and cerium peaks were observed ( $TiO_2$  - JCPDS no. 12-1272 and  $CeO_2$  - JCPDS no. 43-1002). The peaks at  $25.32^\circ$  (101),  $37.01^\circ$  (103),  $37.87^\circ$  (004),  $38.60^\circ$  (112),  $48.09^\circ$  (200),  $54.32^\circ$  (105),  $55.12^\circ$  (211),  $62.73^\circ$  (204),  $68.97^\circ$  (116),  $70.30^\circ$  (220), and  $75.11^\circ$  (215) correspond to anatase  $TiO_2$ . The peaks at  $27.46^\circ$  (110),  $36.11^\circ$  (101),  $41.31^\circ$  (111),  $56.72^\circ$  (220), and  $64.04^\circ$  (310) correspond to rutile  $TiO_2$ . Cerium peaks were found at  $47.05^\circ$  (220),  $56.72^\circ$  (311), and  $60.22^\circ$  (222). No prominent B peaks were detected which suggests the uniform distribution of B due to its lesser ionic radii than that of Ti with the formation of B-O-Ti bonds. Ce ions due its larger ionic radii than that of Ti, either exist on the  $TiO_2$  surface as  $CeO_2$ , or  $Ti^{4+}$  ions enter the Ce lattice with the formation of Ti-O-Ce bonds. These results are consistent with the XRD results observed for the  $B_{0.8}Ce_{0.2}TiO_2$  catalyst (suspended form) with notable anatase, rutile and Ce peaks (section 4.1.4). No changes in the XRD pattern were observed after five times of reuse of the film. This indicates that the degree of crystallinity remains unchanged even after exposing the film under sunlight.



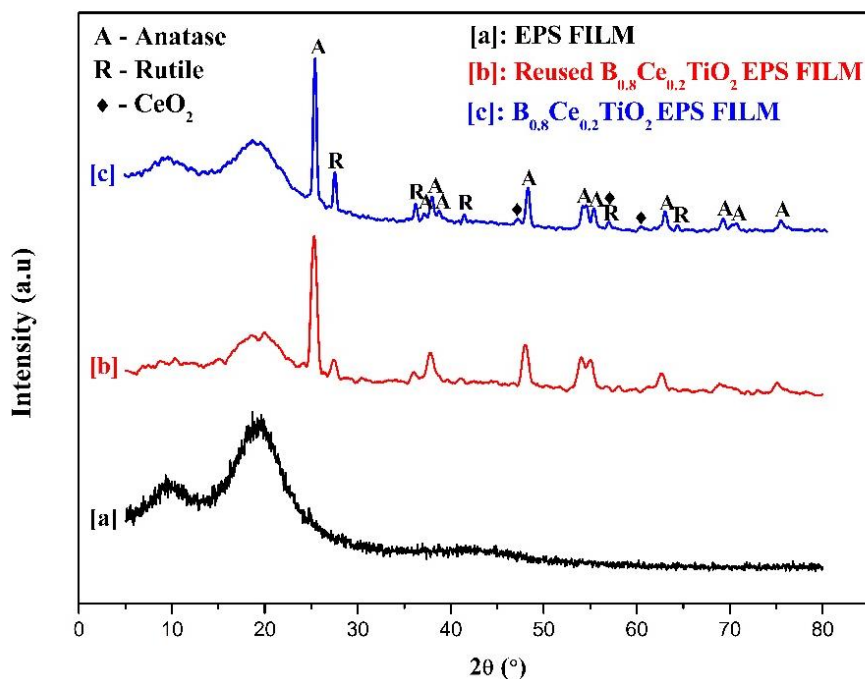


**Figure 5.3.** XRD spectra of [a] EPS film, [b] B<sub>0.8</sub>Ce<sub>0.2</sub>TiO<sub>2</sub> immobilized EPS film after using five times, [c] B<sub>0.8</sub>Ce<sub>0.2</sub>TiO<sub>2</sub> immobilized EPS film

### 5.1.3. FTIR spectra analysis

**Figure 5.4** shows the FTIR spectra of the plain EPS film, unused film, and film after five times of reuse. The peak at 3361.75 cm<sup>-1</sup> corresponds to the O-H stretch. The next peak observed at 3027.47 cm<sup>-1</sup> corresponds to the C-H bond of the benzene ring in polystyrene. The third peak at 2919.71 cm<sup>-1</sup> is due to C-H stretching vibration. Peaks between 1597-1446 cm<sup>-1</sup> correspond to aromatic C=C bond stretch. The next two peaks at 751.40 cm<sup>-1</sup> and 689.59 cm<sup>-1</sup> correspond to the aromatic C-H bend. No major chemical changes were observed after five times of reuse of the film. No additional peaks were observed, which suggests the absence of contaminants. Similar results were observed in the literature (Das and Mahalingam 2019a; Mangalara and Varughese 2016).

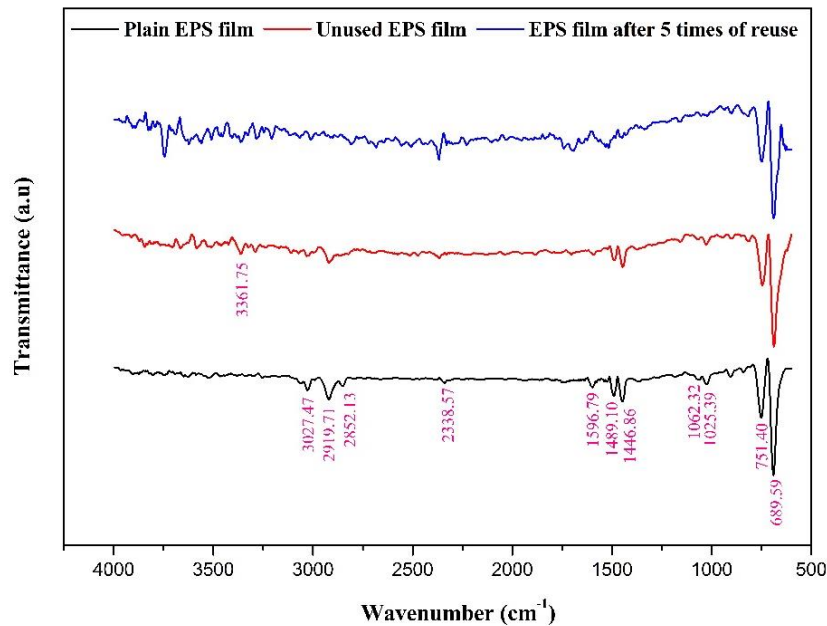


**Figure 5.4.** FTIR spectra of plain EPS film, unused EPS film, and EPS film after five times of reuse

#### 5.1.4. XPS spectra analysis

From XPS analysis, the composition and chemical states of the  $B_{0.8}Ce_{0.2}TiO_2$  immobilized photocatalyst were determined. **Figure 5.5a** indicates the survey spectra of  $B_{0.8}Ce_{0.2}TiO_2$  immobilized film. The Ti 2p peaks were observed at 458.57 eV (corresponds to  $2p_{3/2}$  orbit) and 464.53 eV (corresponds to  $2p_{1/2}$  orbit) (**Figure 5.5b**), which corresponds to  $Ti^{4+}$  (Wang et al. 2016c). A slight shift in the peaks upon doping is observed which can be attributed to the presence of  $Ti^{3+}$ , incorporation of B dopant into the  $TiO_2$  lattice (Shi et al. 2019), partial substitution of O atoms in the  $TiO_2$  lattice by the B atoms (Xu et al. 2009), and also to the efficient transfer of electrons (Maarisetty and Baral 2019). One O 1s peak was observed at 530.47 eV (**Figure 5.5c**), which corresponds to the surface  $OH^-$  group (Jaiswal et al. 2016)/lattice oxygen (Maarisetty and Baral 2019; Zhao et al. 2015b). The higher binding energy observed at around 530 eV (when compared to 529.34 eV observed for  $TiO_2$ ) suggests the existence of a Ti-O-B bond. The lattice oxygen leads to the Ti-O-Ce bond formation. These bond formations are noted from XRD analysis also. A peak at 191.13 eV (**Figure 5.5d**) for B 1s indicates the presence of B in the interstitial lattice position, which promotes the reduction of  $Ti^{4+}$  to  $Ti^{3+}$ . This  $Ti^{3+}$  facilitates the

effective separation of photogenerated charges and thus enhances the photocatalytic activity (Feng et al. 2011; Jaiswal et al. 2016; Patel et al. 2015; Wang et al. 2016c). Two Ce 3d peaks (**Figure 5.5e**) appeared at 884.94 eV and 906.18 eV. This indicates the presence of Ce<sup>4+</sup> (Liu et al. 2005; Wang et al. 2016c).

From the XPS study, the amount of photocatalyst present in the EPS film was quantitatively analyzed, and the actual amount of B<sub>0.8</sub>Ce<sub>0.2</sub>TiO<sub>2</sub> photocatalyst present was 19.96 wt.% of the photocatalyst present in the EPS film, in agreement with the intended catalyst loading (20 wt.%).

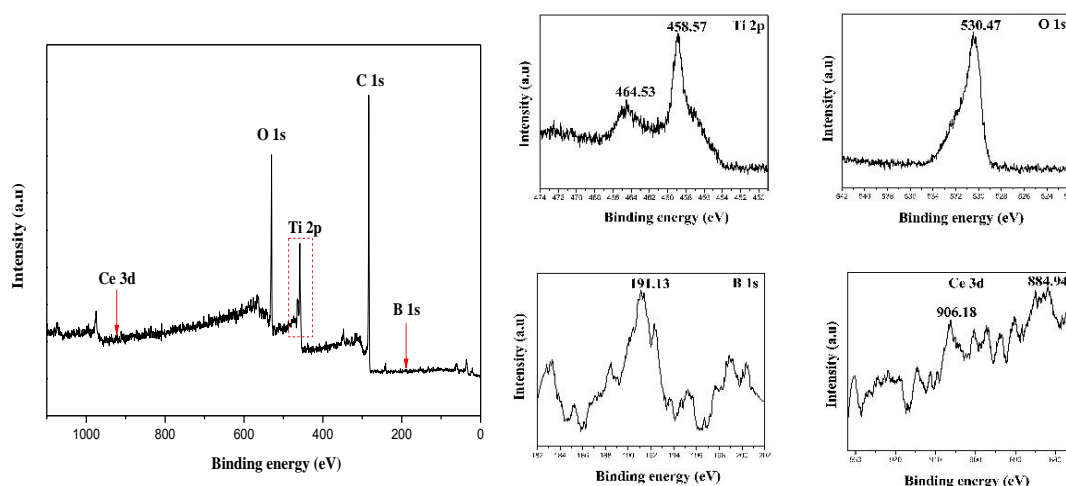


**Figure 5.5.** XPS analysis of the immobilized B<sub>0.8</sub>Ce<sub>0.2</sub>TiO<sub>2</sub> photocatalyst film

### 5.1.5. Contact angle measurement and leaching studies

From contact angle measurements, 82.93° was measured for the B<sub>0.8</sub>Ce<sub>0.2</sub>TiO<sub>2</sub> immobilized EPS film, which indicates that it is hydrophilic. TiO<sub>2</sub> is hydrophilic; B<sub>0.8</sub>Ce<sub>0.2</sub>TiO<sub>2</sub> photocatalyst and EPS beads are hydrophobic. After catalyst immobilization, it is seen that the EPS film behaves as hydrophilic.

Leaching of the photocatalyst from the EPS film was studied by subjecting the film to continuous stirring for 24 h in 200 mL deionized water. The concentration of elements of photocatalyst leached from the immobilized film was quantified using ICP-OES analysis. The results showed minute traces of boron (0.3 ppm) and cerium (0.09 ppm). The Boron concentration values are within the permissible limits specified in the drinking water standards set by WHO (2008). No traces of elemental Ti were observed.

## 5.2. PHOTOCATALYTIC TREATMENT OF CIP

### 5.2.1. Effect of solvent volumes and amount of EPS beads

The solvents i.e., acetone and ethanol, were combined in different ratios (10 ml acetone and 8 ml acetone + 2 ml ethanol), and the amount of EPS beads was varied (3 g and 4 g) to check the resulting performance of the EPS film with respect to the degradation of CIP. The degradation efficiency was found to be only 26% for 5 wt.% (A1 in **Figure 5.6**), and 43% for 10 wt.% (A2 in **Figure 5.6**) of  $B_{0.8}Ce_{0.2}TiO_2$  immobilized EPS film prepared with 10 mL acetone and 3 g EPS. With the addition of 8 mL acetone and 2 mL ethanol, the degradation efficiency was found to be increasing, with 42% degradation observed for 5 wt.% (C1 in **Figure 5.6**) and 57% for 10 wt.% (C2 in **Figure 5.6**). Only 27% degradation was observed for the film prepared with 4 g EPS and 10 mL acetone (B1 in **Figure 5.6**). As mentioned in the literature (Abass 2018), the degradation increases with an increase in the polarity of the solvent, which is observed in this study after the addition of ethanol. Also acetone is considered to be less toxic than the other industrial solvents (Johanson 2012). The presence of pores (as observed from **Figure 5.7**) indicates the existence of active sites, which helps in achieving higher photocatalytic activity.

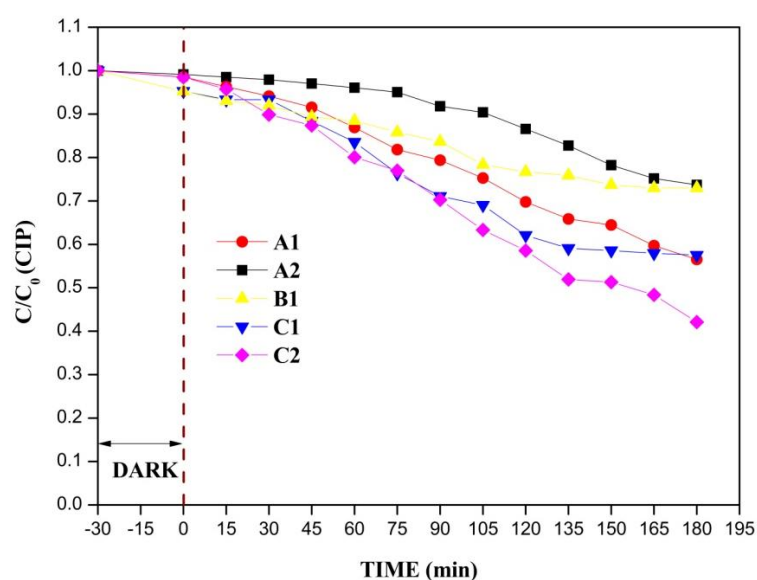


**Figure 5.6.** Effect of solvents on the photocatalytic degradation of CIP using  $B_{0.8}Ce_{0.2}TiO_2$  immobilized EPS film [A1: 3 g EPS + 10 mL Acetone (5 wt.%), A2: 3 g EPS + 10 mL Acetone (10 wt.%), B1: 4 g EPS + 10 mL Acetone (5 wt.%), C1: 3 g EPS + 8 mL Acetone + 2 mL Ethanol (5 wt.%), C2: 3 g EPS + 8 mL Acetone + 2 mL Ethanol (10 wt.%)]

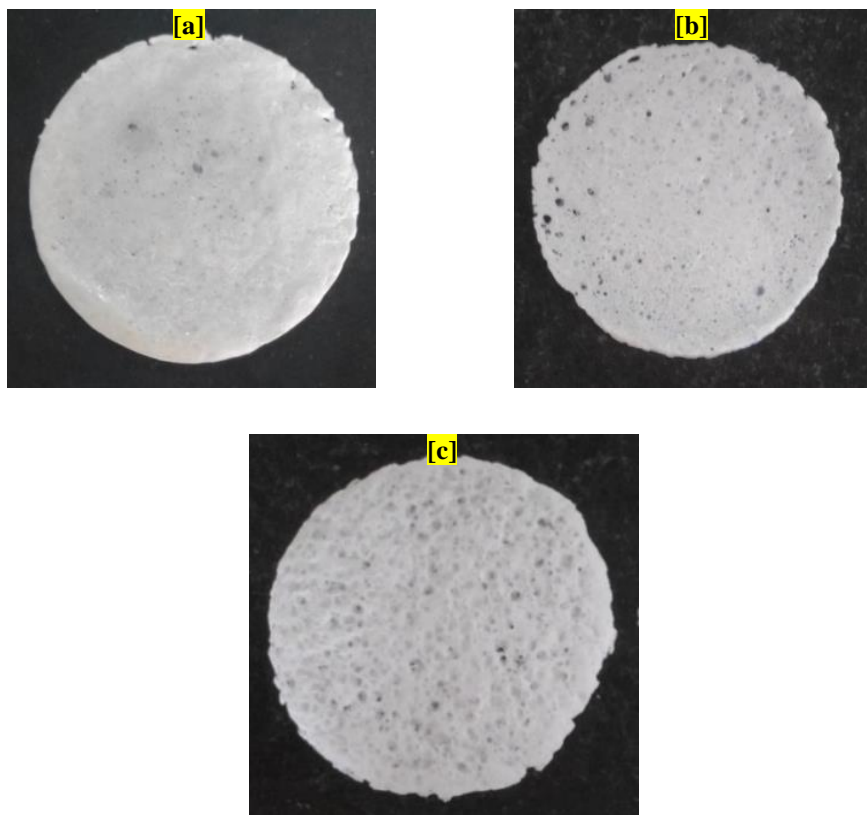


**Figure 5.7.** EPS films prepared by varying the quantity of EPS and solvents: [a] 3 g EPS + 10 mL Acetone, [b] 4 g EPS + 10 mL Acetone, and [c] 3 g EPS + 8 mL Acetone + 2 mL ethanol

### 5.2.2. Effect of catalyst loading

Photolysis experiments (using plain EPS film) showed only 8.44% degradation of CIP under sunlight, thus indicating the need for further treatment using the catalyst immobilized film. The effect of catalyst loading on degradation of CIP was examined by varying the catalyst loading as 5, 10, 15, 20, and 25 wt.% (**Figure 5.8a**). The highest degradation of 81.36% was observed for 20 wt.% after 180 min under sunlight. The degradation efficiency of CIP was found to be increasing with an increase in the catalyst dosage up to 20 wt.% (optimum catalyst dosage). An increase in the catalyst dosage results in an increase of electron-hole pairs, which in turn improves the degradation. However, beyond the optimum catalyst dosage, the degradation decreased, which is due to the reduction in pore size and the number of pores due to the agglomeration of the higher number/excess catalyst particles on the surface of the film. Similarly, in the literature (Das and Mahalingam 2019a),

photocatalytic activity has decreased with an increase in the catalyst dosage. Further, for the 20 wt.% photocatalytic film, a final degradation of 89.17% (**Figure 5.8b**) was observed at the end of 240 min.

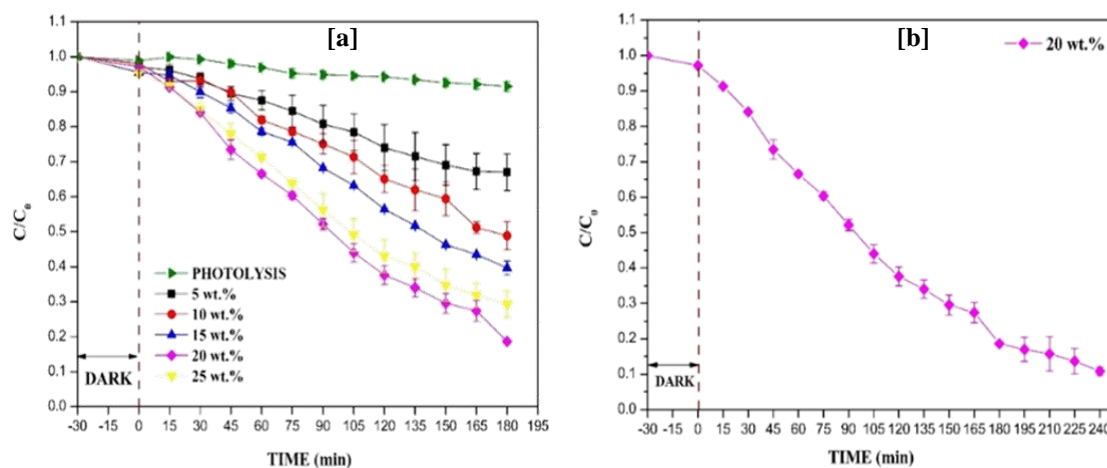


**Figure 5.8.** (a) Effect of catalyst loading on the photocatalytic CIP degradation [CIP = 10 ppm], (b) Photocatalytic degradation of CIP for 20 wt.% EPS film at a longer time scale

### 5.2.3. Effect of CIP initial concentrations and kinetic studies

The effect of the initial concentration of CIP on the degradation was studied with the optimum catalyst loading of 20 wt.% by varying the concentrations of CIP in the range of 10 to 40 mg/L, as shown in **Figure 5.9a**. The degradation was found to be decreasing with an increase in antibiotic concentration. With an increase in the CIP concentration, the reactive species ( $\cdot\text{OH}$  radicals) remain constant for a given catalyst dosage and time of irradiation. A higher pollutant concentration requires a higher number of radicals for the degradation. Also, more pollutant molecules compete for the same active sites in catalysts, thus resulting in a decrease of degradation efficiency. Similar observations are reported in the literature (Das and Mahalingam 2019a).

The reaction kinetics of CIP degradation for the different initial concentrations is shown in **Figure 5.9b**. The kinetics of the reaction was found to be pseudo-first-order. The  $k$  and  $R^2$  values are given in **Table 5.1**. The rate constant  $k$  values were found to be decreasing with an increase in the initial concentrations of CIP.

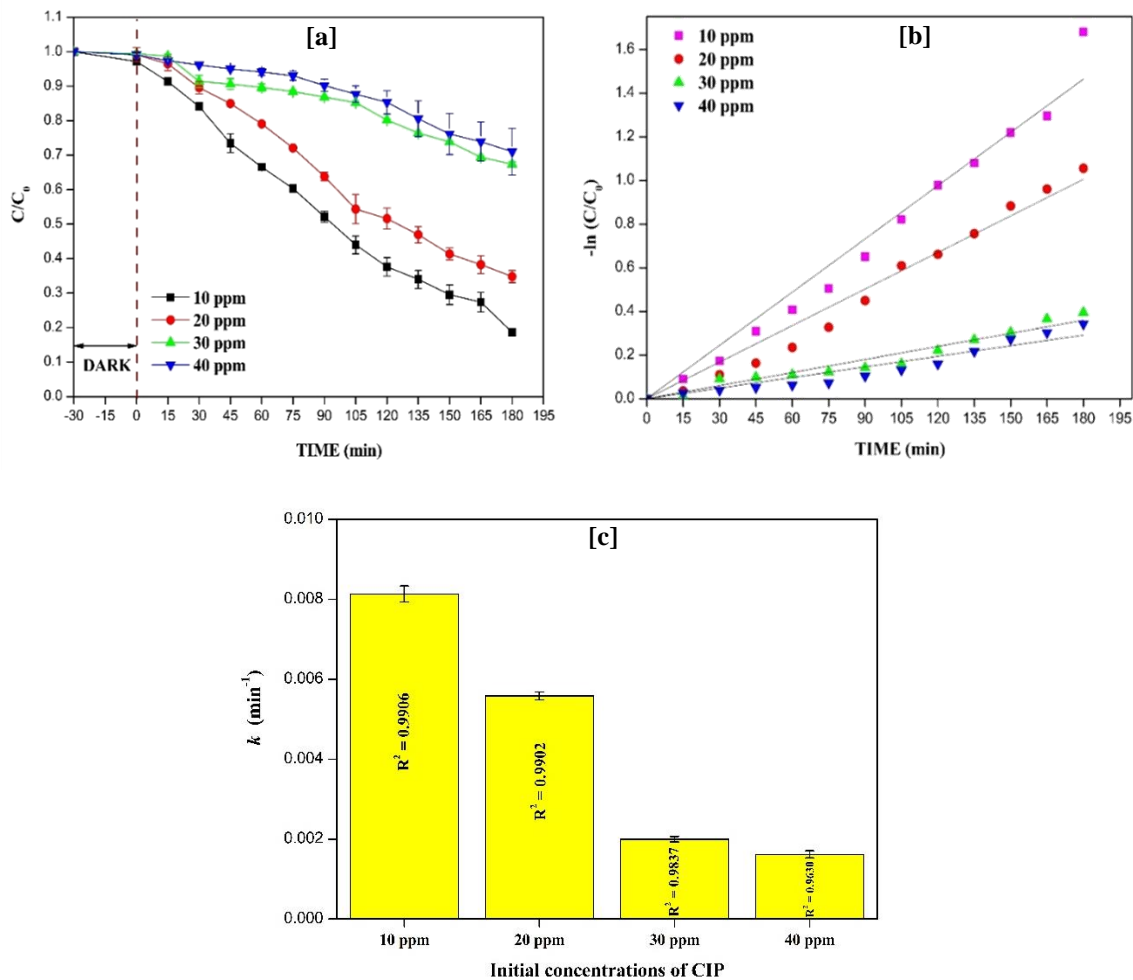


**Figure 5.9.** (a) Variation of initial concentrations of CIP with the optimum catalyst loading of 20 wt.%, (b) Kinetics plot and (c) Summary of kinetics data

**Table 5.1.** Kinetics data of CIP degradation

Immobilized photocatalyst	$k \times 10^{-3}$ ( $\text{min}^{-1}$ )				$R^2$			
	10 ppm	20 ppm	30 ppm	40 ppm	10 ppm	20 ppm	30 ppm	40 ppm
$\text{B}_{0.8}\text{Ce}_{0.2}\text{TiO}_2$	8.13 ± 0.2	5.58 ± 0.1	2.00 ± 0.07	1.62 ± 0.09	0.9906	0.9902	0.9837	0.9630

### 5.2.4. Effect of pH

The effect of pH on CIP degradation was studied by varying the pH as 3, 5, 7, 9, 11 using the optimum conditions of 20 wt.% catalyst loaded film and 10 ppm of CIP for 180 min. The CIP degradation was good at both pH 7 and pH 5. As mentioned in section 4.2.5, the point of zero charge of  $\text{B}_{0.8}\text{Ce}_{0.2}\text{TiO}_2$  was found to be 7.64. From

**Figure 5.10** (Inset figure shows the degradation for different pH values over a period of 180 min), at high pH values (basic pH), both the EPS film and CIP both are negatively charged due to which repulsion occurs and thus a lesser degradation happens. At low pH values (acidic pH), the EPS film and CIP both are positively charged. However, degradation is higher than that at the high pH which might be due to the higher oxidation potential of hydroxyl radicals for the degradation of organic pollutants at low pH. The pH of rivers and lakes in India lies in the range of 6.5-8.5. Also, the effluent with antibiotic residues from the pharmaceutical manufacturing industries or hospital effluent has a pH in the range of 6.7-7.7 (effluent discharge standards for industries and hospitals)(Das et al. 2018). In view of practical and real water sample applications, rest of the studies were performed at a pH of 7.

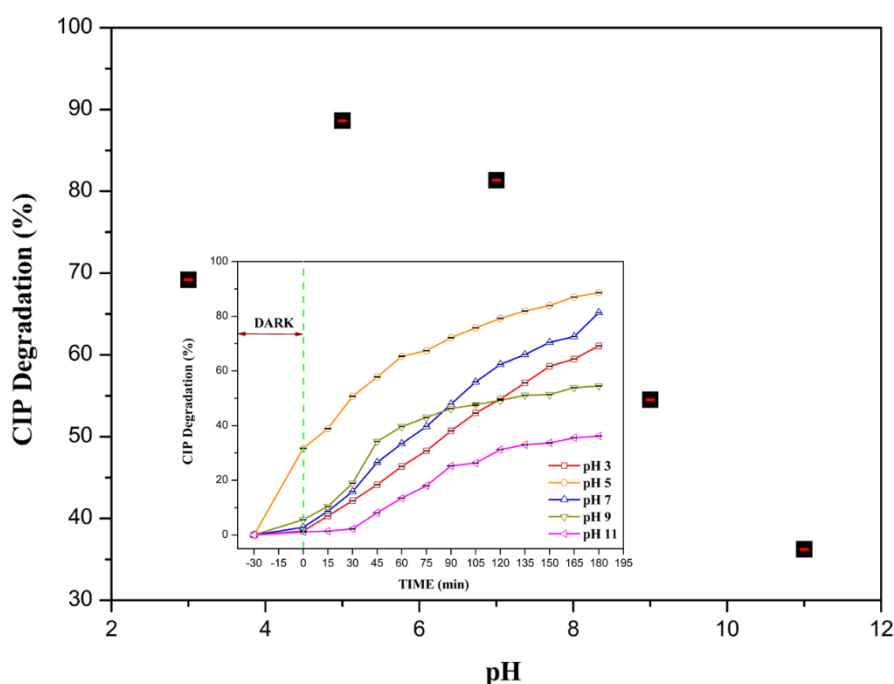


**Figure 5.10.** Effect of pH on CIP degradation

### 5.2.5. Reusability studies

To examine the stability of the  $B_{0.8}Ce_{0.2}TiO_2$  immobilized EPS film, reusability studies were performed five times and with a degradation time of 180 min for each cycle. After each cycle, the EPS film was washed with deionized water and dried at room temperature (overnight). The degradation efficiency of CIP slightly decreased from 81.36% to 71.15% (**Figure 5.11**) after five consecutive cycles of reuse. The



slight decrease in degradation efficiency can be attributed to the adsorbed CIP on the surface of the film, which blocks the active sites available for photocatalytic activity. Thus, these results suggest the stability of the EPS film immobilized with  $B_{0.8}Ce_{0.2}TiO_2$  photocatalyst.

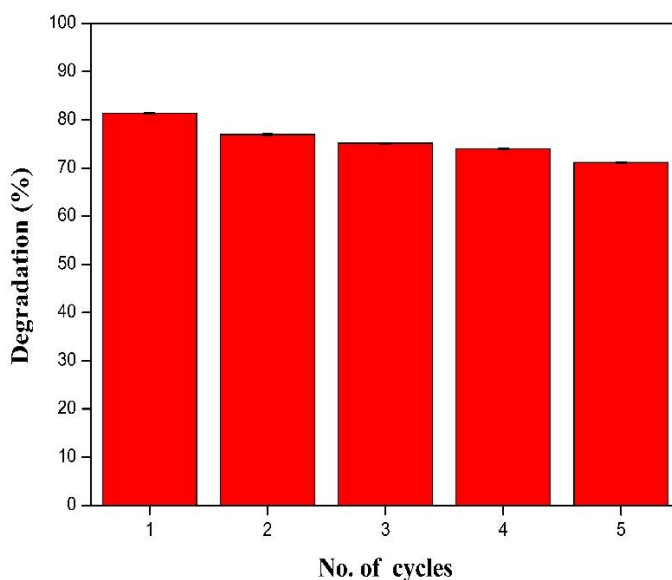


**Figure 5.11.** Reusability of EPS film performed for five consecutive cycles

### 5.3. ANALYSIS OF DEGRADED CIP SAMPLE

#### 5.3.1. TOC analysis and antibacterial activity of the degraded CIP sample

The degraded CIP sample showed a TOC reduction of 46.41% after 180 min and 84.41% after 240 min. These results indicate the mineralization of CIP with an increase in the photocatalytic treatment time. Further, the loss of antibacterial activity of the degraded CIP sample was determined using *E.coli* as the test organism by the agar well diffusion method. As seen from **Figure 5.12**, the zone of inhibition was found to be decreasing with an increase in the treatment time, with no inhibition zones being observed after 195 min and this is in accordance with the degradation observed (**Figure 5.8a**). The decrease in the zone of inhibition suggests the loss of antibiotic activity of the degraded sample.

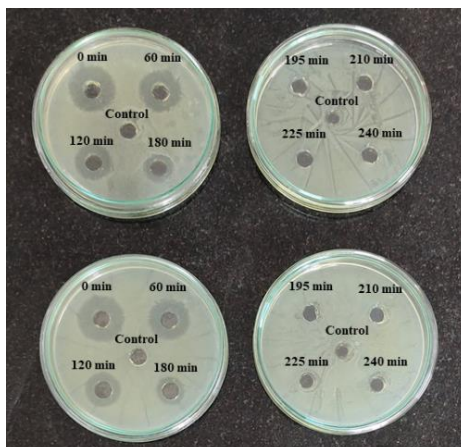


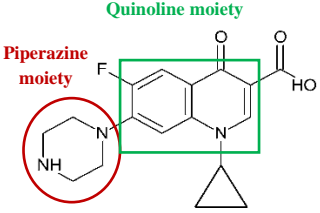
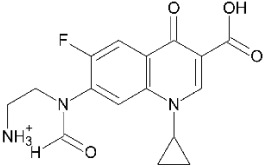
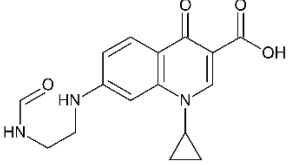
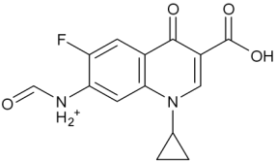
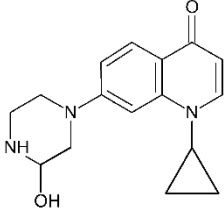
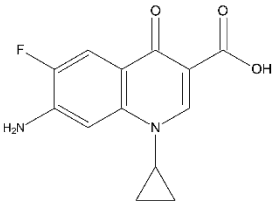
**Figure 5.12.** Antimicrobial activity of the degraded CIP sample

### 5.3.2. LC-MS analysis

**Figure A2** (Appendix I), illustrate the HPLC peaks of initial (pink line) and final (blue line - after 180 min, brown line - after 240 min) CIP samples. The inset graph depicts the MS spectrum of degraded products. The obtained (experimental)  $m/z$  values were compared with  $m/z$  values in the literature, and the degraded product structures were elucidated (**Table 5.2**). The possible pathways of CIP degradation using  $B_{0.8}Ce_{0.2}TiO_2$  immobilized EPS film under sunlight are given in **Figure 5.13**. The degradation has occurred mainly through the transformation of piperazine ring, defluorination, decarboxylation, formation of keto derivatives, and finally, less harmful & low molecular weight products were formed.

In pathway I, the degradation has occurred via transformation of piperazine ring with the formation of  $m/z$ : 263 (degradation of piperazine moiety through the loss of  $CO_2$  from the carboxylate group)  $\rightarrow$  251 (piperazine ring cleavage through loss of  $-C_2H_2$ )  $\rightarrow$  229 (elimination of piperazine moiety). In pathway II, there is formation of the product with  $m/z$ : 315  $\rightarrow$  283, through the loss of F atom (defluorination). In pathway III, the  $m/z$ : 283 was formed by the removal of carboxyl group (decarboxylation). In pathway IV, the formation of keto derivatives has occurred corresponding to the  $m/z$ : 334  $\rightarrow$  291. Finally, the product with  $m/z$ : 200 was formed. Finally, low molecular weight ( $m/z$ : 59) compounds and less harmful products were formed.

**Table 5.2.** Degradation products of CIP

Degradation Products	Experimental m/z	Literature m/z	Structure	References
CIP	331	331	 <p>Quinoline moiety Piperazine moiety</p>	(Gupta and Garg 2018; Haddad and Kümmerer 2014; Hubicka et al. 2013; Maia et al. 2014; Shetty et al. 2017; Zhang et al. 2015)
D1	338	334		(Maia et al. 2014; Wang et al. 2019a; Zhang et al. 2015)
D2	314	315		(Maia et al. 2014)
D3	292	291		(Zhang et al. 2015)
D4	282	283		(Haddad and Kümmerer 2014)
D5	262	263		(An et al. 2010; Gupta and Garg 2018; Maia et al. 2014; Wang et al. 2019a; Zhang et al. 2015)

Degradation Products	Experimental m/z	Literature m/z	Structure	References
D6	251	251		(Shah et al. 2018b)
D7	227	229		(Haddad and Kümmerer 2014)
D8	201	200		(Haddad and Kümmerer 2014)
D9	59	59		(Shah et al. 2018a)

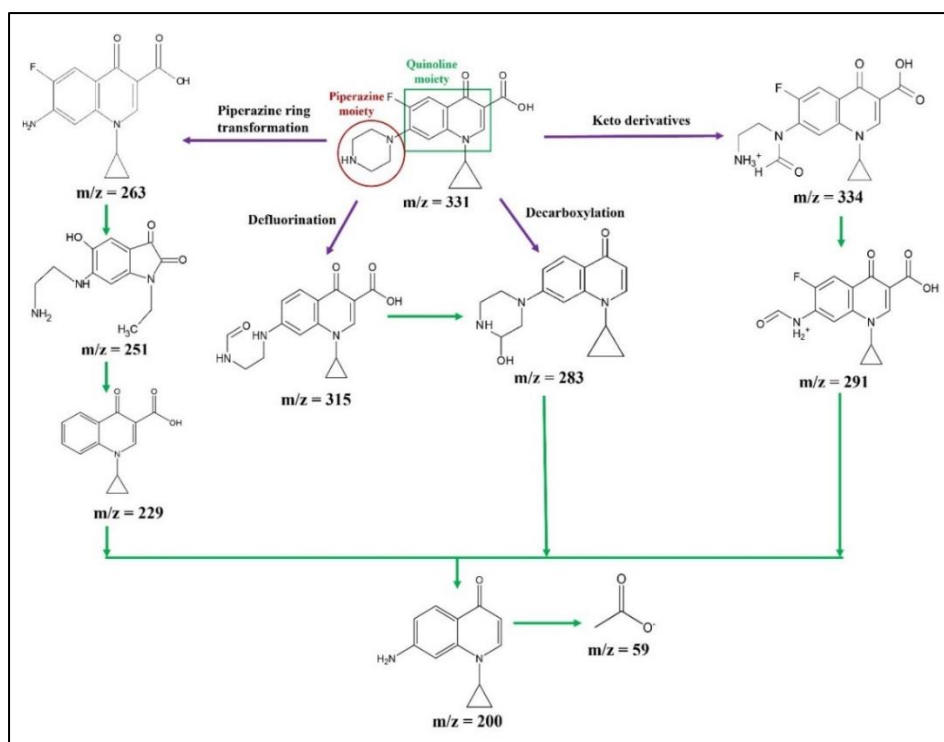


**Figure 5.13.** Possible degradation pathways of CIP from LC-MS analysis

#### 5.4. COMPARISON OF PERFORMANCE OF THE $B_{0.8}Ce_{0.2}TiO_2$ PHOTOCATALYST: SUSPENDED AND IMMOBILIZED FORMS, OTHER ANTIBIOTICS, SUNLIGHT AND UV-A IRRADIATION

It is well-known that the suspended form has better photocatalytic performance than the immobilized form due to the available larger surface area in the suspended form. The degradation efficiency obtained in the immobilized form (89.17%, 240 min) is slightly lesser than that of the suspended form (97.43%, 180 min) (**Figure 5.14a**). An increase in the treatment time/longer timeframes can be considered in order to achieve a higher efficiency. Moreover, in the large-scale applications, the immobilized form helps in catalysts reuse, and thus reduces the operating costs.

**Figure 5.14b** shows the performance of the catalyst for degradation of other antibiotics such as norfloxacin (NOR), levofloxacin (LEV), and moxifloxacin (MOX) performed using the  $B_{0.8}Ce_{0.2}TiO_2$  catalyst, both in suspended and immobilized form under sunlight. In the case of suspended form, the degradation of antibiotics at the end of 180 min is of the following order: CIP (97.43%) > NOR (95.3%) > LEV (92.55%) > MOX (82.31%). In the case of immobilized form, the degradation efficiency at the end of 240 min is of the following order: NOR (97.13%) > LEV (92.53%) > CIP (89.17%) > MOX (79.26%). These significant degradation results suggest the effectiveness of the codoped catalyst -  $B_{0.8}Ce_{0.2}TiO_2$  both in suspended and immobilized forms for the degradation of other antibiotics. However, a difference in the order of degradation efficiency was observed which might be due to the available larger surface area in the suspended form, difference in nature and chemical structure of antibiotics and immobilized form requires more energy (photons) (Bosio et al. 2018; Gaya and Abdullah 2008).

From **Figure 5.14c**, the degradation efficiency of CIP under sunlight is slightly higher than that under UV-A irradiation in the immobilized form whereas in the suspended form a significant effect of sunlight with higher degradation efficiency is observed. These results suggest that sunlight has less effect in the immobilized form. Similarly, in the literature (Bosio et al. 2018), higher degradation of antibiotics is reported under sunlight.

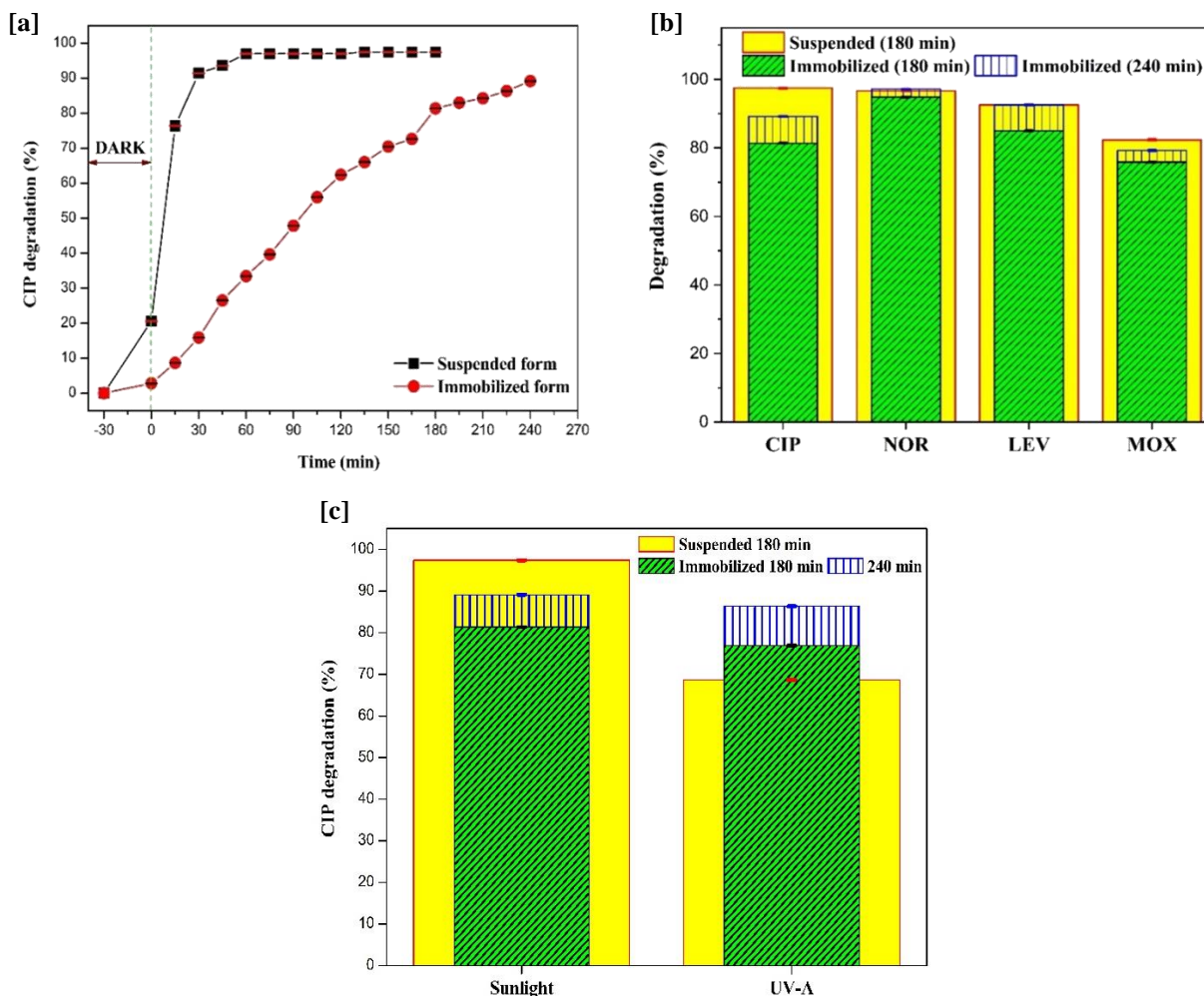


**Figure 5.14.** (a) Comparison of CIP degradation efficiency in suspended and immobilized forms, (b) Comparison of CIP degradation efficiency under sunlight and UV-A irradiation and (c) Degradation of other antibiotics using the  $B_{0.8}Ce_{0.2}TiO_2$  both in suspended and immobilized form

## 5.5. BATCH SCALE-UP STUDY AND EFFECT OF $H_2O_2$ CONCENTRATIONS

A batch scale-up study was performed using 550 mL of the CIP solution to determine the effectiveness of the  $B_{0.8}Ce_{0.2}TiO_2$  immobilized film for treating a larger volume of pollutant solution. The scale-up criteria employed is the ratio of the surface area of the polymer film to reactor volume, and the optimized conditions of the 200 ml reactor were used for the 550 mL reactor. The results are shown in **Figure 5.15a**. The degradation efficiency in both reactor volumes are fairly close to each other, thus confirming the scale-up criteria used. However, a slightly higher degradation for the

larger reactor volume (~ 86% degradation at 180 min compared to 225 min for the smaller reactor volume) is observed.

To enhance the degradation activity, the effect of hydrogen peroxide ( $H_2O_2$ , an oxidizing agent) on CIP degradation (at the optimum condition of 20 wt.% of catalyst dosage with 200 mL of 10 ppm CIP, and 180 min under sunlight) was examined by varying the concentrations of  $H_2O_2$  as 0.25, 0.5, 1, 2, and 4 mL per 200 mL CIP solution. In the photocatalytic degradation process,  $H_2O_2$  has a dual role. It can act as  $e^-$  scavenger (accepts  $e^-$  from conduction band), and it also forms  $\cdot OH$  (Bizani et al. 2006; Chen et al. 2004). As seen from **Figure 5.15b**, at lower concentrations of  $H_2O_2$  (0-1mL per 200 mL CIP solution), degradation efficiency was lesser due to insufficient hydroxyl radicals. However, with an increase in the  $H_2O_2$  concentrations to 2 ml the degradation efficiency increased from 81.36% (absence of  $H_2O_2$ , 0 mL per 200 mL CIP solution) to 89.04% due to the increase in the production of more  $\cdot OH$  by  $H_2O_2$ . Further, with an increase in the  $H_2O_2$  concentration (4 mL per 200 mL CIP solution), degradation efficiency decreased to 81.07% as scavenging of  $\cdot OH$  occurs due to the reaction between the excess amount of  $H_2O_2$  and  $\cdot OH$ , according to the following equations (Eq. 1-2) (Das and Mahalingam 2019b; Dönmez et al. 2020).

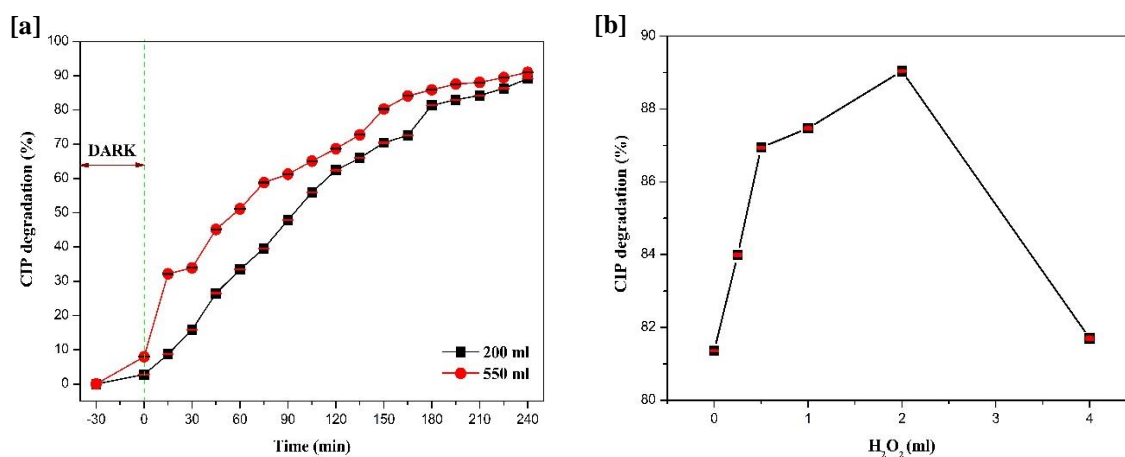
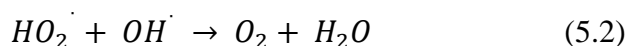
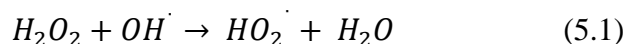


**Figure 5.15.** (a) Batch scale-up studies using 550 ml of CIP solution under sunlight and (b) Effect of  $H_2O_2$  as an oxidizing agent on degradation of CIP

Overall, the  $B_{0.8}Ce_{0.2}TiO_2$  catalyst was effective both in suspended and immobilized forms. Hence it was further explored to disinfect *E.coli* both in the absence and presence of CIP under sunlight.



**This page is left blank**

## CHAPTER 6

### PHOTOCATALYTIC DISINFECTION IN THE ABSENCE & PRESENCE OF ANTIBIOTIC AND EFFECT OF REAL WATER MATRICES

As mentioned earlier in section 1.2, antimicrobial resistance is mainly due to the presence of antibiotics in concentrations exceeding the predicted no-effect concentration postulated for the prevention of resistance development. Hence, the photocatalytic disinfection activity of the best performing catalyst namely  $B_{0.8}Ce_{0.2}TiO_2$  was studied both in the absence and presence of antibiotic (as well as in suspended and immobilized forms). Prior to this, the *E.coli* was tested for its resistance against the CIP (Antibiotic resistance assay - section 3.2.10), and it showed resistance to a concentration of 1 ppm CIP.

#### 6.1. PHOTOCATALYTIC DISINFECTION USING *E.coli*

##### 6.1.1. Disinfection in the absence of antibiotic (suspended and immobilized form)

From the degradation studies (Chapter 4), 1Ce-TiO<sub>2</sub> (0.5 g/L), 1B-TiO<sub>2</sub> (1.0 g/L) and  $B_{0.8}Ce_{0.2}TiO_2$  (0.5 g/L) showed the best performance. Thus, disinfection studies were performed using these catalysts and the immobilized form with  $B_{0.8}Ce_{0.2}TiO_2$  under optimized conditions to evaluate the effectiveness of the synthesized catalyst in terms of both degradation and disinfection. As seen in **Figure 6.1a**, photolysis confirmed the requirement of the photocatalyst to disinfect the *E.coli*. TiO<sub>2</sub> did not show any discernible disinfection activity. 1Ce-TiO<sub>2</sub> showed 1.302 log reduction (95.01%), and 1B-TiO<sub>2</sub> showed 6.426 log reduction (99.9999%).  $B_{0.8}Ce_{0.2}TiO_2$  catalyst showed 7.046 log reduction (99.99999%) after 180 min under sunlight (**Figure 6.1b**). In the case of  $B_{0.8}Ce_{0.2}TiO_2$  catalyst, the bacterial count (CFU/mL) was found to be below the LOD (limit of detection) at the end of 180 min. As the codoped catalyst showed a 1 log higher reduction, it can be considered to be ~10 times more effective than that of the monodoped catalysts (as 1 log reduction corresponds to a decrease in the bacterial count by a factor of 10). In the immobilized form, 6.357 log reduction was observed (**Figure 6.1b**). This result indicates that the immobilized

photocatalytic film is quite effective in disinfecting the target micro-organism as this result is in close proximity to the result obtained for the suspended form. However, further work is needed in this aspect. From the literature (Wang et al. 2016c, 2018), boron is a good disinfectant, and in this study, also B-TiO<sub>2</sub> showed significant activity. The agar plates showing the disinfection activity using photolysis, TiO<sub>2</sub>, 1Ce-TiO<sub>2</sub>, 1B-TiO<sub>2</sub>, and B<sub>0.8</sub>Ce<sub>0.2</sub>TiO<sub>2</sub> are given in **Figure A1** (Appendix II).

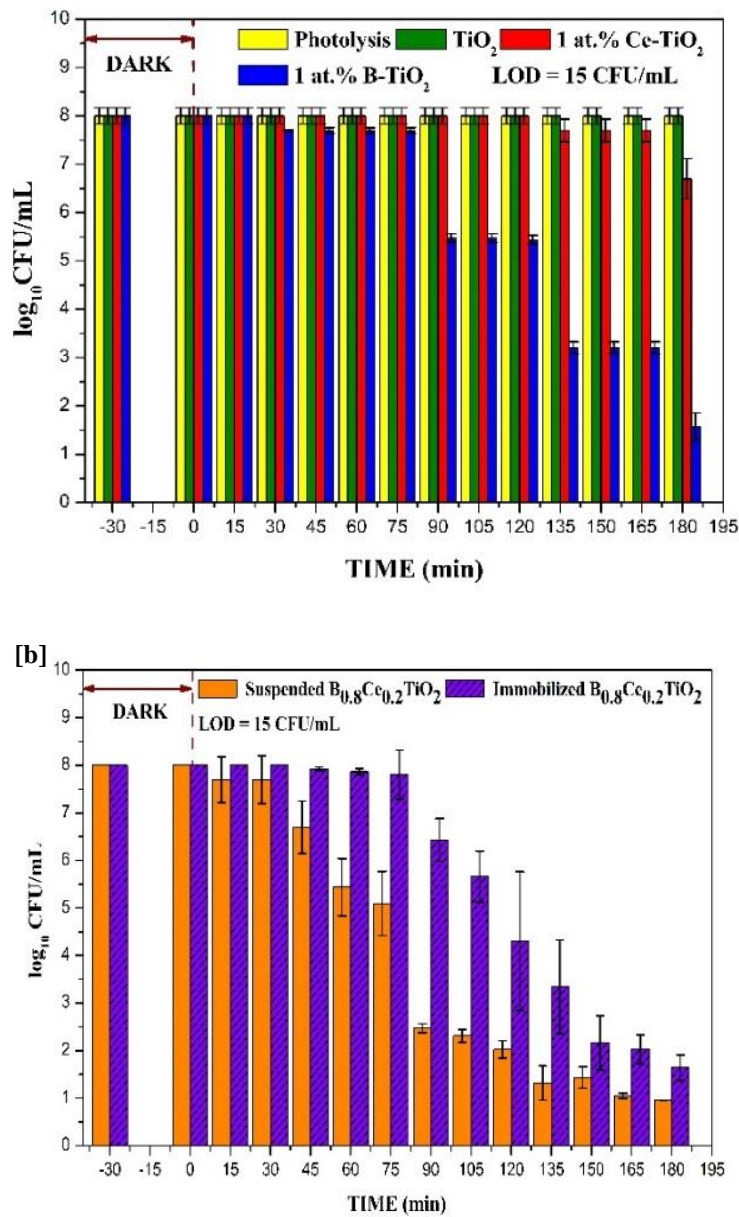


**Figure 6.1.** Disinfection using TiO<sub>2</sub> and best-performing catalysts under sunlight (Initial cell concentration 10<sup>8</sup> CFU/mL, duration -180 min)

### 6.1.2. Disinfection in the presence of antibiotic (suspended and immobilized form)

In the presence of CIP (1 ppm), there is a slight increase in the bacterial log reduction (**Figure 6.2**) which needs further investigation. Similarly, in the literature (Eswar et al. 2016), a slight increase in bacterial disinfection in the presence of antibiotic has been reported. Thus, the  $B_{0.8}Ce_{0.2}TiO_2$  catalyst was effective in terms of both degradation and disinfection (in the absence and presence of antibiotic). The agar plates showing the disinfection activity in the presence of antibiotic using photolysis,  $1Ce-TiO_2$ ,  $1B-TiO_2$  &  $B_{0.8}Ce_{0.2}TiO_2$  are given in **Figure A2** (Appendix II).

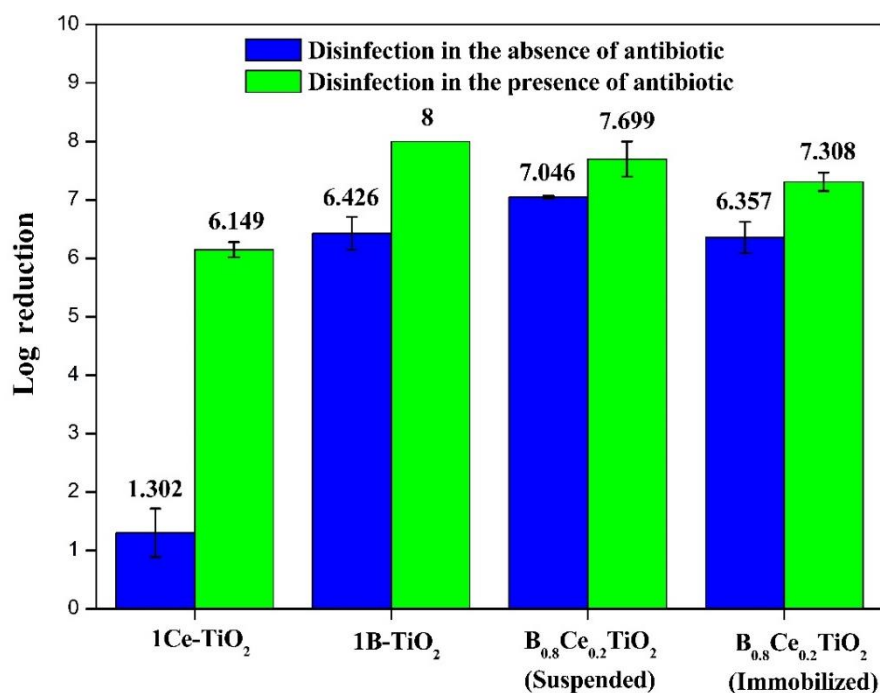


**Figure 6.2.** Photocatalytic disinfection in the absence and presence of antibiotic

### 6.1.3. Regrowth studies

The potential regrowth of bacteria after the photocatalytic treatment (after incubation) was evaluated by storing the bacterial plates for 3 days in the dark at room temperature (Biancullio et al. 2019). The presence of organic content (recalcitrant compounds – here referring to antibiotic) might help to utilize available carbon sources and contribute towards the survival of bacteria (Thayanukul et al. 2013; Zhao

et al. 2014). In this regard, incubated agar plates observed with zero colonies were examined for regrowth. In the case of photolysis, regrowth was observed (**Figure A2**, Appendix), thus suggesting that sunlight alone has no effect on bacterial disinfection and a photocatalyst is required. No regrowth was observed after 3 days in the case of 1B-TiO<sub>2</sub> and B<sub>0.8</sub>Ce<sub>0.2</sub>TiO<sub>2</sub> catalysts (**Figure A2**, Appendix II), thus, confirming the bacterial cell death.

#### 6.1.4. Disinfection kinetics

The kinetics were studied using the following equation (Eq. 6.1) as mentioned in the literature (Geeraerd et al. 2000, 2005) using GlnaFit tool (Version 1.7). From the kinetics plot of {log<sub>10</sub> (N) [CFU/mL]} vs. time, (**Figure 6.3 (a-d)**),  $k_{max}$  and R<sup>2</sup> values are determined (see **Table 6.1**) which has a shoulder (initial flat portion), linear (center portion), and tail (final flat portion).

$$N(t) = \left( \frac{(N(0) - N_{res}) * \exp(-k_{max}t) * (\exp(k_{max} * Sl))}{(1 + (\exp(k_{max} * Sl) - 1) * \exp(-k_{max}t))} \right) + N_{res} \quad (6.1)$$

where,  $N(t)$  = cell concentration at time  $t$  (CFU/mL),  $N(0)$  = initial cell concentration (CFU/mL),  $t$  = reaction time (min),  $k_{max}$  = rate constant (min<sup>-1</sup>),  $Sl$  = Shoulder length (as calculated by the tool),  $N_{res}$  = more resistant subpopulation (tail portion, as calculated by the tool).

The  $k_{max}$  values are higher for disinfection in the presence of CIP (antibiotic) when compared to disinfection in the absence of CIP. These results suggest that the disinfection ability of the immobilized film is better even in the presence of antibiotic (CIP) which is essential in the real-water matrix application as it contains both antibiotic residues and superbugs.

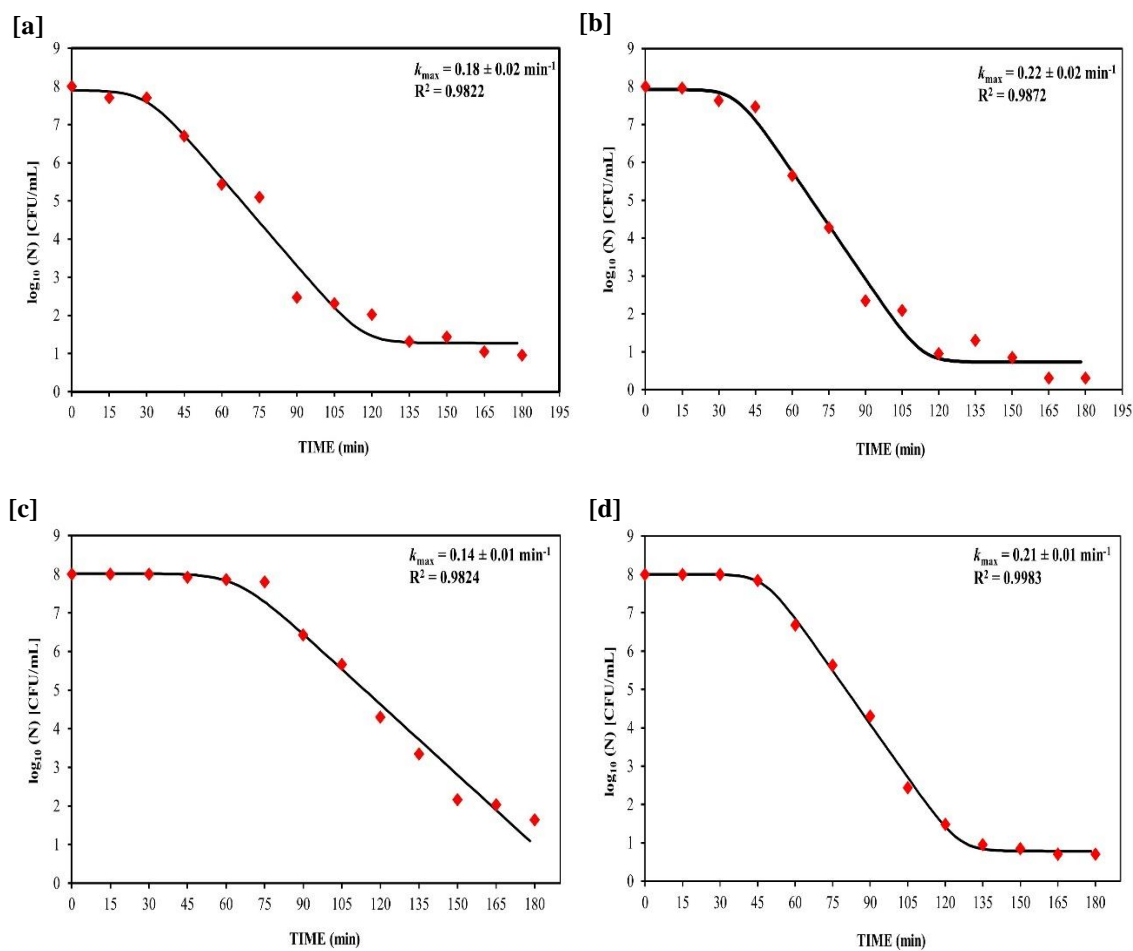


**Figure 6.3.** Kinetics plot of disinfection in the absence and presence of 1 ppm CIP using  $B_{0.8}Ce_{0.2}TiO_2$  (a-b) Suspended form and (c-d) Immobilized form

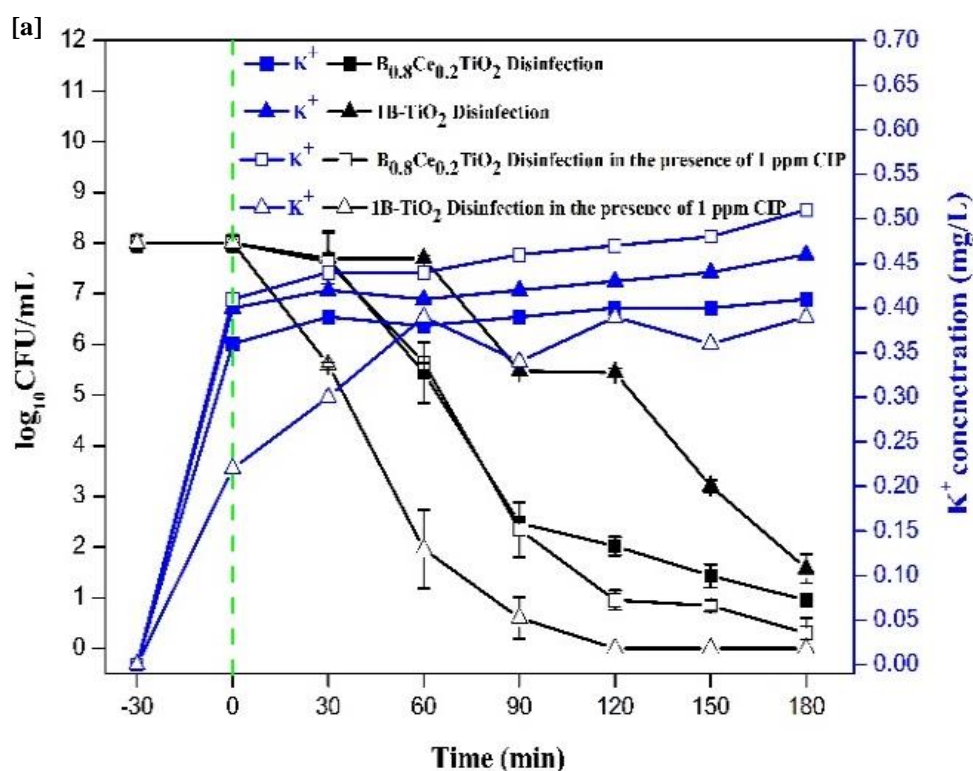
**Table 6.1.** Kinetics of *E.coli* disinfection in the absence and presence of CIP using  $B_{0.8}Ce_{0.2}TiO_2$  catalyst

PHOTOCATALYSTS	$k_{max}$ ( $min^{-1}$ )		$R^2$	
	Absence of CIP	Presence of 1ppm CIP	Absence of CIP	Presence of 1 ppm CIP
$B_{0.8}Ce_{0.2}TiO_2$ (Suspended form)	0.18	0.22	0.9822	0.9872
$B_{0.8}Ce_{0.2}TiO_2$ (Immobilized form)	0.14	0.21	0.9824	0.9983

### 6.1.5. Determination of $K^+$ ions using ICP-OES in the disinfected sample (suspended and immobilized forms)

Potassium ions are the major intracellular cations in bacteria that act as a second messenger molecule. It is involved in the maintenance of a constant internal pH and membrane potential. The generated reactive oxygen species (during photocatalysis) damages the bacterial cell membrane, thus resulting in leakage of  $K^+$  ions. In this regard, as the reaction time increases, the *E.coli* cell concentration decreases, and the concentration of  $K^+$  increases. This indicates the loss of cell membrane permeability thus providing indirect evidence of membrane damage and in turn, cell death.

From **Figure 6.4 (a-b)**, the release of  $K^+$  ions increased, corresponding to a decrease in the cell viability (with an increase in the treatment time). These results are in accordance with the literature (Das et al. 2017; Yan et al. 2020) and thus confirm the cell membrane damage through photocatalytic activity. The concentration of  $K^+$  ions was found to be higher in the sample treated with  $B_{0.8}Ce_{0.2}TiO_2$  compared to  $1B-TiO_2$ , which indicates the synergistic effect of dopants (B and Ce).



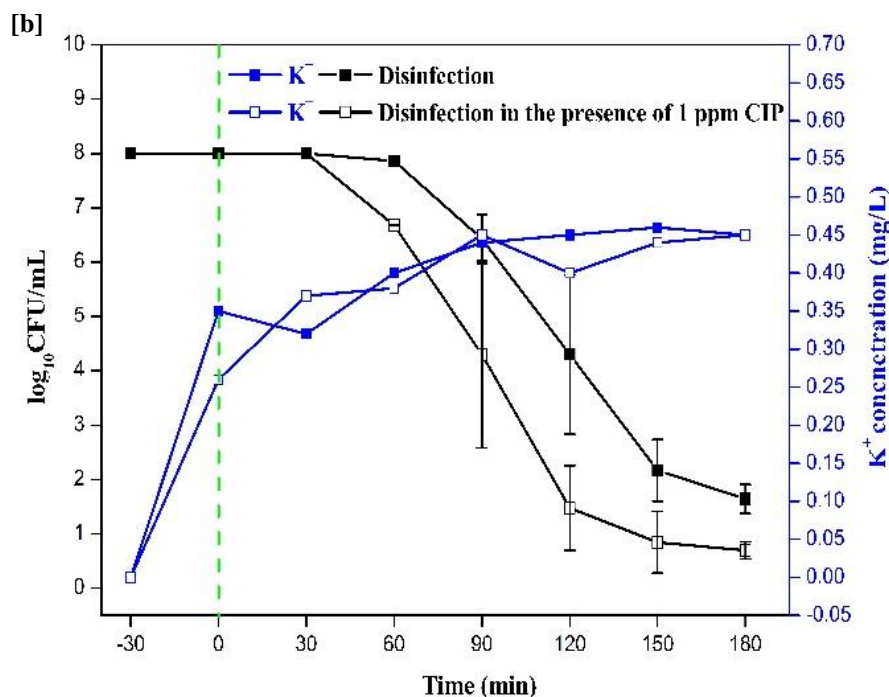


**Figure 6.4.** Release of  $K^+$  ions during disinfection with an increase in the treatment time (a) Suspended form and (b) Immobilized form

## 6.2. EFFECT OF REAL WATER MATRICES

In view of practical application, the water matrices/quality plays a prominent role. Hence, the photocatalytic degradation and disinfection activities of the best performing codoped catalyst (under optimized conditions, both in suspended and immobilized forms) were studied using tap water and river water.

As shown in **Figure 6.5 (a-d)**, CIP degradation efficiency and *E.coli* disinfection in the absence & presence of 1 ppm CIP (under sunlight, 180 min) in river water and tap water were found to be lesser than those observed in the deionized water. This might be due to the presence of anions and natural organic matter present in the real water samples, which react with the generated reactive species, thus resulting in a weaker oxidizing agent (Wang et al. 2012). These species could also act as a scavenging agent for  $\cdot OH$  and  $h^+$  (Wang et al. 2017a). A similar trend for degradation of CIP in different water matrices has been reported in the literature (Sarafraz et al. 2020). The disinfection activity was higher in the case of tap water which might be due to the presence of chlorine ions and this needs further investigation.



**Figure A3 and Figure A5** (Appendix II) show agar plates with disinfection using different water samples in suspended and immobilized form, respectively. **Figure A4 and Figure A6** (Appendix II) show agar plates with disinfection in the presence of 1 ppm CIP using different water matrices in suspended and immobilized form, respectively.

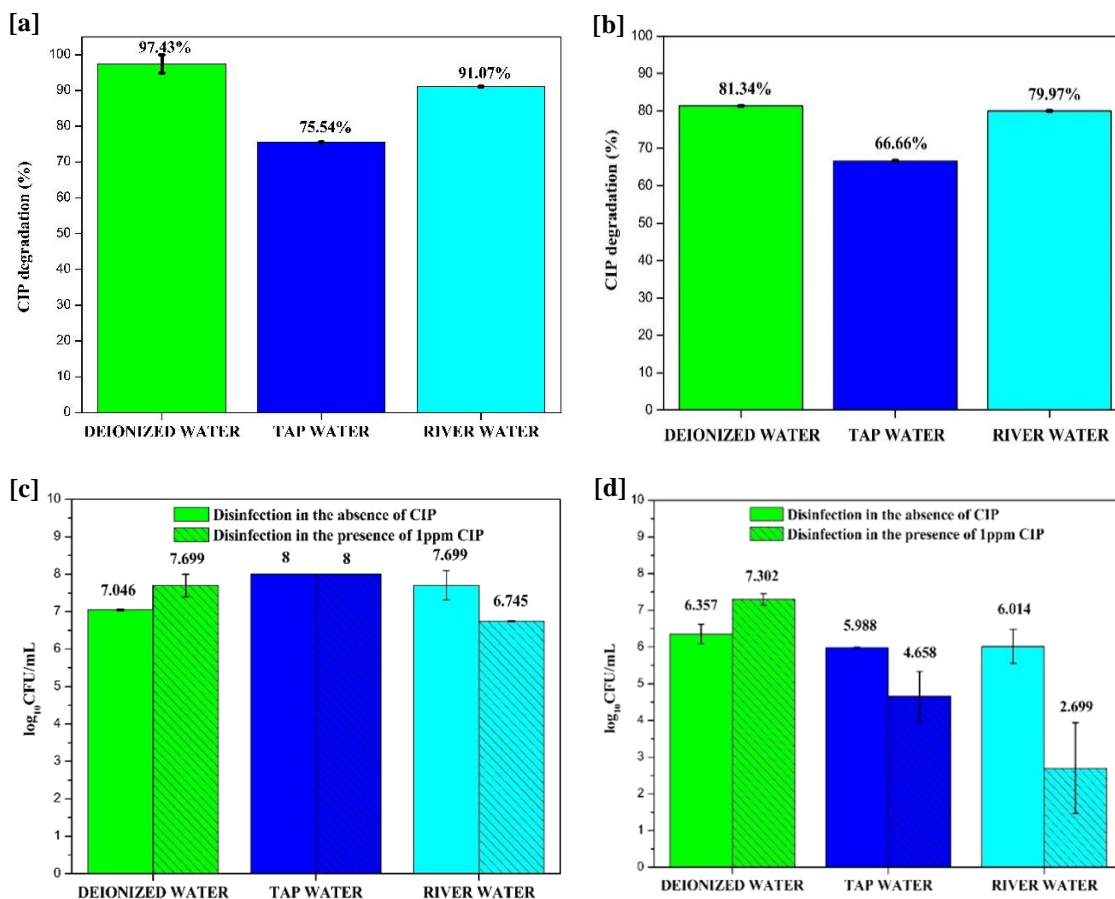


**Figure 6.5.** Photocatalytic degradation of CIP under different water matrices (a) suspended form and (b) immobilized form; Photocatalytic disinfection of *E.coli* (c) suspended form and (d) immobilized form **Experimental conditions:** Suspended form:  $B_{0.8}Ce_{0.2}TiO_2$  - 0.5 g/L, CIP - 10 ppm/ *E.coli* -  $10^8$  CFU/mL, under sunlight - 180 min, Immobilized form: 20 wt.%  $B_{0.8}Ce_{0.2}TiO_2$  EPS immobilized film, CIP - 10 ppm/ *E.coli* -  $10^8$  CFU/mL, under sunlight - 180 min

## CHAPTER 7

### CONCLUSIONS AND SCOPE FOR FUTURE WORK

The results of the present study are summarized, and the major conclusions observed are stated. Overall, the results suggest that doping has a significant effect on both degradation and disinfection, and thus the B and Ce doped photocatalysts under the study serve as an efficient solar light active bifunctional catalyst in solving the emerging global problem of antimicrobial resistance.

#### 7.1. SUMMARY

This study aimed at identifying a bifunctional catalyst suitable for both degradation and disinfection. A series of monodoped and codoped TiO<sub>2</sub> catalysts involving boron and cerium dopants were synthesized using the green EDTA-citrate method. These photocatalysts were investigated for degradation of ciprofloxacin (an antibiotic) and disinfection of *E.coli* under sunlight. B showed its efficacy in terms of disinfection, and Ce showed higher adsorption ability, promoting the degradation. The utilization of visible light has been significantly enhanced upon doping. Thus, these two dopants have shown their synergistic effects. The method of selecting the concentration of dopants (for codoping) by studying the individual dopant photocatalytic activity (through monodoping) helps in identifying the appropriate concentration of a dopant for solving a particular problem and hence, minimizes the chemicals required for bulk synthesis. The immobilized form was found to be effective in terms of both degradation and disinfection. Waste expanded polystyrene beads being used for immobilization, and the catalyst's effectiveness under sunlight makes this process feasible and renewable. The performance of TiO<sub>2</sub> and the synthesized catalysts based on certain parameters obtained from the various characterizations as well as the degradation & disinfection performance, are summarized in **Table 7.1**. Among the synthesized catalysts under the study, 1 at.% Ce-TiO<sub>2</sub>, 1 at.% B-TiO<sub>2</sub> (monodoped) and B<sub>0.8</sub>Ce<sub>0.2</sub>TiO<sub>2</sub> (codoped) are the best-performing catalysts. In terms of disinfection, the codoped catalyst was 10 times more effective than that of the monodoped catalysts.

**Table 7.1.** Performance of photocatalysts under the study based on crystallite size, bandgap energy, adsorption, degradation, COD/TOC reduction, and disinfection (suspended and immobilized forms)

PHOTOCATALYSTS	Crystallite size (nm)	Surface area (m <sup>2</sup> /g)	Bandgap (eV)	Adsorption (%)	CIP degradation (%)	COD/TOC reduction (%)	Disinfection* (log reduction/ equivalent %)
<b>TiO<sub>2</sub></b>	15.99	35	3.29	3.50	69.29	50	0
<b>0.1 at.% Ce-TiO<sub>2</sub></b>	14.06	30.84	2.74	24.77	91.11	68	NE
<b>1 at.% Ce-TiO<sub>2</sub></b>	16.95	41.486	<b>2.50</b>	<b>48.71</b>	<b>93.22</b>	92	1.302 (95.01%) 6.149 (99.9999%) <sup>#</sup>
<b>1 at.% B-TiO<sub>2</sub></b>	19.82	30.124	2.89	12.82	<b>93.16</b>	93	6.426 (99.9999%) 8 (100%) <sup>#</sup>
<b>2 at.% B-TiO<sub>2</sub></b>	17.96	29.955	2.87	16.37	91.37	64	NE
<b>B<sub>0.9</sub>Ce<sub>0.1</sub>TiO<sub>2</sub></b>	20.52	31.323	2.57	9.57	92.55	82	NE
<b>B<sub>0.8</sub>Ce<sub>0.2</sub>TiO<sub>2</sub></b>	17.33	32.115	2.63	20.51	<b>97.43</b>	96	7.046 (99.9999%) 7.699 (99.9999%) <sup>#</sup>
<b>B<sub>0.7</sub>Ce<sub>0.3</sub>TiO<sub>2</sub></b>	16.83	43.198	2.64	13.82	91.57	80	NE
<b>B<sub>0.8</sub>Ce<sub>0.2</sub>TiO<sub>2</sub> immobilized EPS film</b>	NA		NA	2.80	81.36 (180 min) 89.17 (240 min)	46.41 (180 min) 84.41 (240 min)	6.357 (99.9999%) 7.302 (99.9999%) <sup>#</sup>

# - Disinfection in the presence of antibiotic (1ppm CIP), NE - not evaluated or \* - only best performing catalysts evaluated for disinfection,

NA- Not applicable

## 7.2. CONCLUSIONS

The major conclusions that can be drawn from this work are as follows:

- Suspended form:
  - The particle size of the catalysts is in the nanoparticle size range. The highest surface area was shown by  $B_{0.7}Ce_{0.3}TiO_2$  among the codoped series and 1 at.% Ce- $TiO_2$  among the monodoped series.
  - From SEM analysis, the morphology of the catalysts appeared as irregular aggregates with the agglomeration affected by the ionic radius of the dopants. Further, the TEM analysis showed roughly spherical particles, and the SAED pattern indicates the presence of (101, 004) anatase planes and (200) Ce plane.
  - The XRD diffraction peaks indicated the presence of anatase, rutile, and Ce peaks. Ce due to its larger ionic radius than that of  $TiO_2$ , either exists on the surface of  $TiO_2$  or Ti enters the lattice of  $CeO_2$  with the formation of Ti-O-Ce bonds. The absence of prominent boron peaks indicated the uniform dispersion of B in  $TiO_2$  (with the formation of B-O-Ti bonds) due to its ionic radius being lesser than that of  $TiO_2$ . The XPS analysis confirmed the presence of B in both substitutional and interstitial positions at higher concentrations of B (2 at.%) and only in the interstitial position ( $\leq 1$  at.%) along with the existence of  $Ti^{3+}$ , &  $Ce^{4+}$ . Also, the determined elemental composition of the doped catalysts (both monodoped and codoped) was in accordance with the desired composition.
  - The absorption edge of the doped catalysts showed a redshift towards the visible light range. The bandgap energy values of the codoped catalysts were in the range of 2.57-2.64 eV, and these values are in between the range of bandgap energy values observed for the monodoped catalysts (2.5-2.9 eV), suggesting a synergistic effect of the dopants. PL analysis showed lower recombination with effective separation of electron-hole pairs, which are trapped in dopant sites.
  - The enhancement in the photocatalytic activity of 1Ce- $TiO_2$ , 1B- $TiO_2$ , and  $B_{0.8}Ce_{0.2}TiO_2$  catalysts can be ascribed to the higher adsorption capacity of Ce, which provides a better contact between pollutant and catalyst. The higher crystallinity/higher anatase content, as observed from XRD analysis, possibly

significantly influences the mineralization of the pollutant molecule. The narrowed bandgap (as observed from DRS analysis) and higher crystallinity reduce the formation of electron traps and minimize recombination (as confirmed from PL analysis). The presence of B in the interstitial lattice position, as confirmed from XPS, helps in trapping photogenerated charges effectively. These factors have contributed to the synergy of the dopants and thus improved the photocatalytic activity.

- The degradation of CIP obeyed pseudo-first-order kinetics, and  $k$  values are given in **Table 7.2** for the best performing catalysts. The  $k$  values were found to be decreasing with the increasing initial concentrations of pollutant due to the competition of a higher number of pollutants for the active sites on the catalysts.

**Table 7.2.** Kinetics data of best-performing catalysts

PHOTOCATALYSTS	$k$ ( $\text{min}^{-1}$ )
1 at.% Ce-TiO <sub>2</sub>	0.0266 ± 0.0006
1 at.% B-TiO <sub>2</sub>	0.0249 ± 0.0010
B <sub>0.8</sub> Ce <sub>0.2</sub> TiO <sub>2</sub>	0.0452 ± 0.0008

- From the trapping experiments, electrons were the dominant species responsible for the photocatalytic activity, followed by holes and  $\cdot\text{OH}$ .
- The recyclability studies showed a slight decrease in the degradation efficiency of the photocatalysts in five consecutive runs. After the fifth run, ~ 20% decrease in the degradation efficiency was observed for both types of catalysts. These results confirm the stability of the catalysts.
- The photocatalytic degradation of CIP was found to occur mainly through the transformation of piperazine ring, defluorination, decarboxylation, and formation of keto derivatives. The decrease in the intensity of the pollutant peak in the HPLC/LC-MS data validates the effective photocatalytic degradation under sunlight.
- No inhibition zones were observed for residual antibacterial activity of the degraded CIP sample after 60 min and are in agreement with the degradation trend observed. This suggests the loss of antibiotic activity by the degraded sample.

- In real water samples, the degradation efficiency of CIP slightly decreased when compared to that in the deionized water sample due to the presence of anions and natural organic matter.
- Immobilized form:
  - The best performing codoped catalyst ( $B_{0.8}Ce_{0.2}TiO_2$ ) was immobilized using waste expanded polystyrene beads.
  - From the FESEM analysis, the distribution of catalyst particles on the surface of the film was clearly visible along with pores which act as active sites for photocatalytic activity. The average thickness of the film was 1087  $\mu m$  with an average roughness of 15.4323  $\mu m$ .
  - From contact angle measurements, after loading of  $B_{0.8}Ce_{0.2}TiO_2$  photocatalyst, the EPS film behaved as hydrophilic in nature. From the XPS analysis, the actual amount of the immobilized photocatalyst was in accordance with the intended amount during the preparation of the film.
  - The CIP degradation efficiency was found to be 81.36% after 180 min, and a final degradation of 89.17% after 240 min was observed. The degraded sample showed a TOC reduction of 46.41% after 180 min and 84.41% after 240 min. From kinetic studies, the order of the reaction was found to follow the pseudo-first order kinetics with  $k$  value of  $8.13 \times 10^{-3} \pm 0.2$  ( $\text{min}^{-1}$ ) and  $R^2$  of 0.9906.
  - The loss of antibiotic activity/residual antimicrobial activity of the degraded CIP sample was confirmed from the decrease or absence of inhibition zones with an increase in the photocatalytic treatment time.
  - From the reusability studies, the  $B_{0.8}Ce_{0.2}TiO_2$  immobilized EPS film was found to be stable even after five cycles of reuse with a slight decrease in degradation efficiency (~ 10% decrease). No morphological, structural, and chemical changes in the film were observed (after five times of reuse) as confirmed from FESEM, XRD, and FTIR analysis, respectively. Minute traces of doped elements (B and Ce) were observed from ICP-OES analysis (leaching study).
  - The photocatalytic degradation of CIP was found to occur mainly through the transformation of piperazine ring, defluorination, decarboxylation, and formation of keto derivatives. The decrease in the intensity of the pollutant

peak with an increase in the treatment time (HPLC/LC-MS data) validates the effective photocatalytic degradation under sunlight.

- A slightly higher degradation for the larger reactor volume of 550 ml (~ 86% degradation at 180 min compared to the same at 225 min for the smaller reactor volume of 200 ml) was observed using the same optimized conditions of 200 ml for the larger reactor volume (scale-up criteria – ratio of the surface area of the polymer film to reactor volume).
- In the presence of oxidizing agent ( $H_2O_2$  – 2 ml of  $H_2O_2$  per 200 ml of CIP solution), the CIP degradation efficiency increased from 81.36% to 89.04% due to the increase in the production of  $\cdot OH$  by  $H_2O_2$ . With an increase in the  $H_2O_2$  concentration above the optimum concentration, the degradation efficiency decreased due to the scavenging of OH radicals.
- The degradation efficiency of CIP is slightly higher under sunlight (89.17%, 240 min) than that under the UV-A irradiation (86.35%, 240 min).
- The degradation efficiency obtained in the immobilized form (89.17%, 240 min) is slightly lesser than that of the suspended form (97.43%, 180 min). An increase in the treatment time/longer timeframe is required to achieve higher efficiency. However, in the large-scale applications, the immobilized form helps in catalyst reuse and thus reduces the operating costs.
- The codoped catalyst -  $B_{0.8}Ce_{0.2}TiO_2$  was found to be effective against other antibiotics, and the observed degradation efficiencies are given in **Table 7.3**.

**Table 7.3.** Degradation efficiencies of various antibiotics using  $B_{0.8}Ce_{0.2}TiO_2$  catalyst

$B_{0.8}Ce_{0.2}TiO_2$	DEGRADATION (%) after 180 min under sunlight			
	CIP	NOR	LEV	MOX
<b>Suspended form</b>	97.43	95.3	92.55	82.31
<b>Immobilized form</b>	89.17	97.13	92.53	79.26

- Photocatalytic disinfection and application in real water matrices:
  - In the absence of CIP: The disinfection efficiency of the  $B_{0.8}Ce_{0.2}TiO_2$  catalyst was found to be 99.99999% (7.046 log reduction). The monodoped catalysts showed 6.432 log reduction ( $1B-TiO_2$ ) translating into a 1 log difference, and

thus it can be inferred that the codoped catalysts can be considered to be ~10 times more effective.

- In the presence of 1 ppm CIP:  $B_{0.8}Ce_{0.2}TiO_2$  catalyst showed disinfection efficiency of 99.99999% (7.699 log reduction) and 1B- $TiO_2$  showed complete disinfection (8 log reduction). No regrowth was observed in the plates kept under dark for 3 days at room temperature (incubated agar plates) suggesting the complete inactivation of *E.coli*.
- In the immobilized form, the disinfection efficiency was found to be 99.99999% (6.357 log reduction) in the absence of CIP and 99.99999% (7.302 log reduction) in the presence of CIP. These results indicate that the immobilized photocatalytic film is quite effective in disinfecting the target micro-organism as the disinfection efficiency is quite close the efficiency obtained in the suspended form
- From the kinetics plot of  $\{\log_{10} (N) [CFU/mL]\}$  vs. time,  $k$  values of  $0.18 \text{ min}^{-1}$  ( $R^2 = 0.9822$ ) and  $0.22 \text{ min}^{-1}$  ( $R^2 = 0.9872$ ) were observed for disinfection in the absence and presence of CIP respectively for  $B_{0.8}Ce_{0.2}TiO_2$  (suspended form). And for the same catalyst in immobilized form,  $k$  values of  $0.14 \text{ min}^{-1}$  ( $R^2 = 0.9824$ ) and  $0.21 \text{ min}^{-1}$  ( $R^2 = 0.9983$ ) was observed for disinfection in the absence and presence of CIP respectively.
- The degradation efficiency of CIP and disinfection efficiency using tap water and river water (real water samples) was found to be slightly lesser than that observed in the deionized water sample which could be due to the presence of anions and natural organic matter in the real water samples.

Overall, these boron and cerium doped catalysts were effective in terms of both degradation & disinfection under sunlight both in suspended & immobilized forms. In comparison with recent literature involving the ciprofloxacin antibiotic and advanced/latest generation photocatalysts (**Figure 4.12, Table 7.4**), it is evident that these doped catalysts are as efficient or perhaps better than some of the latest generation photocatalysts.



**Table 7.4.** Comparison of CIP degradation efficiency of this work with some latest generation photocatalysts

PHOTOCATALYST	EXPERIMENTAL CONDITIONS/ MAJOR RESULTS	REFERENCE
AgBr/Ag <sub>3</sub> PO <sub>4</sub> @natural hematite heterojunction	Norfloxacin, CIP, ofloxacin, enoxacin, and penicillin C <sub>0</sub> – 15 mg/L Degradation – 83%, 53%, 40%, 70%, and 20% respectively (0.17 g/L) T – 90 min	(Chen et al. 2019)
Zn doped-Cu <sub>2</sub> O	CIP C <sub>0</sub> – 20 mg/L Degradation – 78% (0.6 g/L) T – 60 min	(Yu et al. 2019)
AgNPs@BP (black phosphorus nanosheets)	CIP, NOR, sulfadiazine (SDZ), and tetracycline (TTC) C <sub>0</sub> – 1 mg/L Degradation – 95%, 95%, 93% and 79% respectively (5 mmol/L) T – 30 min	(Chen et al. 2020)
S–C <sub>3</sub> N <sub>4</sub> /ZnO hybrid heterojunction	CIP C <sub>0</sub> – 20 mg/L Degradation – 98.8%, 75.8% (1 g/L) T – 210 min	(Gupta et al. 2020)
TiO <sub>2</sub> /g-C <sub>3</sub> N <sub>4</sub> heterojunction	CIP C <sub>0</sub> – 20 μmol/L Degradation – 93.4% (0.2 g/L) T – 60 min	(Hu et al. 2020)
Black Ti <sup>3+</sup> /N-TiO <sub>2</sub> (b-N-TiO <sub>2</sub> )	CIP C <sub>0</sub> – 0.5 mg/L Degradation – 100% (0.4 g/L) T – 70 min	(Sarafraz et al. 2020)

Bi <sub>2</sub> WO <sub>6</sub> /C <sub>3</sub> N <sub>4</sub> /Ti <sub>3</sub> C <sub>2</sub> composite	CIP C <sub>0</sub> – 10 mg/L Degradation – 87.4% (1.5 g/L) T – 70 min	(Wu et al. 2020)
Zn doped BiOCl nanosheets	CIP C <sub>0</sub> – 10 mg/L Degradation – 98% (1 g/L) T – 80 min	(Xu et al. 2020)
Sm-doped g- C <sub>3</sub> N <sub>4</sub> /Ti <sub>3</sub> C <sub>2</sub> MXene heterojunction	CIP C <sub>0</sub> – 20 mg/L Degradation – 99% (0.2 g/L) T – 60 min	(Yu et al. 2020)
TiO <sub>2</sub> -pillared multilayer graphene nanocomposites	CIP C <sub>0</sub> – 15 mg/L Degradation – 78% (0.5 g/L) T – 150 min	(Zeng et al. 2020)
FeWO <sub>4</sub> /NC (nitrogen doped carbon) nanocomposite	CIP C <sub>0</sub> – 20 mg/L Degradation – 92.23% (10 mg/L) T – 100 min	(Ahamad et al. 2021)
B-TiO <sub>2</sub> Ce-TiO <sub>2</sub> B <sub>x</sub> Ce <sub>1-x</sub> TiO <sub>2</sub>	CIP C <sub>0</sub> – 10 mg/L Degradation – 1 at.% B-TiO <sub>2</sub> – 93.16% (1 g/L) 1 at.% Ce-TiO <sub>2</sub> – 93.22% (0.5 g/L) B <sub>x</sub> Ce <sub>1-x</sub> TiO <sub>2</sub> – 97.43% (0.5 g/L) T – 180 min	This work

### 7.3. SCOPE FOR FUTURE WORK

This study paves the way for some of the following applications/experimental work in the future.

- Application of the developed photocatalysts for the degradation of mixture of antibiotics/other antibiotics, disinfection of multi-drug resistant micro-organisms, other organic pollutants such as heavy metals removal, CO<sub>2</sub> reduction and oil spill removal.
- To evaluate for the simultaneous degradation and disinfection activities using the developed photocatalysts.
- To examine the photocatalytic activity of other emerging contaminants such as pesticides, heavy metals removal etc.
- To study the effect of inorganic ions (present in real water samples) on photocatalytic activity.
- The facile immobilized film prepared can be used for industrial applications (reactor design). Application of biopolymers such as alginate for immobilization of photocatalysts can be considered.
- Development of ternary doped photocatalyst (B/Ce/X-TiO<sub>2</sub>, where X = Ag/Br) using the facile synthesis method or development of doped/heterostructure photocatalyst for the removal of emerging contaminants.
- Cost analysis of the photocatalytic process (reactor studies).

## REFERENCES

- Abass, A. K. (2018). "Effect Type of Solvent , Type of Catalyst and Power of Lamp on Photo Oxidation of Benzene." *J. Univ. Babylon Eng. Sci.*, 26(10), 197–207.
- Ahamad, T., Naushad, M., and Alshehri, S. M. (2021). "Analysis of degradation pathways and intermediates products for ciprofloxacin using a highly porous photocatalyst." *Chem. Eng. J.*, 417(February 2020), 127969.
- Ahmed, M. B., Zhou, J. L., Ngo, H. H., and Guo, W. (2015). "Adsorptive removal of antibiotics from water and wastewater: Progress and challenges." *Sci. Total Environ.*, 532, 112–126.
- Akpan, U. G., and Hameed, B. H. (2010). "The advancements in sol-gel method of doped-TiO<sub>2</sub> photocatalysts." *Appl. Catal. A Gen.*, 375(1), 1–11.
- Ali, Z., Raj, B., Vishwas, M., and Athhar, M. A. (2016). "Synthesis , Characterization and Antimicrobial Activity of Ce Doped TiO<sub>2</sub> Nanoparticles." 5(4), 705–712.
- Alim, S. A., Rao, T. S., Raju, I. M., Kumar, M. R., and Lakshmi, K. V. D. (2019). "Fabrication of visible light driven nano structured Copper, Boron codoped TiO<sub>2</sub> for photocatalytic removal of Lissamine Green B." *J. Saudi Chem. Soc.*, 23(1), 92–103.
- Alrousan, D. M. A., Polo-López, M. I., Dunlop, P. S. M., Fernández-Ibáñez, P., and Byrne, J. A. (2012). "Solar photocatalytic disinfection of water with immobilised titanium dioxide in re-circulating flow CPC reactors." *Appl. Catal. B Environ.*, 128, 126–134.
- Amoresi, R. A. C., Oliveira, R. C., Marana, N. L., Almeida, P. B. De, Prata, P. S., Zaghete, M. A., Longo, E., Sambrano, J. R., and Simões, A. Z. (2019). "CeO<sub>2</sub> Nanoparticle Morphologies and Their Corresponding Crystalline Planes for the Photocatalytic Degradation of Organic Pollutants." *ACS Appl. Nano Mater.*, 2(10), 6513–6526.
- An, T., Yang, H., Li, G., Song, W., Cooper, W. J., and Nie, X. (2010). "Kinetics and mechanism of advanced oxidation processes (AOPs) in degradation of ciprofloxacin

in water.” *Appl. Catal. B Environ.*, 94(3–4), 288–294.

Andrade, F. V. De, Lima, G. M. de, Augusti, R., Silva, J. C. C. da, Coelho, M. G., Paniago, R., and Machado, I. R. (2015). “A novel TiO<sub>2</sub>/autoclaved cellular concrete composite: From a precast building material to a new floating photocatalyst for degradation of organic water contaminants.” *J. Water Process Eng.*, 7, 27–35.

Anh, H. Q., Le, T. P. Q., Le, N. Da, Lu, X. X., Duong, T. T., Garnier, J., Rochelle-Newall, E., Zhang, S., Oh, N. H., Oeurng, C., Ekkawatpanit, C., Nguyen, T. D., Nguyen, Q. T., Nguyen, T. D., Nguyen, T. N., Tran, T. L., Kunisue, T., Tanoue, R., Takahashi, S., Minh, T. B., Le, H. T., Pham, T. N. M., and Nguyen, T. A. H. (2021). “Antibiotics in surface water of East and Southeast Asian countries: A focused review on contamination status, pollution sources, potential risks, and future perspectives.” *Sci. Total Environ.*, 764.

Aoyama, H., Sato, K., Kato, T., Hirai, K., and Mitsuhashi, S. (1987). “Norfloxacin resistance in a clinical isolate of *Escherichia coli*.” *Antimicrob. Agents Chemother.*, 31(10), 1640–1641.

Apopei, P., Catrinescu, C., Teodosiu, C., and Royer, S. (2014). “Mixed-phase TiO<sub>2</sub> photocatalysts: Crystalline phase isolation and reconstruction, characterization and photocatalytic activity in the oxidation of 4-chlorophenol from aqueous effluents.” *Appl. Catal. B Environ.*, 160–161(1), 374–382.

Archana, G., Dhodapkar, R., and Kumar, A. (2016). “Offline solid-phase extraction for preconcentration of pharmaceuticals and personal care products in environmental water and their simultaneous determination using the reversed phase high-performance liquid chromatography method.” *Environ. Monit. Assess.*, 188:512, 1–10.

Arlos, M. J., Hatat-Fraile, M. M., Liang, R., Bragg, L. M., Zhou, N. Y., Andrews, S. A., and Servos, M. R. (2016). “Photocatalytic decomposition of organic micropollutants using immobilized TiO<sub>2</sub> having different isoelectric points.” *Water Res.*, 101, 351–361.

Arumugam, A., Karthikeyan, C., Haja Hameed, A. S., Gopinath, K., Gowri, S., and Karthika, V. (2015). "Synthesis of cerium oxide nanoparticles using *Gloriosa superba* L. leaf extract and their structural, optical and antibacterial properties." *Mater. Sci. Eng. C*, 49, 408–415.

Arun, J., Felix, V., Monica, M. J., and Gopinath, K. P. (2019). "Application of Nano-Photocatalysts for Degradation and Disinfection of Wastewater." *Springer Briefs Inf. Syst.*, 249–261.

Ata, R., Sacco, O., Vaiano, V., Rizzo, L., Tore, G. Y., and Sannino, D. (2017). "Visible light active N-doped TiO<sub>2</sub> immobilized on polystyrene as efficient system for wastewater treatment." *J. Photochem. Photobiol. A Chem.*, 348, 255–262.

Aukidy, M. Al, Verlicchi, P., Jelic, A., Petrovic, M., and Barcelò, D. (2012). "Monitoring release of pharmaceutical compounds: Occurrence and environmental risk assessment of two WWTP effluents and their receiving bodies in the Po Valley, Italy." *Sci. Total Environ.*, 438, 15–25.

Azanu, D., Styryshave, B., Darko, G., Weisser, J. J., and Abaidoo, R. C. (2018). "Occurrence and risk assessment of antibiotics in water and lettuce in Ghana." *Sci. Total Environ.*, 622–623, 293–305.

Balakrishna, K., Rath, A., Praveenkumarreddy, Y., Guruge, K. S., and Subedi, B. (2017). "A review of the occurrence of pharmaceuticals and personal care products in Indian water bodies." *Ecotoxicol. Environ. Saf.*, 137(April 2016), 113–120.

Bardsley, D. (2019). "Dire report finds world's rivers highly polluted with antibiotics." <https://www.thenationalnews.com/uae/environment/dire-report-finds-world-s-rivers-highly-polluted-with-antibiotics-1.866777> (May. 21, 2022).

Basavarajappa, P. S., Patil, S. B., Ganganagappa, N., Raghava, K., Raghu, A. V, and Venkata, C. (2020). "Recent progress in metal-doped TiO<sub>2</sub>, non-metal doped / codoped TiO<sub>2</sub> and TiO<sub>2</sub> nanostructured hybrids for enhanced photocatalysis." *Int. J. Hydrogen Energy*, 45, 7764–7778.

Bayan, E. M., Pustovaya, L. E., and Volkova, M. G. (2021). “Recent advances in TiO<sub>2</sub>-based materials for photocatalytic degradation of antibiotics in aqueous systems.” *Environ. Technol. Innov.*, 24, 101822.

Becker, J., Raghupathi, K. R., Pierre, J. St., Zhao, D., and Koodali, R. T. (2011). “Tuning of the crystallite and particle sizes of ZnO nanocrystalline materials in solvothermal synthesis and their photocatalytic activity for dye degradation.” *J. Phys. Chem. C*, 115(28), 13844–13850.

Bellardita, M., Paola, A. Di, Megna, B., and Palmisano, L. (2018). “Determination of the crystallinity of TiO<sub>2</sub> photocatalysts.” *J. Photochem. Photobiol. A Chem.*, 367, 312–320.

Bengtsson-Palme, J., and Larsson, D. G. J. (2016). “Concentrations of antibiotics predicted to select for resistant bacteria: Proposed limits for environmental regulation.” *Environ. Int.*, 86, 140–149.

Bettinelli, M., Dallacasa, V., Falcomer, D., Fornasiero, P., Gombac, V., Montini, T., Romanò, L., and Speghini, A. (2007). “Photocatalytic activity of TiO<sub>2</sub> doped with boron and vanadium.” *J. Hazard. Mater.*, 146(3), 529–534.

Bharti, B., Kumar, S., Lee, H. N., and Kumar, R. (2016). “Formation of oxygen vacancies and Ti<sup>3+</sup> state in TiO<sub>2</sub> thin film and enhanced optical properties by air plasma treatment.” *Sci. Rep.*, 6(May), 1–12.

Biancullo, F., Moreira, N. F. F., Ribeiro, A. R., Manaia, C. M., Faria, J. L., Nunes, O. C., Castro-Silva, S. M., and Silva, A. M. T. (2019). “Heterogeneous photocatalysis using UVA-LEDs for the removal of antibiotics and antibiotic resistant bacteria from urban wastewater treatment plant effluents.” *Chem. Eng. J.*, 367(February), 304–313.

Bilgin Simsek, E. (2017). “Solvothermal synthesized boron doped TiO<sub>2</sub> catalysts: Photocatalytic degradation of endocrine disrupting compounds and pharmaceuticals under visible light irradiation.” *Appl. Catal. B Environ.*, 200, 309–322.

Bizani, E., Fytianos, K., Poullos, I., and Tsiridis, V. (2006). “Photocatalytic

decolorization and degradation of dye solutions and wastewaters in the presence of titanium dioxide.” *J. Hazard. Mater.*, 136, 85–94.

Bonnefond, A., González, E., Asua, J. M., Leiza, J. R., Kiwi, J., Pulgarin, C., and Rtimi, S. (2015). “New evidence for hybrid acrylic/TiO<sub>2</sub> films inducing bacterial inactivation under low intensity simulated sunlight.” *Colloids Surfaces B Biointerfaces*, 135, 1–7.

Boretti, A., and Rosa, L. (2019). “Reassessing the projections of the World Water Development Report.” *npj Clean Water*, 2(15), 1–6.

Bosio, M., Satyro, S., Bassin, J. P., Saggiaro, E., and Dezotti, M. (2018). “Removal of pharmaceutically active compounds from synthetic and real aqueous mixtures and simultaneous disinfection by supported TiO<sub>2</sub>/UV-A, H<sub>2</sub>O<sub>2</sub>/UV-A, and TiO<sub>2</sub>/H<sub>2</sub>O<sub>2</sub>/UV-A processes.” *Environ. Sci. Pollut. Res.*, (2013), 1–12.

Byrne, J. A., Dunlop, P. S. M., Hamilton, J. W. J., Fernández-Ibáñez, P., Polo-López, I., Sharma, P. K., and Vennard, A. S. M. (2015). “A review of heterogeneous photocatalysis for water and surface disinfection.” *Molecules*, 20(4), 5574–5615.

Cámara, R. M., Portela, R., Gutiérrez-Martín, F., and Sánchez, B. (2018). “Evaluation of several commercial polymers as support for TiO<sub>2</sub> in photocatalytic applications.” *Glob. NEST Journal Global NEST Int. J.*, 16(3), 525–535.

Cantwell, M. G., Katz, D. R., Sullivan, J. C., Shapley, D., Lipscomb, J., Epstein, J., Juhl, A. R., Knudson, C., and O’Mullan, G. D. (2018). “Spatial patterns of pharmaceuticals and wastewater tracers in the Hudson River Estuary.” *Water Res.*, 137, 335–343.

Castro-Puyana, M., Marina, M. L., and Plaza, M. (2017). “Water as green extraction solvent: Principles and reasons for its use.” *Curr. Opin. Green Sustain. Chem.*, 5, 31–36.

Cavalcante, R. P., Dantas, R. F., Bayarri, B., González, O., Giménez, J., Esplugas, S., and Machulek, A. (2015). “Synthesis and characterization of B-doped TiO<sub>2</sub> and their



performance for the degradation of metoprolol.” *Catal. Today*, 252, 27–34.

Cesur, S., and Demiröz, A. P. (2013). “Antibiotics and the Mechanisms of Resistance to Antibiotics.” *Med. J. Islam. World Acad. Sci.*, 21(4), 138–142.

Chao-hai, W. E. I., Xin-hu, T., Jie-rong, L., and Shu-ying, T. A. N. (2007). “Preparation , characterization and photocatalytic activities of boron- and cerium-codoped TiO<sub>2</sub>.” *J. Environ. Sci.*, 19, 90–96.

Chen, D., Yang, D., Wang, Q., and Jiang, Z. (2006). “Effects of boron doping on photocatalytic activity and microstructure of titanium dioxide nanoparticles.” *Ind. Eng. Chem. Res.*, 45(12), 4110–4116.

Chen, J., Liu, M., Zhang, J., Ying, X., and Jin, L. (2004). “Photocatalytic degradation of organic wastes by electrochemically assisted TiO<sub>2</sub> photocatalytic system.” *J. Environ. Manage.*, 70(1), 43–47.

Chen, L., Yang, S., Huang, Y., Zhang, B., Kang, F., and Ding, D. (2019). “Degradation of antibiotics in multi-component systems with novel ternary AgBr/Ag<sub>3</sub>PO<sub>4</sub> @ natural hematite heterojunction photocatalyst under simulated solar light.” *J. Hazard. Mater.*, 371(1), 566–575.

Chen, P., Guo, Z., Cui, K., Guo, W., Li, X., Chen, Y., and Kuang, K. (2020). “Photo-induced degradation of norfloxacin by nanosilver modified two-dimensional black phosphorus.” *Solid State Sci.*, 103(February), 106188.

Chen, Y., Wu, Q., Zhou, C., and Jin, Q. (2018). “Facile preparation of Ce-doped TiO<sub>2</sub>/diatomite granular composite with enhanced photocatalytic activity.” *Adv. Powder Technol.*, 29(1), 106–116.

Colmenares, J. C., and Kuna, E. (2017). “Photoactive hybrid catalysts based on natural and synthetic polymers: A comparative overview.” *Molecules*, 22(5).

Cunha, D. L., Kuznetsov, A., Achete, C. A., Machado, A. E. da H., and Marques, M. (2018). “Immobilized TiO<sub>2</sub> on glass spheres applied to heterogeneous photocatalysis: photoactivity, leaching and regeneration process.” *PeerJ*, 6, e4464.

Dalponte, I., Sousa, B. C. de, Mathias, A. L., and Jorge, R. M. M. (2019). “Formulation and optimization of a novel TiO<sub>2</sub>/calcium alginate floating photocatalyst.” *Int. J. Biol. Macromol.*, 137, 992–1001.

Daneshvar, N., Salari, D., Niaei, A., and Rasoulifard, M. H. (2010). “Immobilization of TiO<sub>2</sub> Nanopowder on Glass Beads for the Photocatalytic Decolorization of an Azo Dye C.I. Direct Red 23.” *J. Environ. Sci. Heal. Part A Toxic/Hazardous Subst. Environ. Eng.*, (October 2013), 37–41.

Das, S., Ghosh, S., Misra, A. J., Tamhankar, A. J., Mishra, A., Lundborg, C. S., and Tripathy, S. K. (2018). “Sunlight assisted photocatalytic degradation of ciprofloxacin in water using Fe doped ZnO nanoparticles for potential public health applications.” *Int. J. Environ. Res. Public Health*, 15(11), 1–11.

Das, S., and Mahalingam, H. (2019a). “Reusable floating polymer nanocomposite photocatalyst for the efficient treatment of dye wastewaters under scaled-up conditions in batch and recirculation modes.” *J. Chem. Technol. Biotechnol.*, 94(8), 2597–2608.

Das, S., and Mahalingam, H. (2019b). “Exploring the synergistic interactions of TiO<sub>2</sub>, rGO, and g-C<sub>3</sub>N<sub>4</sub> catalyst admixtures in a polystyrene nanocomposite photocatalytic film for wastewater treatment: Unary, binary and ternary systems.” *J. Environ. Chem. Eng.*, 7(4), 103246.

Das, S., Sinha, S., Das, B., Jayabalan, R., Suar, M., Mishra, A., Tamhankar, A. J., Lundborg, C. S., and Tripathy, S. K. (2017). “Disinfection of multidrug resistant *Escherichia coli* by solar-photocatalysis using Fe-doped ZnO nanoparticles.” *Sci. Rep.*, 7(1), 1–14.

De, A. K., and Sinha, I. (2022). “Synergistic effect of Ni doping and oxygen vacancies on the visible light photocatalytic properties of Ag<sub>2</sub>O nanoparticles.” *J. Phys. Chem. Solids*, 167, 110733.

Deegan, A. M., Shaik, B., Nolan, K., Urell, K., Oelgemöller, M., Tobin, J., and Morrissey, A. (2011). “Treatment options for wastewater effluents from

pharmaceutical companies.” *Int. J. Environ. Sci. Technol.*, 8(3), 649–666.

Deo, R. P. (2014). “Pharmaceuticals in the Surface Water of the USA: A Review.” *Curr. Environ. Heal. reports*, 1(2), 113–122.

Dever, L. A., and Dermondy, T. S. (1991). “Mechanisms of bacterial resistance to antibiotics.” *Arch Intern Med.*, 151, 886–895.

Dey, A., and Gogate, P. R. (2021). *Nanocomposite photocatalysts-based wastewater treatment. Handb. Nanomater. Wastewater Treat.*, Elsevier Inc., 779-809.

Diamanti-Kandarakis, E., Bourguignon, J. P., Giudice, L. C., Hauser, R., Prins, G. S., Soto, A. M., Zoeller, R. T., and Gore, A. C. (2009). “Endocrine-disrupting chemicals: An Endocrine Society scientific statement.” *Endocr. Rev.*, 30(4), 293–342.

Długosz, M., Zmudzki, P., Kwiecień, A., Szczubiałka, K., Krzek, J., and Nowakowska, M. (2015). “Photocatalytic degradation of sulfamethoxazole in aqueous solution using a floating TiO<sub>2</sub>-expanded perlite photocatalyst.” *J. Hazard. Mater.*, 298, 146–153.

Dönmez, Ö., Dükkancı, M., and Gündüz, G. (2020). “Effects of catalyst preparation method and reaction parameters on the ultrasound assisted Photocatalytic oxidation of reactive yellow 84 dye.” *J. Environ. Heal. Sci. Eng.*, 18(2), 835–851.

Doorslaer, X. Van, Demeestere, K., Heynderickx, P. M., Langenhove, H. Van, and Dewulf, J. (2011). “UV-A and UV-C induced photolytic and photocatalytic degradation of aqueous ciprofloxacin and moxifloxacin: Reaction kinetics and role of adsorption.” *Appl. Catal. B Environ.*, 101(3–4), 540–547.

Duca, C., Imoberdorf, G. E., and Mohseni, M. (2013). “Synthesis, characterization, and comparison of solgel TiO<sub>2</sub> immobilized photocatalysts.” *Int. J. Chem. React. Eng.*, 11(2), 633–639.

El-Bahy, Z. M., Ismail, A. A., and Mohamed, R. M. (2009). “Enhancement of titania by doping rare earth for photodegradation of organic dye (Direct Blue).” *J. Hazard. Mater.*, 166(1), 138–143.

Ellappan, P., and Miranda, L. R. (2014). "Synthesis and characterization of cerium doped titanium catalyst for the degradation of nitrobenzene using visible light." *Int. J. Photoenergy*, 2014.

Eswar, N. K. R., Ramamurthy, P. C., and Madras, G. (2016). "Novel synergistic photocatalytic degradation of antibiotics and bacteria using V-N doped TiO<sub>2</sub> under visible light: The state of nitrogen in V-doped TiO<sub>2</sub>." *New J. Chem.*, 40(4), 3464–3475.

Fabiyi, M. E., and Skelton, R. L. (2000). "Photocatalytic mineralisation of methylene blue using buoyant TiO<sub>2</sub>-coated polystyrene beads." *J. Photochem. Photobiol. A Chem.*, 132, 121–128.

Fagan, R., McCormack, D. E., Dionysiou, D. D., and Pillai, S. C. (2016). "A review of solar and visible light active TiO<sub>2</sub> photocatalysis for treating bacteria, cyanotoxins and contaminants of emerging concern." *Mater. Sci. Semicond. Process.*, 42, 2–14.

Fakhri, A., Gupta, V. K., Rabizadeh, H., Agarwal, S., Sadeghi, N., and Tahami, S. (2018). "Preparation and characterization of WS<sub>2</sub> decorated and immobilized on chitosan and polycaprolactone as biodegradable polymers nanofibers: Photocatalysis study and antibiotic-conjugated for antibacterial evaluation." *Int. J. Biol. Macromol.*, 120, 1789–1793.

Faleye, A. C., Adegoke, A. A., Ramluckan, K., Bux, F., and Stenström, T. A. (2018). "Antibiotic Residue in the Aquatic Environment: Status in Africa." *Open Chem.*, 16(1), 890–903.

Fan, C., Xue, P., and Sun, Y. (2006). "Preparation of Nano-TiO<sub>2</sub> doped with cerium and its photocatalytic activity." *J. Rare Earths*, 24(3), 309–313.

Feng, N., Wang, Q., Zheng, A., Zhang, Z., Fan, J., Liu, S., Amoureux, J., and Deng, F. (2013). "Understanding the High Photocatalytic Activity of (B, Ag)-Codoped TiO<sub>2</sub> under solar-Light Irradiation with XPS, Solid-State NMR, and DFT calculations." *J. Am. Chem. s*, 135, 1607–1616.

Feng, N., Zheng, A., Wang, Q., Ren, P., Gao, X., Liu, S., Shen, Z., Chen, T., and Deng, F. (2011). "Boron Environments in B-Doped and (B, N) -Codoped TiO<sub>2</sub> Photocatalysts: A Combined Solid-State NMR and Theoretical Calculation Study." 2709–2719.

Ferro, G., Fiorentino, A., Alferez, M. C., Polo-López, M. I., Rizzo, L., and Fernández-Ibáñez, P. (2015). "Urban wastewater disinfection for agricultural reuse: effect of solar driven AOPs in the inactivation of a multidrug resistant E. coli strain." *Appl. Catal. B Environ.*, 178, 65–73.

Fick, J., Söderström, H., Lindberg, R. H., Phan, C., Tysklind, M., and Larsson, D. G. J. (2009). "Contamination of surface, ground, and drinking water from pharmaceutical production." *Environ. Toxicol. Chem.*, 28(12), 2522–2527.

Fischer, K., Gawel, A., Rosen, D., Krause, M., Latif, A. A., Griebel, J., Prager, A., and Schulze, A. (2017). "Low-temperature synthesis of anatase/rutile/brookite TiO<sub>2</sub> nanoparticles on a polymer membrane for photocatalysis." *Catalysts*, 7(7).

Fonseca de Lima, J., Harunsani, M. H., Martin, D. J., Kong, D., Dunne, P. W., Gianolio, D., Kashtiban, R. J., Sloan, J., Serra, O. A., Tang, J., and Walton, R. I. (2015). "Control of chemical state of cerium in doped anatase TiO<sub>2</sub> by solvothermal synthesis and its application in photocatalytic water reduction." *J. Mater. Chem. A*, 3(18), 9890–9898.

Foster, H. A., Ditta, I. B., Varghese, S., and Steele, A. (2011). "Photocatalytic disinfection using titanium dioxide: Spectrum and mechanism of antimicrobial activity." *Appl. Microbiol. Biotechnol.*, 90(6), 1847–1868.

Friend, S. , Arlington, S., Swanick, M., Shetty, S., and Vishwakarma, N. (2010). "Global pharma looks to India : Prospects for growth." *Prince Waterhouse Coopers*, 1-40.

Fujisawa, J. ichi, Eda, T., and Hanaya, M. (2017). "Comparative study of conduction-band and valence-band edges of TiO<sub>2</sub>, SrTiO<sub>3</sub>, and BaTiO<sub>3</sub> by ionization potential measurements." *Chem. Phys. Lett.*, 685, 23–26.

- Fujishima, A., and Honda, K. (1972). "Electrochemical Photolysis of Water at a Semiconductor Electrode." *Nature*, 238, 37–38.
- Fujishima, A., and Zhang, X. (2006). "Titanium dioxide photocatalysis : present situation and future approaches." *C. R. Chim.*, 9, 750–760.
- Fujishima, A., Zhang, X., and Tryk, D. A. (2008). "TiO<sub>2</sub> photocatalysis and related surface phenomena." *Surf. Sci. Rep.*, 63, 515–582.
- Fujisawa, J. ichi, Eda, T., and Hanaya, M. (2017). "Comparative study of conduction-band and valence-band edges of TiO<sub>2</sub>, SrTiO<sub>3</sub>, and BaTiO<sub>3</sub> by ionization potential measurements." *Chem. Phys. Lett.*, 685, 23–26.
- Gad-Allah, T. A., Ali, M. E. M., and Badawy, M. I. (2011). "Photocatalytic oxidation of ciprofloxacin under simulated sunlight." *J. Hazard. Mater.*, 186(1), 751–755.
- Gani, K. M., and Kazmi, A. A. (2017). "Contamination of Emerging Contaminants in Indian Aquatic Sources: First Overview of the Situation." *J. Hazardous, Toxic, Radioact. waste*, 21(3), 04016026:1–12.
- Gaonkar, O. (2022). "Menace of antibiotic pollution in Indian rivers." *Toxics link*, 1-41.
- García-Fernández, I., Fernández-Calderero, I., Inmaculada Polo-López, M., and Fernández-Ibáñez, P. (2015). "Disinfection of urban effluents using solar TiO<sub>2</sub> photocatalysis: A study of significance of dissolved oxygen, temperature, type of microorganism and water matrix." *Catal. Today*, 240(PA), 30–38.
- Gaya, U. I., and Abdullah, A. H. (2008). "Heterogeneous photocatalytic degradation of organic contaminants over titanium dioxide: A review of fundamentals, progress and problems." *J. Photochem. Photobiol. C Photochem. Rev.*, 9(1), 1–12.
- Geeraerd, A. H., Herremans, C. H., and Impe, J. F. Van. (2000). "Structural model requirements to describe microbial inactivation during a mild heat treatment." *Int. J. Food Microbiol.*, 59(3), 185–209.

Geeraerd, A. H., Valdramidis, V. P., and Impe, J. F. Van. (2005). “GInaFiT, a freeware tool to assess non-log-linear microbial survivor curves.” *Int. J. Food Microbiol.*, 102(1), 95–105.

Gharagozlou, M., and Bayati, R. (2014). “Photocatalytic activity and formation of oxygen vacancies in cation doped anatase TiO<sub>2</sub> nanoparticles.” *Ceram. Int.*, 40, 10247–10253.

Giannakis, S., Darakas, E., Escalas-Cañellas, A., and Pulgarin, C. (2014). “Elucidating bacterial regrowth: Effect of disinfection conditions in dark storage of solar treated secondary effluent.” *J. Photochem. Photobiol. A Chem.*, 290(1), 43–53.

Giannakis, S., Darakas, E., Escalas-Cañellas, A., and Pulgarin, C. (2015). “Environmental considerations on solar disinfection of wastewater and the subsequent bacterial (re)growth.” *Photochem. Photobiol. Sci.*, 14(3), 618–625.

Giannakis, S., Rtimi, S., and Pulgarin, C. (2017). “Light-assisted advanced oxidation processes for the elimination of chemical and microbiological pollution of wastewaters in developed and developing countries.” *Molecules*, 22(7).

Giraldo-Aguirre, A. L., Erazo-Erazo, E. D., Flórez-Acosta, O. A., Serna-Galvis, E. A., and Torres-Palma, R. A. (2015). “TiO<sub>2</sub> photocatalysis applied to the degradation and antimicrobial activity removal of oxacillin: Evaluation of matrix components, experimental parameters, degradation pathways and identification of organics by-products.” *J. Photochem. Photobiol. A Chem.*, 311, 95–103.

Gnanaprakasam, A., Sivakumar, V. M., and Thirumarimurugan, M. (2015). “Influencing Parameters in the Photocatalytic Degradation of Organic Effluent via Nanometal Oxide Catalyst: A Review.” *Indian J. Mater. Sci.*, 1–16.

Gothwal, R., and Shashidhar, T. (2015). “Antibiotic Pollution in the Environment: A Review.” *Clean - Soil, Air, Water*, 43(4), 479–489.

Gou, J., Ma, Q., Deng, X., Cui, Y., Zhang, H., Cheng, X., Li, X., Xie, M., and Cheng, Q. (2017). “Fabrication of Ag<sub>2</sub>O/TiO<sub>2</sub>-Zeolite composite and its enhanced solar light

photocatalytic performance and mechanism for degradation of norfloxacin.” *Chem. Eng. J.*, 308, 818–826.

Grabowska, E., Zaleska, A., Sobczak, J. W., Gazda, M., and Hupka, J. (2009). “Boron-doped TiO<sub>2</sub>: Characteristics and photoactivity under visible light.” *Procedia Chem.*, 1(2), 1553–1559.

Greczynski, G., and Hultman, L. (2020). “X-ray photoelectron spectroscopy: Towards reliable binding energy referencing.” *Prog. Mater. Sci.*, 107(June 2018), 100591.

Guo, C., Gao, S., Lv, J., Hou, S., Zhang, Y., and Xu, J. (2017a). “Assessing the photocatalytic transformation of norfloxacin by BiOBr/iron oxides hybrid photocatalyst: Kinetics, intermediates, and influencing factors.” *Appl. Catal. B Environ.*, 205, 68–77.

Guo, Y., Qi, P. S., and Liu, Y. Z. (2017b). “A Review on Advanced Treatment of Pharmaceutical Wastewater.” *IOP Conf. Ser. Earth Environ. Sci.*

Gupta, A., and Garg, A. (2018). “Degradation of ciprofloxacin using Fenton’s oxidation: Effect of operating parameters, identification of oxidized by-products and toxicity assessment.” *Chemosphere*, 193(November), 1181–1188.

Gupta, B., Gupta, A. K., Tiwary, C. S., and Ghosal, P. S. (2020). “A multivariate modeling and experimental realization of photocatalytic system of engineered S-C<sub>3</sub>N<sub>4</sub>/ZnO hybrid for ciprofloxacin removal: Influencing factors and degradation pathways.” *Environ. Res.*, (October), 110390.

Gupta, N., Pandey, P., and Hussain, J. (2017). “Effect of physicochemical and biological parameters on the quality of river water of Narmada, Madhya Pradesh, India.” *Water Sci.*, 31(1), 11–23.

Haddad, T., and Kümmerer, K. (2014). “Characterization of photo-transformation products of the antibiotic drug Ciprofloxacin with liquid chromatography-tandem mass spectrometry in combination with accurate mass determination using an LTQ-Orbitrap.” *Chemosphere*, 115(1), 40–46.



Han, X., Yao, C., Yuan, A., Xi, F., Dong, X., and Liu, J. (2018). “Enhanced charge separation ability and visible light photocatalytic performance of graphitic carbon nitride by binary S, B co-doping.” *Mater. Res. Bull.*, 107(November 2017), 477–483.

Hassani, A., Khataee, A., Karaca, S., Karaca, C., and Gholami, P. (2017). “Sonocatalytic degradation of ciprofloxacin using synthesized TiO<sub>2</sub> nanoparticles on montmorillonite.” *Ultrason. Sonochem.*, 35, 251–262.

He, J., Zeng, X., Lan, S., and Lo, I. M. C. (2019). “Reusable magnetic Ag/Fe, N-TiO<sub>2</sub>/Fe<sub>3</sub>O<sub>4</sub>@SiO<sub>2</sub> composite for simultaneous photocatalytic disinfection of E. coli and degradation of bisphenol A in sewage under visible light.” *Chemosphere*, 217, 869–878.

Herman, R. (2014). “Emerging Contaminants Taint Drinking Water Supply.” <https://blogs.scientificamerican.com/guest-blog/emerging-contaminants-taint-drinking-water-supply> (May. 21, 2022).

Hirai, K., Suzue, S., Irikura, T., Iyobe, S., and Mitsuhashi, S. (1987). “Mutations producing resistance to norfloxacin in *Pseudomonas aeruginosa*.” *Antimicrob. Agents Chemother.*, 31(4), 582–586.

Hirsch, R., Ternes, T. A., Haberer, K., Mehlich, A., Ballwanz, F., and Kratz, K. L. (1998). “Determination of antibiotics in different water compartments via liquid chromatography-electrospray tandem mass spectrometry.” *J. Chromatogr. A*, 815(2), 213–223.

Ho, C. Y., Lin, J. K., and Wang, H. W. (2015). “Characteristics of Boron Decorated TiO<sub>2</sub> Nanoparticles for Dye-Sensitized Solar Cell Photoanode.” *Int. J. Photoenergy*, 2015.

Homem, V., and Santos, L. (2011). “Degradation and removal methods of antibiotics from aqueous matrices - A review.” *J. Environ. Manage.*, 92(10), 2304–2347.

Hooper, D. C., Wolfson, J. S., Souza, K. S., Ng, E. Y., McHugh, G. L., and Swartz, M. N. (1989). “Mechanisms of quinolone resistance in *Escherichia coli*:

Characterization of *nfxB* and *cfxB*, two mutant resistance loci decreasing norfloxacin accumulation.” *Antimicrob. Agents Chemother.*, 33(3), 283–290.

Hooper, D. C., Wolfson, J. S., Souza, K. S., Tung, C., McHugh, G. L., and Swartz, M. N. (1986). “Genetic and biochemical characterization of norfloxacin resistance in *Escherichia coli*.” *Antimicrob. Agents Chemother.*, 29(4), 639–644.

Hosseini, M., Esrafil, A., Farzadkia, M., Kermani, M., and Gholami, M. (2020). “Degradation of ciprofloxacin antibiotic using photo-electrocatalyst process of Ni-doped ZnO deposited by RF sputtering on FTO as an anode electrode from aquatic environments: Synthesis, kinetics, and ecotoxicity study.” *Microchem. J.*, 154(September 2019), 104663.

Hosseini, S. N., Borghei, S. M., Vossoughi, M., and Taghavinia, N. (2007). “Immobilization of TiO<sub>2</sub> on perlite granules for photocatalytic degradation of phenol.” *Appl. Catal. B Environ.*, 74(1–2), 53–62.

Hu, K., Li, R., Ye, C., Wang, A., Wei, W., Hu, D., Qiu, R., and Yan, K. (2020). “Facile synthesis of Z-scheme composite of TiO<sub>2</sub> nanorod/g-C<sub>3</sub>N<sub>4</sub> nanosheet efficient for photocatalytic degradation of ciprofloxacin.” *J. Clean. Prod.*, 253, 120055.

Huang, F., Yan, A., and Zhao, H. (2016a). “Influences of Doping on Photocatalytic Properties of TiO<sub>2</sub> Photocatalyst.” *Semicond. Photocatal. - Mater. Mech. Appl.*, 31–80.

Huang, M., Xu, C., Wu, Z., Huang, Y., Lin, J., and Wu, J. (2008). “Photocatalytic discolorization of methyl orange solution by Pt modified TiO<sub>2</sub> loaded on natural zeolite.” *Dye. Pigment.*, 77(2), 327–334.

Huang, Y., Yan, C. F., Guo, C. Q., and Shi, Y. (2016b). “Experimental and first-principles DFT study on oxygen vacancies on cerium dioxide and its effect on enhanced photocatalytic hydrogen production.” *Int. J. Hydrogen Energy*, 41(19), 7919–7926.

Hubicka, U., Zmudzki, P., Talik, P., Zuromska-Witek, B., and Krzek, J. (2013).

“Photodegradation assessment of ciprofloxacin, moxifloxacin, norfloxacin and ofloxacin in the presence of excipients from tablets by UPLC-MS/MS and DSC.” *Chem. Cent. J.*, 7(1), 1–12.

Huo, H., Hu, X., Wang, H., Li, J., Xie, G., Tan, X., Jin, Q., Zhou, D., Li, C., Qiu, G., and Liu, Y. (2019). “Synergy of photocatalysis and adsorption for simultaneous removal of hexavalent chromium and methylene blue by g-C<sub>3</sub>N<sub>4</sub>/BiFeO<sub>3</sub>/carbon nanotubes ternary composites.” *Int. J. Environ. Res. Public Health*, 16(17).

In, S., Orlov, A., Berg, R., García, F., Pedrosa-Jimenez, S., Tikhov, M. S., Wright, D. S., and Lambert, R. M. (2007). “Effective visible light-activated B-doped and B,N-codoped TiO<sub>2</sub> photocatalysts.” *J. Am. Chem. Soc.*, 129(45), 13790–13791.

Inoue, S., Ohue, T., Yamagishi, J., Nakamura, S., and Shimizu, M. (1978). “Mode of incomplete cross-resistance among pipemidic, piromidic, and nalidixic acids.” *Antimicrob. Agents Chemother.*, 14(2), 240–245.

Jaiswal, R., Patel, N., Dashora, A., Fernandes, R., Yadav, M., Edla, R., Varma, R. S., Kothari, D. C., Ahuja, B. L., and Miotello, A. (2016). “Efficient Co-B-codoped TiO<sub>2</sub> photocatalyst for degradation of organic water pollutant under visible light.” *Appl. Catal. B Environ.*, 183, 242–253.

Jaiswal, R., Patel, N., Kothari, D. C., and Miotello, A. (2012). “Improved visible light photocatalytic activity of TiO<sub>2</sub> co-doped with Vanadium and Nitrogen.” *Appl. Catal. B Environ.*, 126, 47–54.

Jamkhande, P. G., Ghule, N. W., Bamer, A. H., and Kalaskar, M. G. (2019). “Metal nanoparticles synthesis: An overview on methods of preparation, advantages and disadvantages, and applications.” *J. Drug Deliv. Sci. Technol.*, 53, 101174.

Johanson, G. (2012). “Acetone.” *Patty's Toxicol.*, 735–752.

Jojoa-Sierra, S. D., Silva-Agredo, J., Herrera-Calderon, E., and Torres-Palma, R. A. (2017). “Elimination of the antibiotic norfloxacin in municipal wastewater, urine and seawater by electrochemical oxidation on IrO<sub>2</sub> anodes.” *Sci. Total Environ.*, 575,

1228–1238.

Joss, A., Keller, E., Alder, A. C., Göbel, A., McArdell, C. S., Ternes, T., and Siegrist, H. (2005). “Removal of pharmaceuticals and fragrances in biological wastewater treatment.” *Water Res.*, 39(14), 3139–3152.

Kalyva, M. (2017). “Fate of pharmaceuticals in the environment -A review.” (March), 1–30.

Kanakaraju, D., Glass, B. D., and Oelgemöller, M. (2018). “Advanced oxidation process-mediated removal of pharmaceuticals from water: A review.” *J. Environ. Manage.*, 219, 189–207.

Karkare, M. M. (2014). “Choice of precursor not affecting the size of anatase TiO<sub>2</sub> nanoparticles but affecting morphology under broader view.” *Int. Nano Lett.*, 4(3).

Kasinathan, K., Kennedy, J., Elayaperumal, M., Henini, M., and Malik, M. (2016). “Photodegradation of organic pollutants RhB dye using UV simulated sunlight on ceria based TiO<sub>2</sub> nanomaterials for antibacterial applications.” *Sci. Rep.*, 6(September), 1–12.

Kaur, A., Anderson, W. A., Tanvir, S., and Kansal, S. K. (2019). “Solar light active silver/iron oxide/zinc oxide heterostructure for photodegradation of ciprofloxacin, transformation products and antibacterial activity.” *J. Colloid Interface Sci.*, 557, 236–253.

Kerli, S., and Eskalen, H. (2020). “Synthesis of titanium oxide thin films by spray pyrolysis method and its photocatalytic activity for degradation of dyes and ciprofloxacin.” *Phys. Chem. Solid State*, 21(3), 426–432.

Khairy, M., and Zakaria, W. (2014). “Effect of metal-doping of TiO<sub>2</sub> nanoparticles on their photocatalytic activities toward removal of organic dyes.” *Egypt. J. Pet.*, 23(4), 419–426.

Kiss, B., Manning, T. D., Hesp, D., Didier, C., Taylor, A., Pickup, D. M., Chadwick, A. V., Allison, H. E., Dhanak, V. R., Claridge, J. B., Darwent, J. R., and Rosseinsky,

M. J. (2017). “Nano-structured rhodium doped SrTiO<sub>3</sub>–Visible light activated photocatalyst for water decontamination.” *Appl. Catal. B Environ.*, 206, 547–555.

Klein, E. Y., Boeckel, T. P. Van, Martinez, E. M., Pant, S., Gandra, S., Levin, S. A., Goossens, H., and Laxminarayan, R. (2018). “Global increase and geographic convergence in antibiotic consumption between 2000 and 2015.” *Proc. Natl. Acad. Sci. U. S. A.*, E3463–E3470.

Konstantinou, I. K., and Albanis, T. A. (2004). “TiO<sub>2</sub>-assisted photocatalytic degradation of azo dyes in aqueous solution: Kinetic and mechanistic investigations: A review.” *Appl. Catal. B Environ.*, 49(1), 1–14.

Koshy, J. (2019a). “Ganga has higher proportion of antibacterial agents : study.” <https://www.indiawaterportal.org/articles/high-proportion-antibacterial-agents-ganga-study> (May. 21, 2022).

Koshy, J. (2019b). “9.3 crore project antibiotic resistance in Ganga.” <https://www.thehindu.com/news/national/ganga-mission-study-to-check-for-antibiotic-resistance-in-river/article29281152.ece> (May. 21, 2022).

Koysuren, O., and Koysuren, H. N. (2017). “Photocatalytic activities of poly(methyl methacrylate)/titanium dioxide nanofiber mat.” *J. Macromol. Sci. Part A Pure Appl. Chem.*, 54(2), 80–84.

Kristiansson, E., Fick, J., Janzon, A., Grabic, R., Rutgersson, C., Weijdegård, B., Söderström, H., and Joakim Larsson, D. G. (2011). “Pyrosequencing of antibiotic-contaminated river sediments reveals high levels of resistance and gene transfer elements.” *PLoS One*, 6(2).

Kumar, A., and Pandey, G. (2017). “A Review on the Factors Affecting the Photocatalytic Degradation of Hazardous Materials.” *Mater. Sci. Eng. Int. J.*, 1(3), 1–10.

Kumar, E., Selvarajan, P., and Muthuraj, D. (2013). “Synthesis and characterization of CeO<sub>2</sub> nanocrystals by solvothermal route.” *Mater. Res.*, 16(2), 269–276.

Kumar, J. V., Karthik, R., Chen, S. M., Muthuraj, V., and Karuppiah, C. (2016). "Fabrication of potato-like silver molybdate microstructures for photocatalytic degradation of chronic toxicity ciprofloxacin and highly selective electrochemical detection of H<sub>2</sub>O<sub>2</sub>." *Sci. Rep.*, 6(1).

Kümmerer, K. (2009). "The presence of pharmaceuticals in the environment due to human use - present knowledge and future challenges." *J. Environ. Manage.*, 90(8), 2354–2366.

Lan, X., Wang, L., Zhang, B., Tian, B., and Zhang, J. (2014). "Preparation of lanthanum and boron co-doped TiO<sub>2</sub> by modified sol-gel method and study their photocatalytic activity." *Catal. Today*, 224, 163–170.

Larsson, D. G. J. (2014). "Pollution from drug manufacturing: Review and perspectives." *Philos. Trans. R. Soc. B Biol. Sci.*, 369(1656).

Larsson, D. G. J., Pedro, C. de, and Paxeus, N. (2007). "Effluent from drug manufactures contains extremely high levels of pharmaceuticals." *J. Hazard. Mater.*, 148(3), 751–755.

Lee, Y. J., Lee, C. G., Kang, J. K., Park, S. J., and Alvarez, P. J. J. (2021). "Simple preparation method for Styrofoam-TiO<sub>2</sub> composites and their photocatalytic application for dye oxidation and Cr(vi) reduction in industrial wastewater." *Environ. Sci. Water Res. Technol.*, 7(1), 222–230.

Legakis, N. J., Tzouvelekis, L. S., Makris, A., and Kotsifaki, H. (1989). "Outer membrane alterations in multiresistant mutants of *Pseudomonas aeruginosa* selected by ciprofloxacin." *Antimicrob. Agents Chemother.*, 33(1), 124–127.

Lester, Y., Mamane, H., Zucker, I., and Avisar, D. (2013). "Treating wastewater from a pharmaceutical formulation facility by biological process and ozone." *Water Res.*, 47(13), 4349–4356.

Li, D., Yang, M., Hu, J., Ren, L., Zhang, Y., and Li, K. (2008a). "Determination and fate of oxytetracycline and related compounds in oxytetracycline production

wastewater and the receiving river.” *Environ. Toxicol. Chem.*, 27(1), 80–86.

Li, D., Yang, M., Hu, J., Zhang, Y., Chang, H., and Jin, F. (2008b). “Determination of penicillin G and its degradation products in a penicillin production wastewater treatment plant and the receiving river.” *Water Res.*, 42(1–2), 307–317.

Li, H., Zhang, W., and Liu, Y. (2020). “HZSM-5 zeolite supported boron-doped TiO<sub>2</sub> for photocatalytic degradation of ofloxacin.” *J. Mater. Res. Technol.*, (x x), 1–11.

Li, J., Liu, F., and Li, Y. (2018). “Fabrication of an Ag/Ag<sub>2</sub>MoO<sub>4</sub> plasmonic photocatalyst with enhanced photocatalytic performance for the degradation of ciprofloxacin.” *New J. Chem.*, 42(14), 12054–12061.

Li, W., Guo, C., Su, B., and Xu, J. (2012). “Photodegradation of four fluoroquinolone compounds by titanium dioxide under simulated solar light irradiation.” *J. Chem. Technol. Biotechnol.*, 87(5), 643–650.

Li, W., Liang, R., Hu, A., Huang, Z., and Zhou, Y. N. (2014). “Generation of oxygen vacancies in visible light activated one-dimensional iodine TiO<sub>2</sub> photocatalysts.” *RSC Adv.*, 4(70), 36959–36966.

Li, Z., and Yang, P. (2018). “Review on Physicochemical, Chemical, and Biological Processes for Pharmaceutical Wastewater.” *IOP Conf. Ser. Earth Environ. Sci.*, 113, 012185.

Lin, A. Y. C., and Tsai, Y. T. (2009). “Occurrence of pharmaceuticals in Taiwan’s surface waters: Impact of waste streams from hospitals and pharmaceutical production facilities.” *Sci. Total Environ.*, 407(12), 3793–3802.

Lin, L., Wang, H., and Xu, P. (2017). “Immobilized TiO<sub>2</sub>-reduced graphene oxide nanocomposites on optical fibers as high performance photocatalysts for degradation of pharmaceuticals.” *Chem. Eng. J.*, 310, 389–398.

Ling, Q., Sun, J., Zhou, Q., Zhao, Q., and Ren, H. (2008). “Visible-light-driven boron/ferrum/cerium/titania photocatalyst.” *J. Photochem. Photobiol. A Chem.*, 200(2–3), 141–147.

Liu, N., Ming, J., Sharma, A., Sun, X., Kawazoe, N., Chen, G., and Yang, Y. (2021). “Sustainable photocatalytic disinfection of four representative pathogenic bacteria isolated from real water environment by immobilized TiO<sub>2</sub>-based composite and its mechanism.” *Chem. Eng. J.*, 426(June), 131217.

Liu, Z., Guo, B., Hong, L., and Jiang, H. (2005). “Preparation and characterization of cerium oxide doped TiO<sub>2</sub> nanoparticles.” *J. Phys. Chem. Solids*, 66(1), 161–167.

Long, Z., Li, Q., Wei, T., Zhang, G., and Ren, Z. (2020). “Historical development and prospects of photocatalysts for pollutant removal in water.” *J. Hazard. Mater.*, 395, 122599.

Low, J., Yu, J., Jaroniec, M., Wageh, S., and Al-Ghamdi, A. A. (2017). “Heterojunction Photocatalysts.” *Adv. Mater.*, 29(20), 1–20.

Lu, X., Tian, B., Chen, F., and Zhang, J. (2010). “Preparation of boron-doped TiO<sub>2</sub> films by autoclaved-sol method at low temperature and study on their photocatalytic activity.” *Thin Solid Films*, 519(1), 111–116.

Lundborg, C. S., and Tamhankar, A. J. (2017). “Antibiotic residues in the environment of South East Asia.” *BMJ*, 358, 42–45.

Maarisetty, D., and Baral, S. S. (2019). “Defect-induced enhanced dissociative adsorption, optoelectronic properties and interfacial contact in Ce doped TiO<sub>2</sub>: Solar photocatalytic degradation of Rhodamine B.” *Ceram. Int.*, 45(17), 22253–22263.

Maddila, S., Kishore, R., and Jonnalagadda, S. B. (2017). “Degradation , Mineralization Of Chloro Phenol Using Ceria Doped TiO<sub>2</sub> Under Photocatalytic Ozonation.” (September).

Magalhães, F., and Lago, R. M. (2009). “Floating photocatalysts based on TiO<sub>2</sub> grafted on expanded polystyrene beads for the solar degradation of dyes.” *Sol. Energy*, 83(9), 1521–1526.

Maia, A. S., Ribeiro, A. R., Amorim, C. L., Barreiro, J. C., Cass, Q. B., Castro, P. M. L., and Tiritan, M. E. (2014). “Degradation of fluoroquinolone antibiotics and



identification of metabolites/transformation products by liquid chromatography-tandem mass spectrometry.” *J. Chromatogr. A*, 1333, 87–98.

Malakootian, M., Nasiri, A., and Gharaghani, M. A. (2019). “Photocatalytic degradation of ciprofloxacin antibiotic by TiO<sub>2</sub> nanoparticles immobilized on a glass plate.” *Chem. Eng. Commun.*, 0(0), 1–17.

Mangalara, S. C. H., and Varughese, S. (2016). “Green recycling approach to obtain nano- and microparticles from expanded polystyrene waste.” *ACS Sustain. Chem. Eng.*, 4(11), 6095–6100.

Marschall, R., and Wang, L. (2014). “Non-metal doping of transition metal oxides for visible-light photocatalysis.” *Catal. Today*, 225, 111–135.

Martin, M. V., Villabrille, P. I., and Rosso, J. A. (2015). “The influence of Ce doping of titania on the photodegradation of phenol.” *Environ. Sci. Pollut. Res.*, 22(18), 14291–14298.

Matějová, L., Kočí, K., Reli, M., Čapek, L., Hospodková, A., Peikertová, P., Matěj, Z., Obalová, L., Wach, A., Kuśtrowski, P., and Kotarba, A. (2014). “Preparation, characterization and photocatalytic properties of cerium doped TiO<sub>2</sub>: On the effect of Ce loading on the photocatalytic reduction of carbon dioxide.” *Appl. Catal. B Environ.*, 152–153, 172–183.

Matějová, L., Šihor, M., Lang, J., Troppová, I., Ambrožová, N., Reli, M., Brunátová, T., Čapek, L., Kotarba, A., and Kočí, K. (2017). “Investigation of low Ce amount doped-TiO<sub>2</sub> prepared by using pressurized fluids in photocatalytic N<sub>2</sub>O decomposition and CO<sub>2</sub> reduction.” *J. Sol-Gel Sci. Technol.*, 84(1), 158–168.

May-Lozano, M., Ramos-Reyes, G. M., López-Medina, R., Martínez-Delgadillo, S. A., J. Flores-Moreno, and Hernández-Pérez, I. (2014). “Effect of the Amount of Water in the Synthesis of B-TiO<sub>2</sub>: Orange II Photodegradation.” *Int. J. Photochem.*, 1–8.

Mazinani, B., Masrom, A. K., Beitollahi, A., and Luque, R. (2014). “Photocatalytic

activity, surface area and phase modification of mesoporous SiO<sub>2</sub>-TiO<sub>2</sub> prepared by a one-step hydrothermal procedure.” *Ceram. Int.*, 40(8 PART A), 11525–11532.

Meador, J. P., Yeh, A., Young, G., and Gallagher, E. P. (2016). “Contaminants of emerging concern in a large temperate estuary.” *Environ. Pollut.*, 213, 254–267.

Mendonsa, K. (2019). “Cancer causing bacteria gains antibiotic resistance, find scientists.” <https://timesofindia.indiatimes.com/city/mysuru/cancer-causing-bacteria-gains-antibiotic-resistance-find-scientists/articleshow/70139537.cms> (May. 21, 2022).

Meng, X., Tang, L., and Jingbo, L. (2010). “Room-Temperature Ferromagnetism in Co-Doped In<sub>2</sub>O<sub>3</sub> Nanocrystals.” *J. Phys. Chem. C*, 114, 17569–17573.

Mikaeili, F., Topcu, S., Jodhani, G., and Gouma, P.-I. (2018). “Flame-Sprayed Pure and Ce-Doped TiO<sub>2</sub> Photocatalysts.” *Catalysts*, 8(9), 342.

Miranda-García, N., Maldonado, M. I., Coronado, J. M., and Malato, S. (2010). “Degradation study of 15 emerging contaminants at low concentration by immobilized TiO<sub>2</sub> in a pilot plant.” *Catal. Today*, 151(1–2), 107–113.

Moongraksathum, B., and Chen, Y. W. (2018). “Anatase TiO<sub>2</sub> co-doped with silver and ceria for antibacterial application.” *Catal. Today*, 310.

Munita, J. M., and Arias, C. A. (1982). “Mechanisms of Antibiotic Resistance.” *Annu. Rep. Med. Chem.*, 17(C), 119–127.

Muñoz-Batista, M. J., Gómez-Cerezo, M. N., Kubacka, A., Tudela, D., and Fernández-García, M. (2014). “Role of interface contact in CeO<sub>2</sub>-TiO<sub>2</sub> photocatalytic composite materials.” *ACS Catal.*, 4(1), 63–72.

Murgolo, S., Yargeau, V., Gerbasi, R., Visentin, F., Habra, N. El, Ricco, G., Lacchetti, I., Carere, M., Curri, M. L., and Mascolo, G. (2017). “A new supported TiO<sub>2</sub> film deposited on stainless steel for the photocatalytic degradation of contaminants of emerging concern.” *Chem. Eng. J.*, 318, 103–111.

Mutiyar, P. K., and Mittal, A. K. (2014). “Occurrences and fate of selected human

antibiotics in influents and effluents of sewage treatment plant and effluent-receiving river Yamuna in Delhi (India).” *Environ. Monit. Assess.*, 186(1), 541–557.

Na, T. W., Kang, T. W., Lee, K. H., Hwang, S. H., Jung, H. J., and Kim, K. (2019). “Distribution and ecological risk of pharmaceuticals in surface water of the Yeongsan river, Republic of Korea.” *Ecotoxicol. Environ. Saf.*, 181, 180–186.

Nagar, A., and Pradeep, T. (2020). “Clean Water through Nanotechnology: Needs, Gaps, and Fulfillment.” *ACS Nano*, 14(6), 6420–6435.

Nawawi, W., Zaharudin, R., Ishak, M., Ismail, K., and Zuliahani, A. (2016). “The Preparation and Characterization of Immobilized TiO<sub>2</sub>/PEG by Using DSAT as a Support Binder.” *Appl. Sci.*, 7(1), 24.

Oliveira, W. V. De, Maria, L., Honorio, C., Almeida, L. C., Viana, B. C., Furtini, M. B., Silva-filho, E. C., and Osajima, J. A. (2020). “TiO<sub>2</sub> Immobilized on Fibrous Clay as Strategies to Photocatalytic Activity.” *Mater. Res.*, 23(1), 1–10.

Omar, K. F. M., Aziz, N. A. A., Palaniandy, P., and Abu Amr, S. S. (2017). “Removal of lindane and *Escherichia coli* (*E.coli*) from rainwater using photocatalytic and adsorption treatment processes.” *Glob. Nest J.*, 19(2), 191–198.

Onesios, K. M., Yu, J. T., and Bouwer, E. J. (2009). “Biodegradation and removal of pharmaceuticals and personal care products in treatment systems: A review.” *Biodegradation*, 20(4), 441–466.

Ounas, O., Foulani, A. A. El, Lekhlif, B., and Jamal-Eddine, J. (2020). “Immobilization of TiO<sub>2</sub> into a poly methyl methacrylate (PMMA) as hybrid film for photocatalytic degradation of methylene blue.” *Mater. Today Proc.*, 22, 35–40.

Owa, F. W. (2014). “Water pollution : sources , effects , control and management.” *Int. Lett. Nat. Sci.*, 3, 1–6.

Pablos, C., Grieken, R. Van, Marugañ, J., and Muñoz, A. (2012). “Simultaneous photocatalytic oxidation of pharmaceuticals and inactivation of *Escherichia coli* in wastewater treatment plant effluents with suspended and immobilised TiO<sub>2</sub>.” *Water*

*Sci. Technol.*, 65(11), 2016–2023.

Pal, M., Mondal, O., Pal, M., Singh, R., Sen, D., and Mazumder, S. (2015). “Influence of doping on crystal growth, structure and optical properties of nanocrystalline CaTiO<sub>3</sub>: A case study using small-angle neutron scattering.” *J. Appl. Crystallogr.*, 48, 836–843.

Palacios-villarreal, C., Manzano, M., Jos, J., Blanco, E., Ramírez, M., and Levchuk, I. (2020). “Photocatalytic degradation of pharmaceutically active compounds (PhACs) in urban wastewater treatment plants effluents under controlled and natural solar irradiation using immobilized TiO<sub>2</sub>.” *Sol. Energy*, 208(March), 480–492.

Patel, M., Kumar, R., Kishor, K., Mlsna, T., Pittman, C. U., and Mohan, D. (2019). “Pharmaceuticals of emerging concern in aquatic systems: Chemistry, occurrence, effects, and removal methods.” *Chem. Rev.*, 119(6), 3510–3673.

Patel, N., Dashora, A., Jaiswal, R., Fernandes, R., Yadav, M., Kothari, D. C., Ahuja, B. L., and Miotello, A. (2015). “Experimental and Theoretical Investigations on the Activity and Stability of Substitutional and Interstitial Boron in TiO<sub>2</sub> Photocatalyst.” *J. Phys. Chem. C*, 119(32), 18581–18590.

Pattnaik, S. P., Behera, A., Martha, S., Acharya, R., and Parida, K. (2019). “Facile synthesis of exfoliated graphitic carbon nitride for photocatalytic degradation of ciprofloxacin under solar irradiation.” *J. Mater. Sci.*, 54(7), 5726–5742.

Paul, B., Martens, W. N., and Frost, R. L. (2012). “Immobilised anatase on clay mineral particles as a photocatalyst for herbicides degradation.” *Appl. Clay Sci.*, 57, 49–54.

Paul, T., Miller, P. L., and Strathmann, T. J. (2007). “Visible-light-mediated TiO<sub>2</sub> photocatalysis of fluoroquinolone antibacterial agents.” *Environ. Sci. Technol.*, 41(13), 4720–4727.

Pawar, M., Sendoğdular, S. T., and Gouma, P. (2018). “A brief overview of TiO<sub>2</sub> photocatalyst for organic dye remediation: Case study of reaction mechanisms

involved in Ce-TiO<sub>2</sub> photocatalysts system.” *J. Nanomater.*, 2018, 1–13.

Prasad, D. H., Park, S. Y., Oh, E. O., Ji, H., Kim, H. R., Yoon, K. J., Son, J. W., and Lee, J. H. (2012). “Synthesis of nano-crystalline La<sub>1-x</sub>Sr<sub>x</sub>CoO<sub>3-δ</sub> perovskite oxides by EDTA-citrate complexing process and its catalytic activity for soot oxidation” *Appl. Catal. A Gen.*, 447–448, 100–106.

Pratap, V., Tomar, S., Dwivedi, D., and Gwalior, M. (2015). “Photocatalytic Degradation of Pharmaceutical Compounds Using Titanium Dioxide Nano Particles.” *Int. J. Adv. Eng. Res. Dev.*, 2(2), 118–122.

Priyanka, K. P., Anu Tresa, S., Jaseentha, O. P., and Varghese, T. (2014). “Cerium doped nanotitania-extended spectral response for enhanced photocatalysis.” *Mater. Res. Express*, 1(1), 1-11.

Qin, D., Lu, W., Wang, X., Li, N., Chen, X., Zhu, Z., and Chen, W. (2016). “Graphitic Carbon Nitride from Burial to Re-emergence on Polyethylene Terephthalate Nanofibers as an Easily Recycled Photocatalyst for Degrading Antibiotics under Solar Irradiation.” *ACS Appl. Mater. Interfaces*, 8(39), 25962–25970.

Renganathan, J., S, I. U. H., Ramakrishnan, K., Ravichandran, M. K., and Philip, L. (2021). “Spatio-temporal distribution of pharmaceutically active compounds in the River Cauvery and its tributaries, South India.” *Sci. Total Environ.*, 800(August), 149340.

Riaz, U., Ashraf, S. M., and Kashyap, J. (2015). “Role of Conducting Polymers in Enhancing TiO<sub>2</sub>-based Photocatalytic Dye Degradation: A Short Review.” *Polym. - Plast. Technol. Eng.*, 54(17), 1850–1870.

Rizzo, L., Sannino, D., Vaiano, V., Sacco, O., Scarpa, A., and Pietrogiacomini, D. (2014). “Applied Catalysis B : Environmental Effect of solar simulated N-doped TiO<sub>2</sub> photocatalysis on the inactivation and antibiotic resistance of an E . coli strain in biologically treated urban wastewater.” *Applied Catal. B, Environ.*, 144, 369–378.

Rtimi, S., and Kiwi, J. (2017). "Bactericide effects of transparent polyethylene photocatalytic films coated by oxides under visible light." *Appl. Catal. B Environ.*, 213, 62–73.

Rtimi, S., Pulgarin, C., Robyr, M., Aybush, A., Shelaev, I., Gostev, F., Nadtochenko, V., and Kiwi, J. (2017). "Insight into the catalyst/photocatalyst microstructure presenting the same composition but leading to a variance in bacterial reduction under indoor visible light." *Appl. Catal. B Environ.*, 208, 135–147.

Rtimi, S., Sanjines, R., Andrzejczuk, M., Pulgarin, C., Kulik, A., and Kiwi, J. (2014). "Innovative transparent non-scattering TiO<sub>2</sub> bactericide thin films inducing increased E. coli cell wall fluidity." *Surf. Coatings Technol.*, 254(July), 333–343.

Rutgersson, C., Fick, J., Marathe, N., Kristiansson, E., Janzon, A., Angelin, M., Johansson, A., Shouche, Y., Flach, C. F., and Larsson, D. G. J. (2014). "Fluoroquinolones and qnr genes in sediment, water, soil, and human fecal flora in an environment polluted by manufacturing discharges." *Environ. Sci. Technol.*, 48(14), 7825–7832.

Sagasta, J. M., Zadeh, S. M., and Turrall, H. (2018). "More people, more food, worse water? - A global review of water pollution from agriculture. Food Agric." *Organ. Int. Water Manag. Inst.*, 1–208.

Sahoo, D. P., Das, K. K., Patnaik, S., and Parida, K. (2020). "Double charge carrier mechanism through 2D/2D interface-assisted ultrafast water reduction and antibiotic degradation over architectural S,P co-doped g-C<sub>3</sub>N<sub>4</sub>/ZnCr LDH photocatalyst." *Inorg. Chem. Front.*, 7(19), 3695–3717.

Sakthivel, S., Shankar, M. V., Palanichamy, M., Arabindoo, B., Bahnemann, D. W., and Murugesan, V. (2004). "Enhancement of photocatalytic activity by metal deposition: Characterisation and photonic efficiency of Pt, Au and Pd deposited on TiO<sub>2</sub> catalyst." *Water Res.*, 38(13), 3001–3008.

Salma, A., Thoröe-Boveleth, S., Schmidt, T. C., and Tuerk, J. (2016). "Dependence of transformation product formation on pH during photolytic and photocatalytic

degradation of ciprofloxacin.” *J. Hazard. Mater.*, 313, 49–59.

Samsudin, E. M., and Hamid, S. B. A. (2017). “Effect of band gap engineering in anionic-doped TiO<sub>2</sub> photocatalyst.” *Appl. Surf. Sci.*, 391, 326–336.

Sanjeev, D. (2020). “Lifeline of Dakshina Kannada and Udupi contain antibiotics , says study.” <https://timesofindia.indiatimes.com/city/mangaluru/lifeline-of-dakshina-kannada-and-udupi-contain-antibiotics-says-study/articleshow/77779358.cms> (May. 21, 2022).

Sarafraz, M., Sadeghi, M., Yazdanbakhsh, A., Amini, M. M., Sadani, M., and Eslami, A. (2020). “Enhanced photocatalytic degradation of ciprofloxacin by black Ti<sup>3+</sup>/N-TiO<sub>2</sub> under visible LED light irradiation: Kinetic, energy consumption, degradation pathway, and toxicity assessment.” *Process Saf. Environ. Prot.*, 137, 261–272.

Sarkar, S., Chakraborty, S., and Bhattacharjee, C. (2015). “Photocatalytic degradation of pharmaceutical wastes by alginate supported TiO<sub>2</sub> nanoparticles in packed bed photo reactor (PBPR).” *Ecotoxicol. Environ. Saf.*, 121, 263–270.

Sato, K., Inoue, Y., Fujii, T., Aoyama, H., and Mitsuhashi, S. (1986). “Purification and properties of DNA gyrase from a fluoroquinolone-resistant strain of *Escherichia coli*.” *Antimicrob. Agents Chemother.*, 30(5), 777–780.

Sayed, M., Khan, J. A., Shah, L. A., Shah, N. S., Shah, F., Khan, H. M., Zhang, P., and Arandiyani, H. (2018). “Solar Light Responsive Poly(vinyl alcohol)-Assisted Hydrothermal Synthesis of Immobilized TiO<sub>2</sub>/Ti Film with the Addition of Peroxymonosulfate for Photocatalytic Degradation of Ciprofloxacin in Aqueous Media: A Mechanistic Approach.” *J. Phys. Chem. C*, 122(1), 406–421.

Sboui, M., Nsib, M. F., Rayes, A., Swaminathan, M., and Houas, A. (2017). “TiO<sub>2</sub>–PANI/Cork composite: A new floating photocatalyst for the treatment of organic pollutants under sunlight irradiation.” *J. Environ. Sci.*, 60, 3–13.

Seddigi, Z. S., Gondal, M. A., Baig, U., Ahmed, S. A., Abdulaziz, M. A., Danish, E. Y., Khaled, M. M., and Lais, A. (2017). “Facile synthesis of light harvesting

semiconductor bismuth oxychloride nano photo-catalysts for efficient removal of hazardous organic pollutants.” *PLoS One*, 12(2), 1–19.

Segura, P. A., Takada, H., Correa, J. A., Saadi, K. El, Koike, T., Onwona-Agyeman, S., Ofosu-Anim, J., Sabi, E. B., Wasonga, O. V., Mghalu, J. M., Santos, A. M. dos, Newman, B., Weerts, S., and Yargeau, V. (2015). “Global occurrence of anti-infectives in contaminated surface waters: Impact of income inequality between countries.” *Environ. Int.*, 80, 89–97.

Sena, M. S., Silva, M. M. de S. e, Santos, A. G. dos, Lopes-Moriyama, A. L., and Souza, C. P. de. (2017). “Synthesis and Characterization of Cerium Molybdate Semiconductor Nanoparticles.” *Mater. Res.*, 20(Suppl.2), 485–491.

Shah, N. S., Ditta, A., Ali, J., Sayed, M., Ul, Z., Khan, H., Murtaza, B., Iqbal, J., Ud, S., Imran, M., Nadeem, M., Al-muhtaseb, A. H., Muhammad, N., Khan, H. M., Ghauri, M., and Zaman, G. (2018a). “Toxicities, kinetics and degradation pathways investigation of ciprofloxacin degradation using iron-mediated H<sub>2</sub>O<sub>2</sub> based advanced oxidation processes.” *Process Saf. Environ. Prot.*, 117, 473–482.

Shah, N. S., Khan, J. A., Sayed, M., Khan, Z. U. H., Rizwan, A. D., Muhammad, N., Boczkaj, G., Murtaza, B., Imran, M., Khan, H. M., and Zaman, G. (2018b). “Solar light driven degradation of norfloxacin using as-synthesized Bi<sup>3+</sup> and Fe<sup>2+</sup> co-doped ZnO with the addition of HSO<sub>5</sub><sup>-</sup>: Toxicities and degradation pathways investigation.” *Chem. Eng. J.*, 351(June), 841–855.

Shan, A. Y., Ghazi, T. I. M., and Rashid, S. A. (2010). “Immobilisation of titanium dioxide onto supporting materials in heterogeneous photocatalysis: A review.” *Appl. Catal. A Gen.*, 389(1–2), 1–8.

Shankaraiah, G., Poodari, S., Bhagawan, D., Himabindu, V., and Vidyavathi, S. (2016). “Degradation of antibiotic norfloxacin in aqueous solution using advanced oxidation processes (AOPs)—A comparative study.” *Desalin. Water Treat.*, 57(57), 27804–27815.

Sharma, B. M., Bečanová, J., Scherlinger, M., Sharma, A., Bharat, G. K., Whitehead,



P. G., Klánová, J., and Nizzetto, L. (2019). “Health and ecological risk assessment of emerging contaminants (pharmaceuticals, personal care products, and artificial sweeteners) in surface and groundwater (drinking water) in the Ganges River Basin, India.” *Sci. Total Environ.*, 646, 1459–1467.

Sharma, I. D., Tripathi, G. K., Sharma, V. K., Tripathi, S. N., Kurchania, R., Kant, C., Sharma, A. K., and Saini, K. K. (2015). “One-pot synthesis of three bismuth oxyhalides (BiOCl, BiOBr, BiOI) and their photocatalytic properties in three different exposure conditions.” *Cogent Chem.*, 1(1), 1–15.

Shen, C., Pang, K., Du, L., and Luo, G. (2017). “Green synthesis and enhanced photocatalytic activity of Ce-doped TiO<sub>2</sub> nanoparticles supported on porous glass.” 1–7.

Shetty, R., Chavan, V. B., Kulkarni, P. S., Kulkarni, B. D., and Kamble, S. P. (2017). “Photocatalytic Degradation of Pharmaceuticals Pollutants Using N-Doped TiO<sub>2</sub> Photocatalyst: Identification of CFX Degradation Intermediates.” *Indian Chem. Eng.*, 59(3), 177–199.

Shi, X., Ding, Y., Zhou, S., Zhang, B., Cai, M., Yao, J., Hu, L., Wu, J., Dai, S., and Nazeeruddin, M. K. (2019). “Enhanced Interfacial Binding and Electron Extraction Using Boron-Doped TiO<sub>2</sub> for Highly Efficient Hysteresis-Free Perovskite Solar Cells.” *Adv. Sci.*, 6(21).

Shiklomanov, I. . (1993). “World fresh water resources: Chapter 2.” *Water Cris. A Guide to World’s Fresh Water Resour.*, 13–23.

Shimizu, A., Takada, H., Koike, T., Takeshita, A., Saha, M., Rinawati, Nakada, N., Murata, A., Suzuki, T., Suzuki, S., Chiem, N. H., Tuyen, B. C., Viet, P. H., Siringan, M. A., Kwan, C., Zakaria, M. P., and Reungsang, A. (2013). “Ubiquitous occurrence of sulfonamides in tropical Asian waters.” *Sci. Total Environ.*, 452–453, 108–115.

Silva, A. R., Martins, P. M., Teixeira, S., Carabineiro, S. A. C., Kuehn, K., Cuniberti, G., Alves, M. M., Lanceros-Mendez, S., and Pereira, L. (2016). “Ciprofloxacin wastewater treated by UVA photocatalysis: contribution of irradiated TiO<sub>2</sub> and ZnO

nanoparticles on the final toxicity as assessed by *Vibrio fischeri*.” *RSC Adv.*, 6(98), 95494–95503.

Silva, G., Draz, G., Silva, M. T., and Faria, J. L. (2009). “Ce-doped TiO<sub>2</sub> for photocatalytic degradation of chlorophenol.” 144, 13–18.

Singh, G. D., and Gupta, K. C. (2014). “Photo and UV degradation of Ciprofloxacin Antibiotic.” *Int. J. Curr. Microbiol. Appl. Sci.*, 3(6), 641–648.

Singh, R., Singh, A. P., Kumar, S., Giri, B. S., and Kim, K. H. (2019). “Antibiotic resistance in major rivers in the world: A systematic review on occurrence, emergence, and management strategies.” *J. Clean. Prod.*, 234, 1484–1505.

Singh, S., Chaki, A., Chand, D. P., Raghuwanshi, A., and Singh, P. K. (2013a). “A novel polystyrene-supported titanium dioxide photocatalyst for degradation of methyl orange and methylene blue dyes under UV irradiation.” *J. Chem. Eng.*, 28(1), 9–13.

Singh, S., Mahalingam, H., and Singh, P. K. (2013b). “Polymer-supported titanium dioxide photocatalysts for environmental remediation : A review.” *Applied Catal. A, Gen.*, 462–463, 178–195.

Singh, S., Singh, P. K., and Mahalingam, H. (2014). “Novel Floating Ag<sup>+</sup> - Doped TiO<sub>2</sub> / Polystyrene Photocatalysts for the Treatment of Dye Wastewater.”

Singh, S., Singh, P. K., and Mahalingam, H. (2015). “An Effective and Low-Cost TiO<sub>2</sub> / Polystyrene Floating Photocatalyst for Environmental Remediation.” *Int. J. Environ. Res.*, 9(2), 535–544.

Sirés, I., and Brillas, E. (2012). “Remediation of water pollution caused by pharmaceutical residues based on electrochemical separation and degradation technologies: A review.” *Environ. Int.*, 40(1), 212–229.

Sökmen, M., Tatlidil, I., Breen, C., Clegg, F., Buruk, C. K., Sivlim, T., and Akkan, Ş. (2011). “A new nano-TiO<sub>2</sub> immobilized biodegradable polymer with self-cleaning properties.” *J. Hazard. Mater.*, 187(1–3), 199–205.

Song, J., Wu, X., Zhang, M., Liu, C., Yu, J., Sun, G., Si, Y., and Ding, B. (2020). “Highly flexible, core-shell heterostructured, and visible-light-driven titania-based nanofibrous membranes for antibiotic removal and E. coil inactivation.” *Chem. Eng. J.*, 379(April 2019), 122269.

Srikanth, B., Goutham, R., Badri Narayan, R., Ramprasath, A., Gopinath, K. P., and Sankaranarayanan, A. R. (2017). “Recent advancements in supporting materials for immobilised photocatalytic applications in waste water treatment.” *J. Environ. Manage.*, 200, 60–78.

Stoyanova, A., Ivanova, N., and Bachvarova-Nedelcheva, Albena Christov, C. (2021). “Synthesis and photocatalytic activity of cerium-doped and cerium-boron co-doped TiO<sub>2</sub> nanoparticles.” *J. Chem. Technol. Metall.*, 56(6), 1294–1302.

Suárez, L., Pulgarin, C., Giannakis, S., Bensimon, M., and Kiwi, J. (2017). “New evidence for disinfection, self-cleaning and pollutant degradation mediated by GF-TiO<sub>2</sub>-Cu mats under solar/visible light in mild oxidative conditions.” *J. Photochem. Photobiol. A Chem.*, 346, 351–363.

Suárez, L., Pulgarin, C., Roussel, C., and Kiwi, J. (2016). “Preparation , kinetics , mechanism and properties of semi-transparent photocatalytic stable films active in dye degradation.” *Applied Catal. A, Gen.*, 516, 70–80.

Tan, Y. N., Wong, C. L., and Mohamed, A. R. (2011). “An Overview on the Photocatalytic Activity of Nano-Doped- TiO<sub>2</sub> in the Degradation of Organic Pollutants.” *ISRN Mater. Sci.*, 2011, 1–18.

Teixeira, S., Mora, H., Blasse, L. M., Martins, P. M., Carabineiro, S. A. C., Lanceros-Méndez, S., Kühn, K., and Cuniberti, G. (2017). “Photocatalytic degradation of recalcitrant micropollutants by reusable Fe<sub>3</sub>O<sub>4</sub>/SiO<sub>2</sub>/TiO<sub>2</sub> particles.” *J. Photochem. Photobiol. A Chem.*, 345, 27–35.

Thamaphat, K., Limsuwan, P., and Ngotawornchai, B. (2008). “Phase Characterization of TiO<sub>2</sub> Powder by XRD and TEM.” *Nat. Sci.*, 42, 357–361.

Thayanukul, P., Kurisu, F., Kasuga, I., and Furumai, H. (2013). "Evaluation of microbial regrowth potential by assimilable organic carbon in various reclaimed water and distribution systems." *Water Res.*, 47(1), 225–232.

Thomas, M. P. (2020). "The killers within." <https://www.theweek.in/theweek/cover/2020/01/03/the-killers-within.html> (May. 21, 2022).

Tian, G., Fu, H., Jing, L., and Tian, C. (2009). "Synthesis and photocatalytic activity of stable nanocrystalline TiO<sub>2</sub> with high crystallinity and large surface area." 161, 1122–1130.

Tijani, J. O., Fatoba, O. O., Babajide, O. O., and Petrik, L. F. (2016). "Pharmaceuticals, endocrine disruptors, personal care products, nanomaterials and perfluorinated pollutants: a review." *Environ. Chem. Lett.*, 14(1), 27–49.

Tsega, M., and Dejene, F. B. (2016). "Structural and Optical Properties of Ce-Doped TiO<sub>2</sub> Nanoparticles Using the Sol-Gel Process." 5(86), 17–20.

Vaiano, V., Matarangolo, M., and Sacco, O. (2018). "UV-LEDs floating-bed photoreactor for the removal of caffeine and paracetamol using ZnO supported on polystyrene pellets." *Chem. Eng. J.*, 350(May), 703–713.

Varnagiris, S., Urbonavicius, M., Sakalauskaite, S., Daugelavicius, R., Pranevicius, L., Lelis, M., and Milcius, D. (2020). "Floating TiO<sub>2</sub> photocatalyst for efficient inactivation of *E. coli* and decomposition of methylene blue solution." *Sci. Total Environ.*, 720.

Vieira, G. B., José, H. J., Peterson, M., Baldissarelli, V. Z., Alvarez, P., and Fátima Peralta Muniz Moreira, R. de. (2018). "CeO<sub>2</sub>/TiO<sub>2</sub> nanostructures enhance adsorption and photocatalytic degradation of organic compounds in aqueous suspension." *J. Photochem. Photobiol. A Chem.*, 353, 325–336.

Villegas- Guzman, P., Giannakis, S., Rtimi, S., Grandjean, D., Bensimon, M., Alencastro, L. F. de, Torres-Palma, R., and Pulgarin, C. (2017). "A green solar photo-

Fenton process for the elimination of bacteria and micropollutants in municipal wastewater treatment using mineral iron and natural organic acids.” *Appl. Catal. B Environ.*, 219, 538–549.

Wang, A., Wang, H., Deng, H., Wang, S., Shi, W., Yi, Z., Qiu, R., and Yan, K. (2019a). “Controllable synthesis of mesoporous manganese oxide microsphere efficient for photo-Fenton-like removal of fluoroquinolone antibiotics.” *Appl. Catal. B Environ.*, 248(July 2018), 298–308.

Wang, B., Leung, M. K. H., Lu, X., and Chen, S. (2013a). “Synthesis and photocatalytic activity of boron and fluorine codoped TiO<sub>2</sub> nanosheets with reactive facets.” *Appl. Energy*.

Wang, C., Zhu, L., Wei, M., Chen, P., and Shan, G. (2012). “Photolytic reaction mechanism and impacts of coexisting substances on photodegradation of bisphenol A by Bi<sub>2</sub>WO<sub>6</sub> in water.” *Water Res.*, 46(3), 845–853.

Wang, H., Li, J., Huo, P., Yan, Y., and Guan, Q. (2016a). “Preparation of Ag<sub>2</sub>O/Ag<sub>2</sub>CO<sub>3</sub>/MWNTs composite photocatalysts for enhancement of ciprofloxacin degradation.” *Appl. Surf. Sci.*, 366, 1–8.

Wang, J., Li, C., Zhuang, H., and Zhang, J. (2013b). “Photocatalytic degradation of methylene blue and inactivation of Gram-negative bacteria by TiO<sub>2</sub> nanoparticles in aqueous suspension.” *Food Control*, 34(2), 372–377.

Wang, J., Svoboda, L., Němečková, Z., Sgarzi, M., Henych, J., Licciardello, N., and Cuniberti, G. (2021). “Enhanced visible-light photodegradation of fluoroquinolone-based antibiotics and E. coli growth inhibition using Ag–TiO<sub>2</sub> nanoparticles.” *RSC Adv.*, 11(23), 13980–13991.

Wang, J., Tang, L., Zeng, G., Deng, Y., Liu, Y., Wang, L., Zhou, Y., Guo, Z., Wang, J., and Zhang, C. (2017a). “Atomic scale g-C<sub>3</sub>N<sub>4</sub>/Bi<sub>2</sub>WO<sub>6</sub> 2D/2D heterojunction with enhanced photocatalytic degradation of ibuprofen under visible light irradiation.” *Appl. Catal. B Environ.*, 209, 285–294.

Wang, S., Wang, L., Zhang, X., Huang, Z.-F., Ma, L., Zou, J.-J., Muhammad, T., and Pan, L. (2016b). "MOF-derived C-doped ZnO prepared via a two-step calcination for efficient photocatalysis." *Appl. Catal. B Environ.*, 189(March), 181–191.

Wang, W., Zeng, Z., Zeng, G., Zhang, C., Xiao, R., Zhou, C., Xiong, W., Yang, Y., Lei, L., Liu, Y., Huang, D., Cheng, M., Yang, Y., Fu, Y., Luo, H., and Zhou, Y. (2019b). "Sulfur doped carbon quantum dots loaded hollow tubular g-C<sub>3</sub>N<sub>4</sub> as novel photocatalyst for destruction of *Escherichia coli* and tetracycline degradation under visible light." *Chem. Eng. J.*, 378, 122132.

Wang, Y., Wu, Y., Yang, H., Xue, X., and Liu, Z. (2016c). "Doping TiO<sub>2</sub> with boron or / and cerium elements : Effects on photocatalytic antimicrobial activity." *Vaccum*, 131, 58–64.

Wang, Y., Wu, Y., Yang, H., Xue, X., and Liu, Z. (2016d). "Co-doping TiO<sub>2</sub> with boron and/or yttrium elements: Effects on antimicrobial activity." *Mater. Sci. Eng. B Solid-State Mater. Adv. Technol.*, 211, 149–155.

Wang, Y., Xue, X., and Yang, H. (2014). "Synthesis and antimicrobial activity of boron-doped titania nano-materials." *Chinese J. Chem. Eng.*, 22(4), 474–479.

Wang, Y. Z., Wu, Y. S., Xue, X. X., Yang, H., and Liu, Z. H. (2017b). "Microstructure and antibacterial activity of ions (Ce, Y, or B)-doped Zn-TiO<sub>2</sub>: a comparative study." *Mater. Technol.*, 32(5), 310–320.

Wang, Y. Z., Wu, Y. S., Yang, H., Wang, M., Shi, X. G., Wang, C., Zhang, S. W., Wu, Y. S., Yang, H., Wang, M., Shi, X. G., and Wang, C. (2018). "Effect of calcination temperature on the microstructure and antimicrobial activity of boron and cerium co-doped titania nanomaterials." 7857.

Wankasi, D., and Dikio, E. D. (2014). "Comparative study of polystyrene and polymethylmethacrylate wastes as adsorbents for sorption of Pb<sup>2+</sup> from aqueous solution." *Asian J. Chem.*, 26(24), 8295–8302.

Wen, X. J., Niu, C. G., Huang, D. W., Zhang, L., Liang, C., and Zeng, G. M. (2017).

“Study of the photocatalytic degradation pathway of norfloxacin and mineralization activity using a novel ternary Ag/AgCl-CeO<sub>2</sub> photocatalyst.” *J. Catal.*, 355(November), 73–86.

Wen, X. J., Niu, C. G., Zhang, L., Liang, C., Guo, H., and Zeng, G. M. (2018). “Photocatalytic degradation of ciprofloxacin by a novel Z-scheme CeO<sub>2</sub>-Ag/AgBr photocatalyst: Influencing factors, possible degradation pathways, and mechanism insight.” *J. Catal.*, 358, 141–154.

Wistrand-Yuen, E., Knopp, M., Hjort, K., Koskiniemi, S., Berg, O. G., and Andersson, D. I. (2018). “Evolution of high-level resistance during low-level antibiotic exposure.” *Nat. Commun.*, 9:1599, 1–12.

Wojcieszak, D., Mazur, M., Kaczmarek, D., and Domaradzki, J. (2017). “Influence of doping with Co, Cu, Ce and Fe on structure and photocatalytic activity of TiO<sub>2</sub> nanoparticles.” *Mater. Sci. Pol.*, 35(4), 725–732.

Wu, K., Song, S., Wu, H., Guo, J., and Zhang, L. (2020). “Facile synthesis of Bi<sub>2</sub>WO<sub>6</sub>/C<sub>3</sub>N<sub>4</sub>/Ti<sub>3</sub>C<sub>2</sub> composite as Z-scheme photocatalyst for efficient ciprofloxacin degradation and H<sub>2</sub> production.” *Appl. Catal. A Gen.*, 608, 117869.

Wu, Q., and Zhang, Z. (2020). “The fabrication of magnetically recyclable Ia-doped TiO<sub>2</sub>/Calcium ferrite/diatomite composite for visible-light-driven degradation of antibiotic and disinfection of bacteria.” *Environ. Eng. Sci.*, 37(2), 109–119.

Xiao, L., Huang, Y., Luo, Y., Yang, B., Liu, Y., Zhou, X., and Zhang, J. (2018). “Organic Cotton Photocatalysis.” *ACS Sustain. Chem. Eng.*, 6(11), 14759–14766.

Xing, X., Du, Z., Zhuang, J., and Wang, D. (2018a). “Removal of ciprofloxacin from water by nitrogen doped TiO<sub>2</sub> immobilized on glass spheres: Rapid screening of degradation products.” *J. Photochem. Photobiol. A Chem.*, 359, 23–32.

Xing, Z., Zhang, J., Cui, J., Yin, J., Zhao, T., Kuang, J., and Xiu, Z. (2018b). “Recent advances in floating TiO<sub>2</sub> -based photocatalysts for environmental application.” *Appl. Catal. B Environ.*, 225, 452–467.

Xu, D., Feng, H., Dong, Y., Wang, Q., Zhang, G., Lv, L., Ren, Z., and Wang, P. (2020). “Enhanced Molecular Oxygen Activation on (001) Facets of Zn-Doped BiOCl Nanosheets for Ciprofloxacin Degradation.” *Adv. Mater. Interfaces*, 2000548(001), 1–11.

Xu, J., Ao, Y., Chen, M., and Fu, D. (2009). “Low-temperature preparation of Boron-doped titania by hydrothermal method and its photocatalytic activity.” *J. Alloys Compd.*, 484(1–2), 73–79.

Xu, J., Gao, Q., Bai, X., Wang, Z., and Zhu, Y. (2019). “Enhanced visible-light-induced photocatalytic degradation and disinfection activities of oxidized porous g-C<sub>3</sub>N<sub>4</sub> by loading Ag nanoparticles.” *Catal. Today*, 332(March), 227–235.

Xu, Q., Yu, J., Zhanga, J., Zhanga, J., and Liu, G. (2015). “Cubic anatase TiO<sub>2</sub> nanocrystals with enhanced photocatalytic CO<sub>2</sub> reduction activity.” *J. Mater. Chem. C*, 3, 10715–10722.

Xu, Y., Wu, S., Wan, P., Sun, J., and Hood, Z. D. (2017). “Introducing Ti<sup>3+</sup> defects based on lattice distortion for enhanced visible light photoreactivity in TiO<sub>2</sub> microspheres.” *RSC Adv.*, 7(52), 32461–32467.

Xue, X., Wang, Y., and Yang, H. (2013). “Preparation and characterization of boron-doped titania nano-materials with antibacterial activity.” *Appl. Surf. Sci.*, 264, 94–99.

Yadav, V., Verma, P., Sharma, H., Tripathy, S., and Saini, V. K. (2020). “Photodegradation of 4-nitrophenol over B-doped TiO<sub>2</sub> nanostructure: effect of dopant concentration, kinetics, and mechanism.”

Yamamoto, T., Ishikawa, T., Ouchi, K., and Nishiya, T. (1986). “Isolation and Characterization of Starch-utilizing Mutants of *Escherichia coli*.” *Agric. Biol. Chem.*, 50(4), 875–882.

Yan, N., Zhu, Z., Zhang, J., Zhao, Z., and Liu, Q. (2012). “Preparation and properties of ce-doped TiO<sub>2</sub> photocatalyst.” *Mater. Res. Bull.*, 47(8), 1869–1873.

Yan, Y., Zhou, X., Yu, P., Li, Z., and Zheng, T. (2020). “Characteristics, mechanisms



and bacteria behavior of photocatalysis with a solid Z-scheme Ag / AgBr / g-C<sub>3</sub>N<sub>4</sub> nanosheet in water disinfection.” *Appl. Catal. A, Gen.*, 590, 117282.

Yang, R., Li, H., Wang, Y., Zhu, Z., Hu, C., Zhao, T., Wang, W., and Liu, B. (2020). “A novel flower-like Z-type heterojunction CuS/Bi<sub>7</sub>O<sub>9</sub>I<sub>3</sub> composite catalyst prepared under mild conditions for degradation of antibiotics and sterilization under visible light.” *Environ. Sci. Nano.* 7(10), 3074-3087.

Yang, S., Xu, D., Chen, B., Luo, B., and Shi, W. (2017). “In-situ synthesis of a plasmonic Ag/AgCl/Ag<sub>2</sub>O heterostructures for degradation of ciprofloxacin.” *Appl. Catal. B Environ.*, 204, 602–610.

Yang, Y. Y., Niu, C. G., Wen, X. J., Zhang, L., Liang, C., Guo, H., Guan, D. L., Liu, H. Y., and Zeng, G. M. (2019). “Fabrication of visible-light-driven silver iodide modified iodine-deficient bismuth oxyiodides Z-scheme heterojunctions with enhanced photocatalytic activity for Escherichia coli inactivation and tetracycline degradation.” *J. Colloid Interface Sci.*, 533, 636–648.

Yoon, Y., Zheng, M., Ahn, Y. T., Park, W. K., Yang, W. S., and Kang, J. W. (2017). “Synthesis of magnetite/non-oxidative graphene composites and their application for arsenic removal.” *Sep. Purif. Technol.*, 178, 40–48.

Yu, H., Huang, B., Wang, H., Yuan, X., Jiang, L., Wu, Z., Zhang, J., and Zeng, G. (2018). “Facile construction of novel direct solid-state Z-scheme AgI/BiOBr photocatalysts for highly effective removal of ciprofloxacin under visible light exposure: Mineralization efficiency and mechanisms.” *J. Colloid Interface Sci.*, 522, 82–94.

Yu, M., Liang, H., Zhan, R., Xu, L., and Niu, J. (2020). “Sm-doped g-C<sub>3</sub>N<sub>4</sub>/Ti<sub>3</sub>C<sub>2</sub> MXene heterojunction for visible-light photocatalytic degradation of ciprofloxacin.” *Chinese Chem. Lett.*, 2–5.

Yu, X., Zhang, J., Zhang, J., Niu, J., Zhao, J., Wei, Y., and Yao, B. (2019). “Photocatalytic degradation of ciprofloxacin using Zn-doped Cu<sub>2</sub>O particles: Analysis of degradation pathways and intermediates.” *Chem. Eng. J.*, 374(January), 316–327.

- Zacchia, M., Abategiovanni, M. L., Stratigis, S., and Capasso, G. (2016). "Potassium: From Physiology to Clinical Implications." *Kidney Dis.*, 2(2), 72–79.
- Zaleska, A. (2008). "Doped-TiO<sub>2</sub>: A Review." *Recent Patents Eng.*, 2(3), 157–164.
- Zammit, I., Vaiano, V., Ribeiro, A. R., Silva, A. M. T., Manaia, C. M., and Rizzo, L. (2019). "Immobilised cerium-doped zinc oxide as a photocatalyst for the degradation of antibiotics and the inactivation of antibiotic-resistant bacteria." *Catalysts*, 9(3).
- Zeng, X. feng, Wang, J. sheng, Zhao, Y. na, Zhang, W. li, and Wang, M. huan. (2020). "Construction of TiO<sub>2</sub>-pillared multilayer graphene nanocomposites as efficient photocatalysts for ciprofloxacin degradation." *Int. J. Miner. Metall. Mater.*
- Zhang, J., Song, Y., Yang, H., Xu, S., Jiang, L., and Dan, Y. (2013). "TiO<sub>2</sub>/T-PVA composites immobilized on cordierite: Structure and photocatalytic activity for degrading RhB under visible light." *Water. Air. Soil Pollut.*, 224(7).
- Zhang, W. F., He, Y. L., Zhang, M. S., Yin, Z., and Chen, Q. (2000). "Raman scattering study on anatase TiO<sub>2</sub> nanocrystals." *J. Phys. D. Appl. Phys.*, 33(8), 912–916.
- Zhang, W., Li, X., Jia, G., Gao, Y., Wang, H., Cao, Z., Li, C., and Liu, J. (2014). "Preparation, characterization, and photocatalytic activity of boron and lanthanum co-doped TiO<sub>2</sub>." *Catal. Commun.*, 45, 144–147.
- Zhang, X., and Liu, Q. (2008). "Preparation and characterization of titania photocatalyst co-doped with boron, nickel, and cerium." *Mater. Lett.*, 62(17–18), 2589–2592.
- Zhang, X. X., Li, R., Jia, M., Wang, S., Huang, Y., and Chen, C. (2015). "Degradation of ciprofloxacin in aqueous bismuth oxybromide (BiOBr) suspensions under visible light irradiation: A direct hole oxidation pathway." *Chem. Eng. J.*, 274, 290–297.
- Zhao, J., Zhang, L., Xing, W., and Lu, K. (2015a). "A novel method to prepare B/N codoped anatase TiO<sub>2</sub>." *J. Phys. Chem. C*, 119(14), 7732–7737.

Zhao, S., Qu, Z., Yan, N., Li, Z., Xu, H., Mei, J., and Quan, F. (2015b). “The performance and mechanism of Ag-doped CeO<sub>2</sub>/TiO<sub>2</sub> catalysts in the catalytic oxidation of gaseous elemental mercury.” *Catal. Sci. Technol.*, 5(5), 2985–2993.

Zhao, W., Ma, W., Chen, C., Zhao, J., and Shuai, Z. (2004). “Efficient Degradation of Toxic Organic Pollutants with Ni<sub>2</sub>O<sub>3</sub>/TiO<sub>2-x</sub>B<sub>x</sub> under Visible Irradiation.” *J. Am. Chem. Soc.*, 126, 4782–4783.

Zhao, X., Hu, H. Y., Yu, T., Su, C., Jiang, H., and Liu, S. (2014). “Effect of different molecular weight organic components on the increase of microbial growth potential of secondary effluent by ozonation.” *J. Environ. Sci. (China)*, 26(11), 2190–2197.

Zhao, X., Yi, X., Tian, S., and Zhang, J. (2018). “Excellent photocatalytic degradation and disinfection performance of a novel bifunctional Ag@AgSCN nanostructure with exposed {-112} facets.” *New J. Chem.*, 42(14), 11811–11818.

Zhao, Y., Tao, C., Xiao, G., and Su, H. (2017). “Controlled synthesis and wastewater treatment of Ag<sub>2</sub>O/TiO<sub>2</sub> modified chitosan-based photocatalytic film.” *RSC Adv.*, 7(18), 11211–11221.

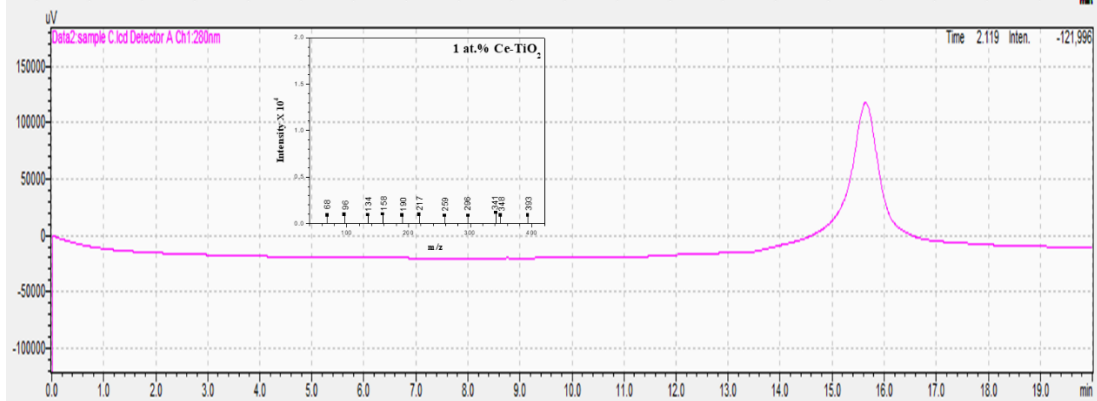
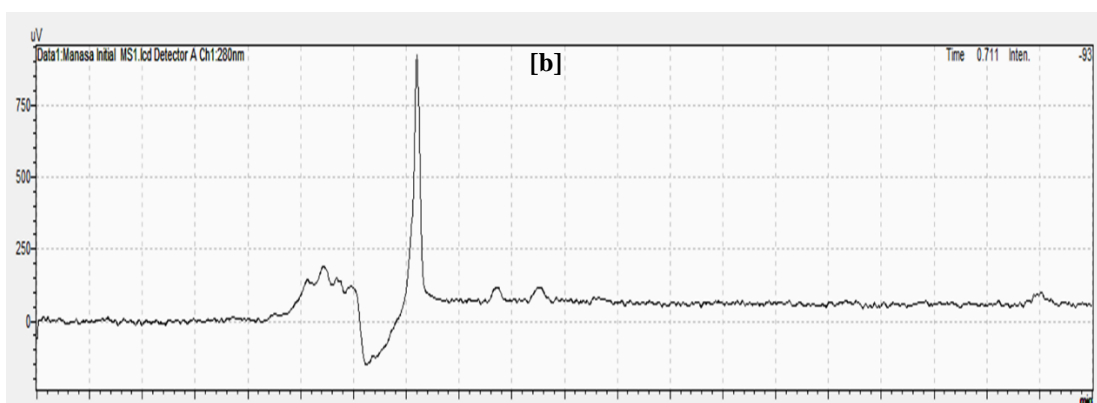
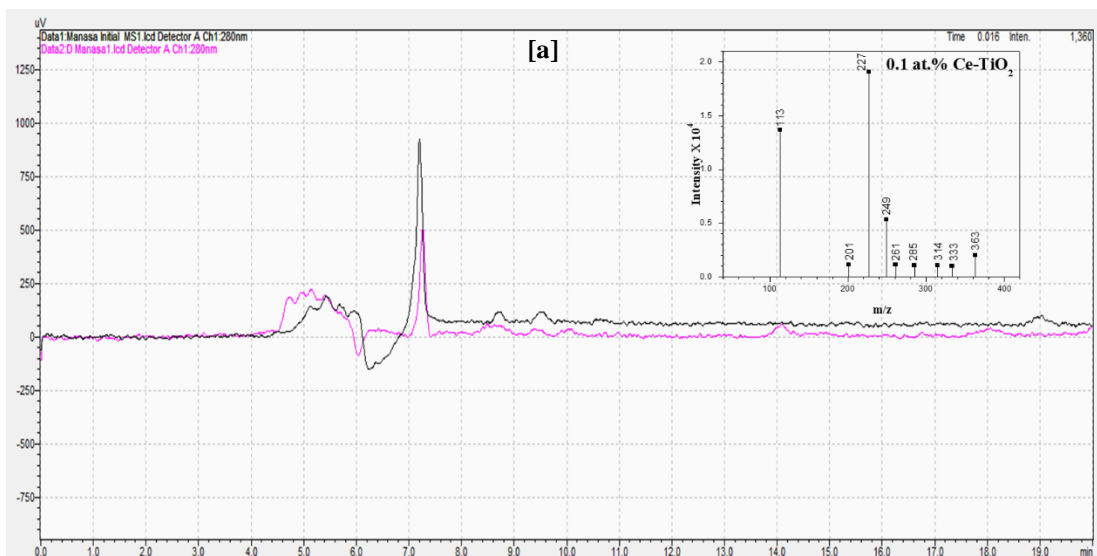
Zheng, X., Xu, S., Wang, Y., Sun, X., Gao, Y., and Gao, B. (2018). “Enhanced degradation of ciprofloxacin by graphitized mesoporous carbon (GMC)-TiO<sub>2</sub> nanocomposite: Strong synergy of adsorption-photocatalysis and antibiotics degradation mechanism.” *J. Colloid Interface Sci.*, 527, 202–213.

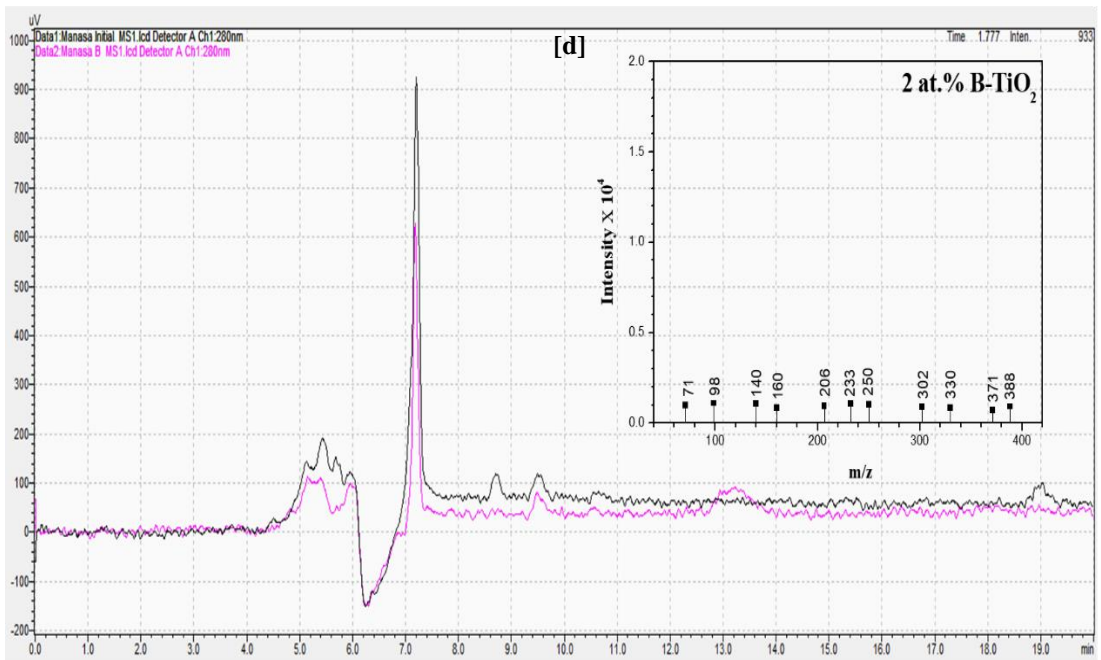
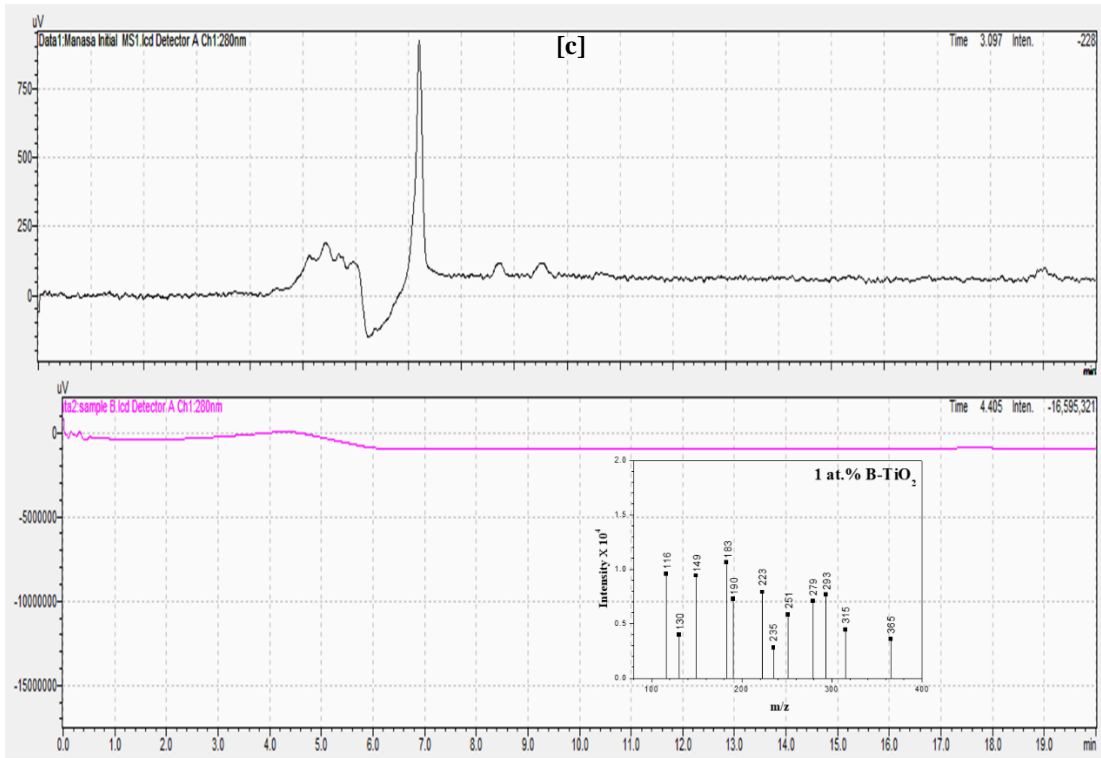
Zhu, W., Li, Z., Zhou, Y., and Yan, X. (2016). “Deposition of silver nanoparticles onto two dimensional BiOCl nanodiscs for enhanced visible light photocatalytic and biocidal activities.” *RSC Adv.*, 6(69), 64911–64920.

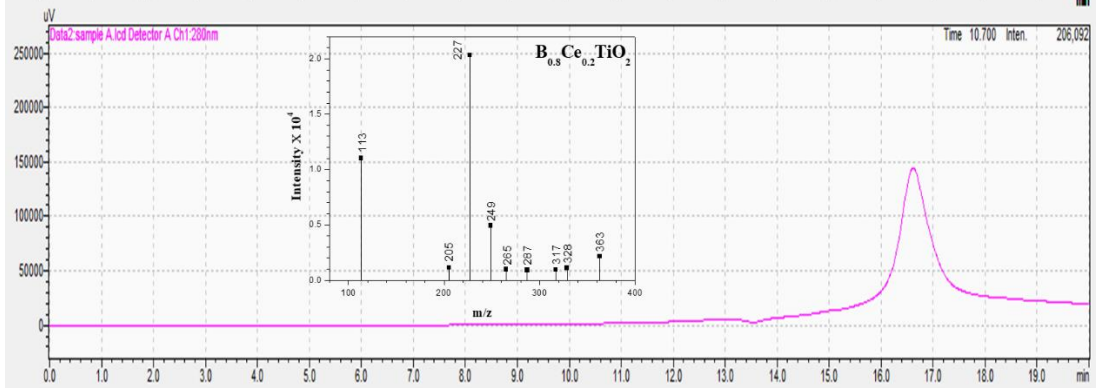
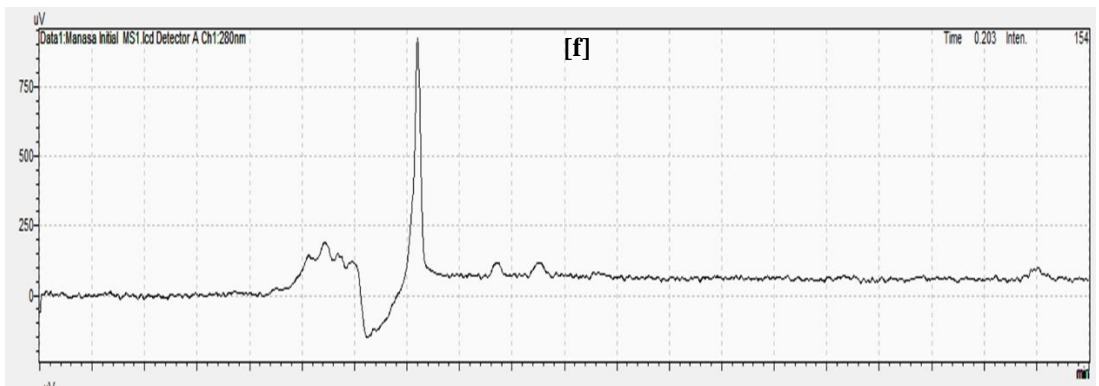
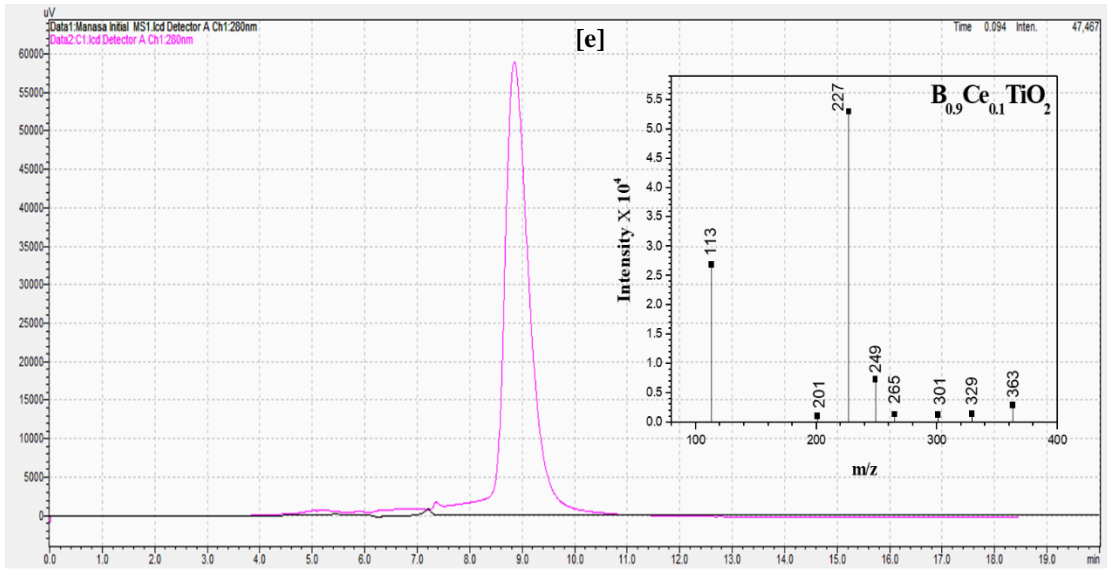
Zuccato, E., Castiglioni, S., Bagnati, R., Melis, M., and Fanelli, R. (2010). “Source, occurrence and fate of antibiotics in the Italian aquatic environment.” *J. Hazard. Mater.*, 179(1–3), 1042–1048.

## APPENDIX I

In this appendix, chromatograms of the CIP treated samples using the synthesized catalysts in this study are given. Black line represents the antibiotic sample before degradation (initial sample) and pink line represents the antibiotic sample after degradation (final sample - after 180 min).







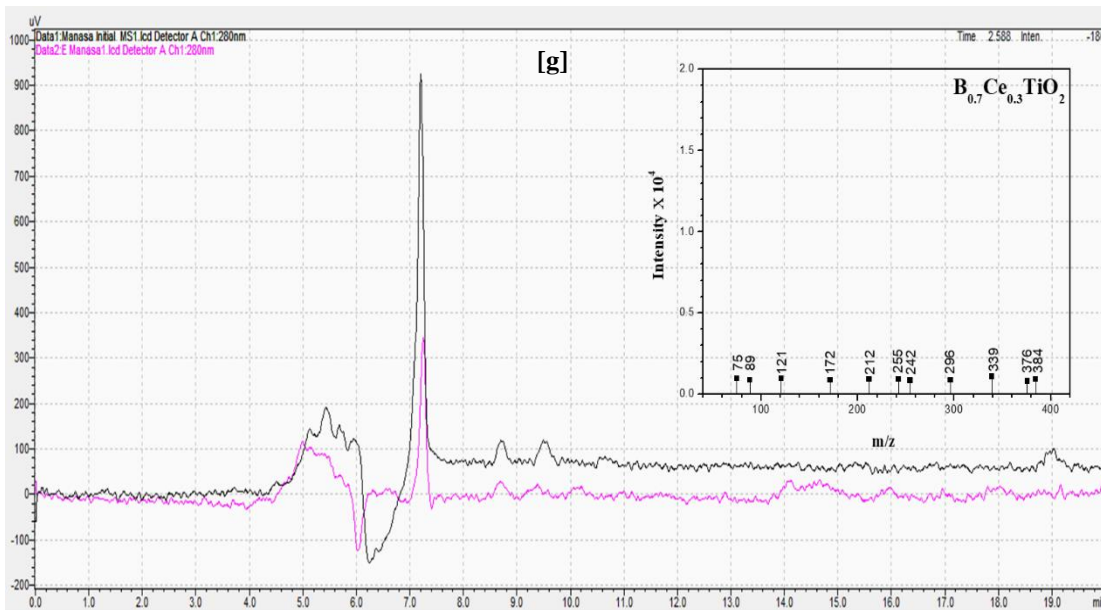


**Figure A1.** HPLC and MS spectra using monodoped (a-d) and codoped (e-g) series of catalysts

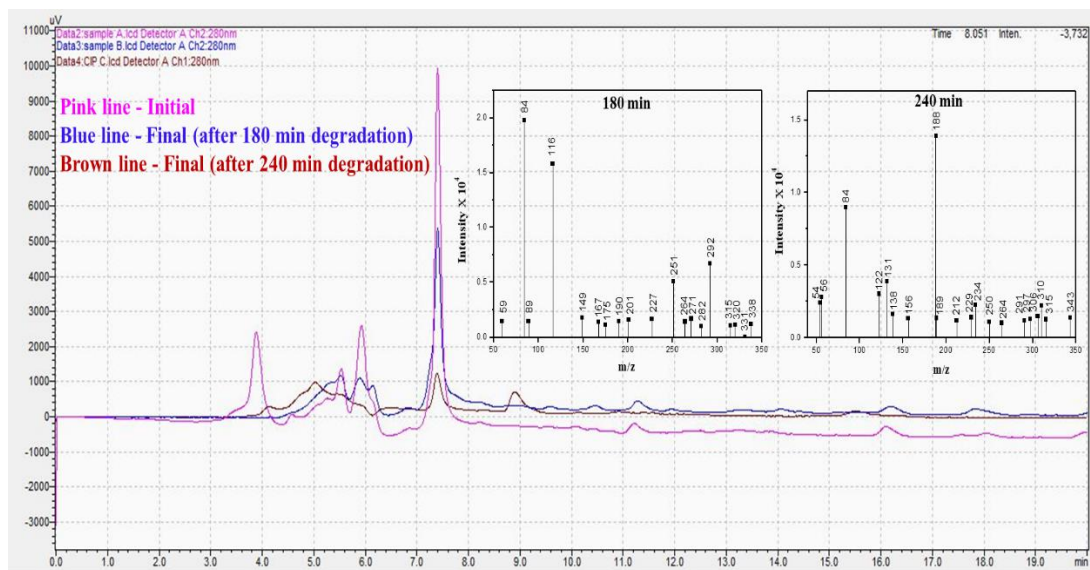
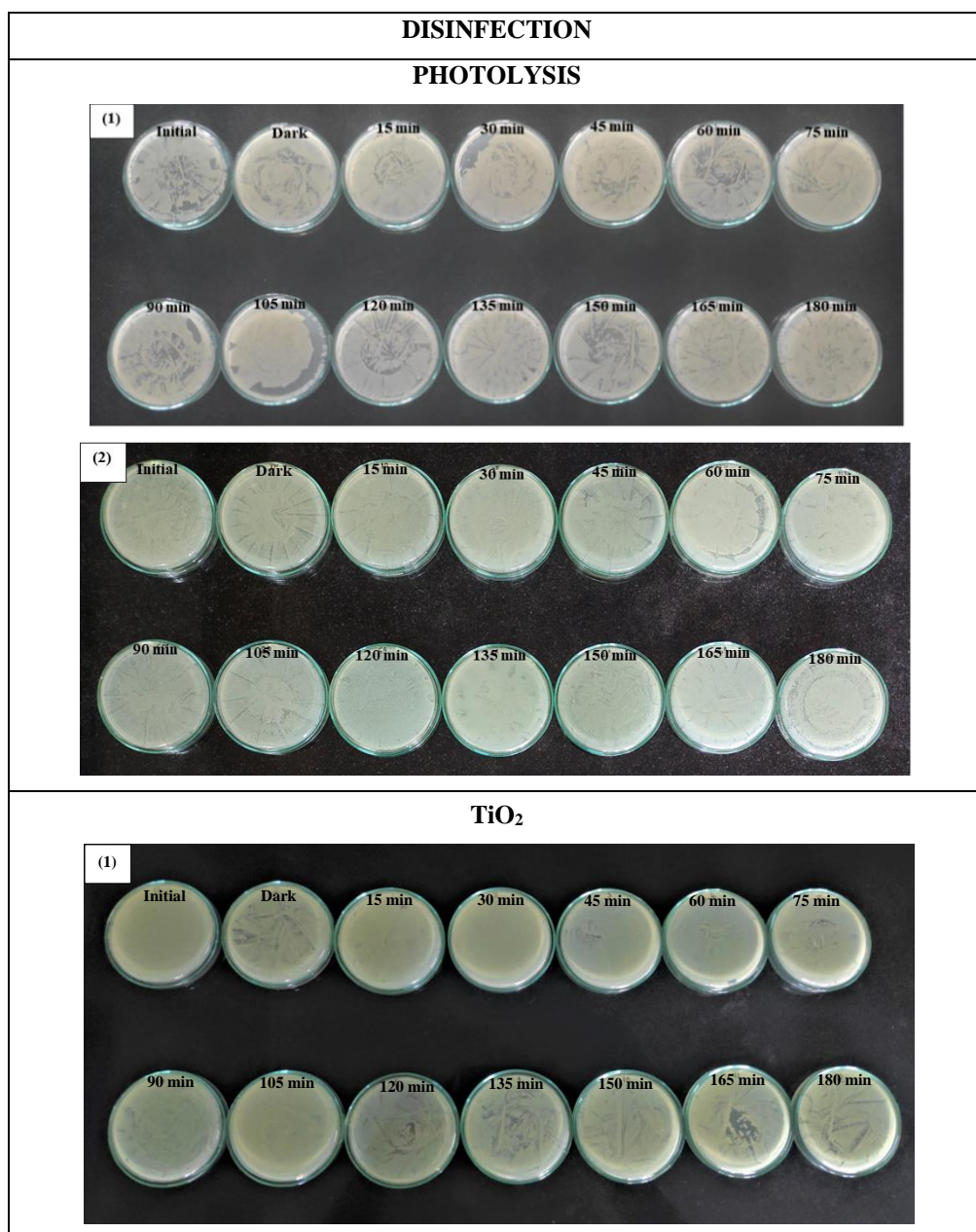


**Figure A2.** HPLC and MS spectrum of CIP degraded products using B<sub>0.8</sub>Ce<sub>0.2</sub>TiO<sub>2</sub> immobilized EPS film

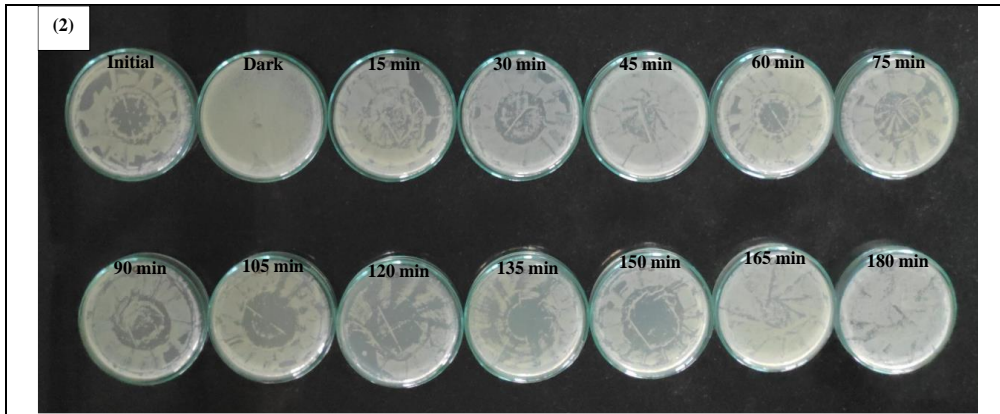


## APPENDIX II

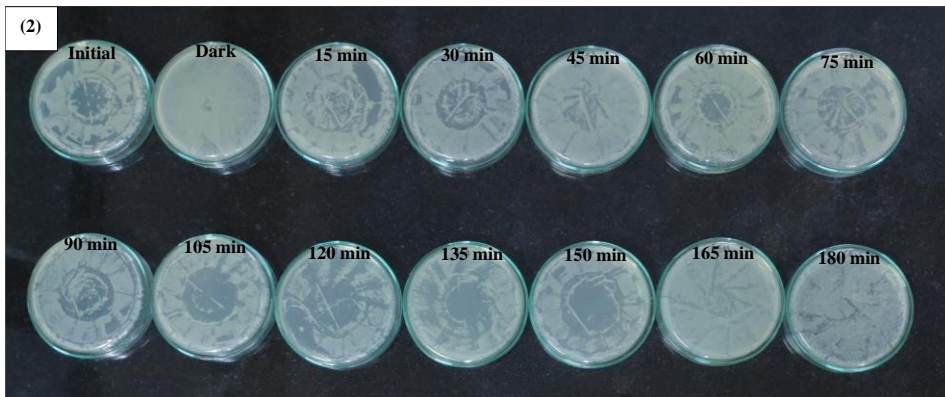
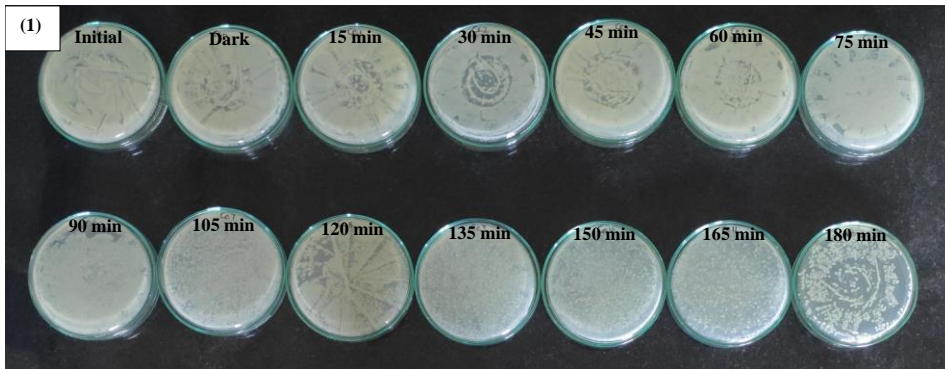
In this appendix, the images of agar plates showing the disinfection activity in different water matrices using the synthesized catalysts in this study are given.



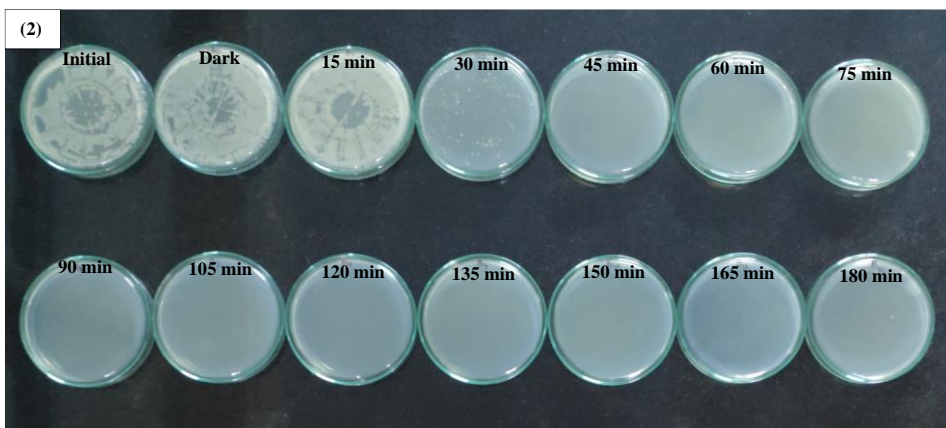
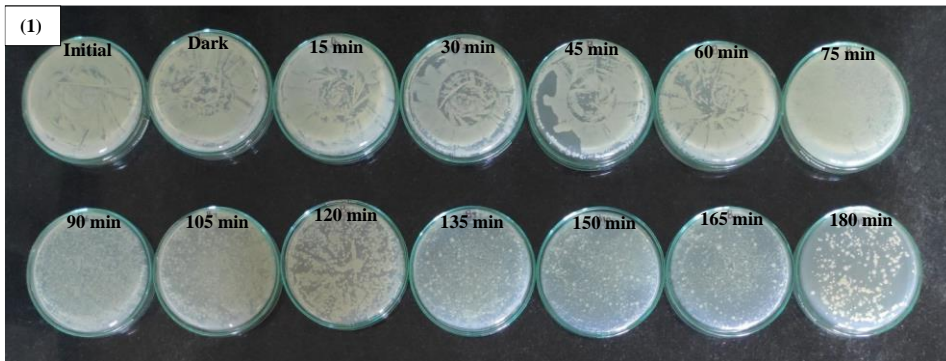




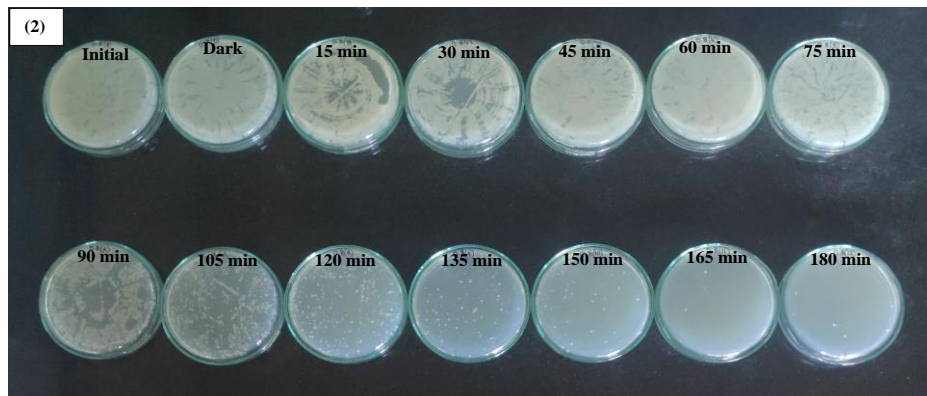
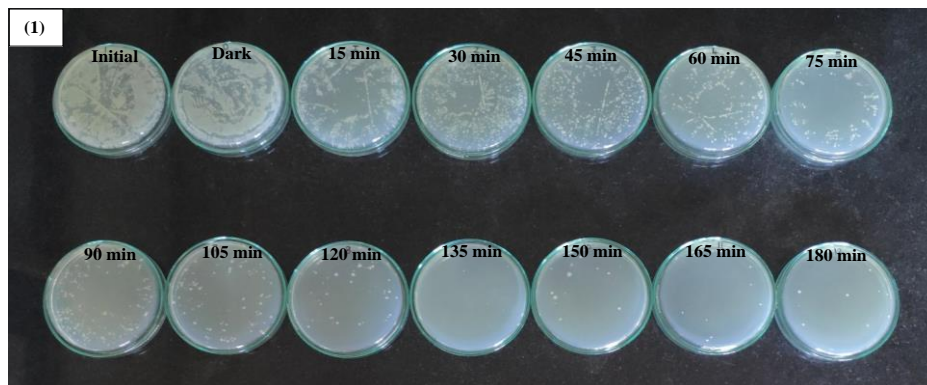
1Ce- TiO<sub>2</sub>



1B- TiO<sub>2</sub>



B<sub>0.8</sub>Ce<sub>0.2</sub>TiO<sub>2</sub> (Suspended form)





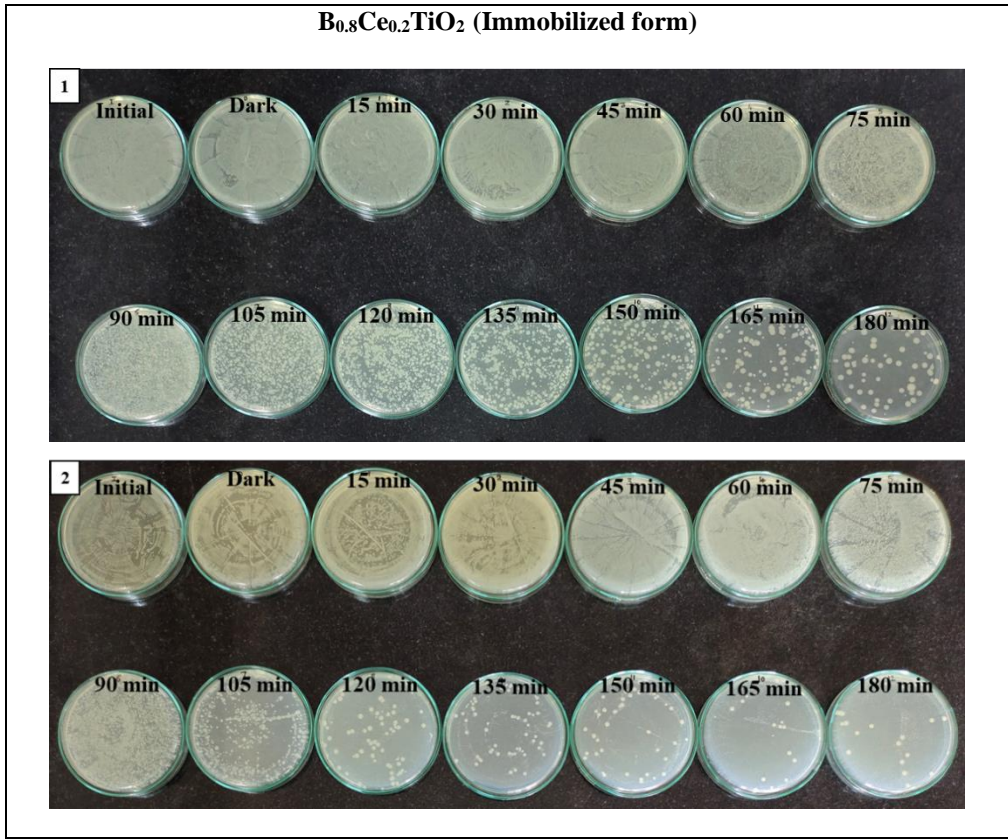
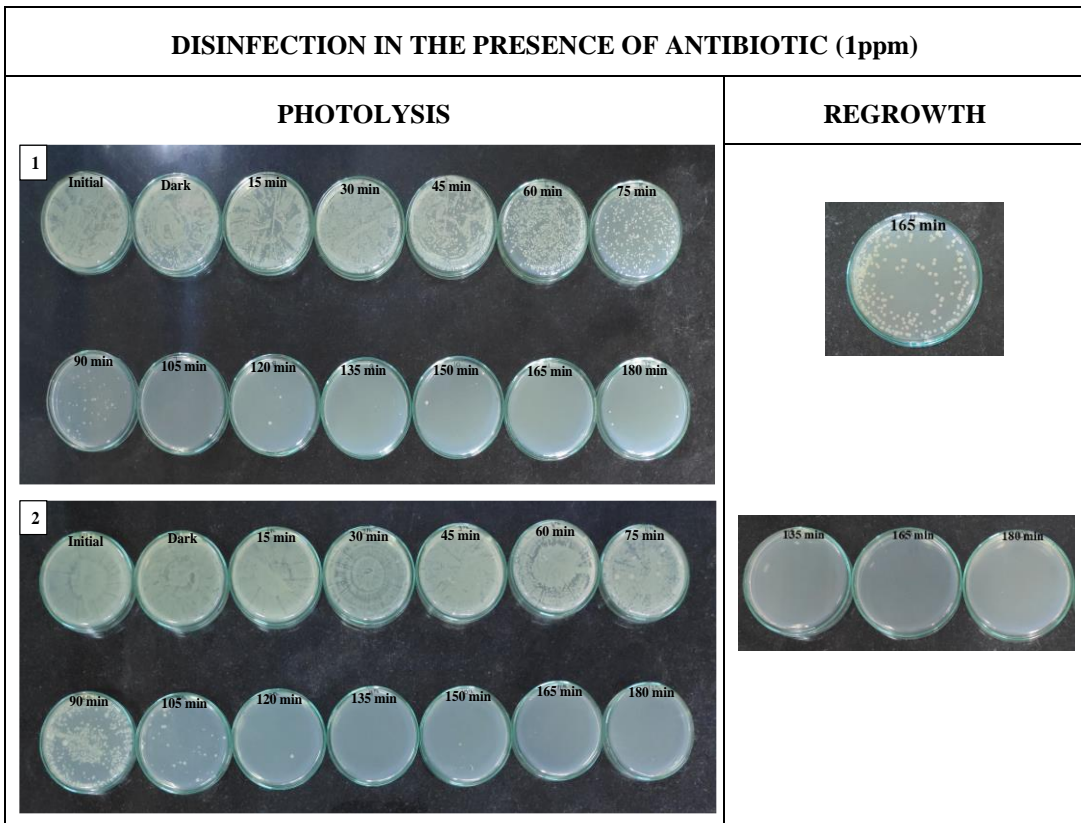


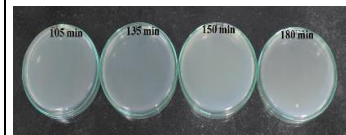
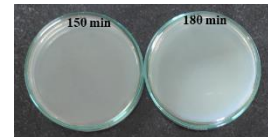
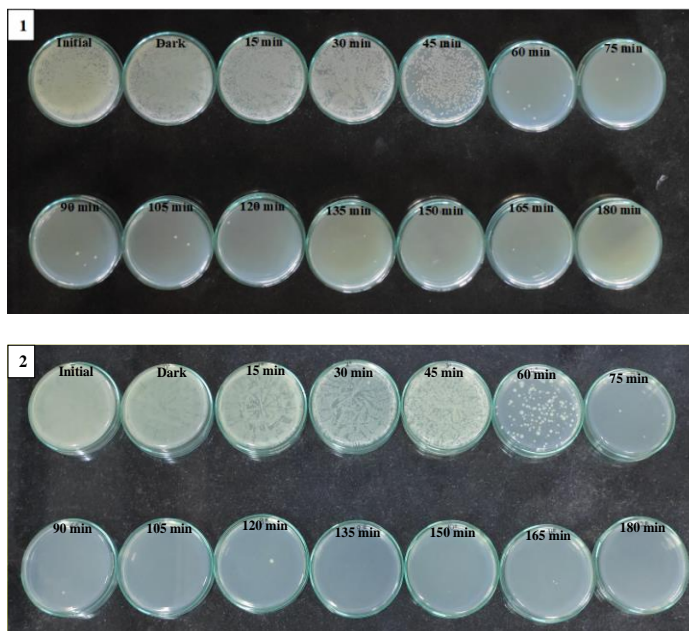
**Figure A1.** Agar plates showing disinfection activity



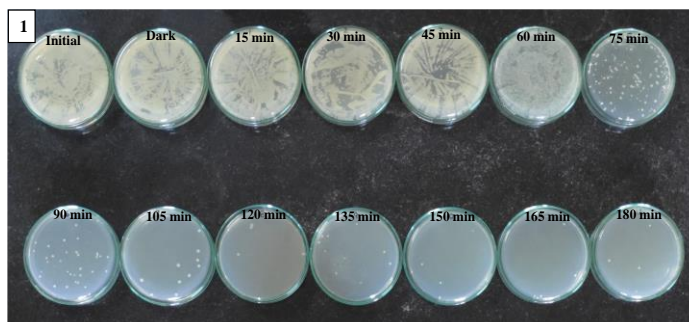
### 1Ce- TiO<sub>2</sub>



### 1B- TiO<sub>2</sub>



### B<sub>0.8</sub>Ce<sub>0.2</sub>TiO<sub>2</sub> (Suspended form)



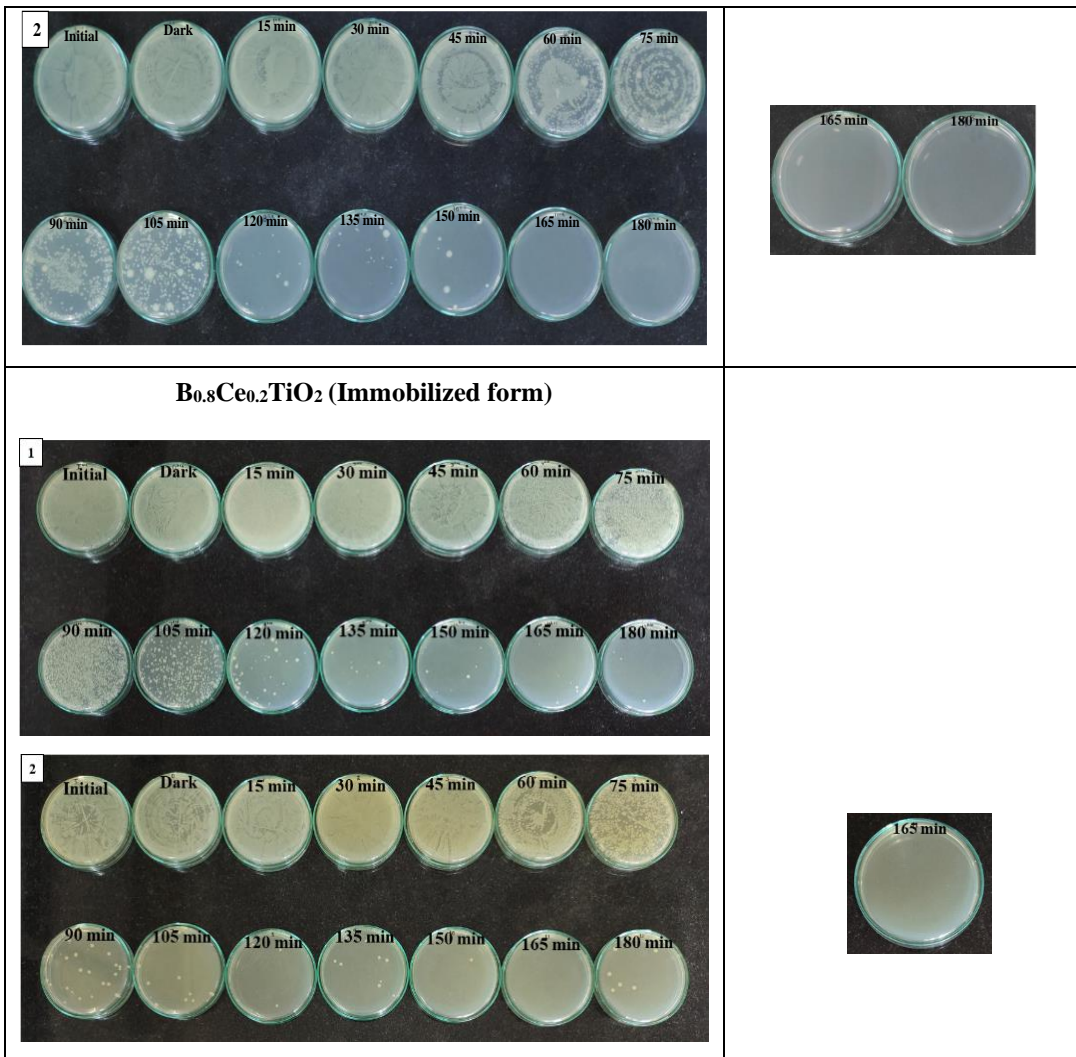


**Figure A2.** Agar plates showing disinfection activity in the presence of 1 ppm CIP



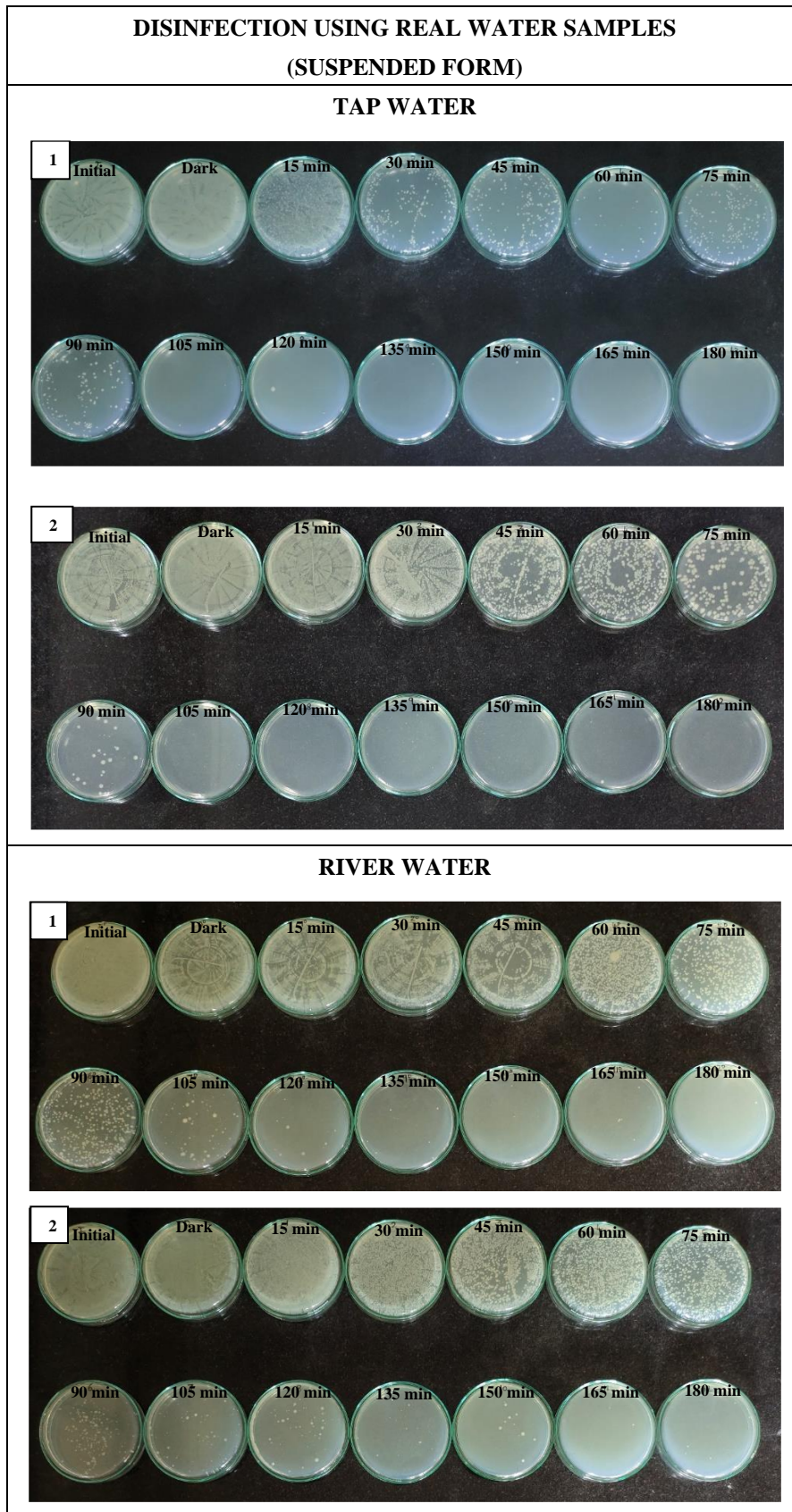


**Figure A3.** Agar plates showing disinfection using different water samples (Suspended form)

**DISINFECTION IN THE PRESENCE OF 1ppm CIP USING REAL WATER SAMPLES  
(SUSPENDED FORM)**

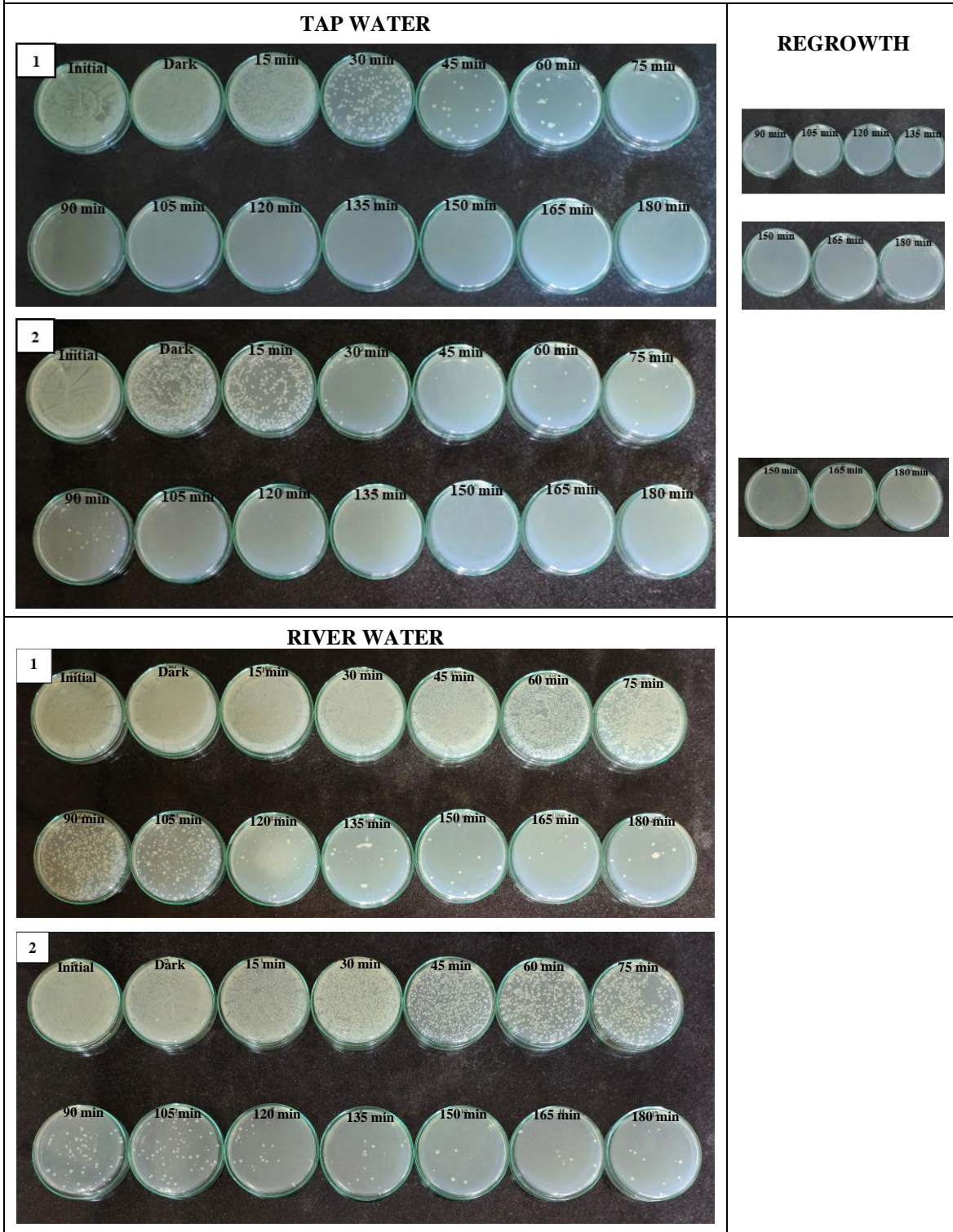


**Figure A4.** Agar plates showing disinfection in the presence of 1 ppm CIP using real water samples (Suspended form)



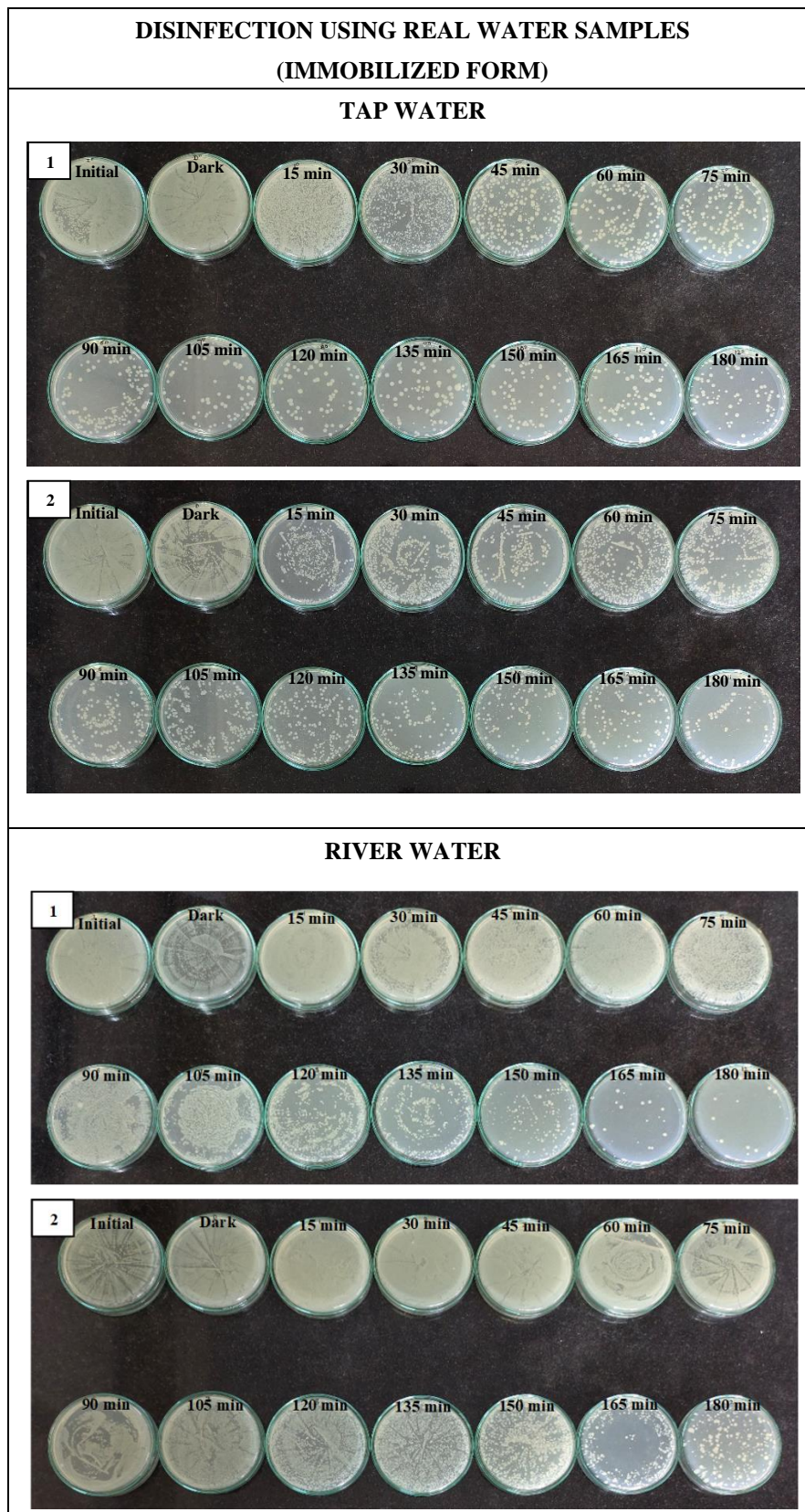


**Figure A5.** Agar plates showing disinfection using real water samples (Immobilized form)



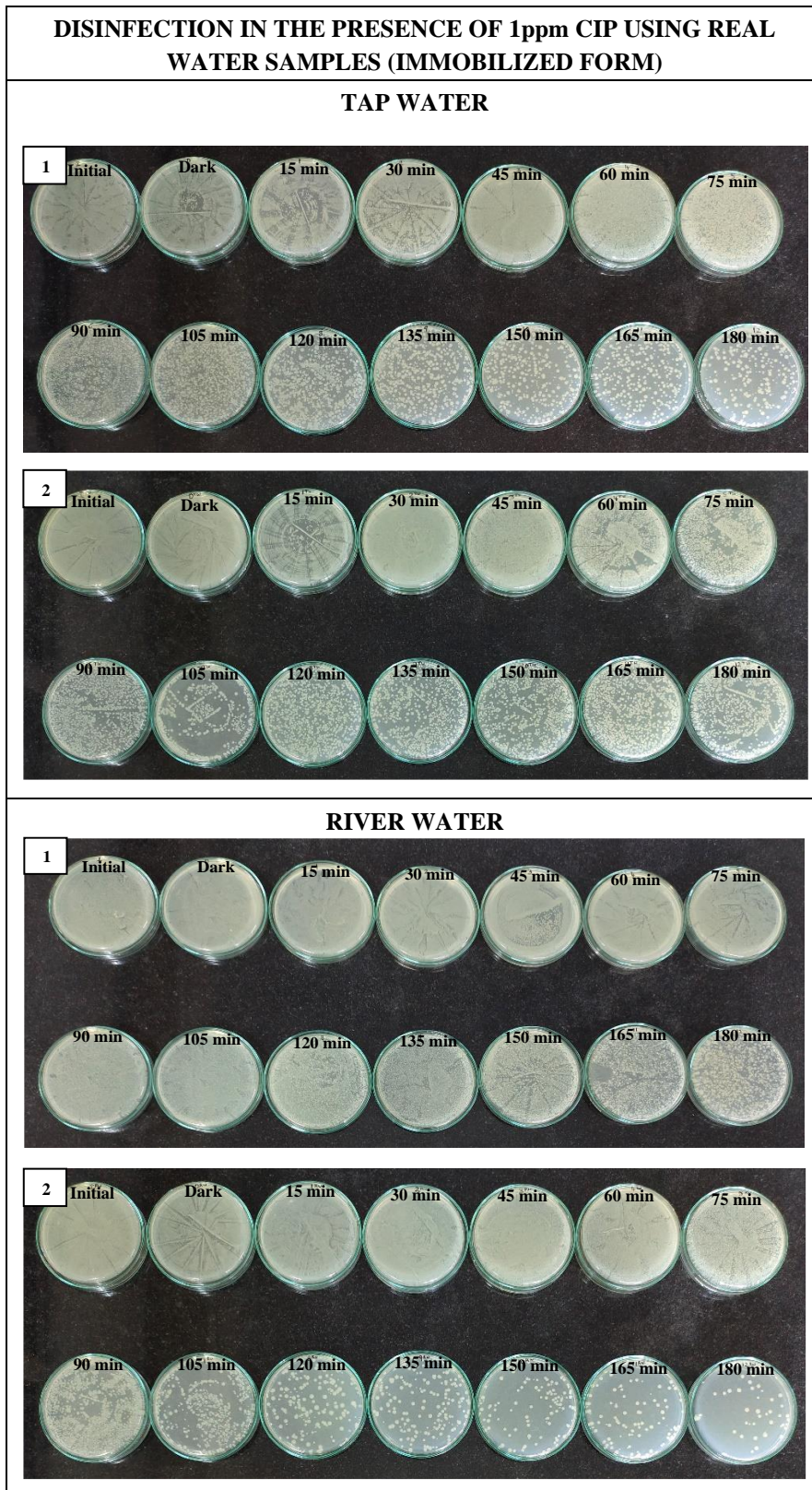


**Figure A6.** Agar plates showing disinfection in the presence of 1 ppm CIP using real water samples (Immobilized form)

## BIO-DATA

**Manasa M**

**Email ID:** [mandhan.m@gmail.com](mailto:mandhan.m@gmail.com)

**Contact no.:** +91-9916701909 / 8095012201

### Personal Details:

**Father's Name:** Manjunatha S

**Date of birth:** 18<sup>th</sup> September, 1990

**Gender:** Female

**Nationality:** Indian

**Permanent address:** H.S.FARM, KURUBARAHALLI, SHIVAKOTE POST,  
HESARAGHATTA HOBLI, BENGALURU-560089,  
KARNATAKA, INDIA

### Educational qualification:

- Ph.D in Chemical Engineering (CGPA-8.0), 2017-2022  
Department of Chemical Engineering,  
National Institute of Technology Karnataka,  
Surathkal, Mangaluru-575025
- M.Tech in Environmental Engineering (82.04%), 2013-2015  
B.M.S College of Engineering, Department of Civil Engineering,  
Bull Temple Road, Basavanagudi, Bengaluru-560019
- B.E in Biotechnology (81.91%), 2009-2013  
Sapthagiri College of Engineering, Department of Biotechnology,  
Hesaraghatta Main road, Chikkasandra, Bengaluru-560057

### Publications:

#### ➤ JOURNAL (Scopus-indexed):

- [1] **Manasa, M.**, Chandewar, P. R., and Mahalingam, H. (2021). "Photocatalytic degradation of ciprofloxacin & norfloxacin and disinfection studies under solar light using boron & cerium doped TiO<sub>2</sub> catalysts synthesized by green EDTA-citrate method." *Catal. Today*, 375, 522–536.

<https://doi.org/10.1016/j.cattod.2020.03.018>

- [2] **Manjunatha, M.**, Chandewar, P. R., and Mahalingam, H. (2022). “Exploring the synergy of B, Ce dopants in codoped titanium dioxide multifunctional photocatalysts for antibiotic degradation and microbial disinfection under solar light.” *Phys. Status Solidi Appl. Mater. Sci.*, 219, 2100581 (1–16).  
<https://onlinelibrary.wiley.com/doi/10.1002/pssa.202100581>
- [3] **Manasa, M.**, and Mahalingam, H. “Upcycling of waste EPS beads to immobilized co-doped TiO<sub>2</sub> photocatalysts: Efficient degradation of antibiotic and disinfection under sunlight.” (under review)

### Other work

- [1] Sukriti, M., **Manasa, M.**, and Mahalingam, H. (2021) “Highly efficient solar light-driven BiOX (X=Br/Cl/I) and BiOY heterojunction (Y=Br/Cl) nano photocatalysts in suspended and immobilized forms for malachite green dye wastewater treatment.”, *Environ. Sci. Pollut. Res.*  
<https://doi.org/10.1007/s11356-021-17636-7>
- [2] Sekar, P., Joshi, D.,S., **Manjunatha, M.**, and Mahalingam, H. (2022) “Enhanced disinfection of *E. faecalis* and Levofloxacin antibiotic degradation using tridoped B-Ce-Ag TiO<sub>2</sub> photocatalysts synthesized by eco-friendly citrate EDTA complexing method.” *Environ. Sci. Pollut. Res.*  
<https://doi.org/10.1007/s11356-022-19268-x>

### ➤ CONFERENCE PROCEEDINGS (ORAL PRESENTATION):

- [1] **Manasa M** and Hari Mahalingam, “Photocatalytic treatment of Emerging contaminants using Ceria-doped TiO<sub>2</sub> under Solar, UV-C and UV-A irradiation”, Proceedings of 8<sup>th</sup> International Engineering Symposium (IES 2019), Kumamoto University, Japan, March 13-15, 2019, pp. A1-1-1 to A1-1-6.
- [2] **Manasa M**, Pranay R Chandewar and Hari Mahalingam, “Photocatalytic degradation of ciprofloxacin and norfloxacin under solar light using boron

doped titanium dioxide catalysts synthesized by green EDTA-citrate method”, APCAT-8, Bangkok, Thailand, August 4-7, 2019, pp. 296.

- [3] **Manasa M**, Pranay R Chandewar and Hari Mahalingam, “Green synthesis of  $B_xCe_{1-x}TiO_2$  catalysts for enhanced sunlight-driven photocatalytic degradation of fluoroquinolone antibiotics and microbial inactivation”, STWTD-2020, December 18-19, 2020, NIT Calicut.

#### **Other work**

- [1] Sukriti Mishra, **Manasa M**, Suman Das and Hari Mahalingam, “Comparison of different Bismuth Oxyhalide photocatalysts for dye wastewater treatment under solar light”, 6<sup>th</sup> IWA-RMTC 2018, Vadodara, Gujarat, December 10-12, 2018 (Poster presentation).
- [2] Sukriti Mishra, **Manasa M** and Hari Mahalingam, “Highly efficient solar light-driven BiOX (X=Br/Cl/I) and BiOY heterojunction (Y=Br/Cl) nano photocatalysts in suspended and immobilized forms for malachite green dye wastewater treatment”, International conference on advances in sustainable research for energy and environment management (ASREEM 2021), NIT Surat, Gujarat, August 6 - 8, 2021 (Best oral presentation award by Econeeds Foundation).

#### **Declaration:**

I hereby declare that the above particulars are true to the best of my knowledge.

**Place:** Surathkal, Karnataka, India

**Date:**

**Manasa M**